Doctoral School of Earth Sciences

Practical applications of geological modelling workflows in the redevelopment of mature hydrocarbon fields – a case study

PHD DISSERTATION

Author

István Nemes

Supervisor

Dr János Geiger

Department of Geology and Paleontology

Faculty of Science and Informatics

University of Szeged

Budapest

2022

TABLE OF CONTENTS

Inventory of units and acronyms		
Acronym	Description	Unit (if any)
1H	shallow wells (upper formations)	-
4H	deep wells (lower formations)	-
A3	Verejskij Formation	-
A4	Bashkirian Formation	-
AOI	area of interest	-
Bb	Bobrikovian/Bobrikovsky Formation	-
bcm	billion cubic metres	-
Boi	initial oil formation volume factor	m^3/sm^3
C	constant depending on units used	-
C1s	Serpukhovian Formation	-
EDA	exploratory data analysis	-
EOR	enchanced oil recovery	-
FWL	free water level	m TVDSS
GRV	gross rock volume	m^3
GUID	globally unique identifier	-
HC	hydrocarbon	-
IBH	Intra-Bobrikovian Horizon	-
IEA	International Energy Agency	-
IOR	improved oil recovery	-
ITH	Intra-Tournasian Horizon	-
km^2	square kilometre	-
m	metre	-
m^3/d	cubic metre per day	-
mmbbl	million barrels of oil	-
mmboe	million barrels of oil equivalent	-
MMm^3	million m^3	-
NtG	net-to-gross	%
OWC	oil-water contact	m TVDSS
pi	initial reservoir pressure	bar
PSTM	pre-stack time migration	-
Rsi	initial dissolved gas content	m^3/m^3
SGS	Sequential Gaussian Simulation	-
SIS	Sequential Indicator Simulation	-
sm^3	standard cubic metre	-
SoW	scope of work	-
SRP	sucker-rod pump	-
STOIIP	stock tank oil initially-in-place	m^3
Swi	initital water saturation	%
TD	total depth	metre
TPM	total property modelling	-
TST	true stratigraphic thickness	metre
TVDSS	true vertical depth subsea	metre
TVT	true vertical thickness	metre
TWT	two-way traveltime	millisecond
v/v%	volume per volume (volumetric percent	-
V1	Tournaisian Formation	-
VPC	vertical proportion curve	-
WC	water-cut	%
Φ	interconnected porosity	%

1 INTRODUCTION

1.1 PREFACE

This thesis concentrates on the practical applications (or applied aspects) of reservoir geological modelling. Accordingly, the theory of the methods applied are of secondary concern, while the in-field implications of an integrated reinvestigation focusing on a mature field are of paramount importance throughout the essay.

The main events and bulk of the work took place between 2015 and 2017; consequently, various aspects of the thesis concentrate on this time period. In some cases, where understanding can be aided, additional data and information are also provided. Due to confidentiality, the hydrocarbon field the study focuses on is anonymised and is referred to as Field A in the documentation (accordingly, well names, precise volumetric data and coordinates remain undisclosed as well).

Structurally, the thesis can be divided into three main parts: 1) an overview of Field A; 2) the process of the reservoir geological modelling, including the preparatory work and the key impacts and results of Phase 1 (first-pass geological model); and 3) the Phase 2 geological model, with the main focus on the integrated workflow established.

This dissertation is strongly connected to the author's related individual and shared publications and conference proceedings; all of the recycled sources are accurately referenced.

1.2 A BRIEF OUTLOOK ON THE PETROLEUM INDUSTRY

Hydrocarbon-related energy sources, that is, oil, gas, condensate and, lately, gas hydrates are a key part of the world's energy mix (Figure 1). Since the dawn of the HC industry, oil and gas (mid-1800s) have been essential members of the energy mix, albeit with changing ratios, as indicated in Figure 1 (n.b., the chart's start date is 1965). During the same time period (from 1965 to 2019), global primary energy consumption increased from 40,000 TWh to 160,000 TWh per year (BRITISH PETROLEUM, 2020), that is, four times, and the increase has been continuous. As a result, the absolute increase in demand is overbalancing the current shrinkage of the relative ratio of oil in the energy basket, resulting in a perpetually growing oil demand and, consequently, oil production. Global oil production climbed from 32 to 95 mmboe per year over the course of six decades, from 1965 to 2019. Meanwhile, natural gas production growth surpassed that of oil, increasing from approximately 2.5 bcm/d in 1970 to 11 bcm/d in 2019 (BRITISH PETROLEUM, 2020). In 2019 the share of fossil fuels is still greater than 80%; oil and gas, without coal, represents 60% (GÜLEN, 2015; Figure 1) of the energy basket.

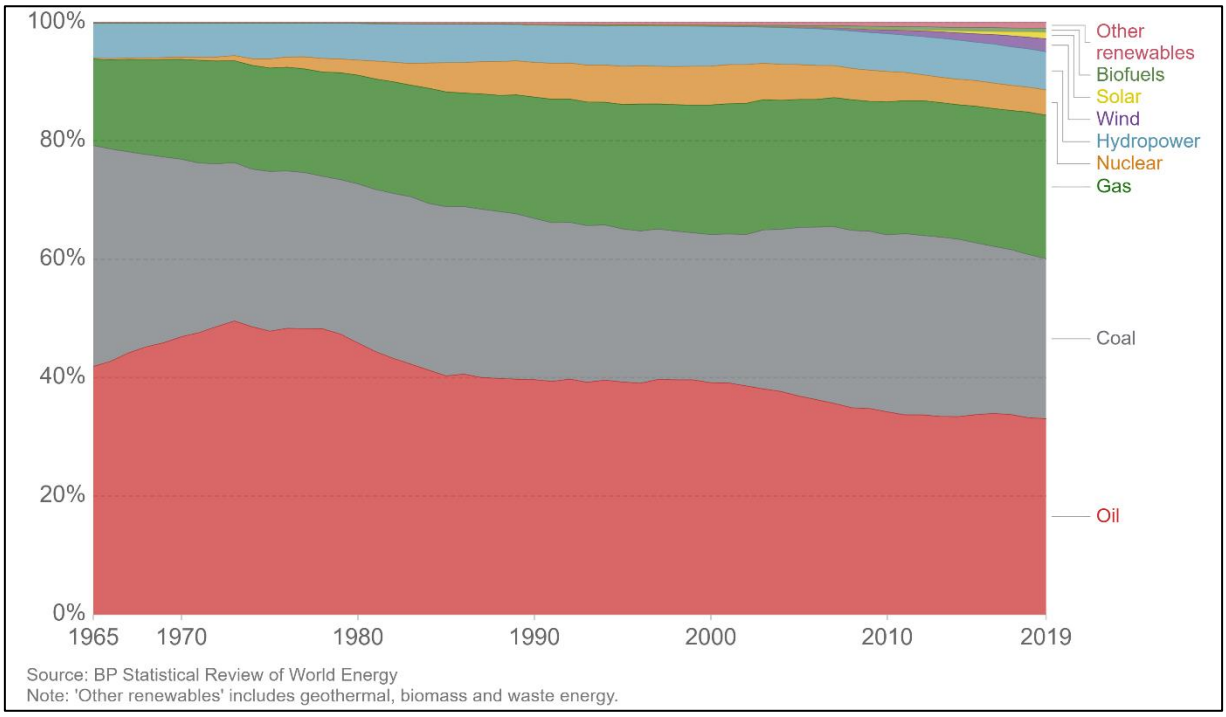

Figure 1: World energy consumption by source. (Source: https://ourworldindata.org/grapher/energy-consumption-by-source-and-region – 24-01-2021)

Figure 2 shows oil price fluctuation since the mid-1800s, indicating a cyclicity in crude prices. There were several crashes in the past, and presumably there will be more in the future as well. In this study the oil price crash in the mid-2010s (from $120 to $45/bbl within a few months) has had a paramount effect as it has directly triggered most of the work outlined in this thesis. Further analysis and the historical background of oil price cyclicity and fluctuations is discussed by various authors with a wide range of views (a few recommended: BRITISH PETROLEUM, 2020; GONG et al., 2021; LANG and AUER, in-press).

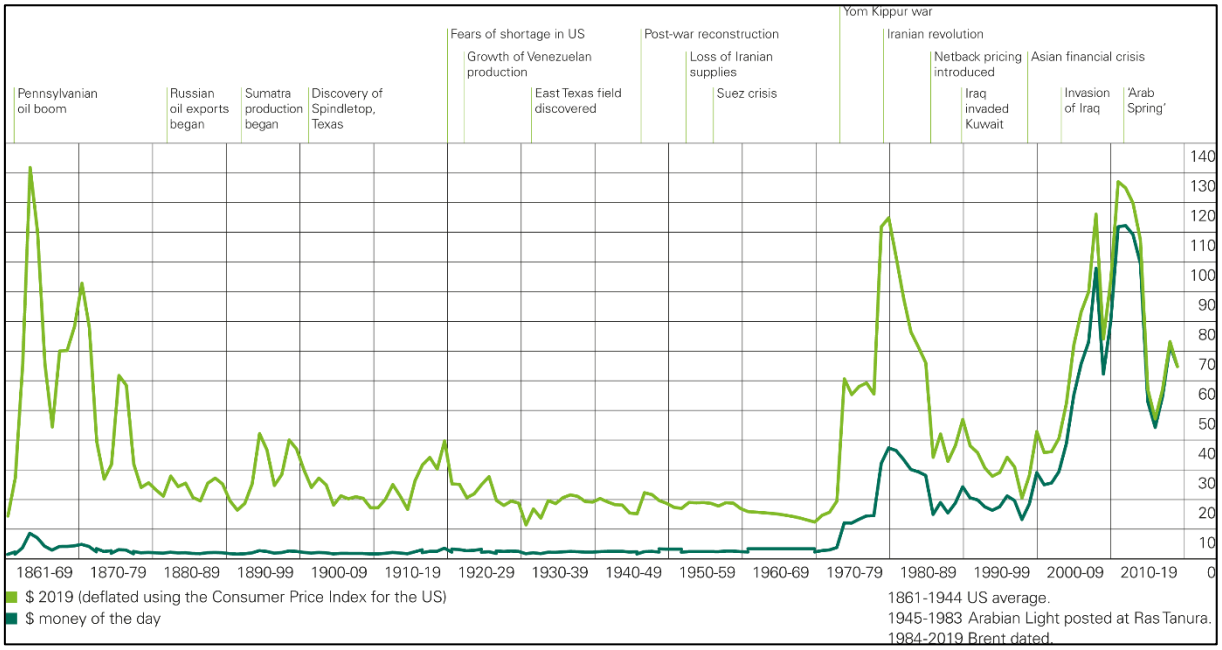

Figure 2: Crude oil prices, 1861-2019. The light green line shows oil price (converted to 2019 USD) changes since the mid-1800s. Important events are missing from the chart, namely, the foundation of the Organization of the Petroleum Exporting Countries (OPEC) in 1960 as well as OPEC+ in 2016 (BRITISH PETROLEUM, 2020).

While the preceding paragraphs reflect on the past, according to IEA, oil and gas demand growth is forecasted to steadily increase in the next decades (Figure 3); it is evident that no abrupt change can be expected. Natural gas shows a steeper growth trend compared to oil, and renewables are indicating noticeably steep growth for the years ahead.

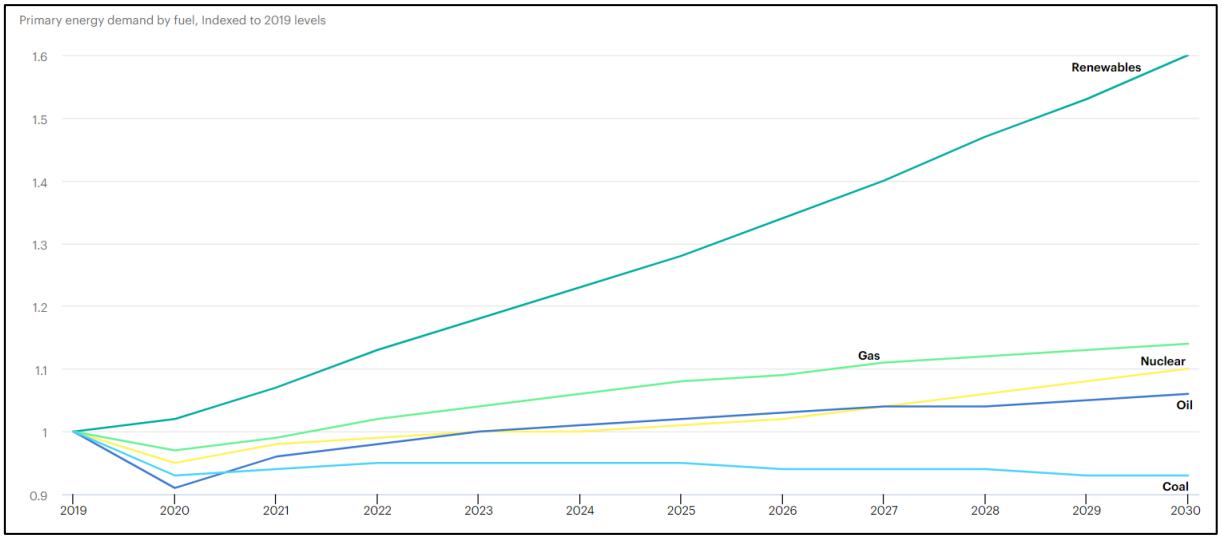

Figure 3: Primary energy demand by different fuel types, reflecting the stated policies scenario, that is, the actual base case Covid-recovery forecasts indexed to 2019 levels (INTERNATIONAL ENERGY AGENCY, 2020).

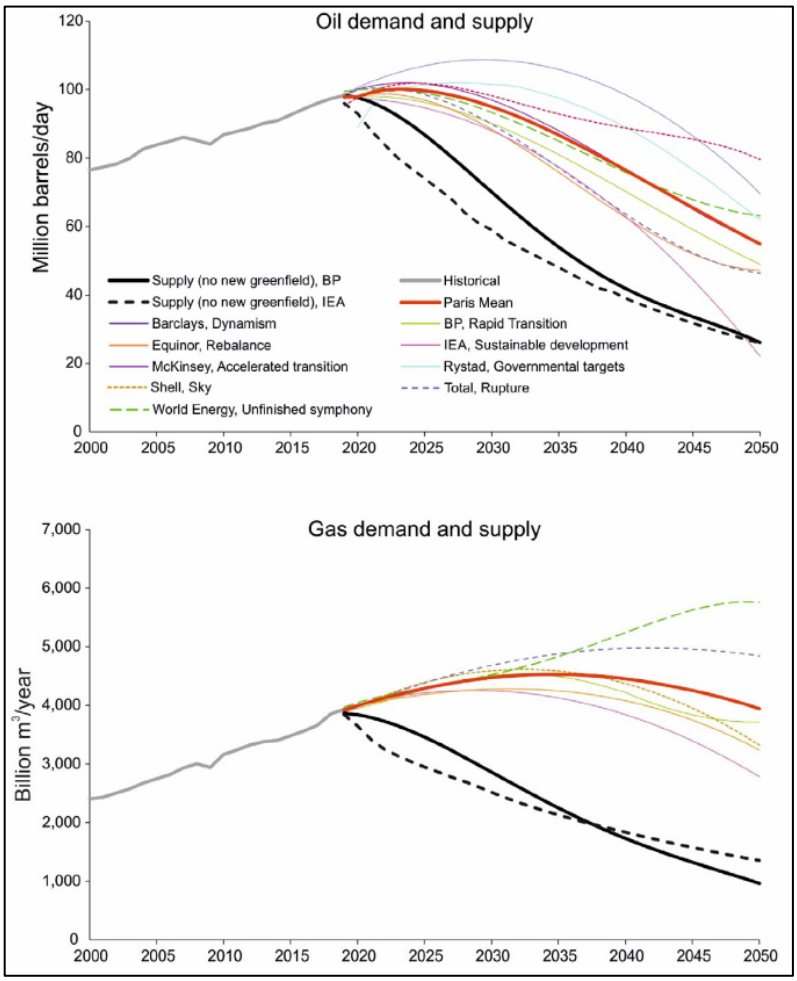

Figure 4: Oil demand and supply is shown in the upper part of the chart, with gas in the lower. The black lines show supply with no green fields, while the coloured lines depict the various forecasts. All forecasts predict demand growth prior to a steady decrease (DAVIES and SIMMONS, 2021).

Based on macro trends, the experience of the past and the forecasts for the future, it is premature to announce the end of the hydrocarbon age. The oil and gas industry will pave the road to renewables, and possibly fusion energy, but will also supply the world with energy in the transitional times ahead.

Figure 4 shows several scenarios for possible future trends focusing on oil and gas supply and demand until 2050. The increase in demand in all scenarios for oil until around 2025-2030 should be noted, as well as for gas demand, which is forecasted to grow until 2035-2040 (DAVIES and SIMMONS, 2021).

1.3 BACKGROUND OF THE STUDY

By the end of the 2010s, approximately 65-75% of the world's total oil and gas production originated from mature fields, which, combined with the desire for reduced unit prices, put pressure on operators to allocate increased efforts to these elements of their portfolios (O'BRIEN et al., 2016; LUPU, 2019; GAFFNEYCLINE, 2020).

Usually, these fields have decades of production history, and a vast amount of data, but consist of a wide vintage and quality range, which makes redevelopment and optimisation planning challenging (VOLZ et al., 2008). On the other hand, the risks of a green field are principally mitigated or even eliminated, the surface facilities are in-place and there is an understanding of the subsurface. The latter usually requires an upgrade or, in some cases, total reconsideration, especially with regard to preparatory work of advanced exploitation technology deployment or piloting (PARSHALL, 2012; NEMES et al., 2021).

Due to the interrelated reasons of slower than anticipated economic growth in China, Russia, India and Brazil, coupled with the upturn in unconventional's exploitation in the US and Canada, crude oil prices dropped significantly in mid-2014 (TARVER, 2015; KRAUSS, 2017; DEPERSIO, 2019). Brent levels, peaking above $110/bbl in the beginning of 2014, plummeted to below $30/bbl, and in time stabilised at around $50/bbl (Figure 5) (CAMPBELL, 2017; REDDEN and STRICKLAND, 2017).

The unconventional (or shale) boom in the United States has had a significant balancing effect on oil prices since the mid-2010s. The technology is becoming cheaper; hence, break-even oil prices are lower. In addition, the drilling and operation of the fields is scalable on some level, providing needed flexibility in a volatile market environment (NEMES et al., 2021).

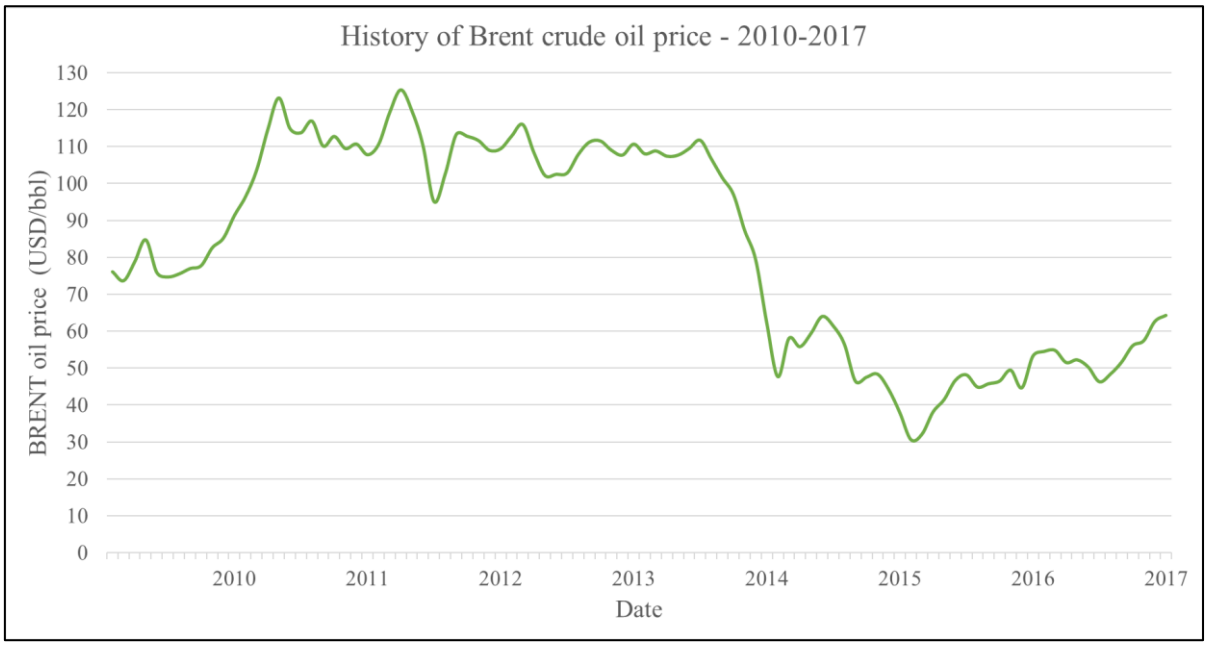

Figure 5: Brent oil price changes between 2010Q1 and 2017Q4. The three-year plateau of 100+ USD/bbl ended abruptly in 2013-2014, leading the industry into a new era of prices and factors, balancing the market both on the supply and demand sides (Source of data: https://www.eia.gov/ – 18-04-2020).

The oil price drop had a significant negative impact on the global oil industry, serving as a kind of wake-up call, but it also triggered unprecedented improvements in cost reduction and optimisation efforts. Cost cutting actions were initiated, portfolio optimisation processes started, started, medium- and high-risk investment projects were suspended for reconsideration, and, unfortunately, tens of thousands of employees were laid off (BOWLER, 2015).

In addition, many painfully learned that errors and overestimations can be overshadowed by high oil prices, but the range for tolerance shrinks significantly in a low oil-price environment. Statistical analyses of multiple projects all over the globe and from several companies have shown that planned and realised results were usually overly optimistic during a period of high oil prices (NANDURIKAR and WALLACE, 2011; NANDURIKAR and KIRKHAM, 2012). The mentioned authors reviewed 150 major capital projects, which showed that they delivered on, on average, only 75% of the forecasts approved at the time of project sanction. Those projects having subsurface issues delivered at even lower rate, at only 55% of the forecasted volumes. Therefore, regular post-evaluations and revisits are advised (they are essentially unavoidable) to develop the tools, applied methods and human capital. A related study was published by MEDDAUGH in 2015, offering different resolutions for the above-mentioned phenomenon, including model sizing, well location identification workflows, sparse data handling and other aspects.

It was compelling for or the upstream departments of oil companies to adjust their strategies to the new macro-environment and revisit mature assets that can yield incremental production with reduced investment (NEMES et al., 2021).

The redevelopment costs of the mature elements of a portfolio can be comparable to (but are usually significantly lower than) exploration costs, but the risk is definitely lower, and tools and methods successful for a given type of reservoir can be transferred to similar items in the portfolio (PARSHALL, 2012; MCCOMB, 2013). Similar processes started worldwide (O'BRIEN et al., 2016), a few examples of which were in the Russian Federation (GOLOVATSKIY et al., 2015; ZOZULYA et al., 2016), India (SARKAR et al., 2015; TIWARI et al., 2015), Indonesia (WASKITO et al., 2015), Malaysia (NG et al., 2016), Australia (MANTOPOULOS et al., 2015), Egypt (EL-BAGOURY et al., 2017), China (RAJPUT et al., 2015) and many others.

The approach chosen by MOL Group was not unique but was in line with international trends toward optimising existing portfolios preceding inorganic growth. This method made it possible to strengthen the portfolio so that it can resist low-price periods due to the low unit costs of production per barrel.

This strategy accelerated the urgent need for a thorough reevaluation of Field A's potential in terms of hydrocarbon and further development. Since, historically, a different approach was normally followed – namely, the supervision of subsurface evaluations and planning conducted by local institutes (i.e., service companies) – the task was complex and highly challenging (NEMES et al., 2021).

1.3.1 OBJECTIVES OF THE STUDY

Naturally, the goals of this thesis are mostly in line with the original scope of work (SoW), which depicted the goals and deliverables of the project's geomodelling stage. However, there are several points that do not strictly belong to the initial scope of work and were added to test ideas.

The objectives of the work summarised in the thesis are as follows:

I. Establish a single quality-checked, standardised database for both static and dynamic subsurface data.
II. Drive a better understanding of the current and past events related to the field that can aid in the future planning of data acquisition.
III. Build an up-to-date 3D geological model to serve multiple purposes.
    a. Serve as a daily tool for reservoir management.
    b. Serve as a tool for data visualisation in one, two and three dimensions.
    c. Serve as a tool for mid- and long-term field development planning, including water injection pattern optimisation, in-fill well drilling placement and upside oil potential identification.

d. Be a direct input to flow simulation modelling.
e. Be the basis, from a geological perspective, of updated field development plan documentation.
f. Reestimate initial in-place volumes and its spatial distribution based on newly available data gathered since the last modelling exercise.

IV. Build a full cycle geomodelling workflow in Petrel to make regular updates faster and smoother.

V. Prove that a complete geomodelling workflow can be built which is capable of automatising routine updates in the geomodel.

VI. Make the continuously current model shareable with business partners and third parties, if necessary.

VII. Introduce the practical implications the executed work can have on field development.

VIII. Highlight opportunities and risks associated with the area of interest and recommend a way forward.

2 GEOLOGICAL BACKGROUND

Field A is an onshore oil field located in the central part of the Volga-Ural Basin, south of the South Tatar Arch and the Romashkinskoe oil field (Figure 6 and Appendix II). It is geographically situated in the southern part of the Russian Federation, 400 kilometres north of Kazakhstan on the border of the Orenburg and Samara regions. The geology of the offset Kazakh fields was analysed in detail by HUVAZ et al. (2007).

Figure 6: A schematic index map indicating the area of interest within the Russian Federation (after SZILÁGYI et al., 2021)

2.1 REGIONAL GEOLOGY AND TECTONIC SETTING

The regional geology and tectonic setting description is mainly based on the overviews compiled by SZILÁGYI et al. (2021) and NEMES et al. (2021). A global overview and detailed correlation of relevant stratigraphic units from Eastern Europe to North America is given by MENNING et al. (2006).

The main structural features of the Volga-Ural Basin have been affected by several structural stages in which many arches and local uplifts (for instance, the Volga-Ural anticline itself), depressions and grabens were formed (Appendix II). Despite later deformations, the basement surface bears the marks of most of the further tectonic movements, except for the younger uncompensated sedimentary troughs and reef buildups (PETERSON and CLARKE, 1983a). The basement of the area consists of Precambrian crystalline rocks deepening toward the Precaspian Basin and the Ural Mountains to the east (Appendix II).

The geological history of the Volga-Ural Basin can be divided into a number of major events. The Silurian was a period of oceanic rifting, and then a tectonic reorganisation changed plate motions and the whole area endured compression in the Lower Devonian (ZONENSHAIN

et al., 1984). The stress regime became extensional again in the Middle Devonian when troughs formed in the interior of the plate.

The Kazakhstan plate and other fragments started to move towards the Russian plate, resulting in an overall compressional setting in the Permo-Triassic (ZONENSHAIN et al., 1984). The Urals fold belt started to elevate as part of the converging motions at this time. The compression rejuvenated itself later in the Cenozoic Era (SZILÁGYI et al., 2021).

The following is a summary of the structural development of the region: The structures of the area are related to six distinct episodes of tectonic activity in the basin (Volga-Ural Basin report, IHS). The events resulted in Riphean-Vendian rift structures, Late Cambrian-Silurian passive margin structures due to the development of the Ural Ocean, Early Devonian compressive structures related to the Caledonian Orogeny, Middle Devonian-Mid Carboniferous rift structures, Late Carbonferous-Triassic Uralian compressive structures connected to the foreland basin formation of the Ural Mountain Belt and Oligocene, and recent compressive structures due to the late reactivation of thrusts and faults (NEMES et al., 2021).

In addition, GOLOV et al. (2000) divided the tectonic evolution into three main stages: a Middle Devonian extension, a passive margin subsidence in the Upper Devonian through the Permian, and a tectonic inversion in the Permo-Triassic, which experienced rejuvenation later in the Cenozoic Era.

Most of the Soviet authors agreed that in the Volga-Ural region, tectonic development played a major role in hydrocarbon accumulation and trapping. A further detailed tectonic and structural scheme of the Volga-Ural anticline and region was provided by SMIRNOV (1958), GUSEVA et al. (1975), ONAKO (1997) and KOLCHUGIN et al. (2014).

As a result of the intensive drilling activity throughout the decades of exploration of and production in the Volga-Ural Petroleum Province, its deep structural elements and tectonic features are relatively well known. Included amongst them are the Sernovodsko-Abdulino graben to the south and the Kazansko-Kirov-South graben to the west surrounding the study area (Appendix II).

2.2 PETROLEUM GEOLOGY

Four major sedimentary sequences are usually disclosed in the literature of the Volga-Ural Basin. These are the Eifelian-Tournaisian, Visean-Bashkirian, Moscovian-Artinskian and above the Kungurian in the Paleozoic. Each of them may be further subdivided into shorter-term sequences that correspond to relative sea level changes (PETERSON and CLARKE, 1983a). In Field A the primary hydrocarbon-bearing reservoirs are the Carboniferous-age Tournaisian (V1), Bobrikovian (Bb), Serpukhovian (C1s) and Bashkirian (A4) formations (Appendix II). A

semi-quantified potential can be also linked to the Devonian formations, as well as to the Carboniferous Verejskij Formation overlying the Bashkirian.

In the middle Frasnian, the Domanik Formation began to form. The Domanik Formation – characterised by high generation potential – later served as source rock (FADEEVA et al., 2015; PETERSON and CLARKE, 1983a; KISELEVA et al., 2017). The Domanik layers are a restricted marine, relatively deep-water, dark grey and black bituminous shale, marl, and argillaceous limestone facies, rich in organic matter, and are believed to be the main source rock in the Volga-Ural Basin (PETERSON and CLARKE, 1983a; BAZHENOVA, 2009). The Domanik Formation can also be a target for shale oil exploitation in the near future in the region (GABNASYROV et al., 2016; MUKHAMETDINOVA et al., 2020).

Carbonate deposition increased markedly during the Famennian age, and reef and organic carbonate deposits covered most of the Volga-Ural province at this time (Appendix II) and continued with no evidence of disconformity into the Tournaisian age, which was the period of regional carbonate deposition (GOLOV et al., 2000).

The general emergence of the Russian platform occurred following the deposition of Tournaisian reefal and other carbonates. A cyclic transgressive-regressive marine deposition took place following Tournaisian, producing a thick interfingering nearshore deltaic-interdeltaic marine and continental-coastal clastic sequence, which had a major effect on the distribution of the petroleum reservoir sediments and source rocks of the Volga-Ural Petroleum Province (PETERSON and CLARKE, 1983a). The deposition of clastic sediments in the Visean age completed the filling of the troughs. The major source area for Visean clastics was the Baltic Shield to the northwest.

The carbonate deposition of the Tournaisian ended suddenly and was replaced by siliciclastics in the Lower Visean, at the Bobrikovian Stage. A detailed overview regarding the Carboniferous hydrocarbon production of the Eastern Hemisphere was given by MEYERHOFF (1984), in which the relationship of tectonics and the oil and gas potential of the Volga-Ural Region can be seen in a broader context compared to other basins. The author emphasised that the most important Carboniferous producing unit in the Volga-Ural Basin is the Visean, which contains the Bobrikovian and Tulsky zones. In this evaluation the Malinov Formation – which is part of the Lower Visean Malinov–Bobrikovian horizon and fills the Kama-Kinel depression in the Volga-Ural Basin over several hundreds of metres – is treated as part of the Bobrikovian Formation.

Visean clastics transform upward to marine carbonate and shale units and finally to the widespread fossiliferous marine carbonate beds of the Namurian (i.e., Serpukhovian –

Appendix II) and Bashkirian ages that covered the entire platform (PETERSON and CLARKE, 1983b).

The rocks of the Serpukhovian age are marine limestone and dolomite; some are interbedded thin grey shale beds. Evidence exists of brief emergence and some erosion, and karstification in parts of the province at the close of the Serpukhovian deposition is present in Field A as well (PETERSON and CLARKE, 1983a).

The rocks of the Bashkirian age are made up of fossiliferous dolomite and limestone. The Bashkirian carbonates are highly fossiliferous with abundant shell debris, foraminifera and algae. Regional emergence of the platform occurred at the close of the Bashkirian deposition. Leaching and karstification of the Bashkirian carbonates occurred at this time, which is considered to be a major element in the reservoir's development (PETERSON and CLARKE, 1983a).

The seal rocks in the region are mainly shales and argillaceous limestones, like the Verejskij Formation deposited on top of the Bashkirian Formation, with alternating silty and calcareous shales, muddy and calcareous sandstones and siltstones in the north of the Tatar Arch (Appendix II) (HUVAZ et al., 2007).

The trapping mechanism in the field is complex; three-way closure is provided by anticline shape and oil-water contact, but in the east the field is bounded by a strike-strip fault.

A detailed tectonic scheme and stratigraphic features of the Orenburg region was given by SUHAREVICH et al. (1975), SHUDOVA (1975), TRAVINA (1975) and SELEZNEVA (2016), amongst others.

2.3 RESERVOIR ROCKS

There are four key reservoir formations in Field A which are of primary importance in the current study (possible additional reservoirs may also occur, although they are not well-appraised). The four formations from the deepest to the shallowest are the Tournaisian (V1) and Bobrikovian (Bb) (i.e., the lower reservoirs) and the Serpukhovian (C1s) and Bashkirian (A4) (i.e., the upper reservoirs) (Appendix II).

In the case of the Tournaisian Formation (V1) (Figure 7), based on the shape and size of peloids, a moderately agitated environment (behind the ooidal/bioclastic shoal) is presumed. It has a shallow water shelf with normal benthic fauna. Lithologically, it is mainly limestone, characterised by vuggy porosity (NEMES et al., 2021). In Field A it is the main reservoir both in terms of in-place and recoverable volumes.

Figure 7: A core section from the Tournaisian Formation from well No. 1xxx (1251-1253m MD RKB), containing porous limestone from white to grey with uneven oil infusion throughout the interval.

The strata separating the Tournaisian and Bobrikovian Formations is the Malinov Shale (or Malinov superhorizon). It starts with dark grey thin bedded shales and claystones with pyrite crystals, deposited in anoxic conditions and relatively deep-water environments (ULMISHEK, 1988). In Field A the Malinov superhorizon was detected and observed in several wells during core investigations. The appearance is dark grey almost-black-coloured thin-bedded shales containing a significant amount of pyrite crystals, which means a fairly good marker for log correlations as well.

Figure 8: A core section from the Bobrikovian Formation from well No. 1xxx (1263-1265 m MD RKB). The sandstone is dark grey – light brown, fine-grained, weakly-cemented, with signs of hydrocarbons. Siltstone is of a dark grey to black colour with weak signs of hydrocarbons. Mudstones are black, dark grey and brittle. The vertical heterogeneity is also reflected in reservoir performance, together with the lateral alterations of different facies.

In Field A the interpreted depositional environment for the Lower Visean Bobrikovian Formation (Bb) (Figure 8) is a nearshore-coastal environment which is located in the broad shallow shelf of the Volga-Ural Basin. Barrier islands were deposited that enclosed the lagoons and estuaries. Tidal deltas, including flood tidal and ebb tidal deltas with tidal channels and bayhead delta sediments were deposited in and in front of the lagoon series. The Bobrikovian Formation is described as an overall transgressive-regressive succession in a nearshore-tidal environment by SZILÁGYI et al. (2021). Transgressive lagoon-estuary and barrier island facies in the lower section turned to regressional lagoon fill-type settings in the upper one.

The pore volume is provided by matrix porosity, which shows that high heterogeneity among different facies, sandstone, siltstone, and shale layers comprise the formation. The high heterogeneity has a significant effect on the productivity of wells perforated to the formation; daily total fluid production ranges from 1-2 m^3 to 60-80 m^3 of gross liquid.

The Serpukhovian (C1s) (Figure 9) Formation is built of marine limestones with a significant imprint of diagenetic dolomitisation. Brief emergence and erosion occurred at the end of the Serpukhovian age, hence, karstification affected the rocks, resulting in vuggy pores and paleokarstic features (NEMES et al., 2021).

Figure 9: A core section from the Serpukhovian Formation from well No. 1xxx (883-885 m MD RKB). White dolomite with strong fracturing and cavernousness observed along section. The upper part of the layer is marked by abundant oil shows, although in the lower part of the layer they become insignificant and are confined to vugs and caverns.

Based on fossil assemblage, a shallow marine, well-circulated environment is suggested for the Bashkirian Formation (A4) (Figure 10). Based on the shape and size of the peloids, a moderately agitated environment (around the ooidal) and an open marine and inner ramp are presumed based on the available information. The most characteristic pore type is vuggy porosity, supplemented by intrafossil pores, showing an average pore size larger than that of the Tournaisian Formation. Lithologically, it is mainly limestone with subordinate dolomite, with a high degree of heterogeneity generated due to diagenetic processes (NEMES et al., 2021).

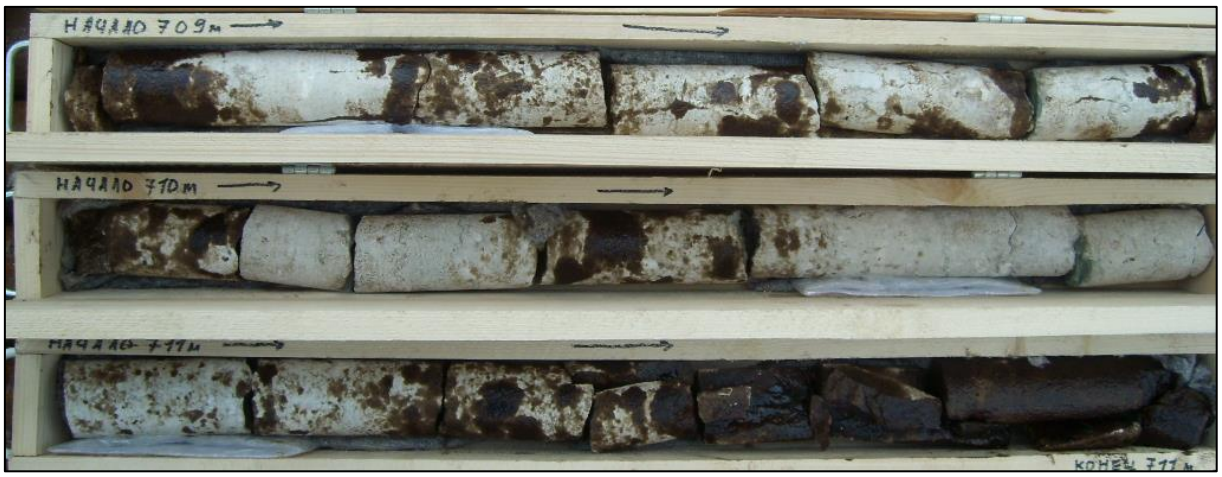

Figure 10: A core section from the Bashkirian Formation from well No. 8xx (709-711 m MD RKB). The vertical heterogeneity is reflected in the abrupt changes to the oil-bearing and tight intervals of the core sample.

Subaerial exposure of carbonates occurred at the end of the Tournaisian, Serpukhovian and Bashkirian. These events induced the karstification and formation of dissolution features in the limestones. The most wide-spread and significant karstification effect is present in the Serpukhovian Formation, with a moderate effect in the Bashkirian Formation and a negligible one in the Tournaisian (NEMES et al., 2021).

3 FIELD HISTORY

As mentioned earlier, by the end of the 2010s approximately 75-80% of the world's total oil production was originating from mature fields (O'BRIEN et al., 2016). Field A is one of the numerous mature fields in Eastern Europe worth considering for reassessment and consecutive redevelopment or production optimisation.

The Volga-Ural basin, with its acreage of approximately 700,000 km^2, is the second-most-prolific HC region in the Russian Federation – after Western Siberia – spreading from the Urals geosyncline in the east to the Volga River and Russian platform in the west and the Caspian Basin at the south (PARFENOV et al., 2008; MEYERHOFF, 1984; VERMA et al., 2000) (Appendix II).

A detailed resume of the oil and gas industry in the Volga-Ural Petroleum Province's two historical centres – Tatarstan and Bashkortostan – was given by KONTOROVIC et al. in 2016. The early exploration activities and geological surveys had been conducted in the second half of the 18th century thanks to the expeditions of academic scientists. The first occasional oil inflow was obtained in 1929 during exploration for potash near the village of Verkhne-Chusovskie Gorodki (KONTOROVIC and LIVSHITS, 2017).

The neighbouring Orenburg (and Samara) oil regions, where Field A is situated, are of the oldest in the Russian Federation; the first discoveries were made in the 1930s. By now the huge and easy-to-recover deposits are at a mature or nearly depleted stage, and new cutting-edge technologies are needed to continue exploitation and extend field lifetime (SHAKIROV et al., 2015; FADEEVA et al., 2015).

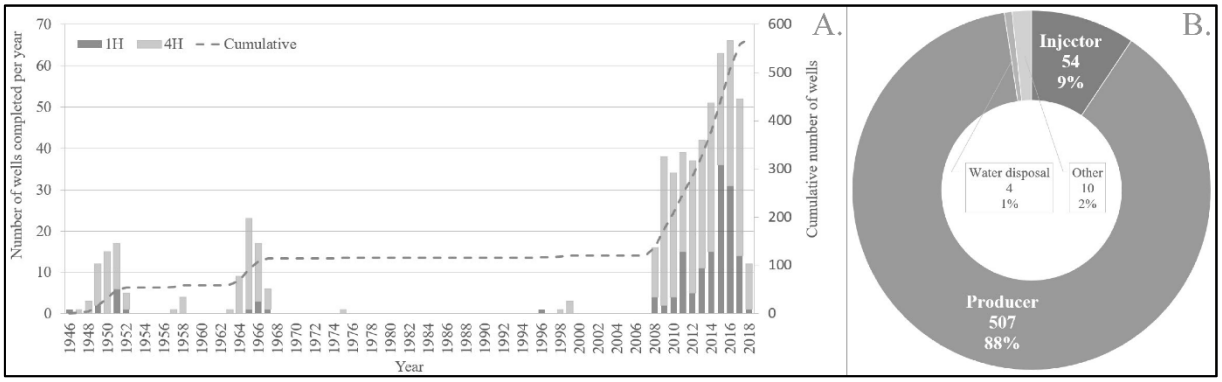

Figure 11: Panel A: A stacked diagram illustrating the number of wells drilled annually in Field A; the dashed line shows the cumulative well number for the same period, which reached 571 wells by 2018Q2. 1H and 4H labels form a distinction between shallow (TD<850 m TVDSS) and deep (TD≥850 m TVDSS) wells, respectively. The lack of drilling activity from 1967 to 2008 should be noted. Panel B: The breakdown of well types as of 2018Q2; the total number of wells is 575, and the delta of the four wells are old, plugged and abandoned unclear ownership drillings (2018 represents only a partial year in the chart). Not all of the existing wells are active; approximately 10% are plugged and abandoned, and ~5% of the wells are temporarily closed due to various technical, environmental or safety reasons.

The field was discovered in 1947 and came on production in 1949. However, an intensive drilling campaign started only after 2007 when the actual operator farmed-in, gaining

100% equity. Since 2007, 40-70 wells have been drilled per year (Figure 11A), providing a significant amount of data and a ramping up of the daily production (Figure 12). The total number of wells drilled in the field is more than 550 wells (Figure 11B).

The total cumulative oil produced as of 2020-03-01 was almost 13 million m^3 (~82 mmbbl), as shown in Figure 12. But the actual recovery factor is only around 10–14% (depending on STOIIP case), providing room for detailed investigation to optimise development strategy through the identification of new opportunities and adjustments in the subsurface and surface elements of the production system. Based on analogous fields and calculations, the expected final recovery in similar reservoirs could be between 25-35%, or even higher with modern secondary and tertiary methods (PÁPAY, 2003).

In Field A there has been active water injection to support pressure maintenance since the mid-1960s. Cumulatively, at the field level, a similar amount of water has been injected as oil produced. (Figure 12).

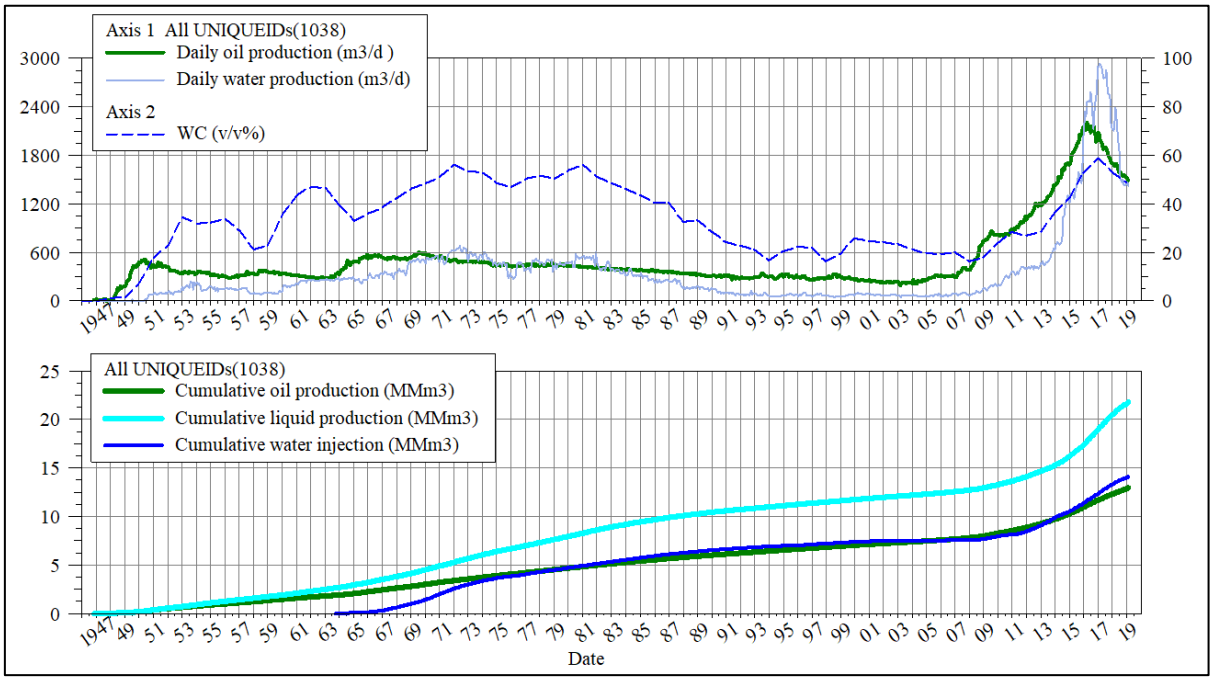

Figure 12: Field-level production parameters are shown in the figure. The accelerated drilling campaign initiated in 2007 had a significant impact on production ramp-up; the water production shows a strong correlation with oil production, in absolute terms, and water-cut (WC) increasing over time should be noted (data is aggregated for 1,038 completion events from 1947 to 2020Q1). (Upper graph: left axis: daily oil and water production (m^3/d); right axis: WC(v/v%); lower graph: cumulative liquid and oil production and cumulative water injection (MMm^3.)

As described in the *Geological background* chapter, there are four productive formations, Tournaisian and Bobrikovian being the deeper horizons at a depth of approximately 900-1000m TVDSS, often produced with commingled wells. The shallow formations, Serpukhovian and Bashkirian, are also often produced with commingled completions; their respective depths are around 500-600m TVDSS (Figure 13). Above the Bashkirian Formation

lies the Verejskij Formation, which can have oil saturation in thin reservoir layers also., though to date this has not been investigated in detail.

The deep reservoirs are most probably hydraulically separated by the Malinov shale layer, with true vertical thickness (TVT) varying between 0.5 and 6 metres and averaging 1.2 metres. The shallow reservoirs can also be partially separated by a high-shale content layer – named Flowbarrier – which is a baffle zone in the flow model (Figure 13). Appendix III shows an example of the depth horizons to illustrate the structural delineation of the AOI. The elevation of the terrain varies between 160 and 340 metres, with an average of 275 metres (Appendix IV).

All of the reservoirs are undersaturated oil reservoirs (hence, no primary gas cap exists), with medium-type black oil having an API gravity of 25-27°. The prevailing driving mechanism is weak to moderate aquifer drive and depletion. The dissolved gas content is low (5–40 m^3/m^3), and therefore plays an ancillary role as a driving mechanism.

The initial reservoir pressures are approximately hydrostatic (~70 bars in the shallow and ~110 bars in the deep reservoirs), while the initial reservoir temperatures are rather low (~20°C in the shallow and ~26°C in the lower reservoirs).

Further parameters and details regarding the geological and dynamic properties of the reservoirs can be seen in Appendix IX.

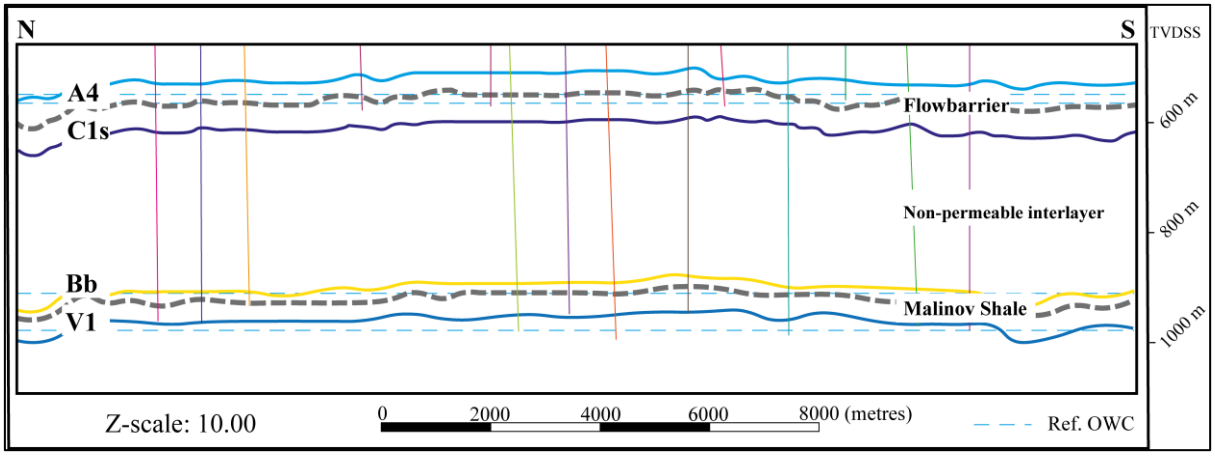

Figure 13: A schematic N-S cross-section of Field A with the stratigraphic framework. Bobrikovian (Bb) and Serpukhovian (C1s) layers are separated from each other by several hundreds of metres of impermeable layers, hence, hydrodynamic communication in the AOI can be ruled out (source: NEMES et al., 2021). The A4 and C1s formations are the upper formation group, with Bb and V1 being the lower (Z-scale=10.00). The vertical lines represent wells projected to the cross-section's pane. The shorter wells are 1H, and the deeper ones reaching at least to the Bobrikovian Formation's top are 4H. The horizontal dashed lines represent the individual initial oil-water contacts (OWC_i) as identified from the well tests in the early life of the field.

4 CONCEPT OF RESERVOIR MODELLING

4.1 INTRODUCTION TO MODELLING

Modelling, as a tool, is applied in a widespread manner in a myriad of sciences, for example, from physics to biology or from finance to meteorology. The most ambitious models describe global weather and climate change DNA, the inheritance model first described by Gregor Mendel, the evolution of the universe since the Big Bang, or the human brain with all of its neural connections, called a connectome (HORN et al., 2014).

The underlying logic is very similar within all models: we determine the possible drivers behind an observed phenomenon; we set up a set of parameters with supposed interactions and rules or laws that are meant to describe the experience; we measure the outputs of the model and validate them against reality; and then we iterate, adjust and restructure until we have a satisfactory modelling result that meets the success criteria against measured reality. At this step the model has the ability to forecast the future based on the past with a given level of uncertainty; this uncertainty gradually increases with distance from the measured realm. Accordingly, models continuously change as new data and understanding become available, or the goodness of the current model no longer meets its predefined purpose.

4.2 INTRODUCTION TO RESERVOIR MODELLING

In these terms a hydrocarbon reservoir model is a consistent representation of all the data and knowledge about a reservoir at a given moment in time relevant to the management and development of the reservoir. In some cases this representation is complex, and sometimes it is simple; the ultimate goal is to fulfil the purpose of its creation. In simple terms a geomodel is meant to describe the size and shape of the reservoir, that is, to place the reservoir in space while its pair, the dynamic model, adds time, fluid movements and pressure to the system. A model must not be a tool to verify prematurely- or partially-made decisions, but should be a tool to eliminate biases and represent the range of possible outcomes. (PYRCZ et al., 2014).

3D reservoir modelling is now the norm, and numerous conventional and unconventional oil and gas fields worldwide are developed each year with the use of reservoir models to determine in-place and recoverable resources and to help predict the expected flow of hydrocarbons and, hence, to identify optimal field development strategy or production optimisation opportunities (Carbonate reservoir modelling in Oman: ABBASZADEH et al., 2000; fast models from Norway: HOLLUND et al., 2005; a case study from Kazakhstan: DEHGHANI et al., 2008; gas hydrates from Japan: AUNG et al., 2011; mature field review: MARTINO et al., 2012; a comprehensive overview of reservoir modelling given by PYRCZ et al., 2014; a giant

field's integrated reservoir study from Kazakhstan: ALBERTINI et al., 2014; a modelling case study from Australia: MANTOPOULOS et al., 2015; a karstic case study from Thailand: LURPROMMAS et al., 2016; a case study from Oman: BELLMANN, 2018; a giant fractured reservoir: SPAGNUOLO et al., 2018; a heavy oil field from Turkey: KAMANLI, 2019; a CO2-storage investigation from Vietnam: VO THANH et al., 2019; a study from West-Siberia: BLOTSKAYA et SARDAROV, 2020; a carbonate reservoir's case study from Egypt: CORLETT et al., 2021).

Although high expectations have been created with the explosion of reservoir modelling software packages and associated geostatistical methods, these packages and methods have also led to regular disappointments in terms of the reservoir modeller's ability to predict reservoir performance. This has given birth to the often-quoted mantra "all models are wrong". In fact, all models are not wrong, but in many cases, models are used to answer questions which they were not designed to answer (RINGROSE and BENTLEY, 2015). (It must also be noted that new data-driven methods are spreading worldwide in diverse industries, including all the branches of the energy sector as well; a good overview of the current status in various areas of the petroleum industry is given by BALAJI et al., 2018, though according to Michael Pyrcz and many others: *"Energy has been big data long before tech learned about big data."*)

What constitutes good design? The core of a good design is simply that it fulfils a specific purpose, so is fit for purpose. "*There is always a balance between probability (the outcomes of stochastic processes) and determinism (outcomes controlled by limiting conditions). We develop the argument that deterministic controls rooted in an understanding of geological processes are the key to good model design. The use of probabilistic methods in reservoir modelling without these geological controls is a poor basis for decision making, whereas an intelligent balance between determinism and probability offers a path to model designs that can lead to good decisions*" (RINGROSE and BENTLEY, 2015).

The principle of parsimony is a good guidance, as it is empirically and statistically proven that the best explanation of a given phenomenon is generally the simplest, the one with the fewest assumptions (SEASHOLTZ and KOWALSKI, 1993; EL-KOUJUK et al., 2011). This is also true for reservoir models; at least in the beginning the model should be simple, interpretable and transparent. Each additional dimension or level of complexity should be tested to determine if it really delivers added value or decreased uncertainty.

The main disciplines involved in this interdisciplinary work are geophysics, petrophysics, fluid and core laboratories, sedimentology, geology, reservoir geology, reservoir engineering, drilling, completions and well testing. The undoubtable advantages of multidisciplinary project teams have been proven worldwide in numerous conventional and

unconventional projects, and nowadays no major projects are initiated without the integration of a wide array of disciplines (RINGROSE and BENTLEY, 2015; BAILLIE et al., 1996; CAMPOBASSO et al., 2005; OKUYIGA et al., 2007; GALINDO et al., 2012; SARKAR et al., 2015; LUKMANOV and IBRAHIM, 2018; NEMES et al., 2021). Data governance and database maintenance are usually provided by a data management department (DAVID et al., 2017; AKOUM AND HAZZAA, 2019; NEMES et al., 2021; SANASI et al., 2021), which is becoming paramount in importance with the exponential growth of available data and the spread of machine learning and deep learning methods.

Although the objective is not for each reservoir discipline to maximise its contribution to the final product, the challenge is rather for each discipline to understand the specific forecasting goal and provide the relevant information in a usable format with an assessment of the uncertainty (JOURNEL, 1995).

Since real hard data at the correct scale are scarce (due to the expenses/technical difficulties), the biggest challenge in reservoir modelling is data integration. Relevant data and information originate from various sources at various scales with varying degrees of reliability. For example, geological data originates at many scales, from the microscopic image of a pore volume to the basin-scale interpretation of a depositional system; geophysical (seismic) data, often the most prevalent, span from the macroscale of well logs to the scale of the entire field (JOURNEL, 1995).

Because data originate from such a variety of sources and at many scales, and because their relevance to the final goal of reservoir performance forecasting is not always clear before the fact, all data must be calibrated, and the uncertainty of their information content assessed. Calibration means that some data are considered reference or ‘hard’ (e.g. well tops, well trajectory), whereas other ‘soft’ (e.g. fault planes) data are calibrated against them. Hard data are usually honoured explicitly by the numerical model. Soft data need not be honoured as precisely; the degree to which they are honoured depends on an assessment of their reliability. In many instances, however, there are not enough data to perform numerical calibration; in these cases, calibration may be borrowed from another field, or from an outcrop, i.e., analogues (JOURNEL, 1995).

In line with PYRCZ AND DEUTSCH (2014), a 3D reservoir model’s key benefits are:

- data transfer between disciplines;
- reconciliation and integration of large amounts and scales of data;
- calculation of in-place hydrocarbon volumes and related spatial and administrative distribution (e.g., different owners, states, counties);
- illustration of 3D spatial connectivity of reservoir layers;

- serving as a tool to focus attention on critical unknowns and risk;
- a geostatistical and visual representation of spatial variations that may enhance or work against a particular production strategy (e.g., well placement, well types, injection strategy and timing);
- serving as a key input for flow modelling and production forecasting and, hence, providing a basis for business decisions (Figure 18).

A partly hidden layer of the modelling job is its underlying psychological effect, similar to talking or writing; that is, it helps to structure thoughts and ideas and knowledge and information, to separate deadends from viable options, and to highlight critical elements while relegating insignificant details. In the case of Field A, it had a vast effect on the next steps in terms of highlighting data and knowledge gaps and inconsistencies and contradictions to be resolved (NEMES et al., 2021).

Modern reservoir models are usually built in 3-dimensional modelling software programmes such as Emerson's RMS, Schlumberger's Petrel, Rock Flow Dynamics's tNavigator or Baker Hughes's JewelSuite, and the fourth dimension – (production) time – is added by the reservoir simulator (like Emerson's Tempest, Schlumberger's Eclipse or Intersect, Rock Flow Dynamics's tNavigator). It is worth noting that beyond on-prem solutions, all the major players in the software market are starting to offer fully cloud-based solutions with fundamentally different licensing and hardware frameworks (e.g., Schlumberger's Delfi Environment).

As described above, a good model is fit-for-purpose, therefore, the purpose needs to be defined upfront, prior to the initiation of the modelling workflow, and aligned amongst interested parties so that expectations can be managed.

According to RINGROSE and BENTLEY (2015), the purpose of a reservoir model can vary greatly from project to project, and some items overlap while others mutually exclude each other. The prerequisites and necessary level of details and resolution alters from type-to-type, along with the time and data needed to create it. (Hence, the expectations about the outputs will also vary accordingly.) The most common possible purposes of a 3D model are listed as follows (after RINGROSE and BENTLEY, 2015):

I. The 'model' is a data repository.
    a. In this case a field model is not constructed, but the corresponding field data is collected, cleaned and structured in a 'Reference Project'. It serves as a source of data, and can usually be modified only by a limited number of experts.

II. The model is a 3D digital representation of the reservoir (or a sector of the reservoir). The subtypes are as follows:
    a. Models for visualisation only (Figure 14).
        i. Simply to visualise the reservoir in 3D.
    b. Models for volume calculation.
        i. Define the spatial distribution of in-place volumes.
    c. Models as a front end to simulation.
        i. Most of the models fall into this category. Most static models are direct inputs to dynamic simulations.
    d. Models for well planning.
        i. The purpose of the modelling exercise is to assist in well planning and geosteering.
    e. Models for EOR/IOR.
        i. IOR schemes generally require very detailed models to give accurate answers and represent the uncertainty range.
    f. Models for storage.
        i. CO_2 (and natural gas) storage generally requires the assessment of quite large aquifer/reservoir volumes and the caprock system – presenting significant challenges for grid resolution and in terms of the level of detail required.

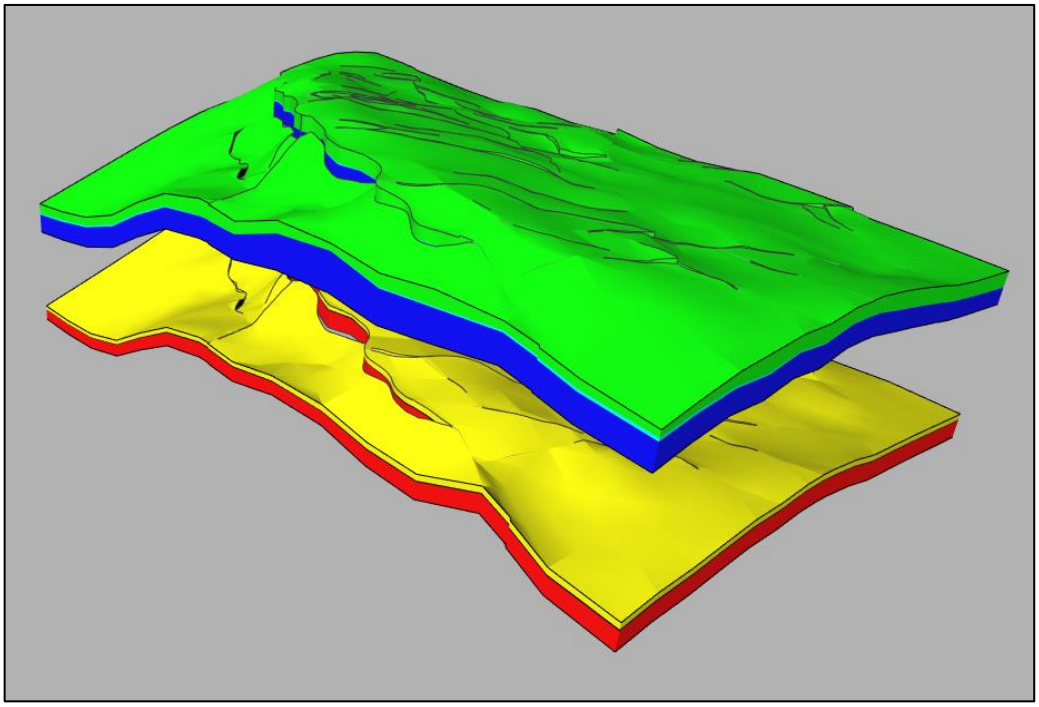

Figure 14: An example of II.a models, serving as visualisation only (from Field A's Phase 1 structural model). Green is Bashkirian, blue, Serpukhovian, yellow represents the Bobrikovian, while red is the Tournaisian reservoir (Z-scale=18.00).

It is best to abandon the notion of a single, all-knowing, all-purpose, full-field model, and replace this with the idea of flexible, faster models based on thoughtful model design, tailored to answer specific questions (RINGROSE and BENTLEY, 2015).

The key takeaway is that the models are representations of the observed and interpreted data and, consequently, always misrepresent reality; the question is to what extent. To put it simply, after RINGROSE and BENTLEY, 2015:

$$\text{data} \neq \text{model} \neq \text{truth}$$

After this general introduction to 3D reservoir modelling, the following chapters focus on Field A and the related modelling steps, with a special focus on workflow creation.

5 DISCUSSION OF THE FIRST PASS GEOLOGICAL MODEL (PHASE 1)

A quick 'first-pass' geological model (a.k.a., Phase 1) was built for Field A so that the business requirements and deadlines for 2016 could be met. The plan was to create a more sophisticated and detailed successor in 2017-2018, later called the 'main' model (a.k.a., Phase 2). As soon as the main model was finalised, the first-pass version was retired and not used for further analysis and planning. It was also planned that the Phase 2 model would mitigate the data and information gaps – where possible – revealed during Phase 1.

A comprehensive introduction to the first pass geological model is published in NEMES et al. (2021). A short(er) summary is given here to highlight the key steps and components.

5.1 SCOPE OF WORK

As described in the *Background of the study* subchapter, the update of the geomodel was a tiny element of a company-level strategy shift. To increase ownership of and insights into the assets of the portfolio, the bulk of the technical work – both surface and subsurface – was transferred in-house. Historically, a different approach was usually followed – namely, the supervision of subsurface evaluations and planning conducted by local institutes (i.e., service companies).

The main deliverable was an integrated, up-to-date and quality-checked 3D geomodel (and a corresponding dynamic model) that can be used for both the current state of the field (maps, initial and remaining volumetric potential, untapped areas, etc.) as well as the testing of different field redevelopment scenarios, such as the drilling of horizontal wells and the restructuring of the water injection well-pattern.

The main quantitative goal of Phase 1 modelling was to have a quick preliminary in-place volume calculation and compare it to the legacy data in order to be able to carry out a sense-check and a rough estimation of volume changes, both in terms of in-place volumes and remaining recoverable resources (NEMES et al., 2021).

5.2 WORKFLOW OF PHASE 1 MODEL

The Phase 1 model was initially built using Emerson's RMS 2013.1 software. Also, it is worth noting that the exact same workflow was repeated in Schlumberger's Petrel 2015.5 due to specific business requirements. There were only slight differences (~3%) in the outputs of the two software programmes. These differences mainly originated from stochastic deviations; all the differences were within a standard deviation of the given parameter (NEMES

et al., 2021), that is, in the case of Field A, there were not any definitive differences identified between the software programmes.

The vintage (the input dataset closing date) of the Phase 1 model is 2016-01-01; no later data was incorporated during the modelling process so that a consistent model could be realised which, once finalised, can be regularly updated, allowing frequent distractions to be avoided.

In order to meet the deliverables, first of all, a standardised, quality-checked and comprehensive subsurface database had to be constructed, and the dataset had to be reinterpreted to reach the goal of substantiating a well-established understanding of the field to translate its actual value into produced barrels (PEDERSON et al., 1998; PARSHALL, 2012).

A schematic overview of the Phase 1 general workflow applied in the 3D geological modelling indicating the main and direct inputs at the corresponding steps is depicted in Figure 15. The steps shown in the figure are explained in more detail in the following subchapters.

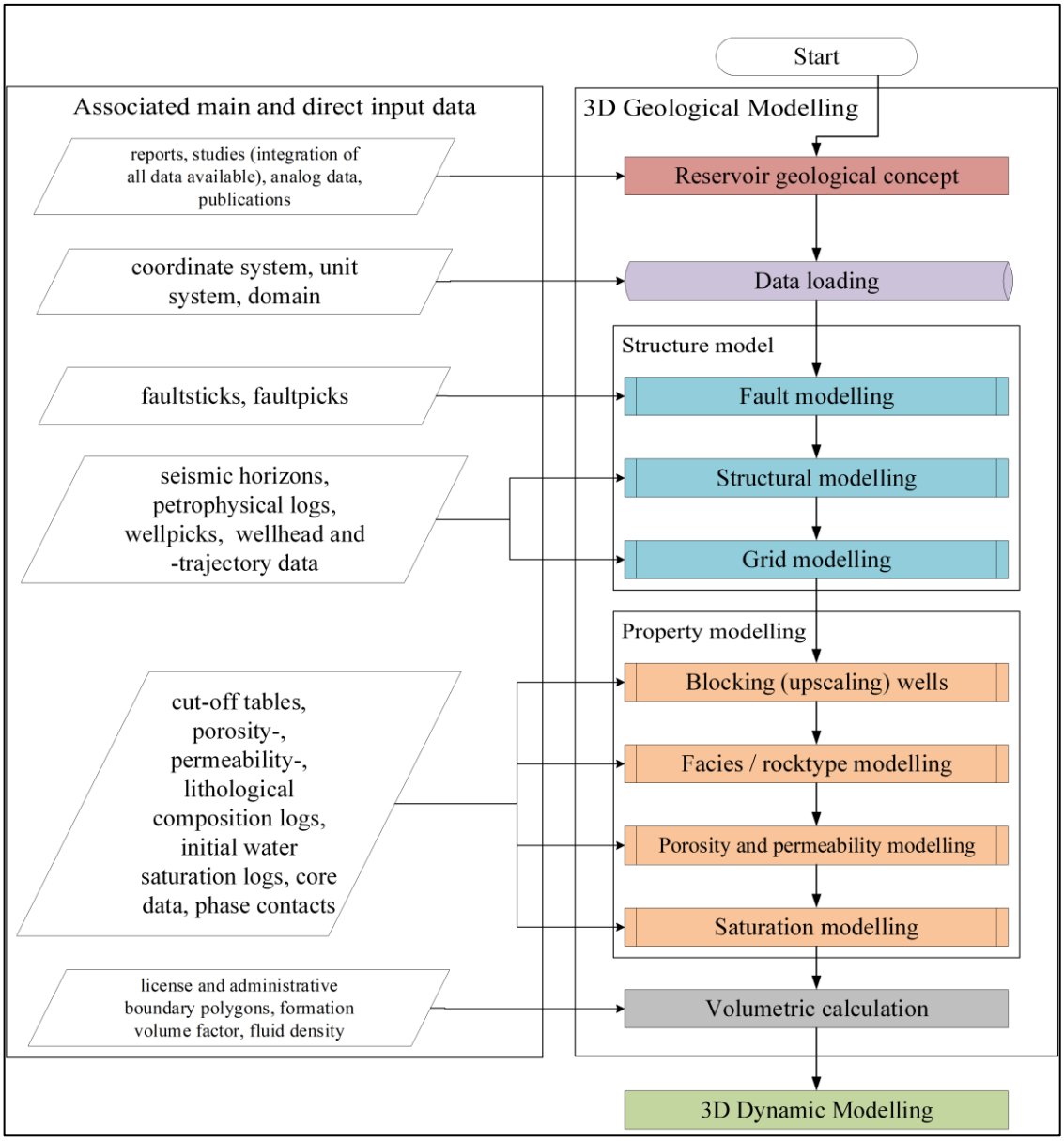

Figure 15: Main steps of a 3D geomodelling workflow on the right, and the key input parameters necessary to make the corresponding step. (It should be noted that the geomodel is only one element in the chain, and not a final product.)

5.2.1 STRUCTURAL MODEL (PHASE 1)

Field A has four productive formations: three carbonate (V1, C1s, A4) formations and one clastic (Bb) interval (Figure 13); all four were part of the 3D geological model. One single geological model was constructed, including the impermeable layer in between the upper and lower formations; in this way, during dynamic simulation, coupled field development options could be tested, and, also, possible cross-flow between the formations could be modelled, if necessary.

At the vintage of the geological model (2016-01-01), the wellstock consisted of 459 wells, of which 349 had measured (and digitised) trajectory data; 46 were only available in paper format, and 64 had no deviation survey at all (NEMES et al., 2021).

The main input parameters for the structural model were the interpreted seismic horizons (stratigraphic tops and bottoms in depth domain, similar to Appendix III) and faultsticks; the sub seismic intralayers were mapped using the well picks (also known as well tops). The total area of interest is covered by 3D seismic (acquired in the late 2000s) (Appendix IV), and the license area is densely populated with wells, hence, the structural interpretation uncertainty is confined.

Well pick filtering was inevitable due to the partial unreliability of the input data: in some cases the well trajectory was questionable; in others, the well log was possibly shifted or the interpretation was dubious. Therefore, after quality checking, the following number of well picks were used to tie the seismic horizons in depth to hard data (Table 1).

Table 1: Number of well picks used during Phase 1 structural modelling, and the average number per unit area (NEMES et al., 2021)

Horizon	Number of well picks (post-filter)	Average number of well picks per unit area (1/km^2)
A4 Top	350	5.3
Flowbarrier Top	325	4.9
C1s Top	319	4.9
C1s Bottom	279	4.2
Bb Top	314	4.8
Malinov Top	311	4.7
V1 Top	312	4.7
V1 Bottom	179	2.7

The initial oil-water contacts (OWC) were identified based on inflow test data. However, contradictions were revealed due to various reasons, for example, measurement quality, cement bond quality, log quality and/or the influence of injection or production in the

vicinity. Hence, initial phase contacts might pose an uncertainty among parameters, and the mitigation of this uncertainty is highly challenging (a case study for the Bashkirian Formation was made by KOLCHUGIN et al. in 2014).

The initial geomodel incorporated all the interpreted faults (~50), but during the iterations with the reservoir engineer the faults were removed as no evidence was identified for them having an impactful effect on the flow pattern of the reservoirs.

5.2.2 GRID MODEL (PHASE 1)

In line with the identified heterogeneity of the individual formations, the vertical resolution of the 3D grid was set to 1 meter in the carbonate reservoirs and 0.4 metres in the clastic. Laterally, the 3D grid was clipped with a predefined polygon to contain cell number in a controllable range. Naturally, the vertical resolution of the impermeable layer was set to fixed, namely, 1 cell.

The horizontal resolution was chosen to be 50 metres in the geological grid, and later it was upscaled for dynamic modelling to 100 metres. Gridding was set up taking into consideration the unconformity at the top of the Tournaisian and Serpukhovian formations, while stair-stepped fault handling was applied for dynamic modelling (NEMES et al., 2021). This technique results in a lower number of distorted cells compared to the alternative pillar fault modelling. The former is preferable for dynamic modelling in heavily tectonised areas where the faults play a key role in the flow pattern and/or segmentation of the reservoir.

The key descriptive parameters of the 3D grid are summarised in Table 2.

Table 2: The main dimensions of the first version (prior to iterations and upscaling) geogrid. The high number of undefined cells is a result of the high number of associated faults.

Grid layout	
Total number of cells	30,801,429
Number of defined cells	14,264,165
Number of undefined cells	16,537,264
Number of columns	223
Number of rows	447
Number of layers	309
Number of zones	7
Rotation angle (degree)	0

5.2.3 UPSCALING (OR BLOCKING) OF WELL LOGS (PHASE 1)

The aim of well log data upscaling – also known as blocking – is to synchronise the vertical resolution of the petrophysical logs with the 3D grid (ZAKREVSKY, 2011).

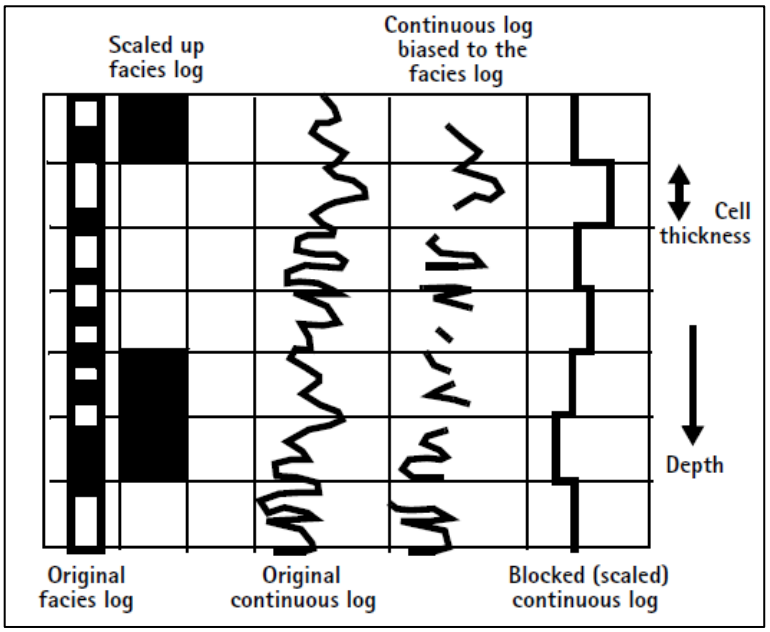

Figure 16: Upscaling (=blocking) of original well logs to the dimensions of the grid cells (EMERSON, 2019).

Interconnected porosity, initial water saturation and reservoir flag parameters were upscaled. Discrete-type reservoir flag using a most-of method, which simply assigns the value to a given grid cell, occurs the most often in the well log within the given cell. The reservoir flag is a simplistic 'rocktype' categorisation based on the cut-off values identified by petrophysical interpretation. (Reservoir flag is 0 if the petrophysical parameters of the rock at a given point suggest that it is not capable of storing and allowing fluids to flow. In other cases, its value is 1.)

Interconnected porosity and initial water saturation were upscaled using arithmetic averaging, but biased to reservoir flag. A visual explanation is given in Figure 16.

The upscaling was cross-validated reservoir by reservoir, with the application of histograms and crossplots.

5.2.4 ROCKTYPE MODELLING (PHASE 1)

Sequential indicator simulation (SIS) technique (pixel-based) was used for discrete rocktype modelling in the case of all formations. In each formation reservoir (code=1) and non-reservoir (code=0), rocks were identified based on well-log analysis, and cut-off criteria were based on this. SIS is useful where the reservoir elements do not have discrete geometries, either because they have irregular shapes or variable sizes, which is the case for the carbonate reservoir in Field A (NEMES et al., 2021).

At this phase no trend maps were used to drive the lateral distribution of either petrophysical parameters or the rocktypes, hence, it is based solely on the well data, variograms and statistical methods.

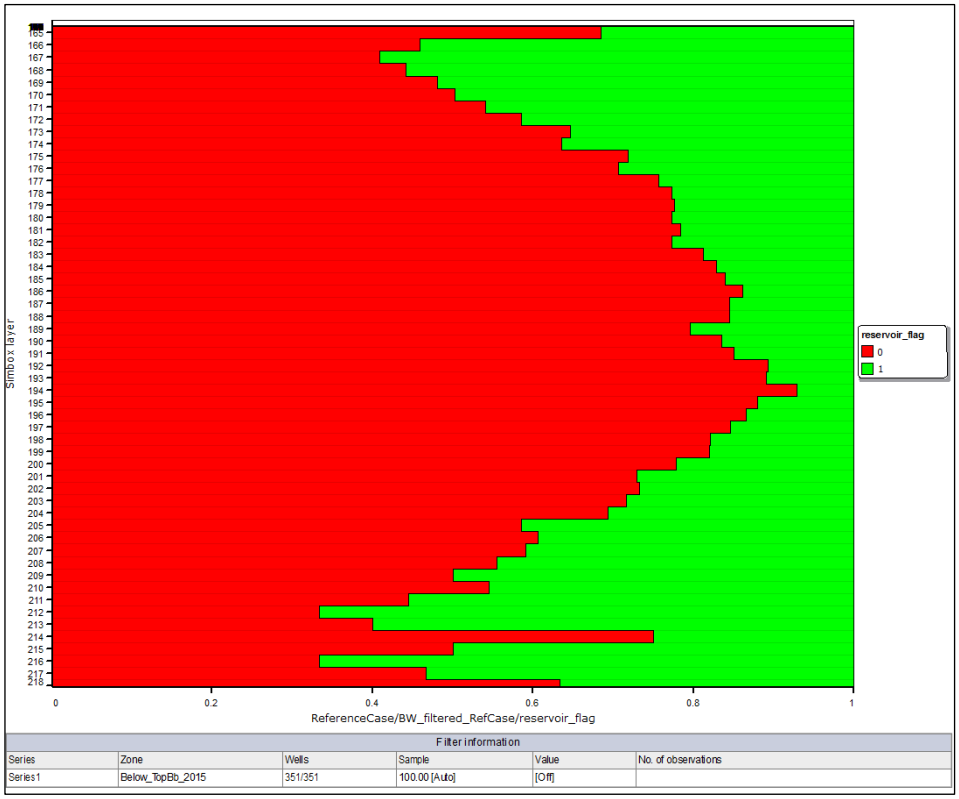

Figure 17: An example of VPCs belonging to the Bobrikovian Formation. Red indicates non-reservoir; green, the reservoir rocktype. Two subzones can be identified, the Upper and Lower-Bobrikovian, interlayered with a shaly, mostly non-reservoir zone.

In order to honour the vertical distribution of rocktypes identified on well logs, vertical proportion curves (VPCs) were put into the indicator simulator (Figure 17). Vertical proportion curves show the vertical variations in simbox depth of a given variable. VPCs contain zone information and by default use the grid resolution (EMERSON, 2019).

5.2.5 PETROPHYSICAL MODELLING AND VOLUME CALCULATION (PHASE 1)

Petrophysical modelling of interconnected porosity and water saturation was performed, biased to the previously modelled reservoirflag parameter. Permeability was calculated based on the porosity, with porosity-permeability regression equations identified on core measurements applied (NEMES et al., 2021).

Interconnected porosity was modelled separately for each formation and corresponding rocktype with the use of variograms, and log-derived water saturation was modelled co-simulating with interconnected porosity. All the wells with interpreted saturation curves were used, resulting in a probable slightly conservative estimation of hydrocarbon pore volume (HCPV) due to the representativity of new wells regarding initial saturation profile (NEMES et al., 2021).

Water saturation cut-off was applied in the 3D grid, resulting in a payflag parameter that was later used during the initial in-place volume calculations.

Equation 1 was used for calculating stock tank oil initially-in-place:

$$STOIIP = \frac{GRV * NtG * \Phi * (1 * S_{wi})}{Boi} \quad \text{Eq.1}$$

where *STOIIP* is stock tank oil initially-in-place (m^3); *GRV* is gross rock volume (m^3); *NtG* is net-to-gross ratio (%); *Φ* is interconnected porosity (%); *Swi* is initial water saturation (%); and *Boi* is the oil formation volume factor at initial reservoir conditions (m^3/sm^3). The calculations were made using different polygon sets based on administrative and legislative requirements. Due to a combination of area and net thickness parameter changes compared to the latest study, the *STOIIP* showed a total increase of 20–40% on the field level, with each individual reservoir showing an increase.

STOIIP refers to the produced volume at surface pressure and temperature (1.01325 bars, 15 °C), also known as standard conditions, as opposed to reservoir conditions (TÖRÖK et al., 2012).

6 DISCUSSION OF THE MAIN GEOLOGICAL MODEL (PHASE 2)

This chapter is structured in such a way that each step of the modelling is described, and then, sequentially, the corresponding Petrel workflow is introduced and explained. The workflow followed (Figure 18) resembles the one in Figure 15. The thesis focuses on the steps up to the volumetric calculation, and only briefly refers to the adjacent steps.

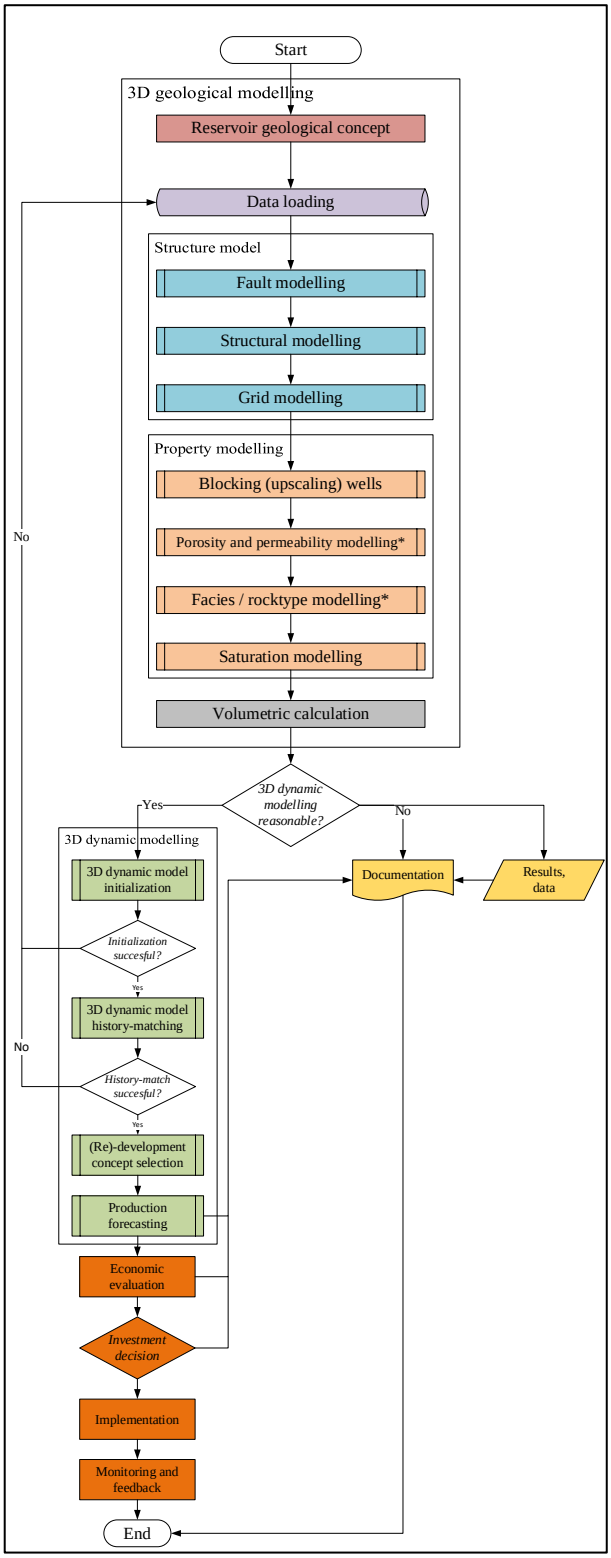

Figure 18: The extended version of the schematic workflow shown in Figure 15. The key difference in the geomodelling part is that the Rocktype modelling and Property modelling steps were switched up (except for Bobrikovian Fm.). The extension reflects the dynamic (flow) modelling and, briefly, the consecutive steps up to implementation.

6.1 PREFACE TO PHASE 2

As was flagged in the *Discussion of the first pass geological* model (Phase 1) chapter, firstly, a low-complexity, quick-look, deterministic geological model was built (Phase 1) and, simultaneously, preparations were made for a second (Phase 2) detailed modelling, aiming to mirror the actual behaviour of the field, incorporate the data and provide an understanding of the non-available or non-interpreted data from the first model.

The incremental value of the Phase 2 model is:

- a more complete and accurate input dataset,
    - including fit-for-purpose data gathering;
- an increased understanding of the field and production history (based on the reservoir engineering work on Phase 1 model);
- more sophisticated modelling methods;
- upgrades based on the lessons learnt from Phase 1;
- a full-cycle, automated workflow to provide a tool applicable for daily operations use and a single-source of truth representation of the subsurface data;
- an incorporation of all the experiences gathered during the Phase 1 model's history-matching process as well as the new data and knowledge acquired during the time interval between the two models;
- the construction of the geomodel in Schlumberger's Petrel, which is the business-preferred software for the given project due to model-sharing reasons with business partners.

Regarding the last point, it must be highlighted that no distinctive functional differences were identified between the two software programmes (RMS and Petrel). The decision was solely based on a non-modelling basis.

The Phase 2 modelling exercise started in August 2017, so not immediately after Phase 1. Hence, approximately ninety new wells were drilled, and new data and information was gathered both from the wells (logs, production) and from existing datasets, both in digital and analog versions. The vintage of the input dataset is 2017-10-31.

The descendants of the Phase 2 model are still in daily use in terms of Field A's life.

6.1.1 PREFACE TO WORKFLOW CREATING AND EDITING

First and foremost, it is critical to mention that the work was done mainly in Petrel 2015.5 (Operating system: MS Windows 7 64-bit) hence, any updates in the software to date – in the last 4 years – are not reflected in the thesis.

A workflow is a sequence of steps making up a process. It can be used for model updates, uncertainty analyses (including experimental design), scenario analyses, idea testing and creation, as well as for general, daily tasks.

Building a geomodel takes hundreds or thousands of steps, all of which represent a subtask, like the lines of a computer code. To be able to run additional stochastic realisations – which honour the same input data but can result in significantly different spatial distributions – knowing the sequence of these steps proves to be useful. The same is true for setting up uncertainty analysis runs, or updating the geomodel with new data or updated information and testing new concepts or hypotheses. Essentially, the sequence of these steps (a.k.a., tasks, jobs), called a workflow, is indispensable for quick idea testing, extensive analysis and running several cases and scenarios during flow modelling.

Besides complex workflows, simple, fit-for-purpose ones can be also created, which can reduce the time needed for repetitive or monotonic tasks with unlimited opportunities (e.g., creating lists of wells in a model, exporting visualisations) (HOFFMAN, 2013).

Examples can be found in the international literature of the use of different types and sizes of workflows to decrease uncertainty, boost collaboration, save time and standardise processes (PYRCZ AND DEUTSCH, 2014; KUMAR et al., 2017; KALETA et al., 2012; SHIRAZI et al., 2010).

The main advantages of creating, maintaining, and developing a workflow for an ‘alive’ subsurface project are the following, according to the author. The project is:

- front-end loaded, so the project benefits in terms of the time consumed in the beginning paying off in the later stages, meaning work speeds up;
- automatable, therefore saving the user time to work on other tasks;
- repeatable, hence, can be used to generate an unlimited number of realisations while minimising the likelihood of human error;
- updateable, as jobs can be added, withdrawn, modified and rearranged without restraints;
- scalable, as the same workflow can run for ten realisations, but also for thousands of them;
- extensible, as additional steps, or child workflows can be added;
- modular, as various subworkflows can be used independently with full functionality also;
- auditable (reproduceable), as the workflow itself is its own documentation and creates transparency;
- archivable, as it can be saved and loaded later on;

- sharable, for example among partners or other parties;
- interpretable, as a third eye can also decipher the steps, which makes handover smoother, when necessary;
- recyclable, as workflows and parts of workflows can be reused in other projects with minor adjustments;
- directly linkable – the flow model's workflow can be directly linked to the geomodel's;
- trackable, in terms of the various versions.

All these advantages make workflows an effective tool in terms of time (by reducing the number of clicks and mouse movements needed to reach the same outcome) and energy being saved and creative capacity being enhanced while minimising the chance of human errors being made during updates and reruns. Therefore, the description of Field A's geomodel workflow is one of the pillars of the current work.

There are two main ways workflows can be created and edited in Petrel: auto-generated workflows, which exploit the functionality so that the software automatically tracks every event impacting a given object in the programme; and manually created workflows, which are generated by the user from scratch. Both use the same module, the Workflow Editor (Figure 19). This thesis focuses on manual workflows.

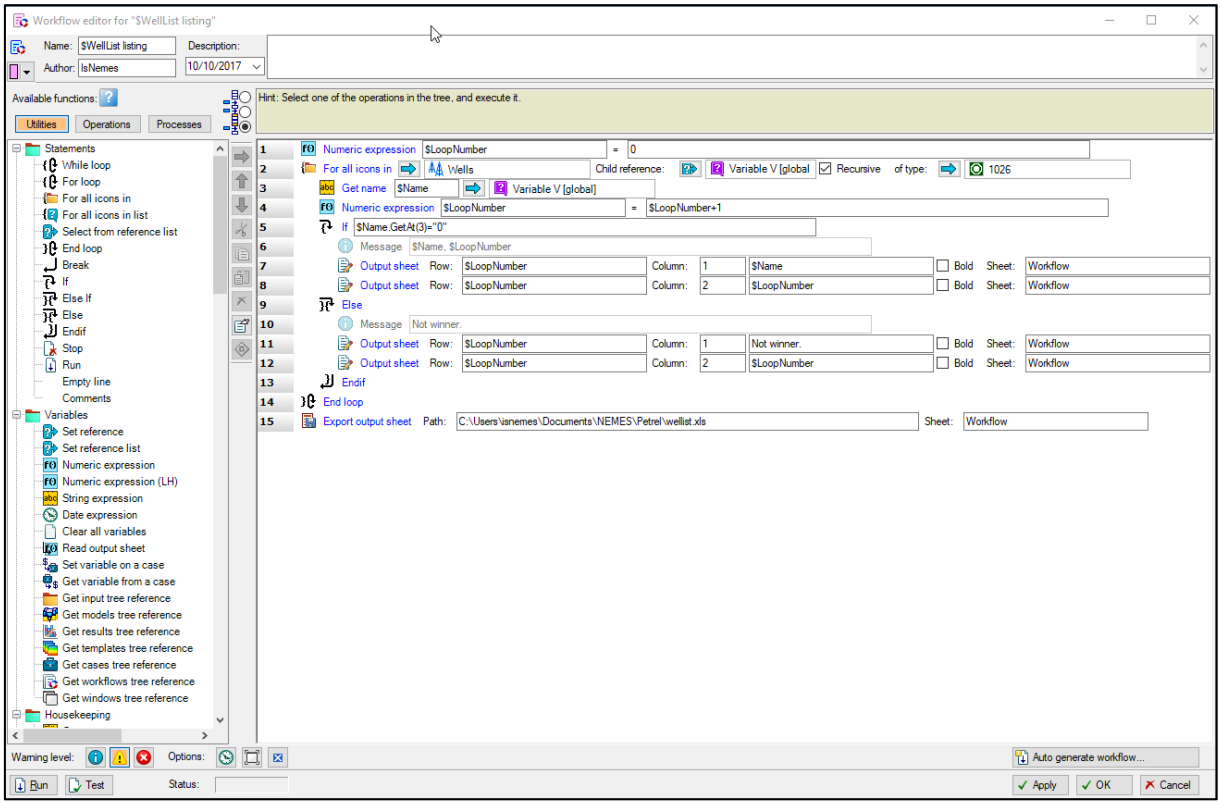

Figure 19: Petrel's Workflow Editor pane. On the left the various building blocks of any workflow are listed in different categories. These can be dragged and dropped to the right pane, which is the working area where the workflow is edited. The example workflow in the figure is a loop, which scrolls through all the wells, lists well names matching an IF function (Line 5) and writes and exports them to an Excel sheet.

In the workflow panel the available, predefined functions are grouped into three main and several subcategories. These main and subcategories will be used in the next chapters of the dissertation to localise the utilised functions.

1) Utilities: general statements widely used in all scripting languages, such as loops or if statements. In total approximately 115 different items are available in Petrel 2015.5.
2) Operations: a collection of operations is available in the programme. In total approximately 290 different items are available in Petrel 2015.5.
3) Processes: a collection of processes is available in the software, for example, structural modelling. In total approximately 205 different items are available in Petrel 2015.5.

The key components of any workflows or scripts are the functions (with their syntaxes) and variables. In Petrel there are several variable types available for use. A variable is like an empty 'box' that temporarily or permanently stores or refers to a given piece of data, information or reference.

In Figure 20 a schematic overview shows the various types of variables. There are two main groups: user-defined (or $variables) and object variables. The former, as indicated by its name, is defined by the user in the workflow and refers to a number, string or date. User-defined variables always start with '$' to differentiate the variable name from general text.

Object variables on the other hand are predefined. Two main subgroups can be distinguished based on the 'radius of influence'. Global object variables are not bound to one workflow, while local ones are created for one specified workflow and cannot be directly referenced in another workflow. In local variables the private is neutral, while if parent-child variable binding – to pass local variables among nested workflows – is necessary input-output differentiation is inevitable (SCHLUMBERGER, 2021).

In Global type there is a predefined number, 52, which is available for use. These variables can be referenced and redefined in any workflow; they are not bound to one, as are the local ones. Their disadvantage can be spotted when complex workflows are used or complete workflows are shared among Petrel projects. Amongst global ones, the Output variable type is somewhat different from the local output type. In this case the output variable's value continuously changes since it references the output of an actual step of the workflow. The Output case follows a similar logic, but the actual output case is assigned to it when the given output of a process is a case (e.g., volumetric calculation) (SCHLUMBERGER, 2021).

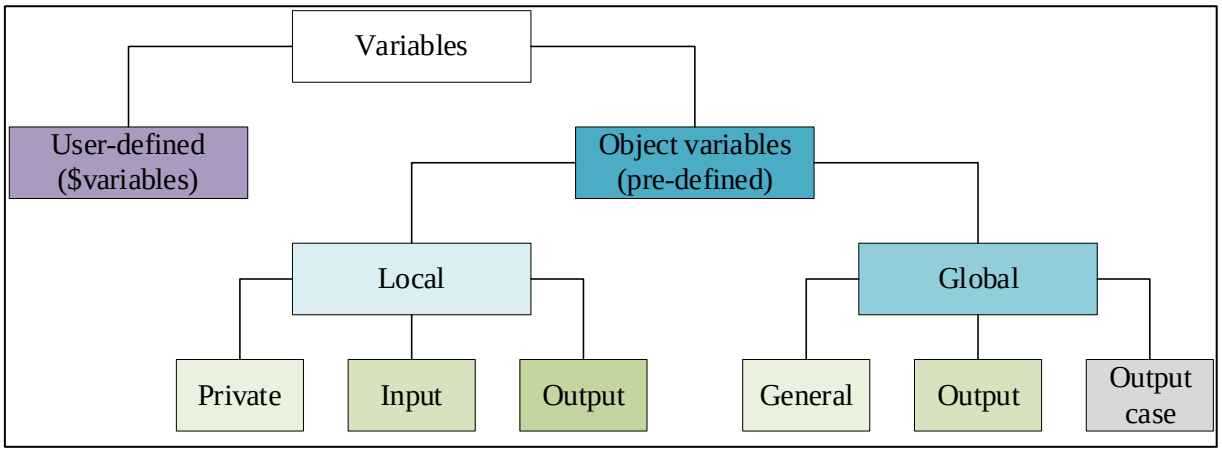

Figure 20: Various types of variables available for workflow building and editing in Petrel.

The Field A geomodelling workflow was split into several subworkflows (eight main elements and two optional), as visualised in Figure 21. The reason for the split is to be able to optimise the update processes in such a way that partial workflows can also be rerun (e.g., only for upper reservoir, or only for lower reservoirs, or only the property model). In addition, dividing up a multi-hundred step workflow makes it more transparent and manageable, especially in case bug hunting becomes necessary.

All these combined subworkflows consist of 818 rows, or steps, the bulk of which is provided by surface manipulation and the property modelling, as shown in Table 3.

Table 3: The breakdown of steps per subworkflow, comprising a total of more than 800 combined, from surface manipulation to volume calculation.

ID	Subworkflow	Reservoir zones	Number of steps
1	Stage 1 – Surface manipulation	A4, C1s, Bb, V1	230
2	Stage 2 – Structural modelling	A4, C1s, Bb, V1	30
3	Stage 3A – Grid modelling	Bb, V1	88
4	Stage 3B – Grid modelling	A4, C1s	68
5	Optional step - Cells penetrated by multiple wells A	Bb, V1	21
6	Optional step - Cells penetrated by multiple wells B	A4, C1s	21
7	Stage 4A – Property modelling	Bb, V1	205
8	Stage 4B – Property modelling	A4, C1s	144
9	Stage 5A – Volumetrics	Bb, V1	6
10	Stage 5B – Volumetrics	A4, C1s	5
Total	10	-	818

Figure 21 shows the structure and relationships of the subworkflows, as well as the decision points that control the path this subworkflows is comprised of in terms of/during the sequence of a given run.

The structural modelling subworkflows (Stage 1, Surface manipulation; Stage 2, Structural modelling) are combined for the upper and lower reservoirs. The reason behind this is that the running time is marginal, and to keep consistency and version tracking doable, the

same structural model feeds both the upper and the lower reservoir's grid. In addition, with this approach, in the case of scenario analysis, a common 3D property model and simulation can also be set up without the need to convert the workflow.

Subsequently, the user can decide whether grid modelling (Stage 3a, 3b), property modelling (Stage 4a, 4b) and volumetrics (Stage 5a, 5b) all need to be run, or if it is satisfactory to update only the upper or lower reservoirs' 3D geomodel. For example, if only a shallow (1H) well is drilled, then the update of the upper reservoirs is necessary, but the rerun of the lower reservoir's post-structural modelling steps is redundant since there is no new data available. Or if the trend maps of the Bobrikovian Formation are updated, then the upper reservoirs' workflow path does not need to be activated for time to be saved and inconsistencies to be avoided.

When the total core workflow is run, then, first, the lower reservoirs' geomodel is fully updated, and then the same is performed for the shallow reservoirs.

Both sides each have one optional subworkflow. These were built in collaboration with the software developer and filter those wells which penetrate the same grid cell. This step is necessary due to the high well density that results in cells being penetrated by two wells. Each of these cases need to be investigated individually, and the decision needs to be made as to which well is the most critical in the given location.

Aspects taken into consideration during the filtering of these well duplets include:

- vertical section where the phenomena occur;
- well log availability;
- log interpretation availability;
- production history (i.e., if the well produced the given layer, it will be used during the history-matching process in the dynamic simulation phase);
- age of the well.

Later on, the petrophysical data of this chosen wellbore is honoured during the upscaling of the well logs and property modelling. The filtered wells were collected in a Saved Search and, with a set operation, removed from the set of wells further used during the property modelling. These are optional since there is no need to run them each time an update happens. With the use of a 50X50-metre horizonal resolution in the shallow reservoirs' geomodel, nine wells were filtered due to the multi-well per one cell phenomena, with three wells in the deep reservoirs' geomodel. This phenomenon was one of the reasons the 50X50-metre horizontal resolution was picked, since any coarser grid would end up with, reasonably, more filtered wells. On the other hand, an even finer resolution could have led to an unmanageable number of cells, both in terms of geomodelling and dynamic simulation.

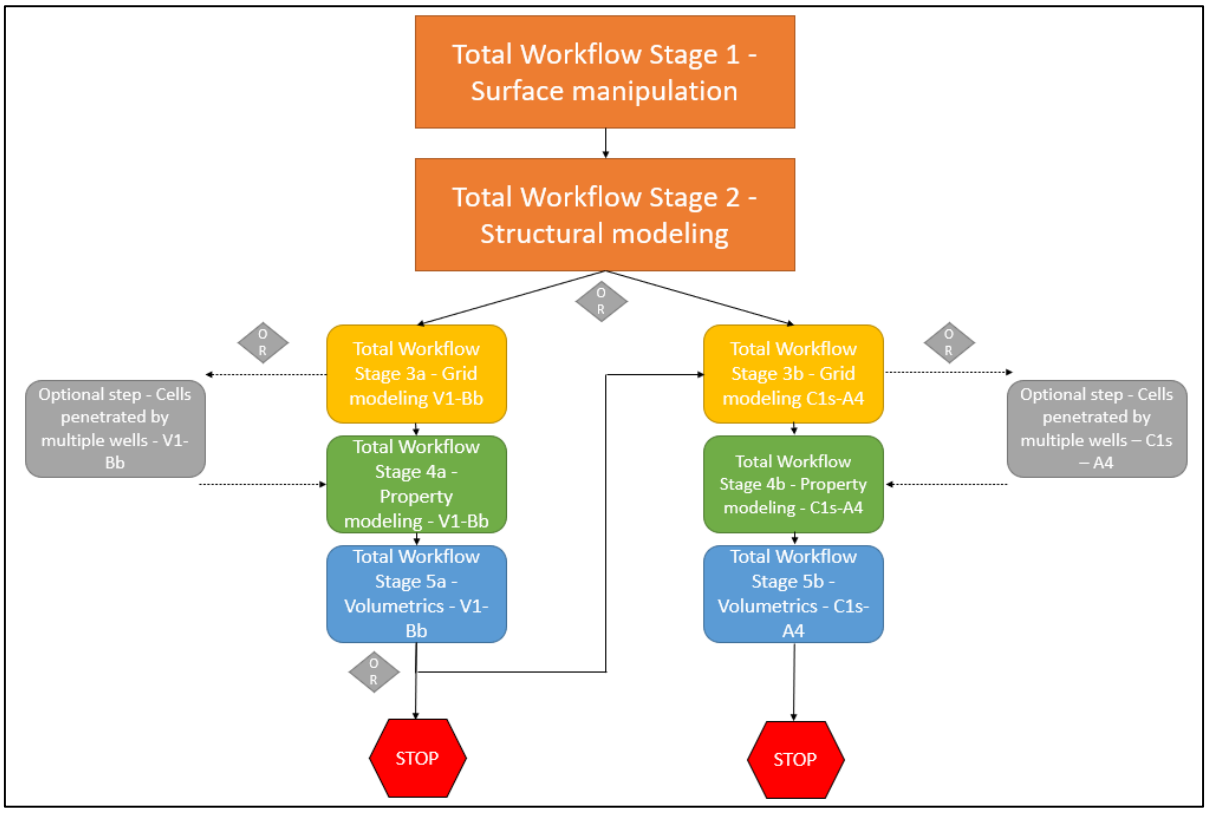

Figure 21: The schema (Level 0) of the workflow built for Field A's geomodelling. The colours are visual aids to distinguish the different stages of the modelling workflow. At each diamond shape there is a decision point that can be set up in the workflows. These decision points make the adjustable set up possible and help to resolve the constraint of rerunning the whole workflow in any case. The OR operators are XOR in logical terms, as both options cannot be chosen (semi-detailed breakdowns (Level 1) are given in Figure 29, Figure 48 and Figure 54) (NEMES, 2022).

6.2 INITIALISATION (PHASE 2)

In subsurface modelling there are different data types that can be categorised, for example, according to the system shown in Figure 22.

Categorical variables in nominal classes can be different facies types, rocktypes or quality flags. Ordinal variables represent more information since their order also has information value, for example, age group of the rock or Mohs scale.

Continuous datatypes can be subdivided into two subdivisions. Interval datatypes are where the intervals between values are equal, for example, the Celsius scale. Ratio datatype are numerical values that indicate the quantity being measured (PYRCZ, 2020), for example, porosity and saturation.

A commonly used category is discrete data, which is frequently used as a synonym for categorical data but can also be used for binned/grouped subsets of continuous data (PYRCZ, 2020).

Data can also be categorised as qualitative or quantitative and soft or hard data. Hard data is that in which there is high confidence e.g., well tops), while soft data is that in which the uncertainty is not negligible (e.g., trend maps).

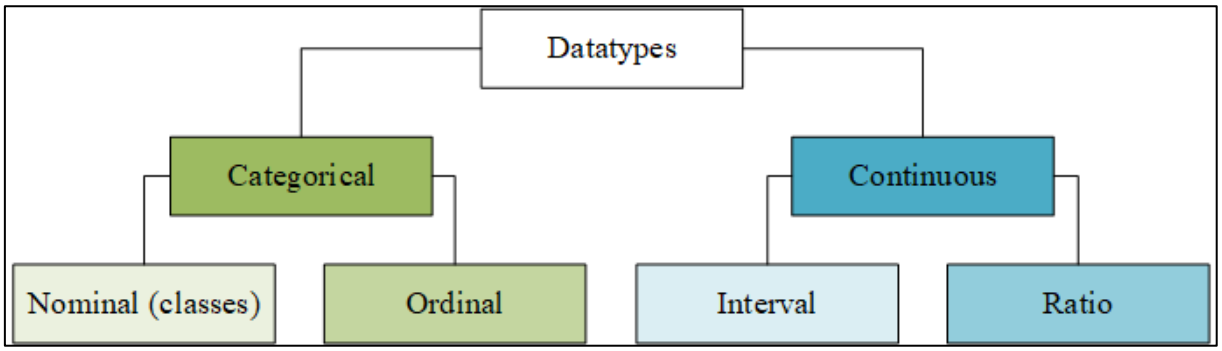

Figure 22: A categorisation system of subsurface datatypes, after PYRCZ, 2020. The two main datatype classes are categorical and continuous. The corresponding subdivisions are the nominal and ordinal in the former and the interval and ratio in the latter.

Data preparation (a.k.a., data wrangling) and loading are inevitable primary steps in any analytical or statistical work (PEDERSON et al., 1998). The conventional 'garbage in, garbage out' is not an empty phrase after all; it shortly sums up the painful experience of skipping the data preparation exercise, which can lead to multiple times more work later, or in the worst case, to decisions based on false conclusions. According to various authors worldwide, one of the key challenges related to mature fields is data availability, reliability and relevancy (PARSHALL, 2012), as case studies from Kazakhstan (ELLIOTT et al., 1998; BIGONI et al. 2010), Russia (CIMIC, 2006), Venezuela (AGBON et al., 2003), Indonesia (HANDAYANI et al., 2012), and India (TIWARI et al., 2015) show (NEMES et al., 2021).

Data preparation or data wrangling is, on the contrary, a time-consuming exercise, which can vary between 40-80% of the total time spent on geomodelling. In other words, 'massaging' the data takes more effort than interpreting and modelling it.

During the data preparation phase, several subtasks are carried out by a multidisciplinary team (BREIT and DOZZO, 2004) involving data experts:

- scanning and digitisation of paper-based data and reports;
- standardization of datatypes;
- unifying naming conventions;
- standardisation and unification of units, coordinate systems, reference levels and undefined values;
- multiple cross-check of data validity and reliability;
- flagging of outlier or extreme data;
- filtering of outlier or extreme data, if necessary;
- removing duplicates;
- individually examining contradictory data and resolving the contradictions;
- loading data into a predefined database and/or reference projects;
- establishing the practice of future data management and perpetual updates.

In Field A, due to the long history of the field, a lot of data were only available in paper/hard copy format. During Phase 2 most of these data were digitised, with a special focus on trajectory and log data, both of which were especially critical in modelling the Bobrikovian Formation as approximately seventy wells that were located in the same southwest area of the field had no digital data beforehand. In addition, fourteen wells still have no trajectory data at all, and approximately forty wells have only dip, but no azimuth data. These wells are amongst the oldest ones, and supposing them to be fully vertical is reasonable.

Most of the well logs were also digitised in the old wells, but the log availability is very limited in these wells (gamma ray and spontaneous potential), which intrinsically defines the interpretability and derivable parameters.

Outlining and implementing a consistent naming convention is inevitable so confusion can be avoided, understanding can be aided and referencing in the Workflow Editor is made univocal. Uniformed naming convention rules were applied to well logs, well tops, seismic surfaces and to production data also.

Datatype standardisation was a comprehensive task that involved various levels of the dataset, from wellhead information to production data. The outlined datatypes and formats have been in use since the standardisation was established.

It is also essential that the coordinate system, units and reference levels be fully unified so that they are comparable, auditable and reliable. The coordinate system is a special local system. All of the coordinates were converted, and in some cases, remeasured (e.g., wellhead coordinates).

Units needed to be unified, starting with the well logs, to the volume-weight conversion. This is usually done during the initial setup, when defining the project unit system. (It is important to note that modelling software usually does not convert units, but only changes them. A cross-check is always necessary.) (Figure 23.)

A critical aspect of every modelling job is the handling and representation of undefined values. Different software programmes use different values, and it is crucial to harmonise them so that contradictions from the statistical analyses, visualisations, data conversion and calculations can be avoided. It should be noted that undefined is not equal to a zero value.

A cross-check and, eventually, a quantification of all data reliability is critical. In the case of Field A – Phase 2, several categories were set up. No data was assumed to be reliable until proven so. (For example, wellhead coordinate contradictions were also revealed when compared against maps. These were also sorted out amongst others.). In the well logs two types of quality-dependent discrete logs were introduced, one that represented the intrinsic reliability of the measurement (dependent on the borehole quality), and another that represented whether

the input data and the interpretation were already quality-checked. This information is particularly useful during history matching, when production history and the well log's conclusions seem to totally contradict each other.

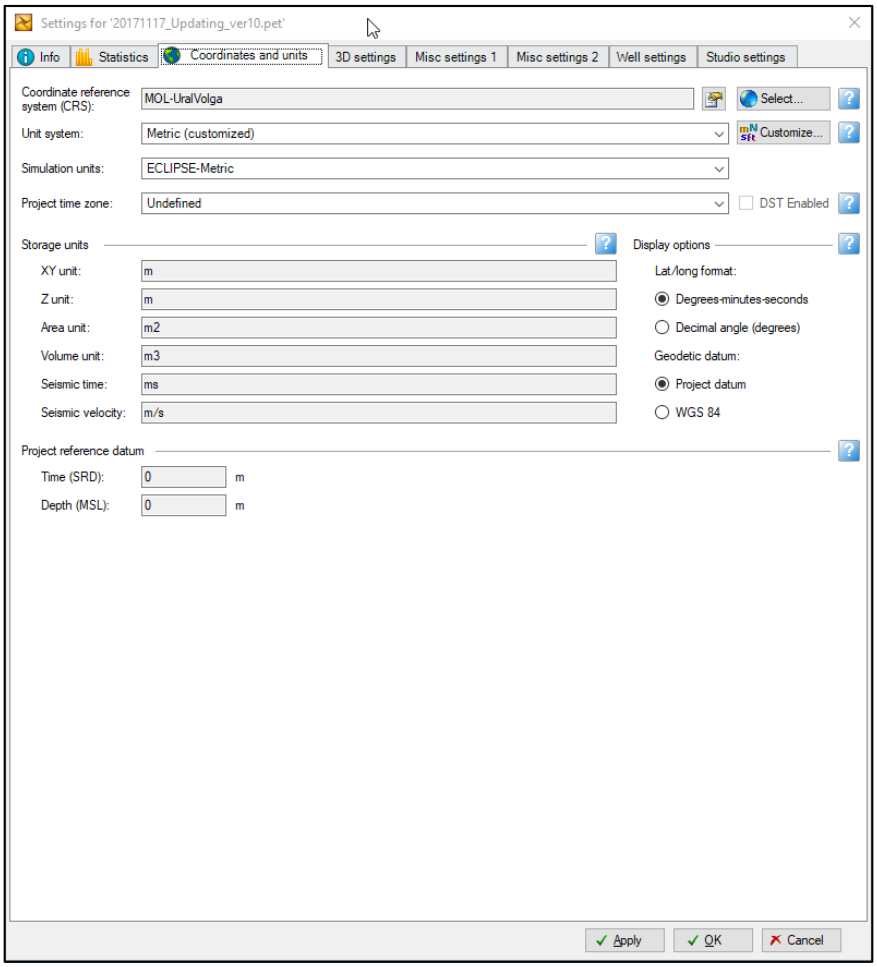

Figure 23: The initial settings of a Petrel Project, where coordinate system, reference levels and units can also be set up.

In the case of well trajectories, eight different groups were setup so that an up-to-date, accessible information source within the Petrel Project (Figure 24) could be obtained.

1) TNG: modern, measured, reliable trajectory (~85% of total wells).
2) NEFI: undisclosed source of digitally available trajectory.
3) NA: no trajectory data, neither on paper, nor in digital format (assumed vertical). (The search is still ongoing.)
4) NAC: no trajectory data, neither on paper, nor in digital format (assumed vertical) (Confirmed by operating company.)
5) NA: Non-OpCo: no trajectory data; the well is not operating company property.
6) PBD-NA: Old, paper-based data was digitised without azimuth. Since these are old wells and based on dips close to vertical, they were used as verticals.
7) PBD-LD: Old, paper-based data was digitised with limited datapoints.
8) PBD-SD: Old, paper-based data was digitised with sufficient datapoints.

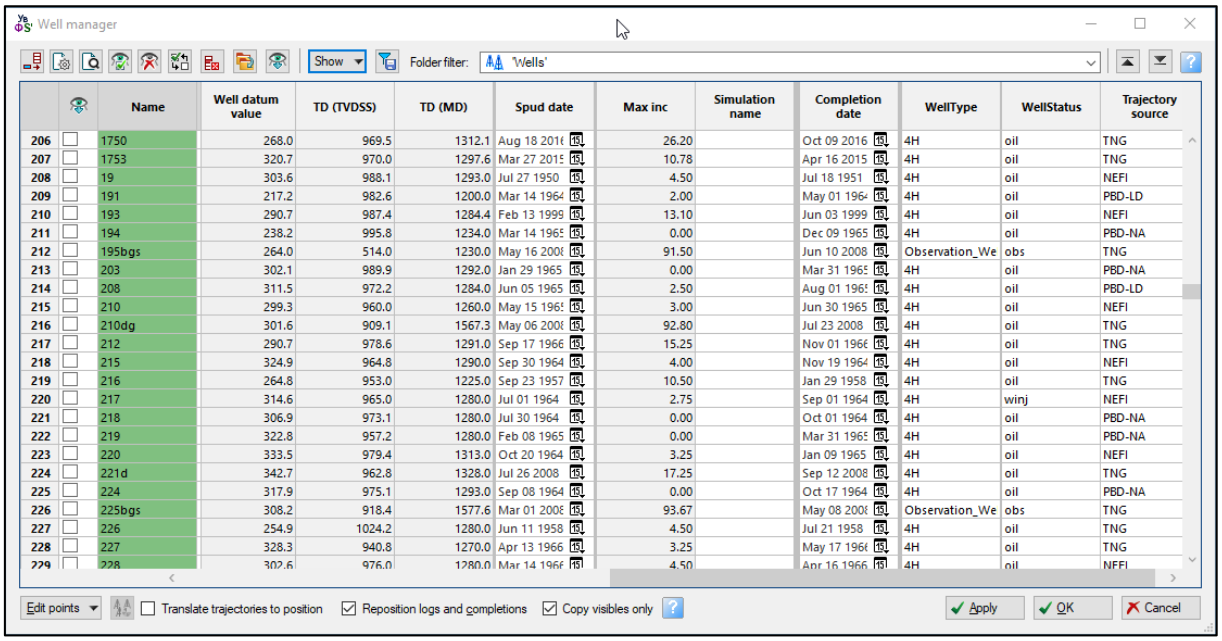

		Name	Well datum value	TD (TVDSS)	TD (MD)	Spud date	Max inc	Simulation name	Completion date	WellType	WellStatus	Trajectory source
206		1750	268.0	969.5	1312.1	Aug 18 201(	26.20		Oct 09 2016	4H	oil	TNG
207		1753	320.7	970.0	1297.6	Mar 27 2015	10.78		Apr 16 2015	4H	oil	TNG
208		19	303.6	988.1	1293.0	Jul 27 1950	4.50		Jul 18 1951	4H	oil	NEFI
209		191	217.2	982.6	1200.0	Mar 14 1964	2.00		May 01 196	4H	oil	PBD-LD
210		193	290.7	987.4	1284.4	Feb 13 1999	13.10		Jun 03 1999	4H	oil	NEFI
211		194	238.2	995.8	1234.0	Mar 14 1965	0.00		Dec 09 1965	4H	oil	PBD-NA
212		195bgs	264.0	514.0	1230.0	May 16 200(	91.50		Jun 10 2008	Observation_We	obs	TNG
213		203	302.1	989.9	1292.0	Jan 29 1965	0.00		Mar 31 1965	4H	oil	PBD-NA
214		208	311.5	972.2	1284.0	Jun 05 1965	2.50		Aug 01 196	4H	oil	PBD-LD
215		210	299.3	960.0	1260.0	May 15 196	3.00		Jun 30 1965	4H	oil	NEFI
216		210dg	301.6	909.1	1567.3	May 06 200(	92.80		Jul 23 2008	4H	oil	TNG
217		212	290.7	978.6	1291.0	Sep 17 1966	15.25		Nov 01 196(	4H	oil	TNG
218		215	324.9	964.8	1290.0	Sep 30 1964	4.00		Nov 19 1964	4H	oil	NEFI
219		216	264.8	953.0	1225.0	Sep 23 1957	10.50		Jan 29 1958	4H	oil	TNG
220		217	314.6	965.0	1280.0	Jul 01 1964	2.75		Sep 01 1964	4H	winj	NEFI
221		218	306.9	973.1	1280.0	Jul 30 1964	0.00		Oct 01 1964	4H	oil	PBD-NA
222		219	322.8	957.2	1280.0	Feb 08 1965	0.00		Mar 31 1965	4H	oil	PBD-NA
223		220	333.5	979.4	1313.0	Oct 20 1964	3.25		Jan 09 1965	4H	oil	NEFI
224		221d	342.7	962.8	1328.0	Jul 26 2008	17.25		Sep 12 2008	4H	oil	TNG
225		224	317.9	975.1	1293.0	Sep 08 1964	0.00		Oct 17 1964	4H	oil	PBD-NA
226		225bgs	308.2	918.4	1577.6	Mar 01 200(	93.67		May 08 200(	Observation_We	obs	TNG
227		226	254.9	1024.2	1280.0	Jun 11 1958	4.50		Jul 21 1958	4H	oil	TNG
228		227	328.3	940.8	1270.0	Apr 13 1966	3.25		May 17 196(	4H	oil	TNG
229		228	302.6	976.0	1280.0	Mar 14 1966	4.50		Apr 16 1966	4H	oil	NEFI

Figure 24: A snapshot of the Well Manager window from the Petrel Project of Field A. Several predefined and user-created well-level attributes can be listed and used for filtering. The trajectory categories are in the rightmost column. It should be noted that only a fraction of the attributes can be visualised in the figure. In the case of multi-hundred-well projects, the use of a well-established and detailed Well Attribute table is highly recommended.

Outlier and extreme data identification and flagging and filtering are not only necessary due to statistical considerations, but can also highlight data export/import malfunctions or human error. The log-end effect, for example, was often encountered – at the end of the well-logs, the datapoints take extreme values due to software malfunctions. Or in other cases the abovementioned undefined values were not synchronised, and some of the well logs were filled with -999.25 values. Quick checks can be made with the use of histograms, boxplots or exploratory data analysis, (EDA) or through visual inspection. In these terms the Type I error corresponds to the removal of only seemingly erroneous data (false positive), while the Type II error accepts false data (false negative).

The removal of duplicates is a straightforward exercise, although this can be tricky if duplicate wells, for example, have slight differences in elevation or total depth, or the trajectories are only slightly different. Each case requires an individual inspection prior to data removal.

After all the data filtering and quality checking, there is a a limit not worth going beyond, usually because there is no hard data available. For example, despite all the effort, there were still wells where the well tops were out of range compared to the seismic or offset wells. These were investigated one by one; in some cases the data gaps and root causes were identified, but for the most part these wells had to be excluded from the structure's conditioning to well tops (this phenomenon impacted approximately ten wells).

Also, a quite unique anomaly occurred infrequently, namely, the well logs were longer in the well than the trajectory itself. In order to do a bulk cross-check of this anomaly, a small

workflow was built and these errors were all corrected individually (either the logs or the trajectory were slightly erroneous, but mostly the trajectory).

A consistent single-source database had to be established so that the generation of multiple versions and copies of the same input data (or data loss) could be avoided. In case of Field A, due to the organisational structure and software availability, a Petrel Reference Project and an OFM (Schumberger's Oil Field Manager software) Reference Project were built. The former is a fully functioning Petrel Project, with the sole purpose of storing and making standardised, quality-checked, up-to-date input data accessible to the project team. Only the Data Management team has the right to add, delete and modify data inside. A great advantage of the Petrel Reference Project is smooth data loading to any other working projects and synchronised project settings; also, there is no need for additional licenses or plugins to connect various databases. Petrel's functionality – the Reference Project Tool (Figure 25) – makes data loading fast and auditable, from the Reference Project to the working project.

Key datatypes in the Petrel Reference Project are of different scales and sources, but are all in line with the principles listed in this chapter and use an extraordinarily strict, predefined convention in terms of names, units, coordinate systems and templates:

- well data:
  - wellhead data,
  - trajectories,
  - completion history,
  - measured well logs,
  - interpreted well logs,
  - additional well attributes (e.g., date of drilling);
- well tops;
- seismic surfaces;
- seismic cube;
- faults;
- phase contacts;
- trend maps;
- license and other administrative boundaries.

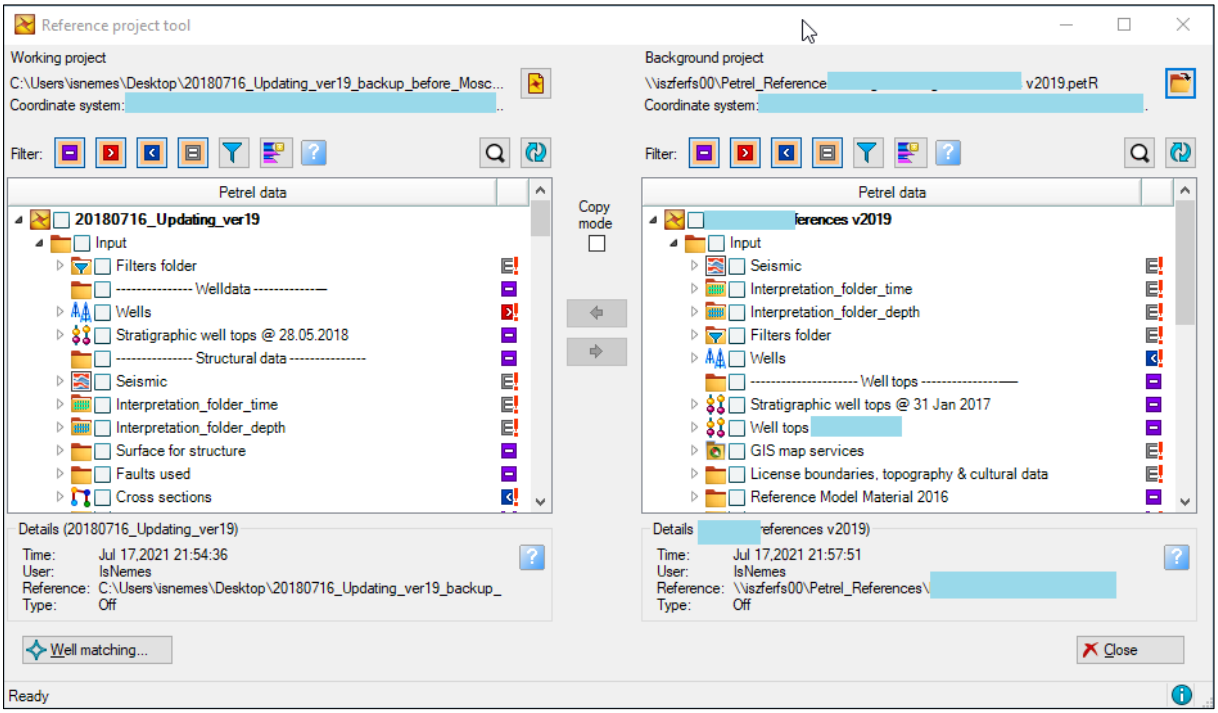

Figure 25: The user interface of the Petrel Reference Project tool; on the right is the Background Project (i.e., the Petrel Reference Project), and the left side shows the working project. The different data objects/items are labelled with a globally unique identifier (GUID) to make matching explicit.

The OFM Reference Project of Field A is a data repository for production, injection, and pressure data, with the same data governance logic as its pair in Petrel. The key data types in the OFM database in the case of Field A on a completion level include:

- production data:
  - for oil, gas and water,
  - daily and monthly rates, and cumulative production,
  - given in cubic meters and tons;
- injection data:
  - for water,
  - daily and monthly rates, and cumulative production,
  - given in cubic meters and tons;
- uptime (i.e., the number of days the completion was in production in a given time interval);
- water-cut (ratio of water produced and total liquid produced);
- additional derived parameters (average production and injection rates, liquid rates, cumulative volumes, first day of production).

Once the Reference Project(s) is/are set and the dataflow processes are established, it is advisable to construct a process for the recuring updates of the database so that a quick deterioration of the Reference Projects can be avoided. In this case new well data was loaded

without delay, but the production database was updated on a fixed, monthly basis, as per the user requirement.

6.2.1 WORKFLOW STAGE 0 – PRIOR TO MODELLING

The majority of the data preparation and validation took place prior to the geomodelling in Petrel, i.e. prior to the Surface manipulation step of the workflow (Figure 21). In Petrel a series of Saved Searches were set up for further use during modelling and visualisation. The sequence of folders was optimised, and after loading each well, a short sequence of double-checking was done. The main critical steps during this phase were the following:

- visual inspection of wellhead data using 2D/3D window;
- visual inspection of well trajectory using 3D window;
- a qualitative inspection of well log data (focusing on interconnected porosity, water saturation and shale-content) using simple exploratory data analysis via built-in statistics;
- checking of well top set completeness, amending where necessary;
- checking of well attribute completeness, amending where necessary;
- visual inspection of completion events.

The list below gives a more detailed overview of the key input data used during the geomodelling workflow that was loaded into the Petrel Reference Project and the working project subsequently as well.

1) Seismic data
    a. interpreted depth surfaces of the stratigraphic top of reservoir zones
        i. uncertainty analysis was performed for all the horizons, and the P50 case was used for base case geomodelling;
    b. faultsticks (i.e., a skeleton) for the eastern bounding fault.
2) Well data
    a. wellhead coordinates, elevation, trajectories (where available, directional surveys were used) – 557 wells;
    b. well completions (historical and actual perforations and squeezes) loaded from corresponding OFM database;
    c. various well attributes (see Figure 24).
3) Petrophysical data
    a. core data, where applicable;
    b. processed well logs

i. typically, gamma ray, one to three different resistivity curves, spontaneous potential, density, neutron, calliper and occasionally other log types;

c. interpreted well logs (417 wells with interpreted interconnected porosity log)
    i. total and interconnected porosity, lithological composition (sand, shale, dolomite, limestone, gypsum-content), initial water saturation, permeability,
    ii. uncertainty analysis was performed using Monte Carlo method for the interconnected porosity, the initial water saturation and the shale volume, hence, P90-P50-P10 cases were calculated for each;
    iii. the sampling rate of the logs is 0.2 metres;
d. well tops (or wellpicks), identified on well logs;
e. recommended reservoir and pay cut-off sets;
f. facies distribution trend maps;
g. initial oil-water contacts identified on well-test and well log data.

4) Dynamic data
    a. production data loaded from OFM database;
    b. well-testing information (production rates and pressure build-up interpretations);
    c. oil initial formation volume factor (Boi) per reservoir;
    d. absolute oil and water density at ambient conditions.
5) Other data
    a. georeferenced surface topography map;
    b. production license boundary;
    c. 3D acquisition(s) boundary polygons;
    d. natural reserve area boundary polygons;
    e. border of administrative regions.

6.3 STRUCTURAL MODEL (PHASE 2)

Structural modelling is the process of establishing the tectono-stratigraphic skeleton of the reservoir by integrating seismic and well data in line with the regional geological concept. A structural model defines the fault-fault, horizon-horizon and fault-horizon relationships, fault

throws and pinch-outs. It describes the seismic-level spatial shape of the reservoir, which provides the direct shape and high-level layering of the grid model (SAIKIA et al., 2015).

Field A's structural modelling was based on (manually) interpreted seismic horizons that were converted to depth domain using a velocity model. The horizon interpretation was done in the PSTM (pre-stack time migration) volume, and the results were depth-converted (Figure 26). The uncertainty range of the interpreted surfaces was quantified, and P90, P50, P10, mean and min-max cases were loaded into the Petrel Reference Project and the working project. The P50 cases were used in further modelling; the quantification of in-place volume uncertainty was not part of this stage. The scheme followed is very similar to the one published by EBONG et al. (2019) or by ADELU et al. (2019), and is common in the industry.

The 3D seismic acquisition over the AOI was completed in 2008 (Appendix VII with green polyline) and was first processed in 2009, and then reprocessed in 2014 and merged with a neighbouring exploration block's seismic volume, acquired in 2014.

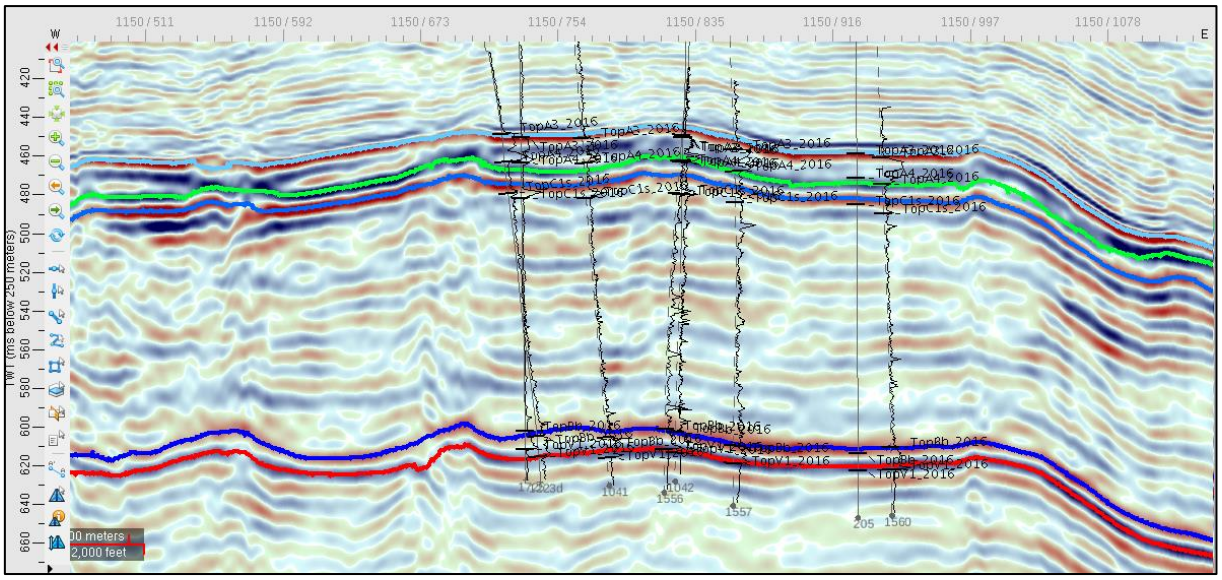

Figure 26: A time domain (TWT) W-E seismic cross-section of Field A indicating the top horizons of the four productive formations; in light blue an additional top, the Verejskij Fm., is also interpreted. The black straight lines are well trajectories projected to the section, with well tops. The log curves next to the trajectories are DTs (P-wave velocities) (Source: D. Holló's Seismic Report).

Only the top horizons were interpretable (A3, A4, C1s, Bb, V1 and one supplementary marker) (Figure 26); hence, the bottom of C1s, Bb and V1 were modelled based on the corresponding top and with the use of the well tops identified in the wells. The Bb bottom is the top of the Malinov Shale, stratigraphically a member of the Bobrikovian, but acting as a vertical flow barrier. A similar approach was followed to generate the intralayers in V1 and Bb – the former separating the Upper and Lower Tournaisian, the latter separating the Upper and Lower Bobrikovian.

To generate the bottom Surface resampling algorithm used key input data from the closest top horizon (in the case of the Bb bottom, the V1 top is the input), and the well tops of

the target surface. The mapping increment was always 50X50 metres in order to accommodate sporadically high well density.

The consistency of the surfaces was checked to ensure that they do not intersect each other and that unreasonable positive/negative bullseyes do not occur. Some seismic-related errors had to be manually removed from the surfaces by eliminating datapoints within these relatively small polygons (max. 100 metres in diameter).

The resulting surfaces were smoothed and interpolated in the formerly eliminated bullseyes where necessary. Wells still causing unrealistic peaks were investigated individually, and where no resolution could be revealed, the well was removed from the dataset (old wells without trajectory).

The well top adjustment was performed in Petrel during the geomodelling; the target was to reach an approximate residual value of 0.2-metres. A convergent interpolation algorithm was used for this process in order to accommodate multiple data sources and so that unrealistic shapes could be avoided. An example of the resulting surfaces is shown in Appendix V. The number of well tops per structural horizon is shown in Table 4.

Table 4: The number of quality-checked and passed well tops that were used for the surface adjustment of the corresponding depth surface (also see Appendix X).

Horizon	Number of well tops
A4 top	551
C1s top	542
C1s bottom	410
Bb top	415
Bb bottom	413
V1 top	413
V1 bottom	165

With the use of the top and bottom surfaces as input data, the true vertical thickness and true stratigraphic thickness maps were derived. In the Stage 2 model the Flowbarrier zone was not modelled in the Structural modelling step, but is represented in the rocktype modelling, suggesting that A4 and C1s may communicate hydrodynamically, at least in a limited way.

The average thickness of the main formations is listed in Table 5, and a TVT map of the Tournaisian Formation is shown in Appendix VI. The Malinov Shale is thin, but according to the analysis of the well tops, it is regionally existent throughout the area of interest, which makes it highly probable that the Tournaisian and Bobrikovian Formations are separate hydrodynamic units.

Table 5: Partial descriptive statistics of true vertical thickness values of the four main reservoirs and the Malinov Shale. The thickest formation is the Serpukhovian, although the oil is trapped only in the very dome of the structure. (The number of digits in the case of the Malinov Shale is different in order to illustrate the range close to 0 metres.

Formation	Minimum TVT (m)	Average TVT (m)	Maximum TVT (m)	Std. dev. (m)
Bashkirian	15	37	53	4
Serpukhovian	42	57	68	2
Bobrikovian	9	17	32	3
***Malinov Shale**	0.5	1.2	1.9	0.3
Tournaisian	40	44	51	1

The eastern bounding fault was modelled based on the fault sticks interpreted on seismic and converted to depth domain. The pillar gridding technique was applied since it is almost vertical, therefore, the number of distorted cells is minimal (FONTANA et al., 2015). This fault provides the closure of the structure to the east and penetrates all reservoirs, having a throw of around 100-150 metres (Appendix V). Although on seismic it seems like a series of smaller faults, for the purposes of reservoir modelling a simplified approach is adequate. In-field structural elements were not incorporated into the geomodel.

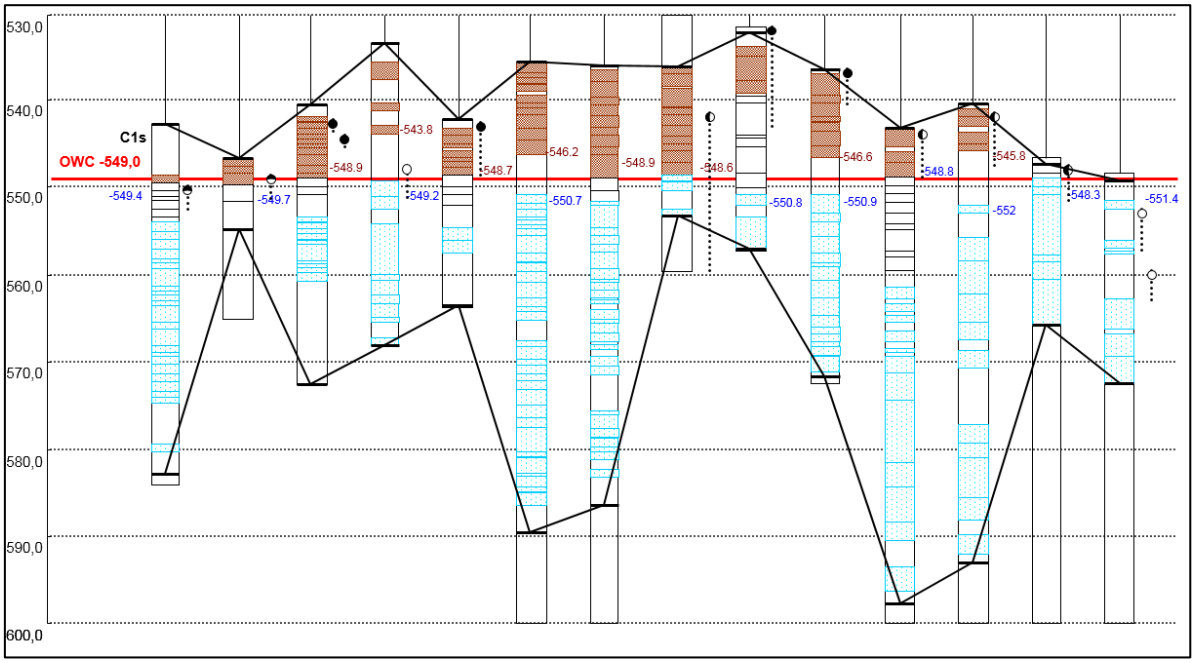

Figure 27: An illustration of initial OWC estimation integrating logging and well-testing data for the reservoir of C1s. The columns indicate the log responses (brown is hydrocarbon, blue is water), while the signs on the right represent the nature of the inflow – oil/oil with water/water/dry) (source: internal materials).

Initial oil-water contacts were identified for each formation based on logging and inflow testing information (Figure 27). Despite some contradictions, one flat initial oil-water contact (OWC) was established for each formation (an example for C1s is illustrated in Appendix VII).

The most informative drillings are the earliest ones (drilled before the 1970s), since these represent the initial state of the individual reservoirs. The new wells (drilled after 2000) have a more sophisticated logging suite, but are inherently exposed to the risk of not penetrating

the reservoir in their initial state, but an altered one caused by seventy years of production and injection history.

The identified initial OWC parameters are shown in Table 6.

Table 6: The reference case initial oil-water contacts applied during geomodelling, based on preliminary investigations.

Reference OWC_i (m TVDSS)	
A4	535
C1s	549
Bb	930
V1	941

Although it is not directly linked to surface manipulation, the creation of reservoirflag is equally essential, hence, its place in the Stage 1 subworkflow. Reservoirflag is a discrete well log that has two values; it is 0 (Tight) if the cut-off conditions are not met, and it equals 1 (Reservoir) when they are.

The reservoirflag=1 parts of the reservoir are presumed to be of good enough quality to contribute to the storage capacity as well as the flow capacity.

The applied cut-off criteria were based on a petrophysical evaluation of the well logs and core data, especially core flooding experiments. The base case cut-off sets identified are summarised in Table 7. For the reference case only porosity cut-offs were used. The resulting reservoirflag discrete log is visualised in a well section in Figure 28.

Water saturation cut-off was not applied, as it is initial water saturation and not irreducible water saturation; consequently, high water saturation does not directly mean that a given cell is not capable of having flowing fluids. However, if necessary, for volume comparison purposes with historical studies, the additional cut can be applied in the 3D grid directly, arriving to net pay from net reservoir. It is crucial that this method presupposes that during 3D dynamic simulation, the relative permeabilities will dictate the flow of various saturation-level cells. This does not necessarily mean that all the cells which exist as reservoirs will be able to have flowing hydrocarbons.

Table 7: A summary of the applied interconnected porosity cut-offs per formation. For the reference case only porosity cut-offs were applied.

	POR_EF cutoffs - ReservoirFlag (%)
A4	8.7
C1s	8.0
Bb	11.0
V1	8.4

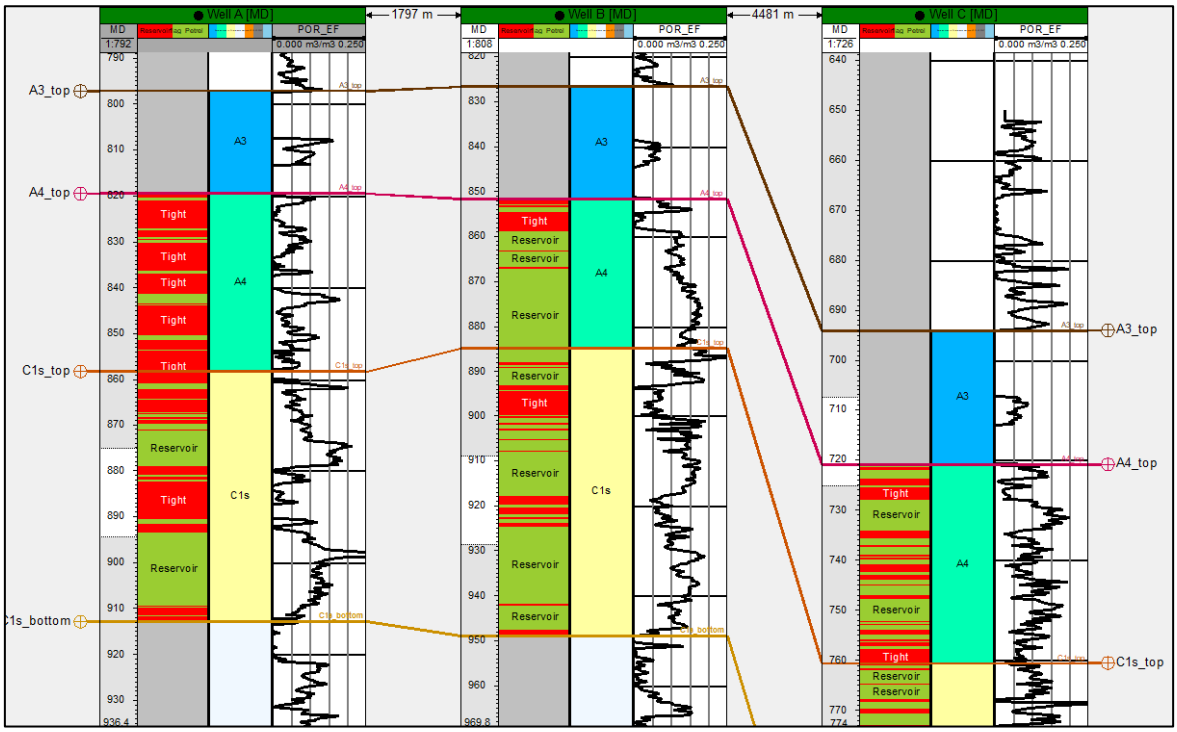

Figure 28: An illustration of a well section with three log tracks: the left one shows the reservoirflag; red represents tight rocks, while green shows the reservoir. In the middle is the zonelog showing in which reservoir the given depth point is situated. The rightmost is the interconnected porosity (in fraction) curve, P50 case.

6.3.1 Workflow Stage 1 – Surface manipulation

Stage 1 – Surface manipulation subworkflow consists of 230 steps and, as the name suggests, is mainly scripted to create, adjust and update structural surfaces. Also, as mentioned earlier, the calculation of the reservoirflag well log is incorporated into the subworkflow.

A semi-detailed (Level 1) overview of the subworkflow is given in Figure 29 as a guidance prior to the introduction of the step-by-step description. (Similar Level 1 breakdowns will also be introduced for Stage 3a – Grid modelling (*Workflow Stage 3a and 3b – Grid modelling*) and Stage 4a – Property modelling (Workflow *Stage 4a and 4b – Property modelling*) subworkflows, as these are the most extensive and multi-layered. The rest of the subworkflows are simpler, with a significantly fewer number of steps.)

The steps of the Surface manipulation subworkflow (Figure 21) can be split into seven groups, as indicated in Figure 29. A general ‘housekeeping’ and creation of backups is followed by the reservoir top maps well-top matching and adjustments. With the use of the created reservoir tops, TVT and TST maps are calculated; subsequently, OWC_i polygons are generated, ending the steps related to mapping.

The last group of steps in this subworkflow encompasses the calculation of the discrete reservoirflag log based on the predefined cut-off criteria per reservoir subzone.

In the following part the step-by-step (Level 2) description of the subworkflow is given, starting with the housekeeping as Step 1.

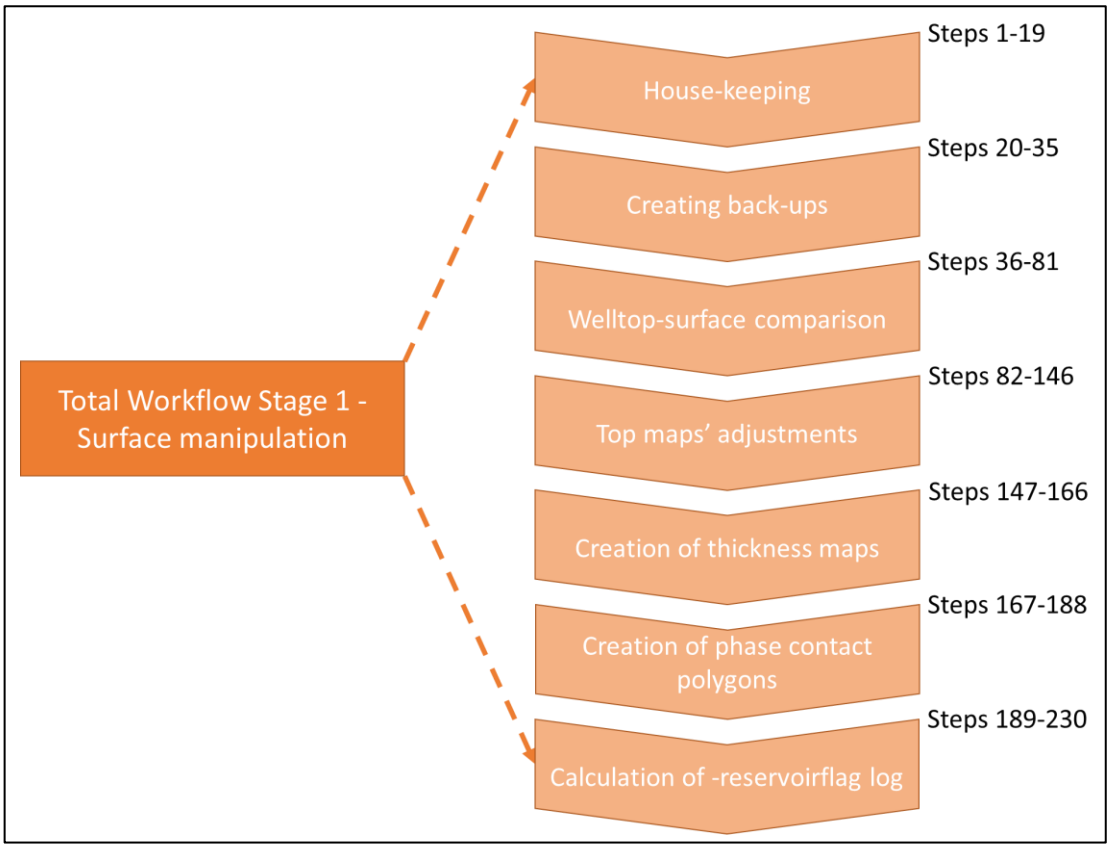

Figure 29: A semi-detailed (Level 1) breakdown of the main groups of steps in the Surface Manipulation subworkflow indicating the steps belonging to the given group. Each step is introduced in the subchapter in detail (Level 2). An overview of the Level 0 subworkflows is given in Figure 21.

A few recommended steps at the beginning of each subworkflow are provided so that contradictions can be avoided, and step order can be maintained. (Steps 1-9) (Figure 30). Using *Comments* (Utilities/Statements), critical text-based reminders can be added and the subworkflow can be further structured.

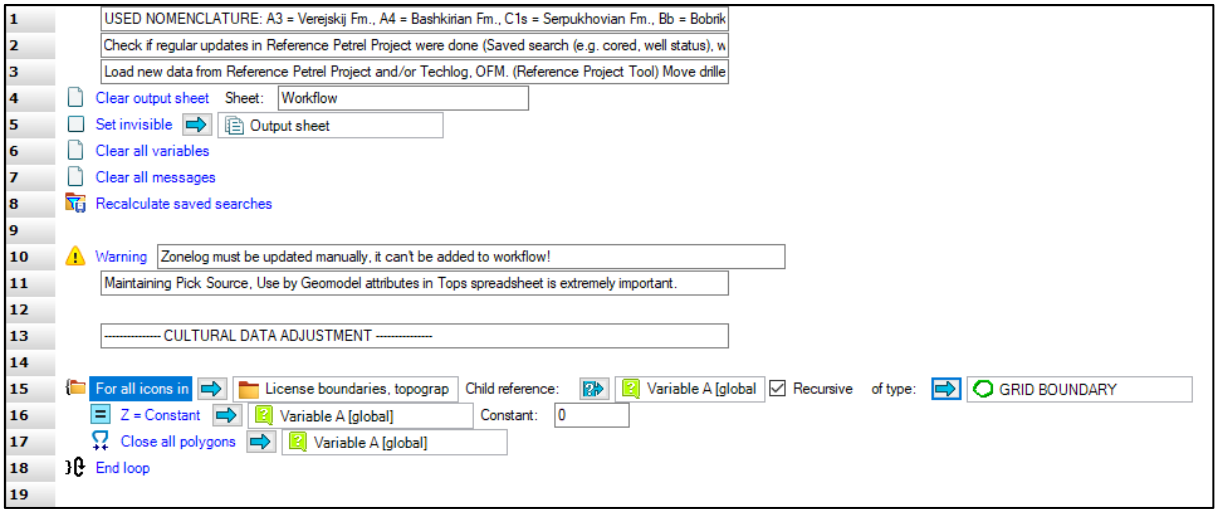

Figure 30: Steps 1-19 in the Stage 1 – Surface manipulation subworkflow. The first steps are critical background information, housekeeping steps, and warnings to the geomodeller or to anyone using the workflow.

Clear output sheet (Utilities/Information) clears the sheet where the Workflow Editor exports the output data by default. This step sets the scene and clears any remaining output data from former runs so that misunderstandings can be avoided.

Clear all variables (Utilities/Information) removes all loaded data to the Global or Local variables, resulting in a clean sheet before the start of data manipulation. *Clear all messages* (Utilities/Information) cleans up the message panel of Petrel so that confusion between relevant and irrelevant and old and fresh messages can be avoided.

Recalculate saved searches (Operations/Saved searches operations) is essential in order to make sure all the newly loaded wells are loaded into the corresponding Saved Searches (example in Figure 31) so they are incorporated into upcoming steps or, in some cases, are deliberately excluded. More than fifty different Saved Searches were set up throughout the geomodel for modelling, visualisation and statistical purposes.

Step 10 is *Warning* (Utilities/Information), which stops the workflow and brings up a prompt the user needs to click on before the run continues. In Petrel 2015.5 the Zonelog update was not part of the available functions to be added to a workflow, so it had to be updated semi-automatically. (It should be noted that in newer versions it is already available.) Zonelog is a discrete log type that has a distinct numeric value for each layer based on the well tops set. Its availability and reliability are critical in performing pre-model statistics. Its special feature is that if a well stops within a formation and has no well top for the next reservoir, the zonelog value will be undefined. This was corrected manually by adding pseudo-well tops to the TD of these wells.

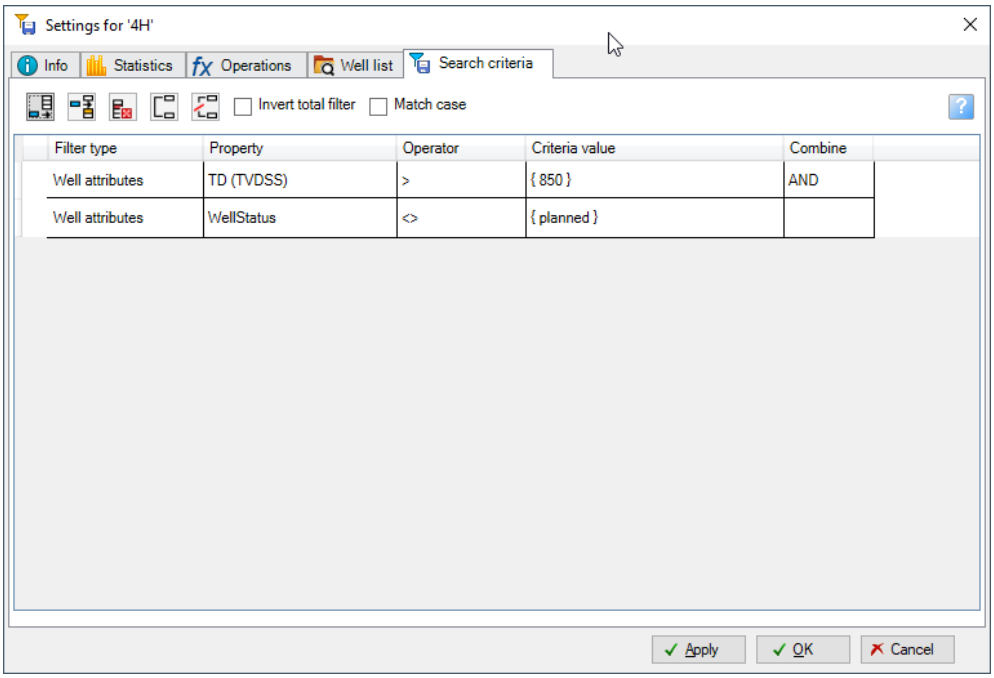

Figure 31: An example for a simple Saved Search, which keeps wells that have a total depth (TD) higher than 850 metres and are drilled, not only planned.

Steps 15-18 aim to ensure that the cultural data (i.e., administrative and other polygons; examples are shown in Appendix VII) depth values are uniform, that the polygons are closed, and any unintentional change is annulled with this simple loop. The *For all icons in*

(Utilities/Statements) loop search in the predefined folder, for all objects equal to the defined type (polygon), adds the object to the Variable A global object variable and runs the *Z= constant* (Operations/Arithmetic operations) and *Close all polygons* (Operations/Polygons operations) commands. This loop is repeated until all the objects have been processed. Step 18 *End loop* (Utilities/Statements) is of critical importance as this step tells the for loop to stop and jump back to the beginning. It's an indispensable part of the 'for' syntax.

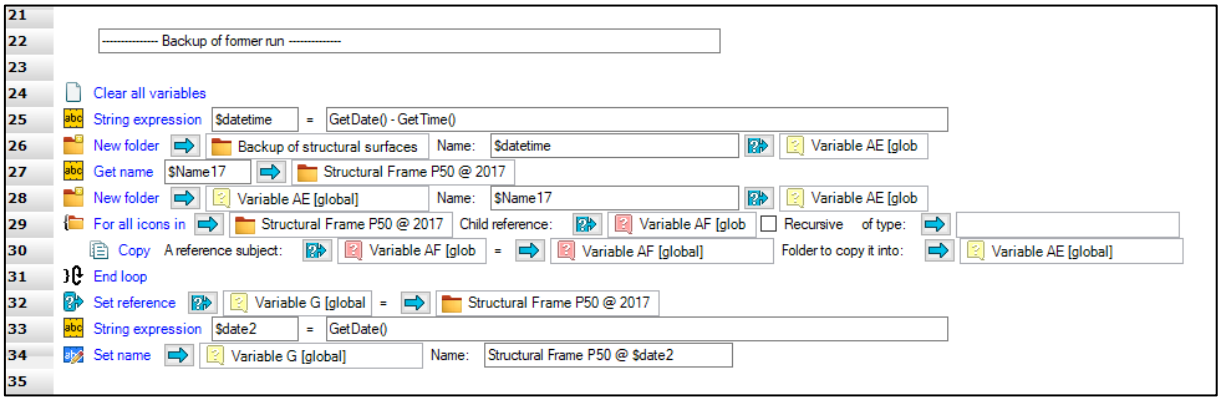

Figure 32: Steps 21-35 in the Stage 1 – Surface manipulation subworkflow creates a backup of the previous run's output surfaces.

Step 25, *String expression* (Utilities/Variables), is a commonly used function that creates a string as the content of a $variable (see Figure 20). GetDate() and GetTime() are string functions, retrieving the current system date and time. There are approximately forty different string functions and additional possibilities available for use providing the opportunity for complex string operations (Figure 32).

With the $datetime variable the target folder for the backup objects is created, and the current time in the folder name ensures unidentical naming. Step 27, *Get name* (Utilities/Housekeeping), is a useful function to read into a $variable the precise (Petrel) name of any objects in the Petrel project. In steps 29–31 a loop is created to use the *Copy* (Utilities/Housekeeping) command for each element of the source folder (Figure 32).

Set reference (Utilities/Variables) is a simple command to add an object to a variable, while *Set name* (Utilities/Housekeeping) provides the ability to rename specific objects.

The outcome of these steps is a backup version of the surfaces prior to rerunning the bulk of the workflow. The goal is to always have a safety backup version in case there is a need for it to be restored and to be able to compare pre- and post-update versions if necessary. Without this step the original ones could be overwritten (Figure 32).

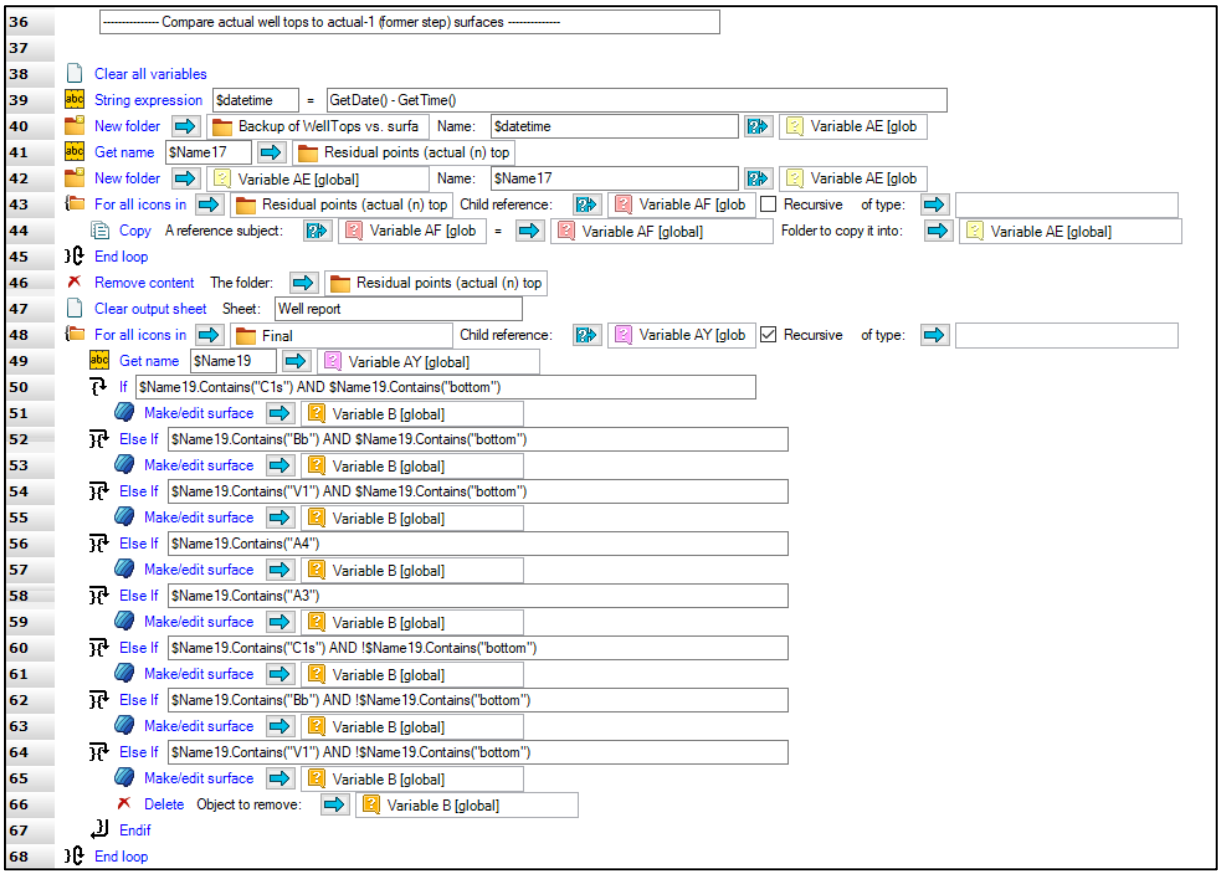

Figure 33: Steps 36-81 in the Stage 1 – Surface manipulation subworkflow creates a comparison of the new well tops versus the former version of depth surfaces. It provides a good indication about any anomalies, which are then investigated individually.

The output of this set of steps are residual points in a folder structure similar to Steps 21-35. Also, Steps 38-45 create a backup of the previous run in order to make a comparative analysis, if necessary (Figure 33). In Step 46 the *Remove content* (Utilities/Housekeeping) command cleans the main directory, where the newest residual point sets are created in the upcoming steps.

Steps 48-68 represent a loop using the *For all icons in* command. This loop generates the residual points comparing the n-th set of well tops and the n-1-th surfaces (in other words, a post-evaluation based on the newly acquired data). In Step 48 the command reads the subsequent 'icon' (i.e., object) in the target folder, called Final, added from the Input tree. (It should be noted that the Petrel Workflow Editor identifies folders and objects based on GUID, and not by the name. Hence, the renaming of objects does not confuse the workflow – although the latter is not applicable for Calculator syntaxes; this is discussed in a later section.). In the loop the different surfaces are distinguished by a series of nested *If* and *Else if* statements (Utilities/Statements), based on their name. (So in this case the name stated is of utmost importance.) In order to be able to use the name of the object as a string, a *Get name* command is used in each loop in Step 49, which reads the name as a string in the $Name19 variable.

In each If or Else if statement, a string description is used. (For example: “$Name19.Contains("V1") AND !$Name19.Contains("bottom")” translates to: if the name of the actual object contains V1 but does not contain bottom, then run the *Make/Edit surface* (Processes/Utilities) operation shown in Figure 34.) .contains() is a string function, while the “!” in front of $Name19 alters the string operation from contain to does not contain.

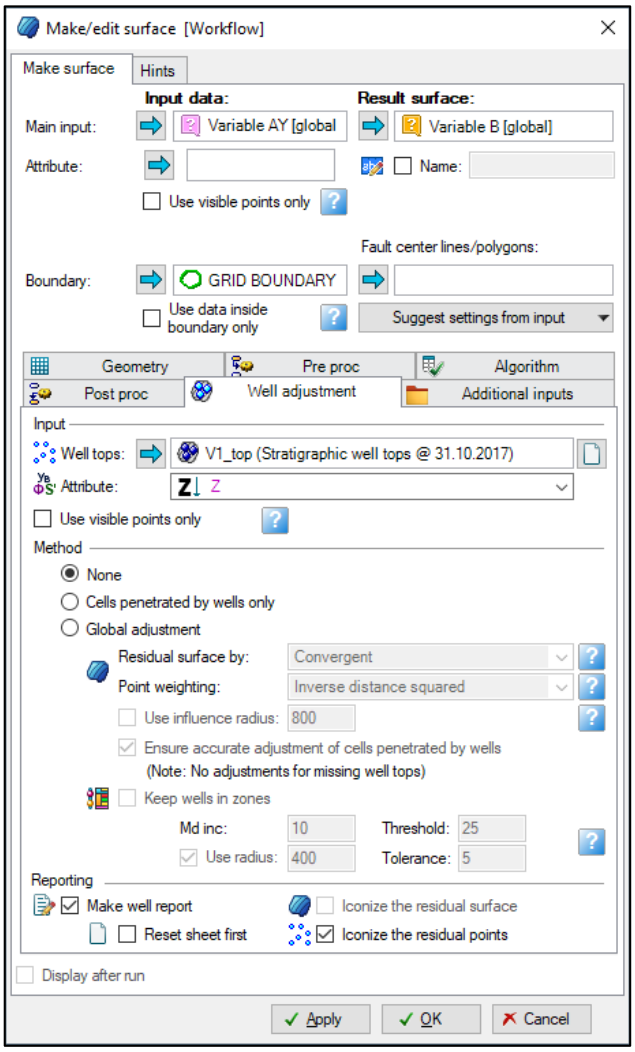

Figure 34: Operation window of Make/edit surface, showing the Well adjustment tab for V1 top surface.

As the previous loop’s outputs (namely the residual pointsets) are placed in the Input tree directly, they will be moved to a newly defined folder that is uniquid so that a transparent structure can be kept with the addition of a suffix containing the actual date generated by the *GetDate()* string operation (Step 71) (Figure 35). A unique command is applied to the Input tree in a variable so that it can be referred to: *Get input tree reference* (Utilities/Variables). And with a short loop of *For all icons in*, all the residual points are moved from the root directory to a unique user-defined folder with the use of a basic *Move* (Utilities/Housekeeping) command. Closing the if statements with *Endif* (Utilities/Statements) and the loops with *End loop* is of crucial importance so that avoid syntax errors can be avoided.

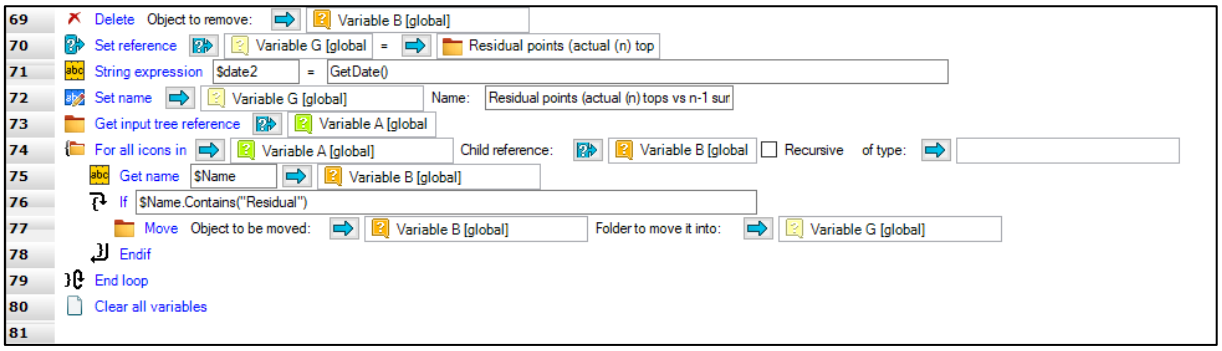

Figure 35: Steps 69-81 in the Stage 1 – Surface manipulation subworkflow belong to the same subtask as Steps 36-81.

With the ending of Step 80, all the backups and "non-invasive" operations are finished. From Step 82 the operations alter the surfaces (see Figure 36). Although the original seismic-derived surfaces are always kept intact, and copies are used for all operations (e.g., Step 90's *Copy* (Utilities/Housekeeping) command), this is a precautionary protocol allowing the user to get the unaltered input data back if any unintentional modifications occur.

Steps 84-87 are the usual housekeeping steps to clear the scene from the remnants of any previous runs so that consistency and structure can be maintained. It should be noted that backups are only generated for the final output surfaces (Step 22-34), but not for the intermediate versions so that time can be saved and transparency maintained.

In Step 88 a reference list is created using the *Set reference list* (Utilities/Variables) (Figure 37). This creates a table where the columns are different variables, while the rows represent linked input data. The next loop *For all icons in list* (Utilities/Statements) follows the reference list row by row, using the predefined variable content strictly in each loop's row.

Within the loop in Steps 90-94, the actual surface is copied and renamed, and the *Get name* and *Set name* (Utilities/Housekeeping) operations and the Replace string operator for the $Name2 variable are applied.

The *Eliminate inside* (Operations/Eliminate where) operation clears (setting to undefined) the datapoints in the depth surface within the pre-aligned irregularity polygons. This step removes the unrealistic positive and negative spikes from the surfaces. These polygons impact approximately 0.8% of the total area and are mostly outside the production license area. A further elimination is carried out so that horizon inconsistencies can be fixed (i.e., the surfaces which intersect each other without geological reason). This phenomenon occurs on the eastern flanks of the fault, affects approximately 8.2% of the total area in the A4, C1s (and A3) reservoirs, and are totally outside the production license area. These operations are handled in two consecutive manoeuvres (Step 95 and Steps 96-98).

Step 99 uses *Smooth operation* (Operations/Surface operations) with two iterations to slightly smooth the surfaces. Thus the name of the target folder in Step 90, 'Post-Smooth' (see Figure 36).

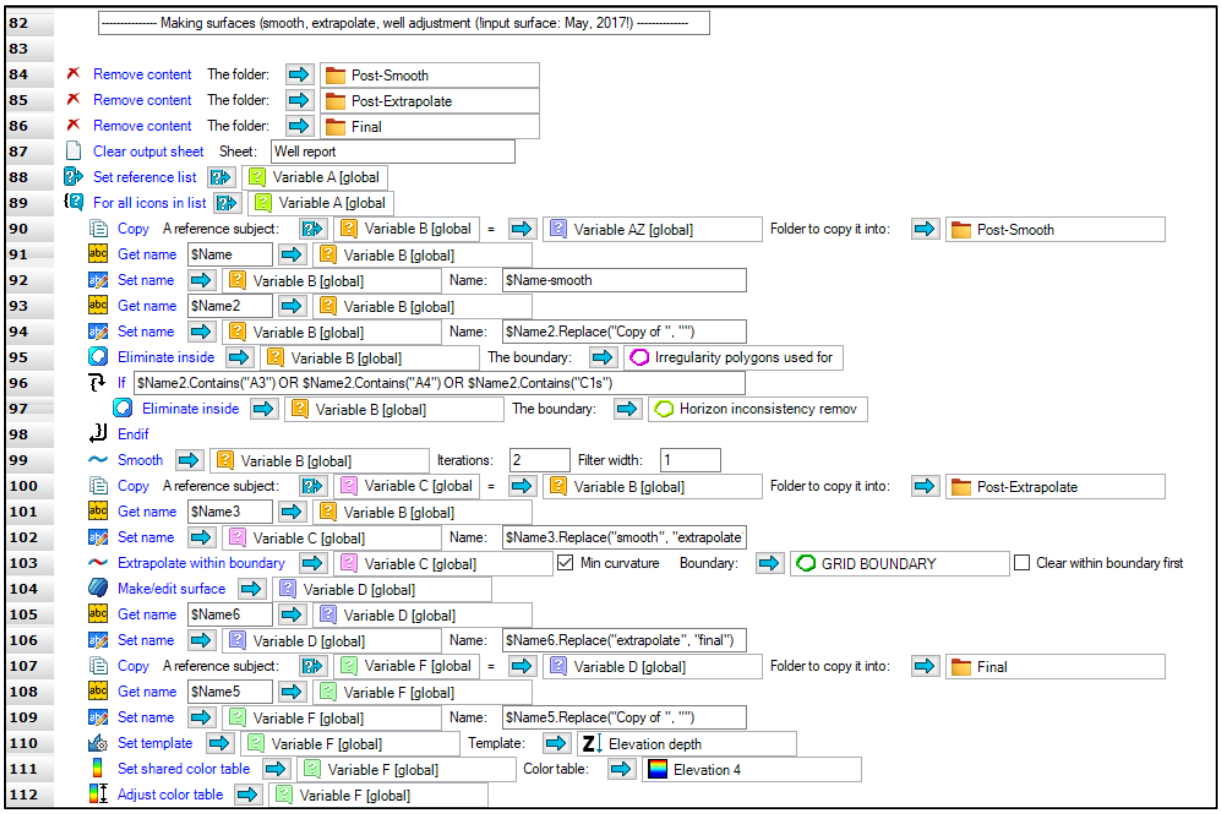

Figure 36: Steps 82-112 in the Stage 1 – Surface manipulation subworkflow smooth, extrapolate and well adjust the top and base surfaces of the reservoirs.

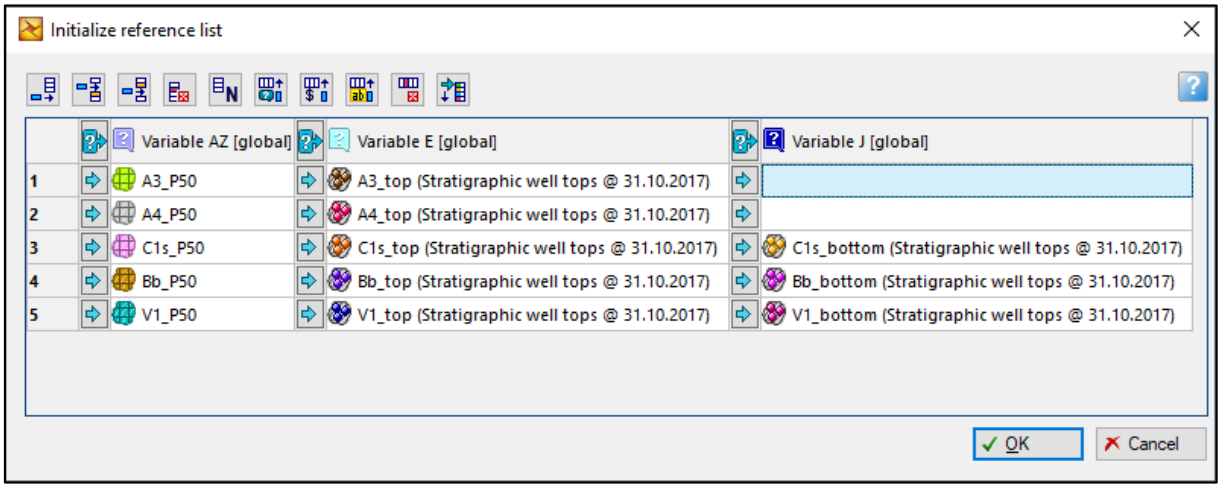

Figure 37: A reference list initialised where the first column (Variable AZ) contains the input main depth surfaces, the second column (Variable E) has the well tops for the top horizons, while the third column (Variable J) provides the well tops for the base surfaces (where applicable). It should be noted that A3 was not modelled, and A4's base is C1s's top.

Steps 100-102 create a copy of the smoothed and partially eliminated surface into a predefined folder and rename each object consistently.

Step 103 extrapolates (or interpolates) the surfaces using a minimum curvature approach (which maintains trends), using the operation *Extrapolate within boundary* (Operations/Surface operations). This step aims at achieving a consistent surface set within the future 3D grid area, which is depicted by the green polygon in Appendix VII. The previously eliminated irregularities are interpolated and, where necessary, the surfaces are extrapolated to the 3D grid boundary within the boundary.

Step 104 adjusts the main surfaces to the corresponding well tops, as a final step in the set of preparatory steps belonging to the data of the main surfaces. This step is critical as it links the soft data (surfaces) to the hard data (well tops), which has a very high impact due to the high well density (average well distance is approximately 400 metres).

Step 105-112 are miscellaneous operations where the final surfaces are renamed and moved to the target folder and are coupled with a predefined template and colour table. *Set template* (Utilities/Housekeeping), *Set shared colour table* (Utilities/Housekeeping) and *Adjust colour table* (Utilities/Visualisation & Plotting) are combined to perform this latter part.

It should be noted that all the steps from 89 to 140 are within a *For all icons in* loop. So the majority of the operations shown in Figure 36 and Figure 38 are performed for all the surfaces listed, as shown in Figure 37.

Steps 113-124 are preparatory steps for TVT and TST calculations in the next part of the subworkflow. These steps link the main final surfaces to object variables with the *Set reference* command (Utilities/Variables) as part of a nested *If* and *Else if* operation using the name of the surfaces. (Hence, it is highly important that the naming conventions are kept consistent.) For example, Step 116 is a logical yes if Variable F contains the A4 reservoir's top surface in the given n-th loop. So the A4 final surface – named A4_P50-final – will be linked to Variable N.

Steps 125-138 are two nested *If* operations; in the first part the non-seismic interpreted surfaces (the stratigraphic bottom surfaces or the V1, Bb, and C1s reservoirs) are created by the *Make/Edit surface*. The method used is Surface resampling and well top adjustment as all these surface-well intersections were identified on well logs; hence, hard data is available to guide the algorithm. Steps 132-138 serve the same purpose as Steps 113-124, described in the previous paragraph, but for the newly created bottom surfaces.

The long loop that started at Step 89 ends at Step 140, and two variable cleaning steps were added to clean the scene. It should be noted that the *Delete* (Utilities/Housekeeping) command removes the data object directly from the Input tree without further notifications.

As scripted in Steps 134-135, the bottom of Bb (also known as the top of Malinov Shale) was created based on the top of the Bb. During the quality check of the resulting surface, there were multiple areas where the Malinov Shale pinched out, although the well data suggests otherwise.

A few patching steps (Step 143-146) were added to mitigate the problem, as shown in Figure 39. *Z = Surface(x,y)* (Operations/Arithmetic operations) assigns the Z-value of the newly created surface to the original object, in this way saving several steps of additional scripting (Figure 39).

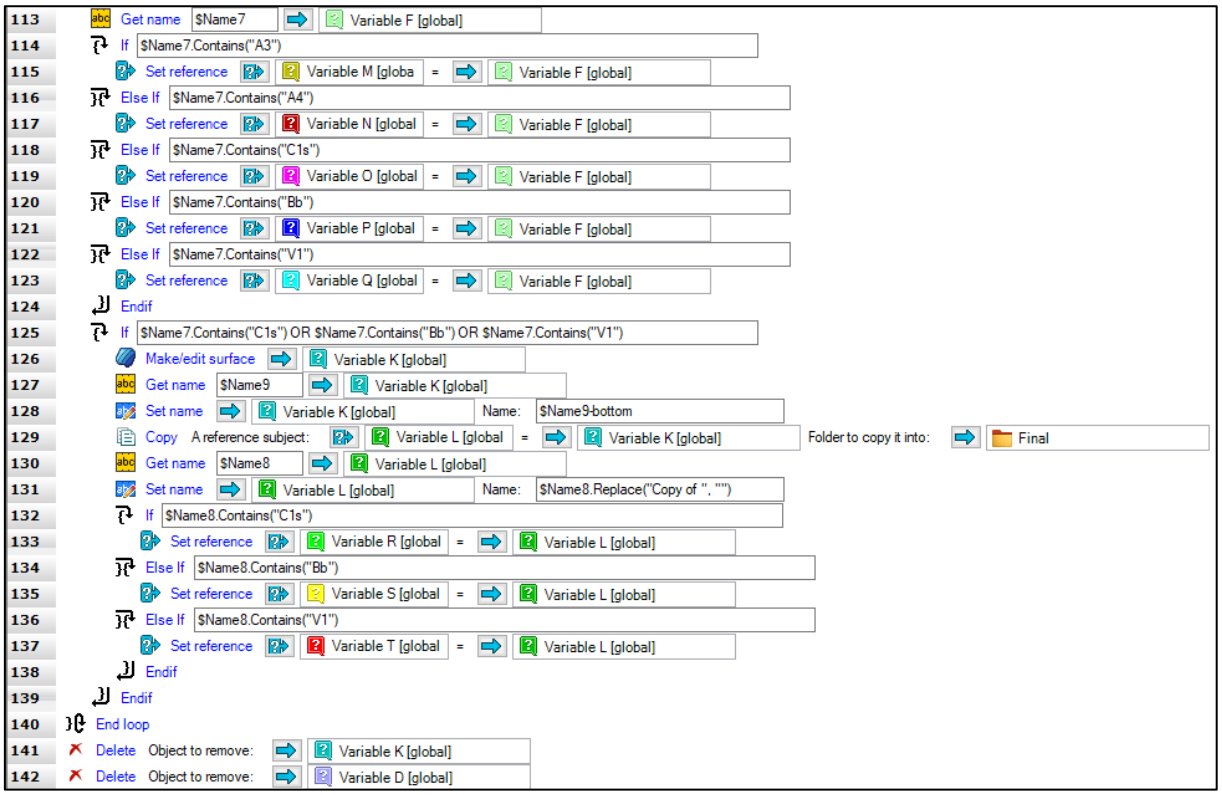

Figure 38: Steps 113-142 in the Stage 1 – Surface manipulation subworkflow are on one hand preparations for the steps beyond 142, but the key outputs are the calculated surfaces that are based on the nearest main (seismic interpreted) surfaces.

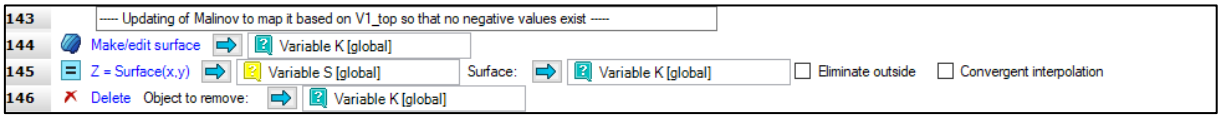

Figure 39: Steps 143-146 in Stage 1 – Surface manipulation subworkflow is a 'patch' to alter the source surface in generating the Malinov Shale top surface so that inconsistencies can be mitigated.

The main and derived depth surfaces are finished at Step 146, and are ready for further use during Structural modelling.

From Steps 148 to 166 true vertical thickness (TVT) and true stratigraphic thickness (TST) maps are calculated based on the depth surfaces (Figure 40).

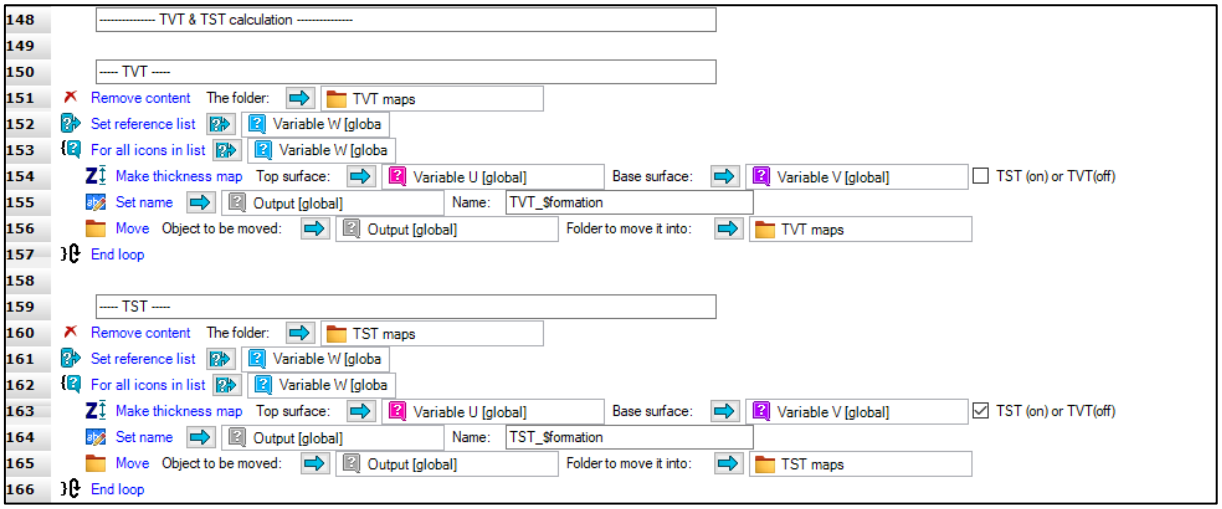

Figure 40: Steps 148-166 in Stage 1 – Surface manipulation subworkflow calculates all the TVT and TST maps of the reservoirs and separating layers.

In both cases a reference list (Figure 41) is used to define the top-base pairs for the calculations as well as the name of the actual formation, the latter as a string $variable. The variables in the list were defined in the previous steps (Steps 114-137). In the loop the thickness maps are calculated with the use of the *Make thickness map* command (Operations/Calculations). Step 155 renames the output map, which is temporarily stored in the Output variable; it has to be moved to be permanently saved, as Step 156 shows. The same set of steps is repeated for the TST calculation also; only the naming and the calculation method is adjusted.

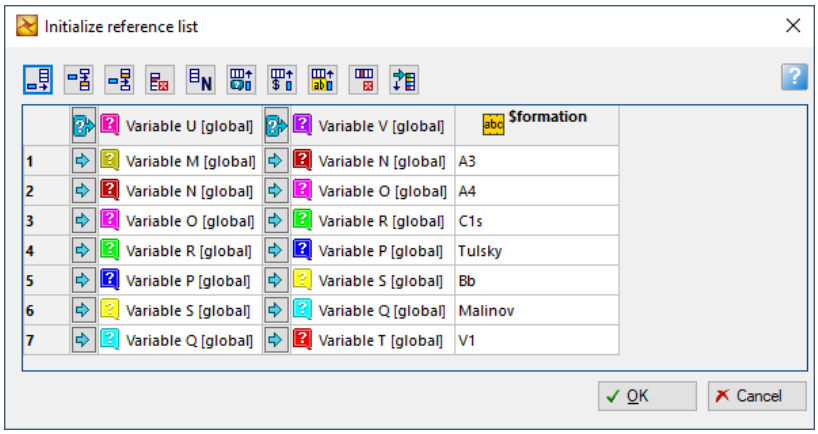

Figure 41: A reference list structuring and linking the previously defined object variables and corresponding formation names in a $variable.

The last operation in the realm of surface manipulation is the creation/update of oil-water contact polygons (Figure 42). Within these fifteen steps, both the backup of the earlier run's results and the creation of the new set is encoded. Steps 170-176 generate the backup while the loop starting at Step 177 builds the inner and outer OWC polygons for each main depth surface (top and bottom). An example of the results is shown in Appendix VII.

Like TVT and TST generation, the loop also works with a predefined reference list. The same object variables are used as in the earlier calculations, and the OWC surfaces were consistently predefined (Table 6) and are used in Step 182, *Create intersection with surface* (Operations/Convert points/polygons/surfaces), which is the key operation in the generation of the polygons. These polygons require additional manual post-processing to remove minor closures or other artifacts.

Step 188 is a reminder that unnecessary backups from the Temp folder within the Input tree need to be deleted. This step could be automatised as well, though it was deemed safer to prompt the user.

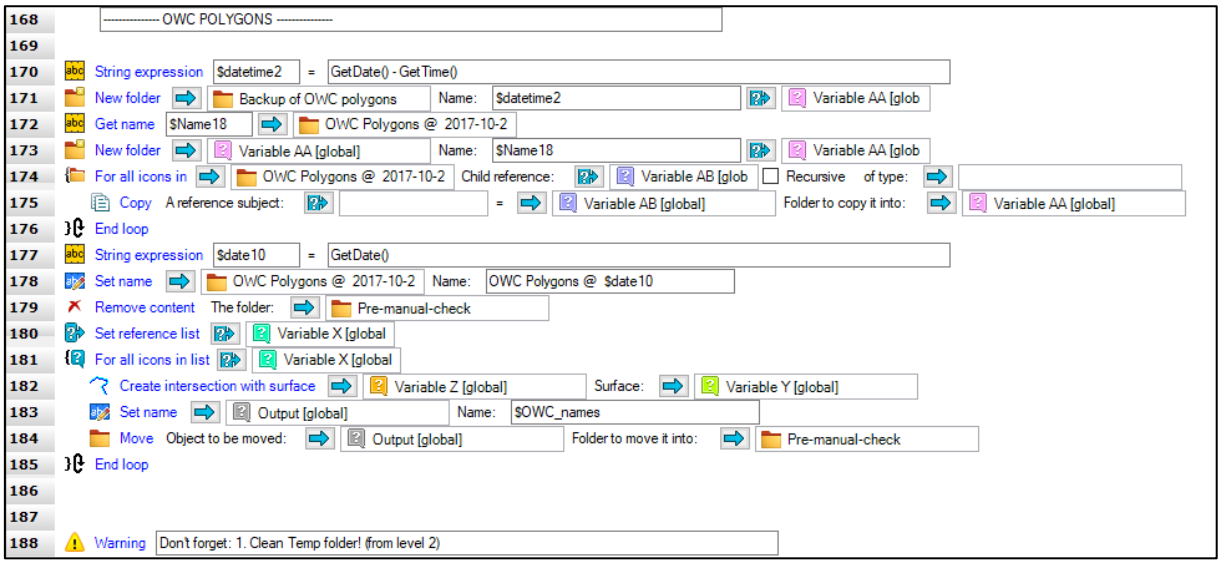

Figure 42: Steps 168-188 in Stage 1 – Surface manipulation subworkflow saves and creates the inner and outer OWC polygons for each reservoir zone.

6.3.1.1 Reservoirflag calculation

Although it is not directly linked to the surfaces, the reservoirflag calculation and update workflow was also added to Stage 1. Step 192 is a reminder that pseudo-well tops need to be added where necessary, as described earlier.

Steps 193-197 define the cut-off criteria shown earlier in Table 7, and add each of them to a $variable using the *Numeric expression* (Utilities/Variables) command (Figure 43). With this approach the values can be referenced in multiple calculations, but need to be altered only in one line when an update or a sensitivity analysis is necessary. Hence, referencing, instead of the use of static values is preferable throughout the workflow building. A similar operation is performed in Step 198.

Since the log calculations are executed in Petrel's Calculator, a few supplementary steps are inevitable (in Petrel 2015.5). The *Get calculator name* (Utilities/Housekeeping) command creates a reference via $variable to any of the objects in the Input tree or in the Model Pane. This $variable can be directly used in the calculator's input line.

Steps 202-207 are necessary for the calculator to work smoothly and without syntax errors.

In Steps 208-210 a specific subset of the wells is treated. In some of the old Bobrikovian wells (~100), there are only a very limited number of logs available, and a unique (as well as uncertain) technique must be applied that can provide some idea about the reservoir distribution in these wellbores, though porosity cannot be calculated. At this stage these logs were not updated, but were directly used as they were created prior to the in-house model building. These wells are critical since they have produced the majority of Bb's cumulative production to date

and are located uniformly over the field. Step 208, the *Set visible* (Utilities/Visualization & plotting) command, switches on Saved Search, which filters only these wells, so Step 209 – setting the $Res to undefined (i.e., deleting the former run) – and Step 210 are only applied on this subset of the total wellcount. It is critical to have the Use search filter active in these *Well log calculator* (Operations/Calculators and filters) steps so that the calculation is only applied for the filtered wells. Step 211 switches off the Saved Search with the *Set invisible* (Utilities/Visualisation & plotting) command.

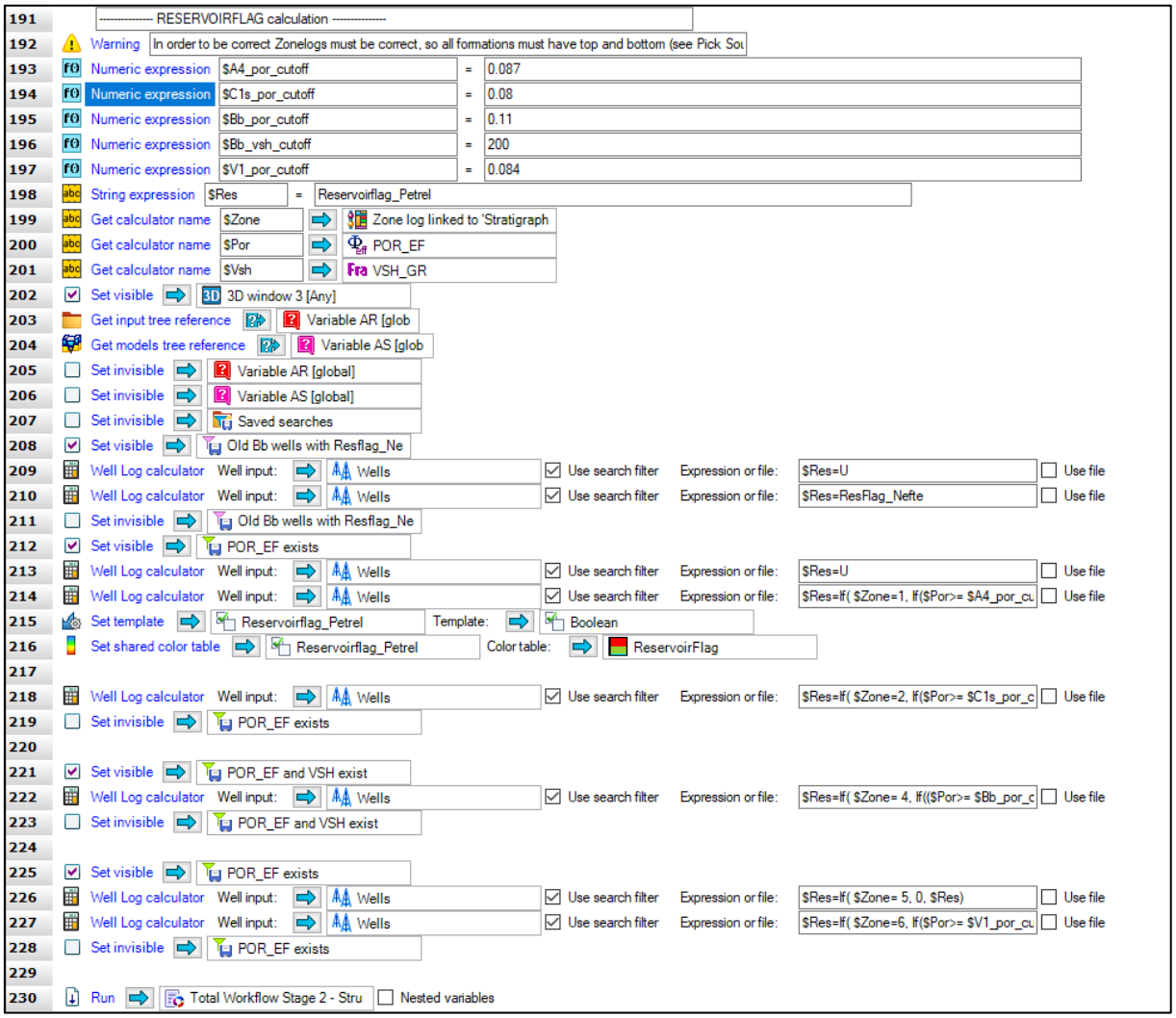

Figure 43: Steps 191-230 in the Stage 1 – Surface manipulation subworkflow are scripted to calculate the reservoirflag, i.e., a discrete log that consists of two values: 0, if the given data point does not meet the cut-off criteria; 1, if it does fulfil each criterion. This part is not related to surface operations, hence, is an outlier in this workflow grouping.

Steps 212-228 calculate the $Res (=ReservoirFlag log) for A4, C1s, Bb, and V1 respectively. In the case of Bb, VSH cut is also scripted, although in the base case only a porosity cut-off is applied. But in order for different approaches to be tested, the necessary coding was placed in the workflow to save the time associated with a possible future insertion. The general syntax used is shown in Equation 2:

$$\$Res = If\left(\$Zone = 4, If\left(\left(\$Por \geq \$Bb_{por_{cut}}\ AND\ \$Vsh \leq \$Bb_{vsh_{cut}}\right), 1, 0\right), \$Res\right)$$

The first If function is for the zonelog so that the calculation is only performed for the Bobrikovian Formation ($Zone=4). The nested If checks each datapoint to see whether both the porosity AND (logical operator) shale-content meet the cut-off criteria. An illustration of the final outcome, when the workflow is run for all four oil-bearing formations, is shown in Figure 28.

Step 230 is a *Run* (Utilities/Statements) command, which runs a chosen workflow if active. In this case it runs the Stage – Structural modelling subworkflow, so that the running of all the subworkflows chosen by the user is ensured. If the defined variable is inherited by the next subworkflow, the Nested variables tick box shall be active.

6.3.1.2 Results

A short list of the outputs and visual aids (where applicable) created during the Stage 1 – Surface manipulation subworkflow is given below:

- backups of previous run results for main and derived depth surfaces and corresponding OWC polygons;
- updated Saved Searches;
- residual report and points comparing the n-1 and n versions of main depth surfaces;
- well adjusted, fine-tuned depth surfaces of the main reservoir tops (Figure 26, Appendix V);
- derived depth surfaces of base for all reservoirs;
- updated inner and outer OWC polygons for all four reservoirs (Appendix VII);
- true vertical thickness maps (Appendix VI);
- true stratigraphic thickness maps;
- updated zonelog (Figure 28);
- updated reservoirflag discrete log (Figure 28);
- an exhaustive Petrel workflow covering the bullet points above.

6.3.2 WORKFLOW STAGE 2 – STRUCTURAL MODELLING

The Petrel workflow representing the structural modelling process contains approximately thirty rows (as in Figure 21). The upper and lower reservoirs were handled together up until the end of structural modelling (Stage 2), but they are split into two grid models (in Stage 3) due to practical reasons (time needed for updating the geomodel, time needed to run uncertainty workflows, avoidance of unnecessary updates, the number of cells being kept

to a manageable level). The geological concept suggests that the upper and lower reservoirs are hydrodynamically separated (Figure 13), hence, the related dynamic model can be decoupled; consequently, the geomodel can be in separate grid models.

The Stage 2 – Structural modelling subworkflow processes the eastern bounding fault (and processes any other faults if incorporated into the model).

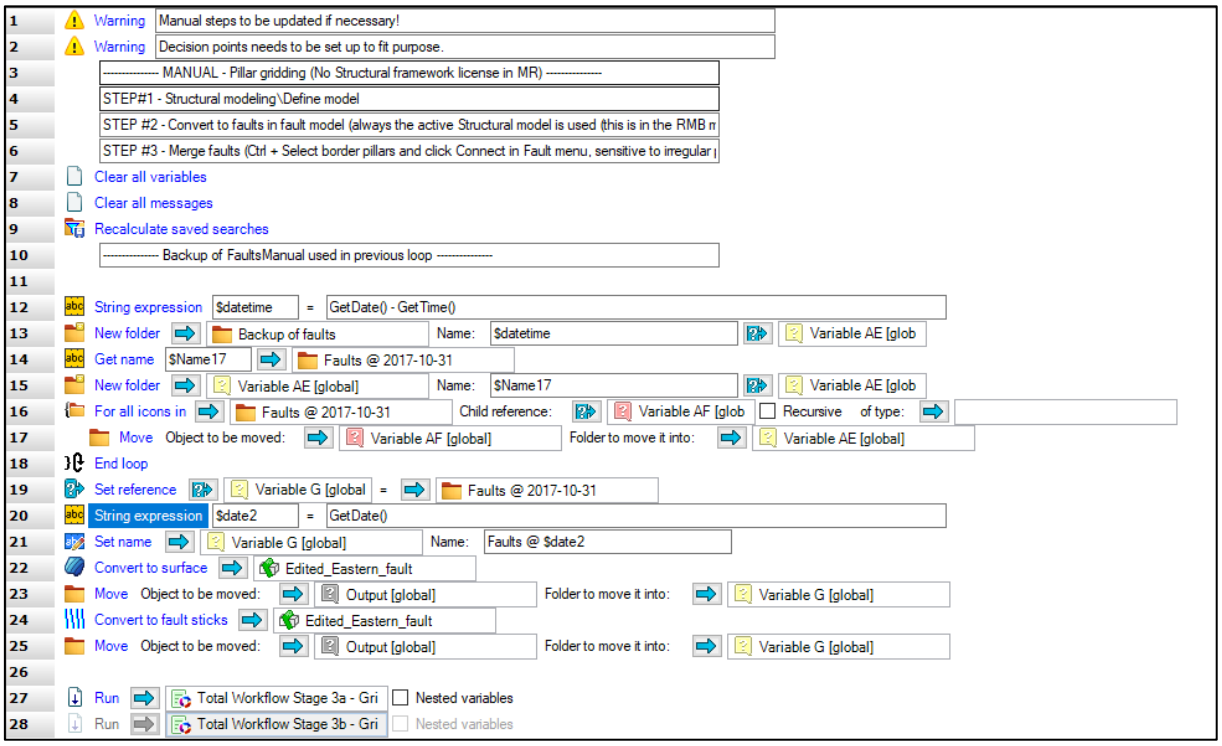

Figure 44: Steps 1-28 in the Stage 2 – Structural modelling subworkflow. The key result of this short subworkflow is the preparation of the fault(s) to be modelled.

Steps 1-9 (Figure 44) are general reminders for the user (since the fault modelling was done manually), and sets the scene by clearing variables and messages. (It should be noted that *Clear all variables* is only activated when nested variables are not used across subworkflows.)

Steps 10-18 create a backup of the former run's results regarding the eastern bounding fault, and the next steps generate fault sticks (Step 24 – *Convert to fault sticks* (Operations/Model extraction)) and the fault surface (Step 22 – *Convert to surface* (Operations/Model extraction)) from the modelled fault.

Steps 27 and 28 reflect a decision point on the to-be updated grid models, adopting the logic of Figure 21.

6.3.2.1 Results

A short list of the outputs and visual aids (where applicable) created during the Stage 2 – Structural modelling subworkflow is given below:

- backups of previous run results of surface conversion;
- (manually) updated eastern bounding fault (if update is necessary);

- updated derived fault surface;
- updated derived fault sticks;
- an exhaustive Petrel workflow covering the bullet points above.

6.4 GRID MODEL (PHASE 2)

A grid model – 3D grid model – can be described as a 3-dimensonal representation of the relevant characteristics of a reservoir with a predefined resolution. Each grid cell represents a data point for each modelled property, and its shape is dictated by the structural framework and the grid's user-defined dimensions. These data are based on geological, geophysical, petrophysical and engineering measurements, calculations and estimations. The overall goal is to interpolate to the interwell space and extrapolate beyond that the spatial distribution of pivotal properties for investigations of the current study. Mainly, the well data are the anchor points, and by extensive stochastic or deterministic (inter/extra)polation, the reservoir's spatial variability can be described with an intrinsic level of uncertainty (modified after ODEZULU et al., 2014 and SAIKIA et al., 2015).

A 3D cellular grid allows the user to do facies and property modelling, volume calculations and, eventually, run a flow simulation, do production forecasting and test field development scenarios. A high-quality grid is fundamental for all further modelling (EMERSON, 2019).

The 3D grid modelling methodology applied for the creation of an integrated structural model based on the input data described above was pillar gridding (within the corner point gridding group). Pillar gridding is the process of generating structural grids. Gridding begins with the creation of a 2D grid (skeleton) between the midpoints of the key pillars. Top and bottom grids are then generated from the top and bottom points of the key pillars (this is still a dimensionless stage, a skeleton) (SCHLUMBERGER, 2021).

This technique was used since the structure is a 'semi-layercake'; simple and nearly atectonic in the model. (A more modern method is volume-based modelling, but its advantages are not decisive in a geological environment similar to Field A's.) As interpreted during Phase 1 dynamic simulation, and as further geological analysis shows, the in-field faults have no, or a negligible effect on flow, and thus were not incorporated into the model so that needless complexity could be avoided. The method results in a structured, regular 3D grid, where the horizontal dimension of the cells is equidistant.

Zig-zag type fault handling (also known as stair-stepped – FONTANA et al., 2015) was applied – it helps regular shaped grid cells along the eastern bounding fault be obtained – to

minimise the number of distorted cells along the fault plane (SCHLUMBERGER, 2021). Distorted cells slow down the modelling run, both in the static and dynamic phases, hence, if possible, their number was controlled. Prior to fault modelling, the fault sticks were manually adjusted where necessary, and anomalous shapes and artifacts were removed, but any major change to the original dip and azimuth were avoided.

From this stage the modelling pathways are split into two 3D grid models (Figure 21) – the upper two reservoirs (A4 and C1s), and the lower reservoirs (Bb and V1), respectively – the workflows and the description of the applied methods is also split in the study (NEMES, 2022). The overlapping aspects will be described one time and merely referred to afterwards so that a significant amount of redundant information and description can be avoided.

The lower reservoirs, Bb and V1, constitute the first 3D grid model. Both the Bobrikovian and the Tournaisian reservoir layers were split into two subzones.

In the case of the Bobrikovian, the base of splitting was sedimentological change, which could be identified on the well logs throughout the region. Transgressive lagoon-estuary and barrier island facies in the lower section turned to regressional lagoon fill-type settings in the upper one (SZILÁGYI et al., 2021). Consequently, the Lower-Bobrikovian is more shaly and silty, and thus has poorer lithological properties though more favourable petroleum storage and flow capacity, while the Upper-Bobrikovian is sandier, resulting in a higher net-to-gross ratio and higher porosity and permeability values, which is favourable for fluid production (Figure 45).

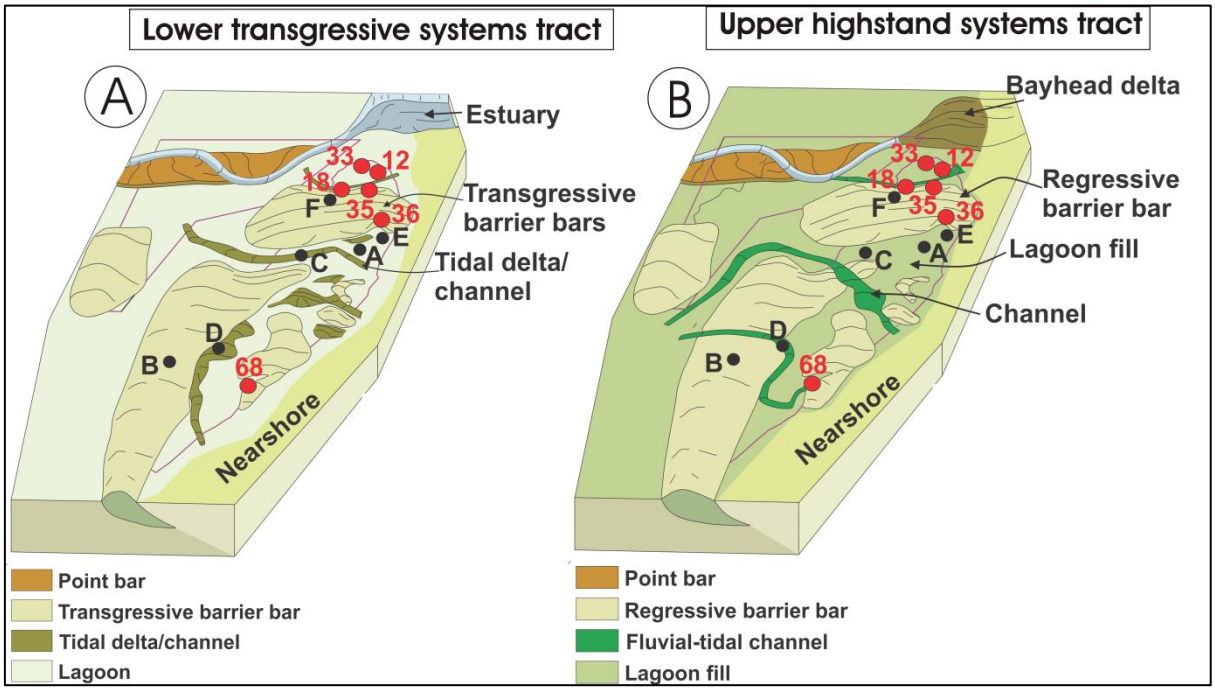

Figure 45: Block diagrams depicting the Lower (Panel A) and Upper Bobrikovian (Panel B) facies distribution. The black discs are key wells for well log analysis, while the red discs are wells with core data. Naturally, core data played a main role in establishing the facies settings of the formation (source: SZILÁGYI et al., 2021).

The subzonation of the Bobrikovian Formation is based on well log data that is validated by core descriptions. The detailed process and results were published by SZILÁGYI et al. (2021). In each well penetrating the formation and having satisfactory logsuite, the IBH (Intra-Bobrikovian Horizon) was identified and added as a well top. These well tops were later used to represent the subdivision on a 3D grid level also (Table 8). The Malinov Shale was also modelled as a separate subzone so that its existence regionally, regardless of its thickness, could be ensured.

Table 8: Number of well tops identified and used during modelling for the IBH (Intra-Bobrikovian Horizon) and ITH (Intra-Tournaisian Horizon), respectively.

Intra-horizon	Number of well tops
IBH	408
ITH	386

The subzonation of the Tournaisian Formation is based on permeability contrast; more specifically, the core data in the Lower Tournaisian shows a lower permeability range compared to the Upper Tournaisian (Figure 46). The subzonation is based on well log interpretation, similar to the Bobrikovian Formation. The number of identified well tops are shown in Table 8. The geological reason beyond the observed phenomena is most probably a loss of pore throat diameter due to secondary fluid migrations and related crystallisation processes. It is also a possibility that the Upper Tournaisian's permeability remained high relative to the lower part due to its oil saturation (WORDEN et al., 1999).

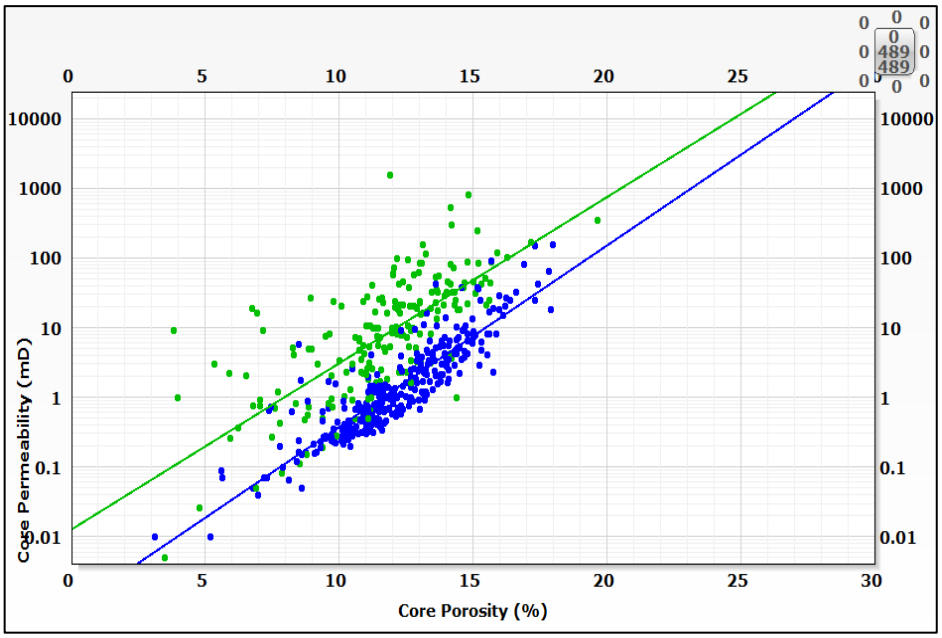

Figure 46: The blue set of dots depicts the porosity-log-permeability relationship in the Lower Tournaisian reservoir, while the green dots show the same relationship in the Upper Tournaisian. The green set shows permeability values, on average, which are approximately one order of magnitude higher (source: Petrophysical Report by N. Lavrenkova, 2017).

The upper reservoirs, the Bashkirian and the Serpukhovian Formations comprise the second 3D grid. In this case subzonation was advisable so that the cell number could be

decreased. The total thickness of the C1s is high, although only the crestal part (Figure 47) of the reservoir stores oil. Henceforth, the reservoir was subdivided and the lower part was coarser in the grid, saving a significant number of cells (cca. 75%) – and speeding up the flow modelling process – without losing valuable information.

In both cases first the main surfaces were used to create a primary 3D grid, and the main reservoir zones were consecutively subdivided into subzones.

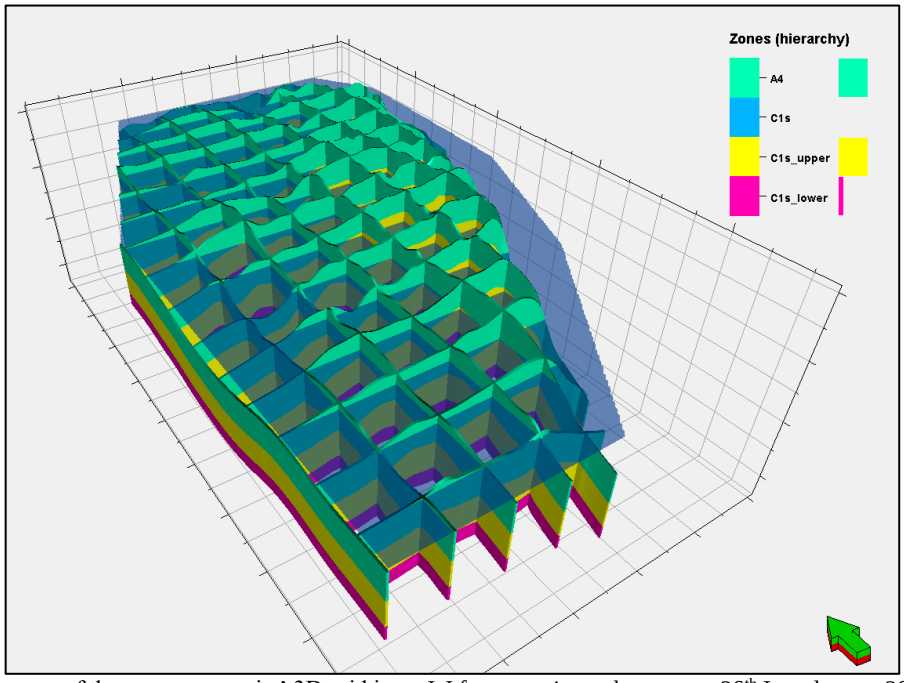

Figure 47: The zones of the upper reservoirs' 3D grid in an I-J fence section, where every 26th I- and every 26th J-direction is visualised. Z (vertical exaggeration) =18.00. The blue semi-transparent surface is the OWC_i of the Serpukhovian Formation, revealing that only the crestal part of the structure is oil-saturated.

Table 9 shows the number of cells with the corresponding average vertical resolution. Since the total reservoir thicknesses show a low standard deviation (Table 5), cell thickness is also close to permanent within the AOI of each formation.

Table 9: The resulting number of cells for each subzone and the targeted vertical cell resolution (NEMES, 2022).

Main zone	Average TVT (m)	Target vertical cell dimension (m)	Number of layers	Number of 3D cells (in simbox)
A4	37	0.6	60	5,157,000
C1s Upper	37	0.6	60	5,157,000
C1s Lower	20	6	10	859,500
Subtotal (Upper)	94	-	130	11,173,500
Bb Upper	9	0.5	18	1,547,100
Bb Lower	8	0.5	16	1,375,200
Malinov Shale	1	1	1	85,950
V1 Upper	8	0.5	16	1,375,200
V1 Lower	37	1	37	3,180,150
Subtotal (Lower)	63	-	88	7,563,600
Total	157	-		18,737,100

Vertical resolution was estimated based on the consideration that it is high enough to be able to represent the heterogeneity of the smallest objects/geological layers (RINGROSE and BENTLEY, 2015). In other terms each layer of interest is represented by a minimum of 2-4 cells.

The horizontal resolution in each case was chosen to be 50X50 metres in order to incorporate the maximal number of wells in the property modelling and to not have to filter them due to the several-wells-in-one-cell phenomena described in the chapter *Preface to workflow creating and editing*. In addition, the high horizontal resolution makes the lateral heterogeneity (e.g., in the Bobrikovian Formation) more emphasised in the 3D model.

In the reservoir geological 3D grid, there was no rotation angle applied during grid creation – due to the lack of a distinctive orientation in permeable pathways providing flow capacity – so the main (default) direction of N-S was followed.

The 3D grid area was clipped (to decrease cell number) with a predefined polygon, depicted as AOI. The polygon is shown in Appendix VII with a solid green line.

6.4.1 WORKFLOW STAGE 3A AND 3B – GRID MODELLING

The Stage 3A – Grid modelling subworkflow describes the generation of the lower reservoirs' geocellular grid (without properties). It consists of 88 steps.

The Stage 3B – Grid modelling subworkflow describes the generation of the upper reservoirs' geocellular grid (also without the properties yet) and consists of 68 steps. The two workflows are very similar and the concept behind them is identical, though the number of steps is different. The reason for this phenomenon resides in the number of subzones. In the upper reservoirs' grid only the C1s reservoir is subdivided, while both reservoirs are in the lower one. Since the Stage 3A subworkflow is of slightly greater complexity, the description is based on that.

A semi-detailed (Level 1) overview of the subworkflow is given in Figure 48 as a guidance prior to the introduction of the step-by-step description.

Stage 3A – Grid modelling subworkflow's steps (Figure 21) can be split into six groups, as indicated in Figure 48. A general 'housekeeping' and the creation of backups is followed by grid modelling and a set of steps aimed at the quality checking of the created grid. Subsequently, 3D grid's layering is performed, and the predefined OWC_i values are linked to the corresponding grid zones.

In the following part the step-by-step (Level 2) description of the subworkflow is given, beginning with housekeeping as Step 1.

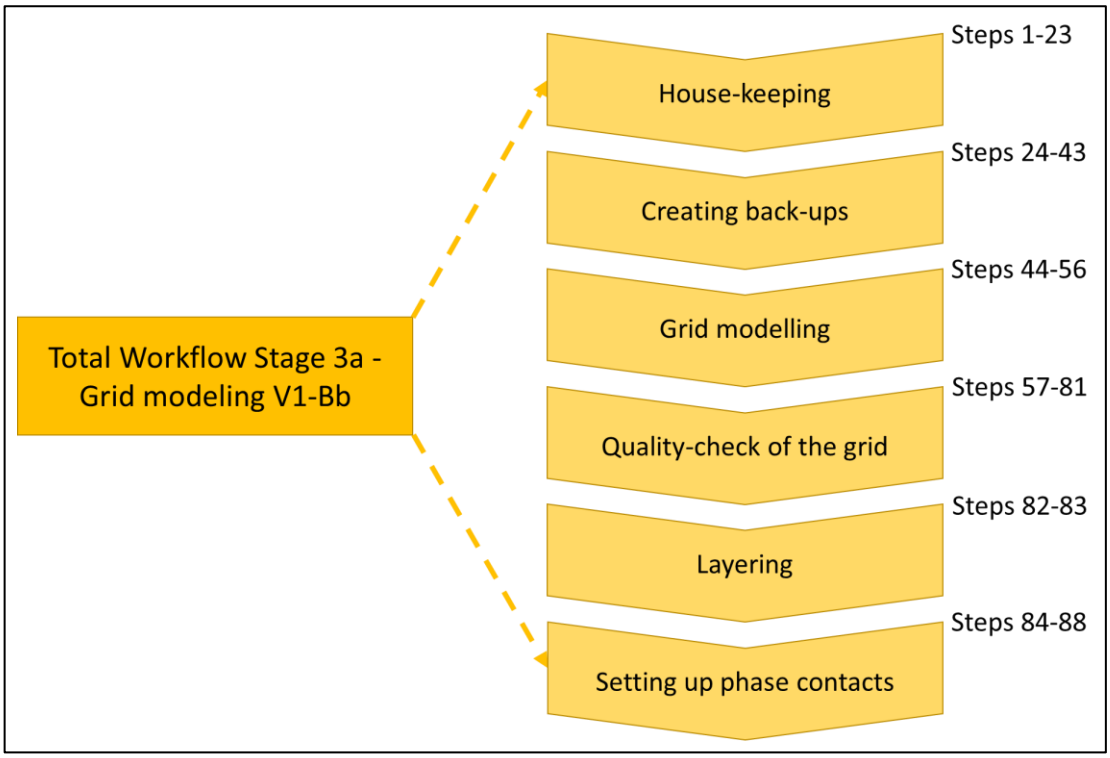

Figure 48: A semi-detailed (Level 1) breakdown of the main groups of steps in the Stage 3a – Grid modelling subworkflow (V1-Bb) indicating the steps belonging to the given group. Each step is introduced in the subchapter in detail (Level 2). The Level 0 overview of the subworkflows is given in Figure 20.

Steps 1-3, as shown in Figure 49, are general housekeeping operations. As in-between subworkflow nested variables are not applied, it is safe to execute *Clear all variables*, and since it is not obligatory to rerun all the subworkflows – since they are modular – executing *Recalculate saved searches* is also a necessary step.

The next Comments (Steps 6-8) are for the user, as the grid boundary polygon must be of a 'grid boundary' data type in order for it to be attachable to the next steps. In addition, it is critical to visualise the faults in a 2D window for the *Pillar gridding* operation so that error messages and aborted runs can be avoided.

Steps 10-22 is a *For all icons in* loop with a nested *If/Else if* function, where the depth surfaces are linked to global variables Bb top, Bb bottom (or Malinov top), V1 top and V1 bottom. For instance, the V1 top is added to Variable I in Steps 19-20.

Step 21 closes the nested *If/Else if* with an *Endif*, while Step 22 closes the loop with an *End loop* command. Both are compulsory as per the syntax of the respective operations.

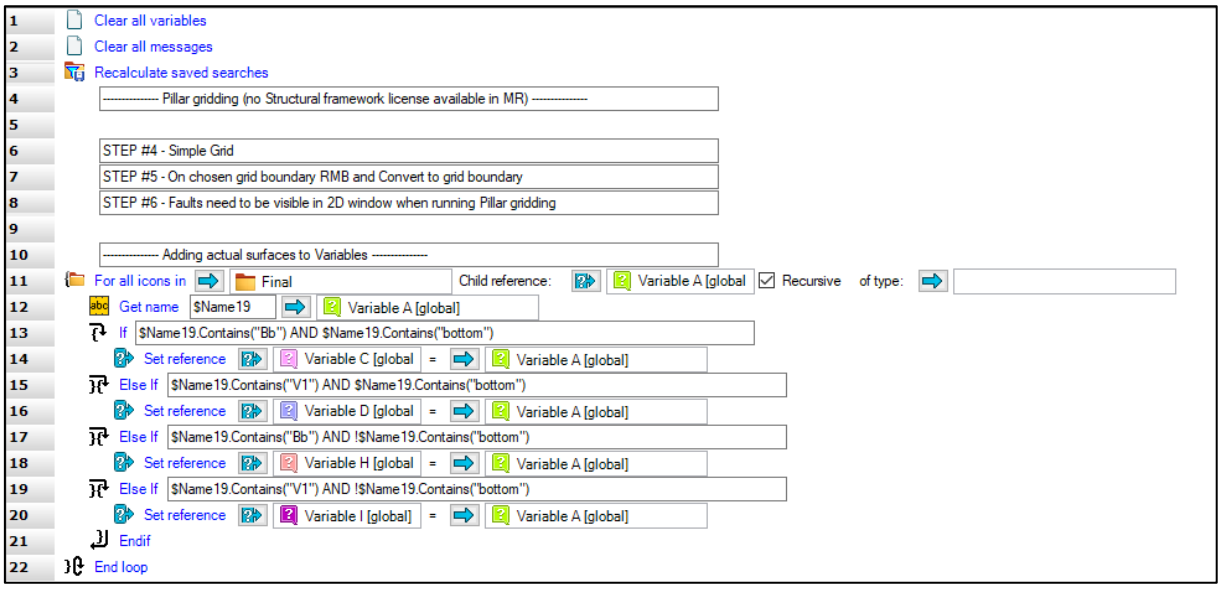

Figure 49: Steps 1-22 in the Stage 3A – Grid modelling subworkflow are about general housekeeping and adding the to-be used depth surfaces to object variables.

Steps 24-43 (Figure 50) create copies of the previous subworkflow run's quality-checking outputs, more specifically, the residual point sets comparing the input depth surfaces and the outputs of the grid modelling steps discussed in the next paragraphs. If, during an update, an anomaly occurs, having the backups of previous runs can be advantageous so that investigations and analyses can be performed. The practical logic behind this is analogous to the identical jobs in the Stage 1 – Surface manipulation subworkflow, that is, new folders are created that are distinguished with a date and time stamp from the *Getdate()* and *GetTime()* string expressions, and the *Set name* command is used to finish the naming. The working folders are emptied after the backups are done with the *Remove content* command in Steps 34 and 42.

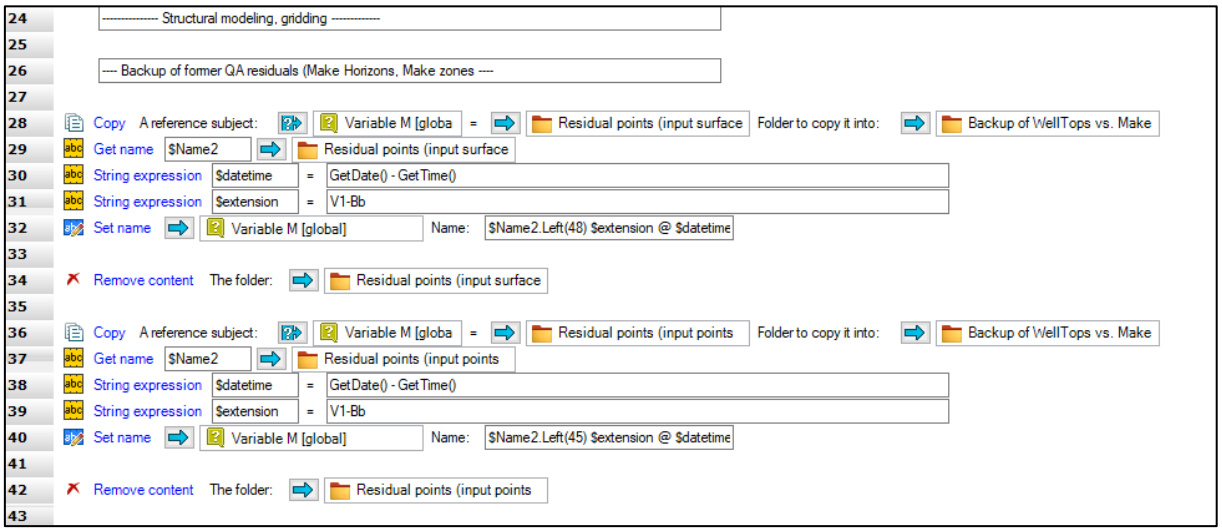

Figure 50: Steps 24-43 in Stage 3A – Grid modelling subworkflow create backups (or safe copies) of the residual points created during the grid modelling in the previous run of the subworkflow.

Steps 44-56 (Figure 51) are the core of the present subworkflow, as these few operations generate the frame of the 3D geocellular model and the 3D structural grid. Only vertical layering (i.e., setting up the vertical resolution and methodology) is covered below.

Steps 46-48 cover an obligatory task so that a smooth pillar gridding run can occur. In the used version of Petrel pillar gridding's prerequisite is the visualisation of the faults in a 2D window when running the operation. In this case it is advisable to have a separate folder for saved windows that are used in the workflow so that accidental deletion can be avoided.

Set visible activates and brings forward the 2D window, which is saved for solely this purpose. To ensure that nothing is visualised, *Clear displayed objects* (Utilities/ Visualisation & plotting) is run for the active window, and only after that is the fault visualised.

Step 50 defines which 3D grid the adjacent operations are applied to. In this case, it is the V1-Bb grid (i.e., the lower reservoirs). (It should be noted that the workflow does not create new 3D grids, but overwrites existing ones.)

Step 51, *Make simple grid* (Processes/Utilities), is redundant; it is not critical in the workflow. (It is a part which remains from the trial-and-error runs.) It is an alternative to the pillar gridding process, when you create 3D grids with no faults (SCHLUMBERGER, 2021). Creating a simple 3D grid in this manner gives the user access to the more rigorous volume calculations without the need to go through the pillar gridding and make horizons processes (SCHLUMBERGER, 2021).

Pillar gridding (Processes/Corner point gridding) is necessary due to the eastern bounding fault. Step 52 is the start of the pillar gridding process, which will result in the 3D geocellular model. In this process the skeleton of the grid is created, fault handling is set up, the grid boundary is defined and the I and J (horizontal) resolution is set. The output is a dimensionless skeleton, with three pseudo-surfaces and a top-mid-base which are not linked to geology, but are only needed for the following steps. As this is a very delicate process, it is not always recommended to run it via workflow, and it requires additional attention and quality checking so unwanted results can be avoided.

The real geological vertical layering of the grid is defined in three steps. The first is Step 53, *Make horizons* (Processes/Corner point gridding), which is usually based on the seismic interpreted horizons. In the current model the non-seismic interpreted horizons are also added, namely, the top of the Malinov Shale and the bottom of the Tournaisian Formation (Figure 52). In this step the model horizons are created, hence, becoming the coarsest vertical layering of the grid. The well tops are used and honoured throughout the process as hard data. To be able to validate the goodness of the process well tops, an output horizon comparison is run, and the differences for each well top are calculated as a residual point.

Steps 54-55 are the middle steps in defining the vertical layering of the grid. *Make zones* (Processes/Corner point gridding) inserts the subzonation into the horizons. In the current example in Step 54, the IBH (Intra-Bobrikovian Horizon) horizons are added to the grid, and

the same thing occurs in Step 55 for the ITH (Intra-Tournaisian Horizon) horizons. In this case the sole input to the intra-horizon generation is the well top sets. The goodness of the adjustment is critical, and a quality-check is done as it is in the main horizons.

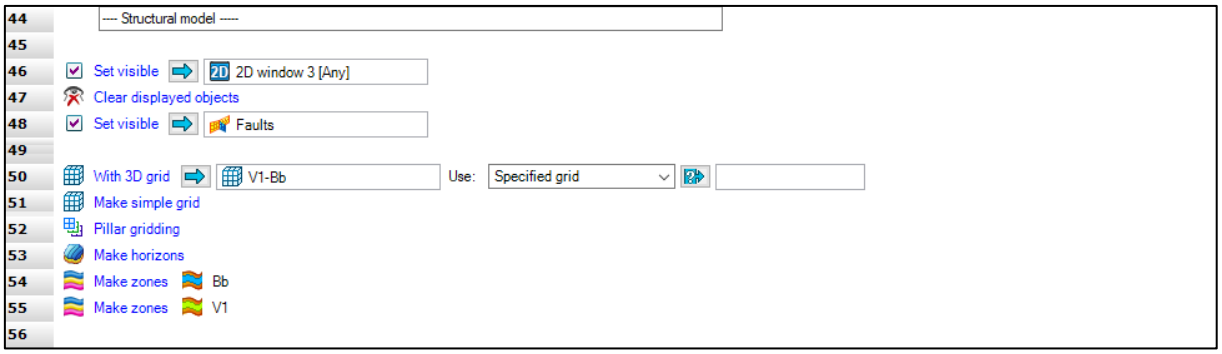

Figure 51: Steps 44-56 in Stage 3A – Grid modelling subworkflow frame the grid model, create/edit the grid, and make horizons and zones.

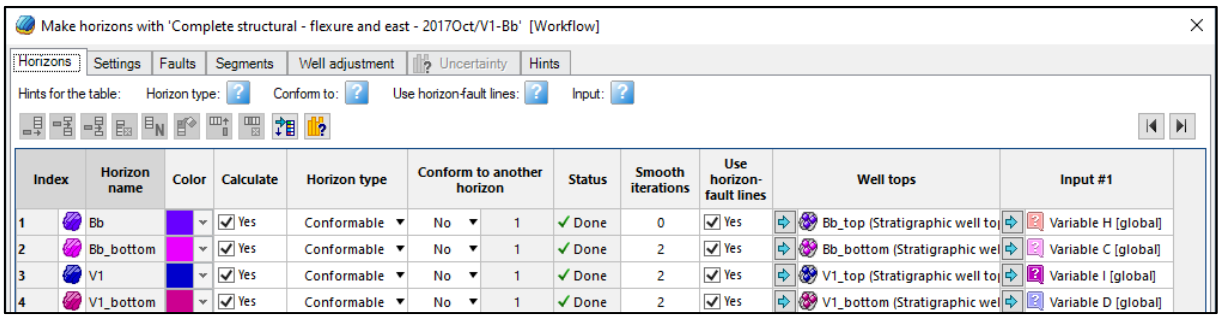

Figure 52: The Make horizons window with the Horizons tab. The key input data for the horizon modelling are the previously finalised depth surfaces for each horizon as well as the well tops that are honoured during the process.

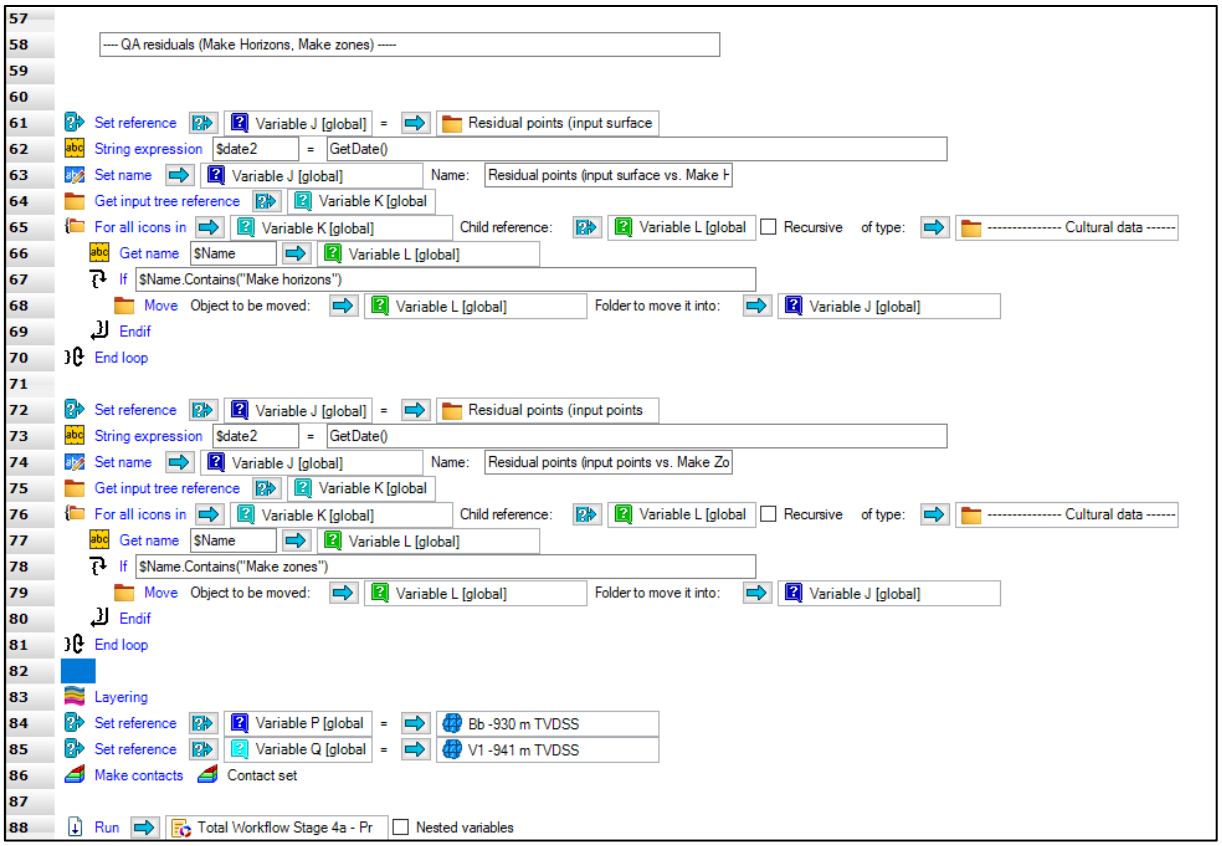

Figure 53: Steps 58-88 in the Stage 3A – Grid modelling subworkflow describe the quality-check of the newly created horizons and zones, and subsequently includes the layering and the corresponding OWC_i values which are linked to the reservoirs. The last step (Step 88) provides continuity to the next subworkflow.

Figure 53 shows the last section of this subworkflow, where Steps 61-70 are a quality-check; more specifically, the residual point sets created during the *Make horizons* job are moved from the Input tree to a predefined, date-stamped folder. Steps 72-81 have the same script as 61-70, except for the output residual points of the Make zones job.

Step 83, *Layering* (Processes/Corner point gridding), is a key step as this process sets up the vertical layout and number of layers, that is, the thickness of the cells or vertical resolution. In Field A all the reservoirs were set up to be subdivided with a proportional approach, where the number of layers is defined for each pillar (or column) of the 3D grid; hence, the exact thickness varies based on the local TVT. Although the thickness is moderately heterogenous, this does not cause extreme deviations. The quantitative figures are shown in Table 9.

The main principle in the layering was to make the grid capable of representing the reservoir layer's effective (net) sections. The Bobrikovian Formation is very heterogenous, so the vertical resolution was targeted at around 0.5 metres, while the Upper Tournaisian has lower heterogeneity but is of upmost relevance, hence, the fine grid. In the Lower Tournaisian, on the other hand, the resolution is one metre/cell on average.

The Bashkirian and the Upper Serpukhovian are, on average, 0.6 metres fine vertically in the grid due to their heterogeneity (Table 9).

The Malinov Shale and the Lower Serpukhovian are coarse so that the total cell number is decreased. The former is one cell thick, while the latter is ten cells, which results in six metres of layer thickness, on average.

Steps 84-85 solely link the OWC_i surfaces of the Bobrikovian and Tournaisian to object variables.

Step 86 is an operation using the *Make contacts* (Processes/Corner point gridding) command to link the OWC_i values with the corresponding reservoirs or reservoir segments in the 3D grid.

Step 88 is a turning point, where the running of the next subworkflow starts if activated, following the logic of Figure 21.

Stage 3B – Grid modelling subworkflow is very much like 3A, and it contains the same steps for the Bashkirian and Serpukhovian reservoirs.

The Bashkirian is modelled as one zone, while the Serpukhovian is subzonated with a ratio of 7:13, that is, 65% of the Serpukhovian belongs to the lower part. It is not a geological subzonation, but is based on modelling considerations. The split ratio is based on OWC_i, so that the oil cap is securely in the fine resolution upper section.

The eastern bounding fault is similarly handled as in the lower reservoir with the use of zig-zag handling; its horizontal resolution is also 50X50 metres.

Due to the high degree of similarity to the 3B subworkflow, 3A is not described in detail here.

6.4.1.1 Optional subworkflows

There are two optional subworkflows, one for each 3D grid, indicated by the grey background and dotted connectors in Figure 21. The Optional step – Cells penetrated by multiple wells subworkflows are not described in detail as the rights do not belong to the author, although their role is unique and is introduced shortly.

In Field A the well density is high, and the average well distance is 400 metres – and the wells are drilled from well pads, with 2-6 wellheads located within a few metres of each other – in some cases the well tops are less than 50 metres from each other. This can result in multiple wells penetrating the same grid cell(s), which can cause errors or misleading results in the property modelling. Hence, these well pairs were identified and – as mentioned before in the Preface to workflow creating and editing subchapter – investigated pair by pair.

The workflow consists of 21 steps and uses a loop, which results in a 3D parameter showing, for each cell, how many well trajectories penetrated it. Consequently, the grid can be filtered, and the well pairs identified. In the lower reservoirs three wells needed to be filtered due to this phenomenon, while in the upper reservoirs nine wells (the former three wells overlap naturally) required filtering.

6.4.1.2 Results

A short list of the outputs and visual aids (where applicable) created during Stage 3A and 3B – Grid modelling subworkflows is given below:

- backups of previous run results of residual points for both the main zones and the subzones;
- two 3D grids ready for further modelling with 50X50-metre horizontal resolution and fit-for-purpose vertical;
- quality-checked (residual points) model representation of surfaces;
- linked initial fluid contacts to corresponding reservoir layers and segments;
- wells filtered manually where multiple ones went through the same cells;
- an exhaustive Petrel workflow covering the bullet points above.

6.5 ROCKTYPE AND PROPERTY MODELLING (PHASE 2)

With the creation of the empty 3D grid, the next step is the distribution of the petrophysical parameters to the interwell space – where each grid cell represents the a value for each parameter – while preserving realistic reservoir heterogeneity and matching the well data (SCHLUMBERGER, 2021). There are several approaches available in terms of algorithms, approaches and methods. The palette of these is comprehensively described in detail by RINGROSE and BENTLEY, 2015.

Prior to any modelling exercise, either facies or petrophysical property modelling well log upscaling is necessary, which blocks the log resolution to the grid's vertical resolution, as shown in Figure 16. (Although with the exponential growth of computing power and algorithms, the need for upscaling may fade away soon.) This step is basically an averaging operation, which can be biased to facies/rocktype. It is applicable both in the case of discrete and continuous parameters, but with different methods. In the case of discrete parameters, the 'most of' method is widely used, which assigns the value to the given cell and which has the highest ratio in the given depth interval on the well logs. It is used for Bobrikovian's reservoirflag parameter in the current modelling workflow.

Most of the statistical methods and the probability theory are also founded in normal distribution. Hence, data transformation sequences are inevitable prior to the running of any modelling algorithms so that the actual input dataset is normally distributed and spatial trends are removed.

For stochastic modelling a data transformation sequence is set up that splits the input (upscaled) well date into a trend component and a residual component. The trend component (lateral and vertical) is the result of geological processes, while the residual is white noise that cannot be explained by geology. The aim of the data transformation sequence is to arrive at a normally distributed residual component with an average of zero (EMERSON, 2019). The residual component is modelled using variogram models and correlations (if any); after the modelling sequence, the transformation sequence is reversed and the trend components are reimplanted. Data truncation can be also added to the transformation sequence, ensuring that neither the input nor the output contains outlier data points (e.g., negative or extremely high porosity). The sequence of the transformation steps is considered individually for each parameter as it has an impact on the result. Input truncation is usually the first step, with normal score transformation being the last in the sequence.

Conventionally (like in Phase 1), the facies modelling precedes the petrophysical property modelling, as the latter is usually biased to the former (ZAKREVSKY, 2011). In the case

of Bobrikovian, this traditional approach is used since in approximately 100 wells only reservoirflag could be interpreted based on the limited legacy logsuite, so to honour these the discrete facies modelling method was chosen. In all the other formations a relatively novel approach, total property modelling, was applied.

Total property modelling (TPM) is more general than the net-to-gross method (RINGROSE, 2008). While the net-to-gross method models first the discrete reservoir flag, the TPM first models the petrophysical properties, and the cut-off is applied on the grid, hence, providing a higher degree of flexibility in model updates and sensitivity analyses.

In the current model for both rocktype and property modelling, stochastic methods are applied, just as in Phase 1 (NEMES et al., 2021). For the rocktype modelling, pixel-based indicator simulation is applied, and 2D trend maps are used to guide the distribution. Indicator simulation method uses indicator variograms to create the model architecture by assigning the model element type on a cell-by-cell basis. The indicator variogram is simply a variogram that has been adapted for discrete rather than continuous variables (RINGROSE and BENTLEY, 2015).

The property modelling workflow will be described in a slightly different way than the previous subworkflows; modelling theory will be described in parallel with the workflow's introduction.

6.5.1 WORKFLOW STAGE 4A AND 4B – PROPERTY MODELLING

Prior to the introduction of the details of the workflow, a fundamental difference between Phase 1 and Phase 2 must be noted. A complete petrophysical reinterpretation was performed, which involved revisited well picks, all available core data and manual interpretations for old wells where there weren't any antecedent usable logs. Consequently, the cut-off values were also adjusted, and the statistical analysis had to be updated prior to 3D property modelling.

Since there are two distinct property modelling subworkflows, one for each reservoir pair, the more complex one (i.e., 4A) is used to illustrate the subworkflow (Figure 21). Stage 4A and 4B – Property modelling subworkflows contain all the steps, from a blank 3D grid to a fully flagged geomodel ready to be used for volume calculation and flow modelling initialisation.

4A describes the process for the Bobrikovian and Tournaisian reservoirs; 4B, the upper reservoir pair. 4A consists of 205 steps, while 4B comprises 144 steps. The difference is due to the differing modelling approach in the case of Bobrikovian compared to the other three formations. As described above, in the case of Bobrikovian, first the reservoirflag ("rocktype") is modelled and, subsequently, the petrophysical parameters are constrained by the

reservoirflag. For all of the other reservoirs, the TPM approach is used, hence, 4A is used to illustrate the process.

A semi-detailed (Level 1) overview of the subworkflow is given in Figure 54 as a guidance prior to the introduction of the step-by-step description.

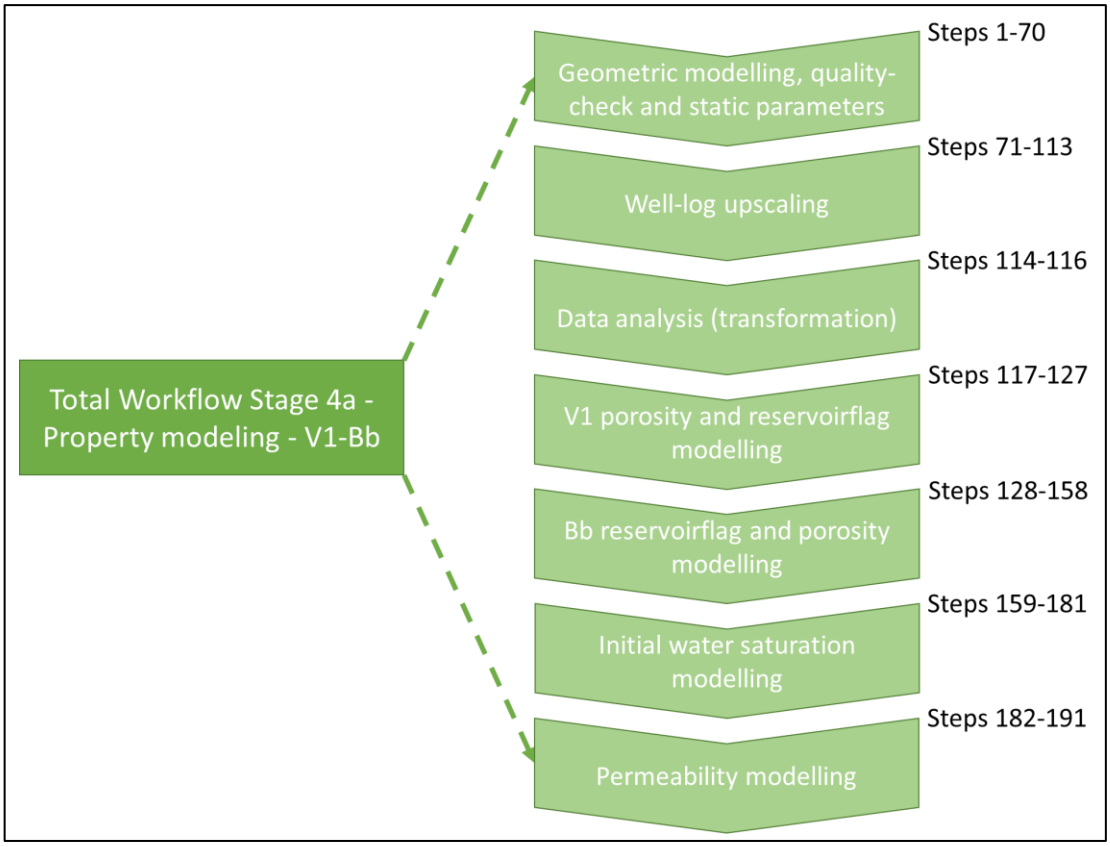

Figure 54: A semi-detailed (Level 1) breakdown of the main groups of steps in the Stage 4a – Property modelling subworkflow (V1-Bb) indicating the steps belonging to the given group. Each step is introduced in the subchapter in detail (Level 2). The Level 0 overview of subworkflows is given in Figure 20.

Stage 3A – Property modelling subworkflow's steps (Figure 21) can be split into seven groups, as indicated in Figure 54. The first group includes the creation of geometric properties, auxiliary parameters and quality-checking properties. It is followed by the well log upscaling process, which transforms the log-resolution to the resolution of the 3D grid.

A short step (at least in terms of subworkflow steps), but one of utmost importance, precedes the actual property modelling – the data analysis. This step ensures the transformation of input data to the statistical realm of the applicable algorithms.

Consequently, porosity and reservoirflag are modelled in the V1 formation and, in a separate loop, are modelled in the Bb formation. The distinction is necessary due to the differing modelling approaches for the two formations.

The last two groups encompass the initial water saturation and the permeability modelling.

In the following part the step-by-step (Level 2) description of the subworkflow is given, starting from Step 1.

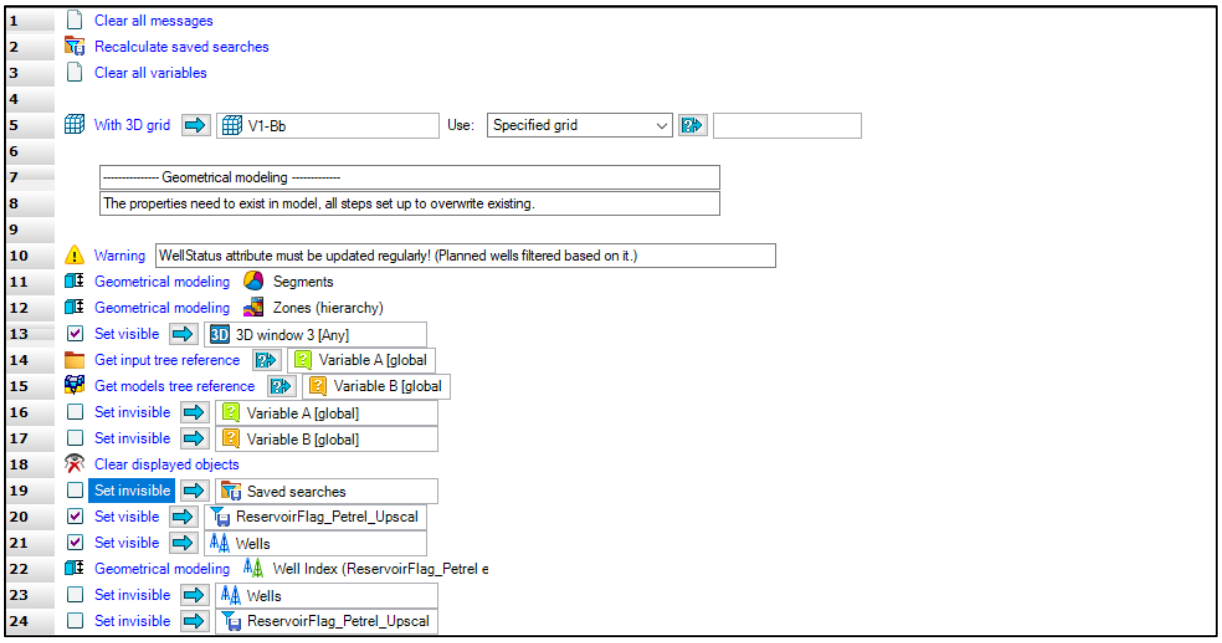

Figure 55: Steps 1-24 in Stage 4A – Property modelling subworkflow represent the first third of the geometrical modelling. The first part is comprised of the general housekeeping steps, while from Step 5 Geometrical modelling starts.

Steps 1-3 are general housekeeping steps, enabling the user to start with a clean sheet, while Step 5 defines the 3D grid where the successive operations will be performed.

From Step 7 the first subsection, Geometrical modelling, starts, which creates a set of properties representing general grid properties such as depth of the grid cell's central point, zone index and cell volume. Each cell gets a numerical value corresponding to the selected system variable. These properties are important in processes such as volume calculation and arithmetic operations, statistics and filtering on petrophysical properties (SCHLUMBERGER, 2021).

The presented workflow is built in such a way where the target properties are pre-existing, and in each rerun of the workflow the values within the properties are overwritten (not recreated), but the 'cod' remains the same; more specifically, each property present in the workflow is created during the initial construction of the property model and the workflow.

Step 10 *Warning* is a reminder to the user that the well attributes must be consistently updated since the attributes are used for Saved searches, and those define the list of wells subject to current operations and processes. Here it is worth reemphasising the crucial need for a perpetually clean and consistent dataset, which is the basis of a smooth and spotless run that does not miss valuable information due to a lack of fundamental setups.

Steps 11-12, *Geometrical modelling* (Processes/Property modelling), assign Segments and Zones discrete parameters. Segments indicate areas of the grid separated by faults, that is, show two segments in the grid of interest, while zones represent the formerly created zones and subzones in a hierarchical order.

Steps 13-24 are preparatory steps for the creation of the first of two Well Index properties. The calculation is based on Saved Search indicated in Step 20 (Figure 55). Each cell penetrated by a well that has reservoirflag calculated (or defined) and is to be upscaled will have a unique, discrete property value, meaning that in this step the wells that are not in the set of inputs for further modelling are filtered out. The last steps involve cleaning the scene (3D window) for the generation of the second Well index property. It is critical that windows used during the workflow must not be deleted so that syntax errors during the running of the workflow can be avoided.

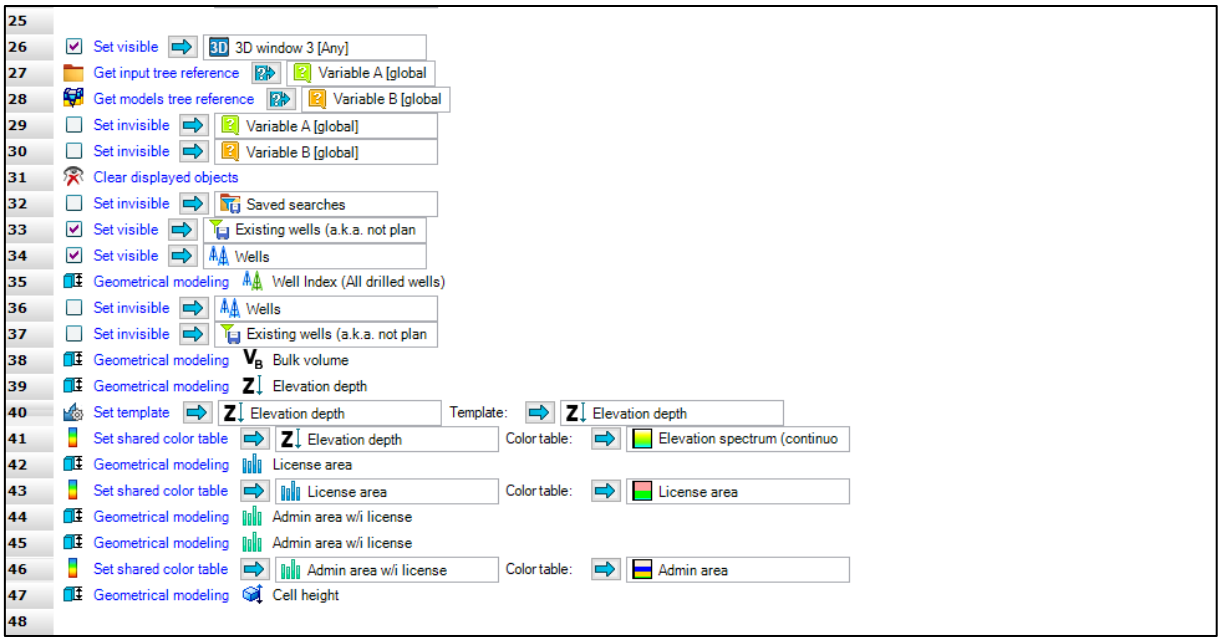

Figure 56: Steps 25-48 in the Stage 4A – Property modelling subworkflow represent the second third of the geometrical modelling. All the auxiliary properties are created to support the further modelling steps.

Steps 26-37 create the second Well index parameter, which assigns a unique value to each cell penetrated by a drilled well (Figure 56). All the physically existing wells are in the list of this Saved Search; naturally, the planned trajectories are filtered. The process uses only the visible wells, so multiple steps are necessary to set it up in a predefined 3D window.

Step 38 calculates the Bulk volume of each cell (i.e., GRV – gross rock volume). Nowadays this parameter is not critical; earlier it was created to speed up the volume calculations.

Step 39 assigns the true vertical depth of each cell's centre. The same process can be used to generate relative depth properties also, for example, HAFWL – height above free water level, which is an essential input into saturation height modelling (NEMES, 2016).

Steps 40 and 41 set up the template and the colour table of the newly created depth property. These steps play a role a role in making visualisations smoother and consistent.

Step 42 assigns distinct values to separate the area within the production license boundary and beyond it. This parameter is crucial for the filtering of both calculations and

visualisations. The method used within Geometrical modelling is Assign between surfaces and polygons, where a sole boundary polygon can be used also. Step 43 assigns the colour table.

Steps 44-46 generate a discrete property, where within the production license area the administrative distinction is also indicated (see Figure 57). (The field is on the border to two administrative regions in the Russian Federation.) This property is used for volume split calculations, which are inevitable for any documentation and resource reports.

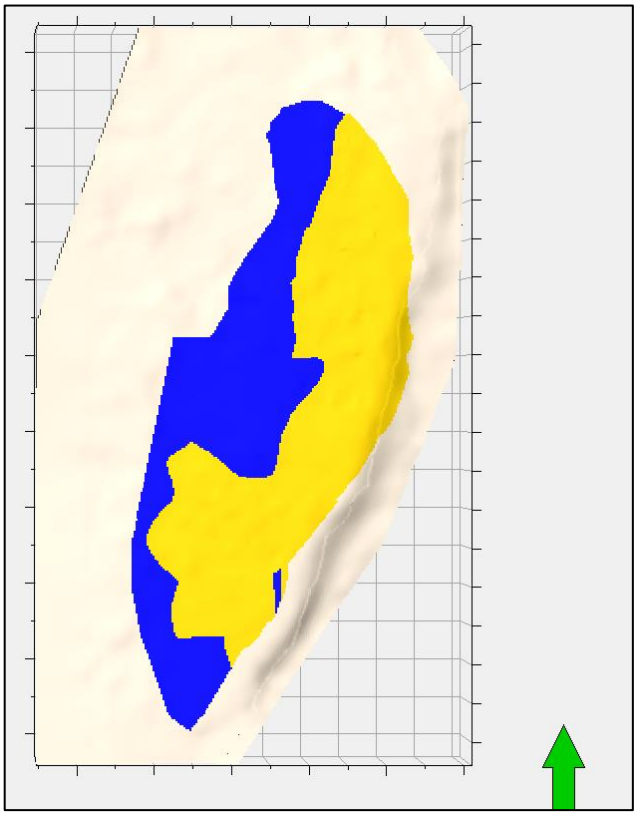

Figure 57: Light yellow represents the 3D grid area outside the production license boundary, while blue and yellow show the separation along the border in between two administrative regions.

Step 47 generates a continuous property, storing the cell height value, which is the TVT of the cell with current settings. It calculates the distance between the upper and lower faces of a cell (SCHLUMBERGER, 2021).

Within Geometrical modelling there are approximately 25 built-in operations with a wide range of setup options, providing flexibility in the support of various tasks and goals.

Steps 49-50 are *Numeric expression*s, more specifically, Bo_i values are assigned to $variables for each zone (Figure 58). Bo_i shows the ratio of oil volume in the reservoir compared to standard conditions; since the oil loses its dissolved gas content the volume shrinks, hence, the value is ≥ 1.0 (TÖRÖK et al., 2012).

Steps 51-52 assign the absolute density of the oil at standard conditions to $variables. These fluid properties are necessary for the conversion of volume to mass due to reporting and financial reasons.

Both the Bo_i and absolute density are derived from the PVT analysis of oil samples taken from the corresponding reservoirs and are referenced to initial reservoir pressure and temperature conditions. Steps 53-54 generate 3D properties from these parameters, namely, a static value for each cell per subzone.

Steps 55-58 calculate a coefficient applicable to directly calculate, during volumetric calculations, the in-place volumes in mass (in tonnes) instead of volume. In order to make 3D properties referenceable in the *Property calculator*, the *Get calculator name* expression is applied (Steps 55-57). The simple equation to generate the coefficient is depicted in Step 58, as follows:

$$Boi - Density\ Quotient\ (m^3/ton) = \frac{Boi\ (m^3/sm^3)}{Absolute\ density\ (ton/m^3)}$$

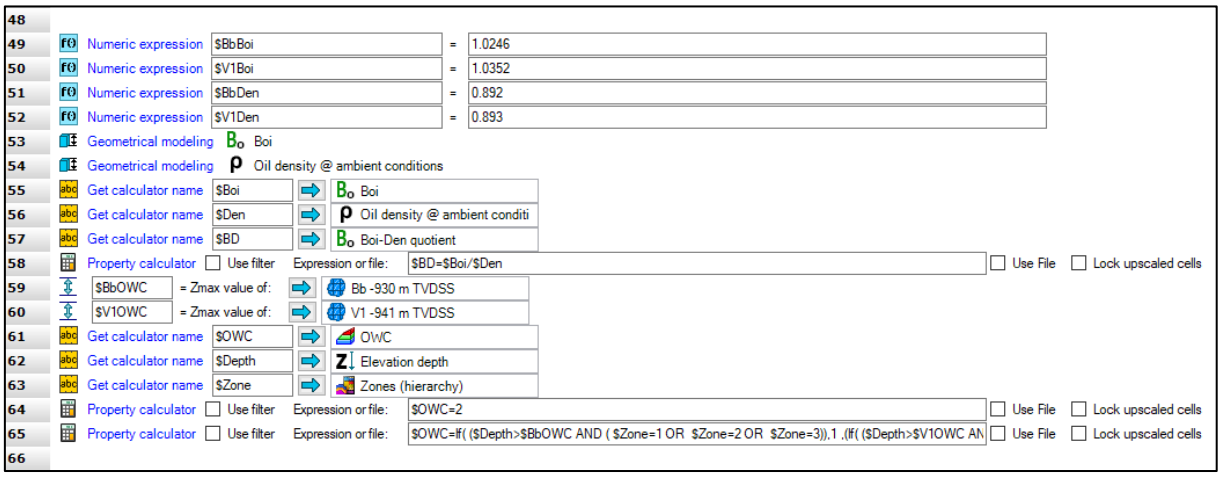

Figure 58: Steps 29-66 in the Stage 4A – Property modelling subworkflow represent the last third of the geometrical modelling. It describes the generation of fluid properties necessary for the STOIIP calculation and the generation of the OWC parameter.

The following steps generate 3D properties from the OWC_i values for visualisation and filtering purposes (Figure 58). Steps 59-60 generate the OWC depth $variables by applying a *Get Zmax value of data* expression (Operations/Get result of calculations). The next steps generate calculator parameters, and Step 64 removes any earlier values and makes cross-checking possible (i.e., assigns a discrete value of 2 everywhere, representing a water zone). Step 65 is a multiple nested *If* function with *Or* and *And* logical operations to generate the oil zones within the 3D property.

The optional subworkflow (Optional step – Cells penetrated by multiple wells, V1-Bb) filtering for multiple penetrations of wells of the same cell can/should be run here if deemed necessary, although it is not presented in detail due to its rights belong to the software vendor and not the author. A reminder is added at Step 68, as at this stage all the input properties of the optional subworkflow have already been created (Figure 59).

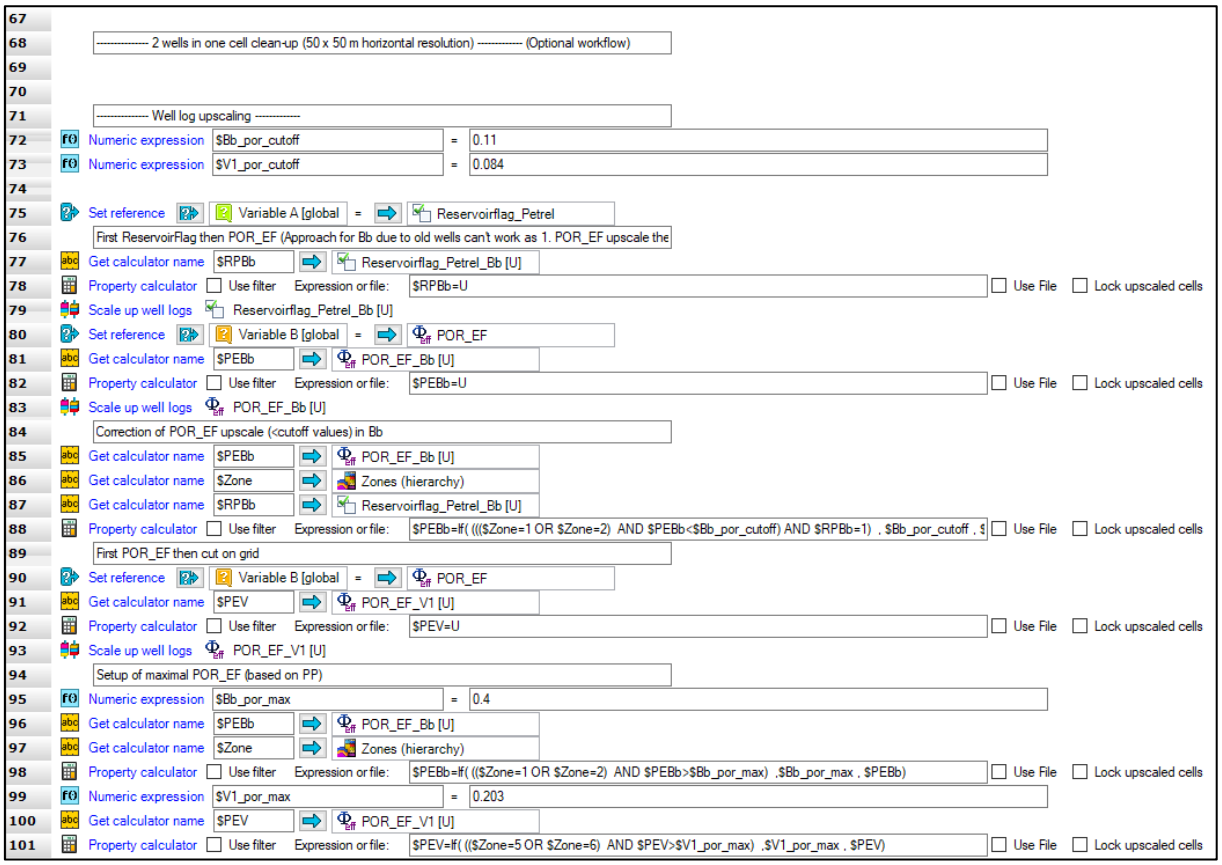

Figure 59: Steps 67-101 in Stage 4A – Property modelling subworkflow contain the upscaling process of well logs for reservoir flag (in Bb) and for effective porosity (both for Bb and V1).

Steps 72 and 73 assign the porosity cut-off values to corresponding $variables with the *Numeric expression* operation. The porosity cut-off value for the Bobrikovian Formation was identified based on petrophysical interpretation as 11%, while that of the Tournaisian Formation was 8.4%.

Step 75 (*Set reference*) links the Reservoirflag discrete global log to Variable A, as this will be a main input for the following steps.

Steps 76-83 describe the upscaling process for the Bobrikovian Formation, as detailed in Chapters 5.2.3 and 6.5. In this reservoir approximately 100 wells only have reservoirflag log due to the limited logset available. To be able to utilise the interpreted reservoirflag information, a non-TPM process was applied; first the reservoirflag was upscaled and modelled in space and (biased to this) the interconnected porosity was subsequently upscaled and distributed spatially.

Steps 77 and 78 retrieve the calculator name for the upscaled reservoirflag property and, using the *Property calculator*, set its value to undefined (U) so that consistent overwriting of any former runs is assured (Figure 59).

Step 79 is the *Scale up well logs* (Processes/Property modelling) process, which parameterises the log-to-grid upscaling job. (For statistical and quality assurance purposes, the reservoirflag parameter is also upscaled for the Tournaisian reservoir in the same step).

Multiple options are set up as lists of input wells where Saved Searches function can be applied. (Approximately 520 wells were incorporated into the upscaling process, where reservoirflag was calculated and no other excluding criteria occurred; for example, eleven horizontal wells were excluded from further analysis due to incomplete and relatively uncertain datasets.)

For this parameter the ‘most of’ sampling method was applied, with minor weighting factors, where pre- and post-upscale differences were identified on histograms. This method selects the value which is most represented in the log for each individual grid cell and assigns it to the cell. This method is only available for discrete data (SCHLUMBERGER, 2021).

Zone correction was applied, which shifts and scales input data in the grid and also to the exact matching zone.

The output properties were cross-checked with the application of subzone level histograms so that possible deviations from the input data could be filtered (Figure 60).

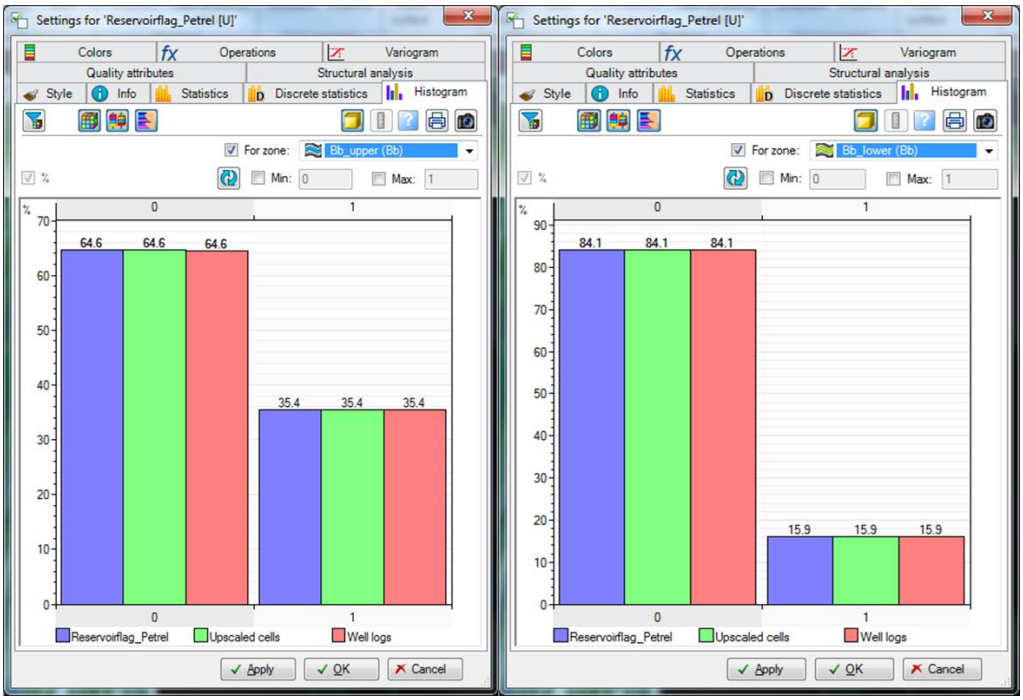

Figure 60: Histograms used for quality checking of the upscaling process (and also property modelling). The left histogram shows the Upper Bobrikovian, while the right one shows the Lower Bobrikovian’s reservoirflag parameter in terms of the relationship amongst modelled property, upscaled log and well log.

Steps 80-83 show the upscale process specifically for the Bobrikovian Formations; in contrast to the other reservoirs, here bias to reservoirflag had to be applied due to the above-described modelling method. Arithmetic averaging was used during the upscaling for the porosity, with a similar setup and quality check as previously described. An additional measure was necessary, as in some cases unrealistically low averages occurred as a result of the upscaling, which were corrected by Steps 85-88 (Figure 59). More specifically, if the upscaled porosity value of a reservoir cell is under the cut-off value (it should not be mathematically), then it is corrected and assigned the exact cut-off value by removing the contradiction. This

measure was only applied in the Bobrikovian Formation, and a marginally low number of cells were involved.

In the Tournaisian (and also Bashkirian and Serpukhovian), the total property modelling (TPM) approach was used, so the interconnected porosity logs were upscaled without biasing. Arithmetic averaging was used, and a Saved Search filtered the excluded wells from the process. Approximately 400 wells were eligible to be upscaled and used in further modelling steps. Steps 90-93 contain the upscaling steps for the Tournaisian reservoir's porosity logs (Figure 59), having similar preparatory steps as in the case of Bobrikovian (e.g., setting the earlier run's results to undefined).

In a similar way to the to the manual correction of unrealistically low values of upscaled porosity in some cases mentioned above, the maximum values are also controlled. The honouring of the input data's statistical range is assured by this preventative measure. The maximum porosities as identified by petrophysics are 40.0% for Bobrikovian and 20.3% for Tournaisian (for the sake of completeness: 28.6% and 30.0% for Bashkirian and Serpukhovian, respectively).

Steps 94-101 describe this quality assurance measure for both formations. The calculation is performed in *Property calculator* postliminary to set up the necessary $variables and retrieve calculator names. Steps 98 and 101 are two simple *If* statements coding the reset of any porosity value above a given maximum to that value.

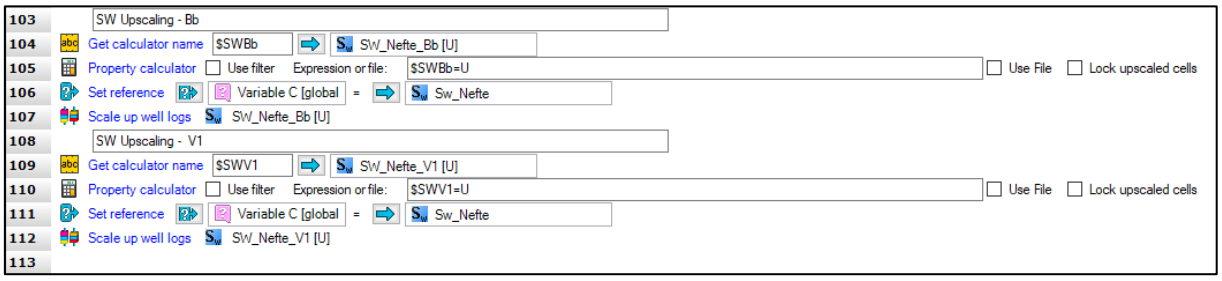

Figure 61: Steps 102-113 in the Stage 4A – Property modelling subworkflow describe the upscaling process of initial water saturation well logs for both Bb and V1.

In the case of water saturation logs, the key difference between Phase 1 and Phase 2 is the interpretation method; in Phase 2 the Archie method was applied with parameters based on core measurements.

Steps 103-107 show the upscaling process of initial water saturation for the Bobrikovian Formation, where the calculation is biased to the reservoirflag discrete values. (It should be noted that initial water saturation is mostly not the case, since most of the wells were drilled after approximately 60-70 years of production. Hence, the newer wells (at least part of them) penetrated and provided data about non-initial conditions. This means that there might be a slight inherent overestimation of initial water saturation at the reservoir level. It is not quantifiable, and there was no correction applied to balance it.) The steps of the workflow are

similar to the earlier upscaling processes, using the *Property calculator* and *Scale up well logs* operations (Figure 61). Zone correction and Saved searches were applied in both the Bb and V1 formations. Arithmetic averaging was used during the upscaling process in all subzones.

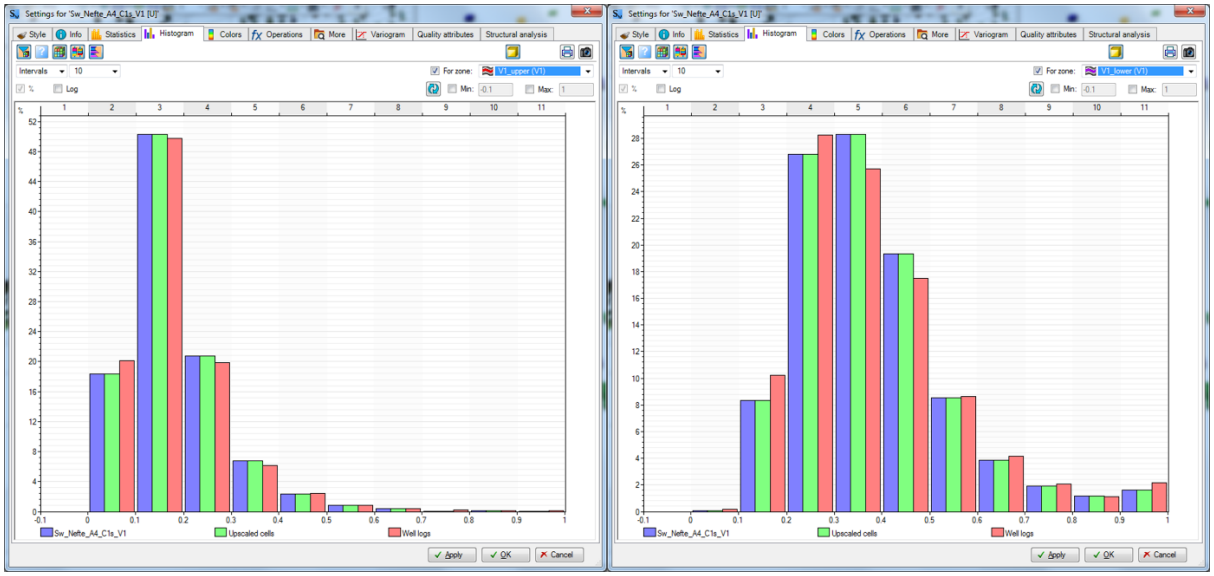

Figure 62: Histograms showing the goodness of upscaling and (subsequent modelling) versus the well logs. The dataset is filtered to above OWC_i in both the Upper (left) and Lower (right) Tournaisian subzones.

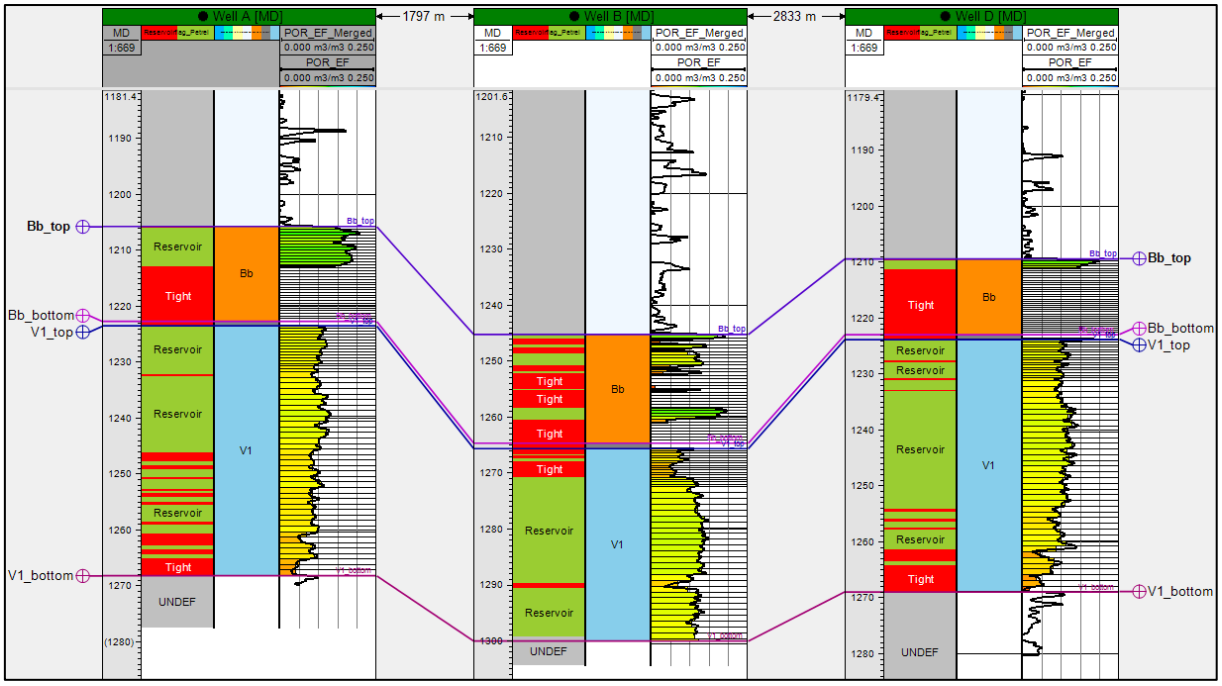

Figure 63: An example of a quality check of the upscaling process using a well correlation pane of three random wells (Well A, B, D). The rightmost track shows the original porosity well log (black line), while the coloured bars show the upscaled values. It is noticeable that the two sets of values show a high degree of similarity.

Steps 108-112 describe the upscaling process for the Tournaisian reservoir's initial water saturation (Figure 61). Except for biasing to reservoirflag, all the rest of the methods applied were the same as for Bobrikovian. For quality assurance purposes histograms were applied, but they focused only on the reservoir cell above the OWC_i of the corresponding subzone (Figure 62). (Water saturation below OWC_i is set to 100% in a subsequent step.) A

similar visual comparison was also done in the well section view, comparing well logs with upscaled logs (Figure 63).

For both the interconnected porosity and initial water saturation, approximately 400 wells comprised the inputs that had sufficient input well logs, were not filtered due to two wells in one cell or other inconsistencies and were not horizontal.

Step 115 (Figure 64) is a reminder for the user to update the data analysis manually, since the setup of this task has a fundamental impact on the outcomes of the following steps. Data analysis is the process of exploring and quality controlling the input data to prepare the primary and secondary inputs used for discrete and continuous property modelling during the Facies and Petrophysical modelling processes. Data analysis enables a detailed analysis of both discrete and continuous properties. One can use and setup facies proportion (e.g., vertical proportion curve - VPC), thickness, and variogram modelling for discrete properties, with data transformation and modelling variograms for continuous properties (SCHLUMBERGER, 2021). Further background was provided in Chapter 6.5.

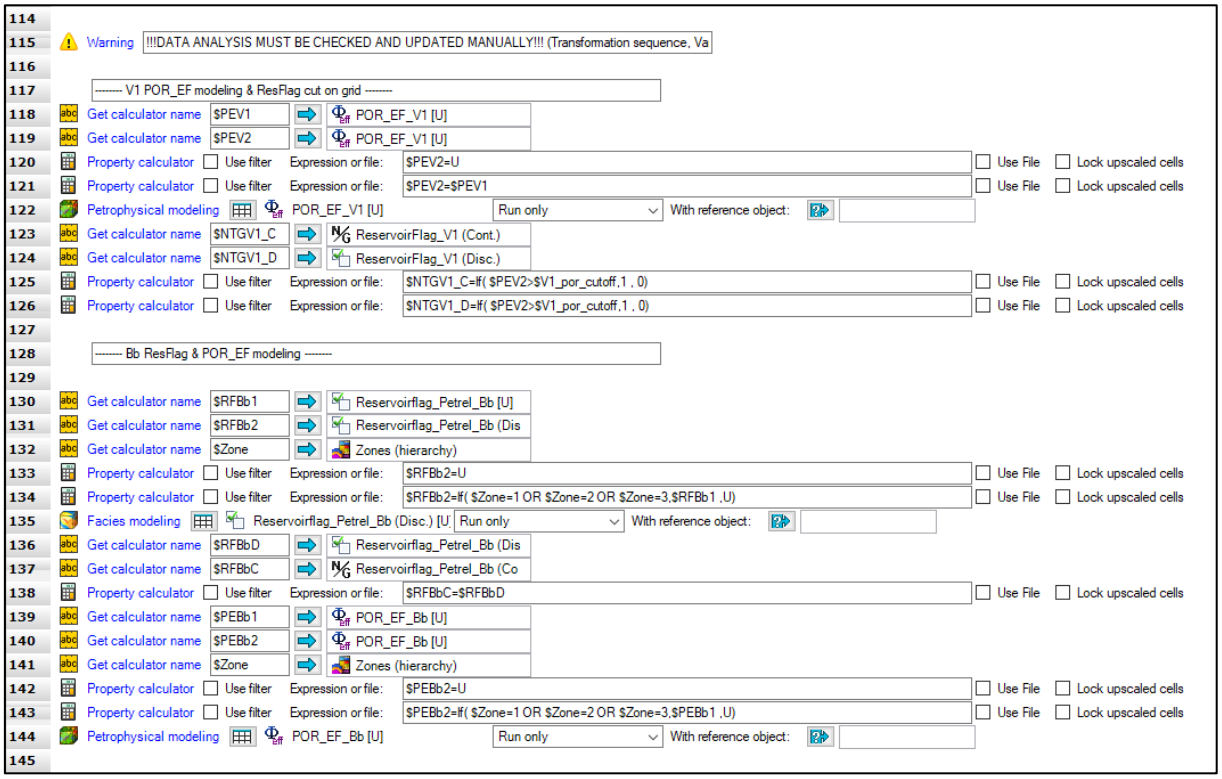

Figure 64: Steps 114-145 in the Stage 4A – Property modelling subworkflow show the porosity modelling and consecutive reservoirflag calculation for V1. Conversely, Bb expressly starts with facies modelling for the reservoirflag, and then the petrophysical modelling of porosity is performed, biased to the output of facies modelling.

In the case of the Tournaisian reservoir, the *Data Analysis* pane was set up for the porosity and, later on, for the water saturation parameters, where the input data is the upscaled well log (which is actually a 3D property having values only along the wellbores in the grid). "*Data transformation makes the data stationary and standard and is normally distributed before the actual modelling process. Back-transformation is performed automatically in the*

reverse order of the modelling result. This preserves the spatial trends and original data distribution in the final result property" (SCHLUMBERGER, 2021).

Stationarity is a prerequisite for most of the algorithms, and assumes that elements are randomly but homogeneously distributed in the inter-well space, that is, there are no trends that show a correlation with spatial coordinates (PYRCZ et al., 2006). This is the opposite of natural geological systems in which elements are heterogeneously distributed and show significant non-stationarity: they are commonly clustered and show patterns in their distribution (based on RINGROSE and BENTLEY, 2015).

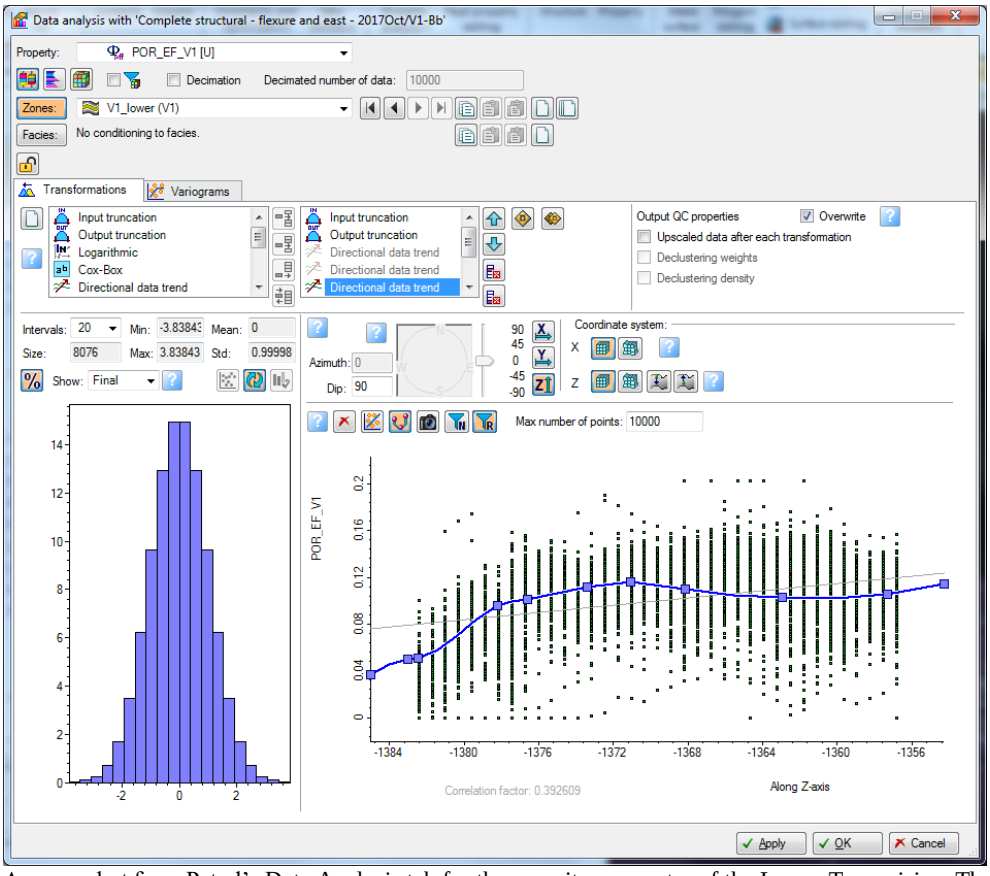

Figure 65: A screenshot from Petrel's Data Analysis tab for the porosity parameter of the Lower Tournaisian. The histogram shows the distribution of residuals, while the chart shows a trend removal in X-direction (W-E, i.e., 90° azimuth).

In the case of porosity for both the Upper and Lower Tournaisian zones, an individual data transformation sequence was created (Figure 65).

1. Input truncation: ensuring that input data is only used within a predefined range (i.e., removing extreme values, if any).
2. Output truncation: ensuring that output data is only within a predefined range (i.e., removing extreme values, if any). (It is only run at the back-transformation.)
3. Directional data trend: removing X-Y-Z (or I-J-K) direction trends from the dataset to prepare stationarity.

4. Normal score (transformation): removing any remaining non-stationarity and converting the dataset to Gaussian-distribution. (Normal score transformation should always be the last in the transformation sequence.)

To have the upscaled well logs intact and to avoid directly using them as the property for petrophysical modelling, a copy is created. Steps 118-121 represent this move; $PEV1 and $PEV2 differ, and only the property name is common. $PEV1 is the output of upscaling, while $PEV2 is the 3D property that is used for *Petrophysical modelling* (Processes/Property modelling) in Step 122. This 'hack' was necessary so that the set up values of the Data Analysis could be saved after each run.

For each subzone, a spatial variogram model was defined for porosity in the Data Analysis tab. Major, minor and vertical direction semi-variograms were fit to the data, and, where necessary, nested variograms were applied. An example of a vertical semi-variogram of exponential type with a range of approximately 5-7 metres is shown in Figure 66.

The variogram is a mathematical tool/function used to describe the expected spatial variation of a property. In general, the similarity between two observed points depends on the distance between them, that is, the variability increases with increasing separation distance. Variograms are used as input for petrophysical modelling and facies indicators modelling. They are important because they provide information regarding the confidence with which the value of a cell can be estimated, based on its distance from a cell of known or calculated value (e.g., a well) (EMERSON, 2019). Further details and application in variograms in reservoir modelling can be accessed (amongst others) in OLEA, 1994; CAERS, 2005; RINGROSE and BENTLEY, 2015 and PYRCZ AND DEUTSCH, 2014.

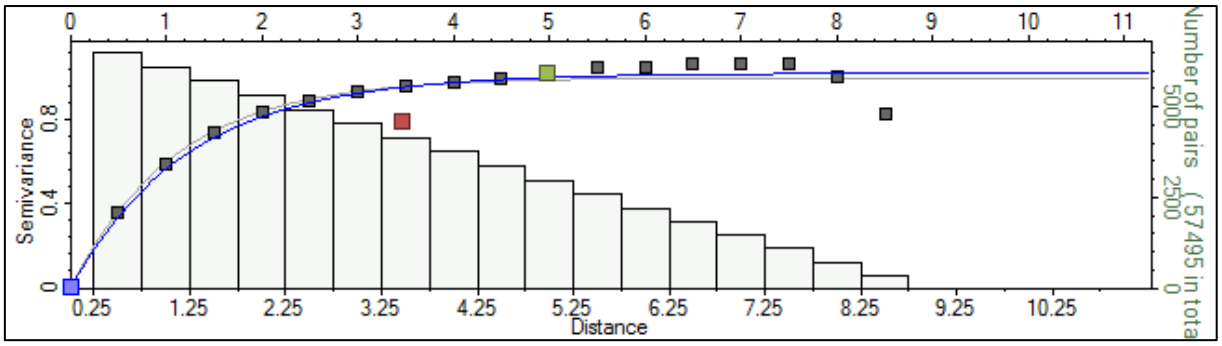

Figure 66: A vertical direction semi-variogram with exponential fitting for the porosity of the Lower Tournaisian reservoir, where the dots represent empirical values, while the blue line is the fitted theoretical semi-variogram.

Step 122 represents the *Petrophysical modelling* process, where all the modelling tasks can be set up. Most of the inputs (data distributions, variograms) are directly linked to the Data Analysis, and there were not any available trends (e.g., seismic attributes) available for modelling. Sequential Gaussian Simulation (SGS) was chosen, which uses well data, input distributions, variograms, and trends (if available) (RINGROSE and BENTLEY, 2015). Upscaled

wells were honoured, that is, not overwritten by the modelling process. A random global seed number was set up as, which is a starting value of a stochastic run and allows one to be replicated.

Naturally, the petrophysical modelling setup is required per subzone (and per facies, if applicable). In this case it was initialised separately for the Lower and Upper Tournaisian. Since TPM was applied at this stage, there were not any facies properties available, making the parametrisation straightforward and simpler.

Steps 123-124 retrieve the calculator name of the to-be updated reservoirflag properties (both continuous and discrete types are created to provide flexibility for further use) (Figure 64). It should be noted that at this stage the parameters for Tournaisian and Bobrikovian are separated from each other; they are merged in the last steps of the subworkflow.

Steps 125-126 use a simple calculation in the *Property Calculator* to generate the reservoirflag parameters in 3D based on the previously modelled porosity property, which means applying the predefined cut-off values on the 3D grid, resulting in a discrete "rocktype" model where 0 represents non-reservoir and 1 represents reservoir zones. (The cut-off values were predefined as $variables in Steps 72-73.) (Figure 59.)

From Step 130 (Figure 64) the reservoirflag and the porosity modelling of the Bobrikovian Formation are scripted. As discussed earlier, the sequence of the petrophysical and facies modelling of Bobrikovian follows a conventional approach, where the facies modelling precedes the petrophysical modelling. The need for this emerges from the fact that in approximately 100 Bobrikovian wells, only reservoirflag can be interpreted, but interconnected porosity cannot be calculated. Hence, to squeeze the information from these old wells, the log reservoirflag discrete parameter is modelled, biased to these old (and, naturally, to the new) wells also. In this manner the Bobrikovian is unique among the four modelled formations, as all the rest are modelled using total property modelling (TPM).

Steps 130-134 are preparatory steps, so the creation of the relevant calculator names and safety overwriting of former runs happen prior to *Facies modelling*.

The *Data Analysis* window is similar to that described in the case of Tournaisian, although, necessarily, the Facies modelling's input parameter, namely, the reservoirflag upscaled log, has differences compared to that of the continuous parameter. In the case of discrete parameters, there are two key tools which drive the spatial distribution:

1. VPC (Vertical Proportion Curve) (Figure 67): Widely used tool for representing the proportion of different facies in each layer of the 3D model, aiding the description of facies spatial distribution (DOLIGEZ et al., 2011; KETINENI et al., 2019; ODEZULU et al., 2014).

2. Variograms (e.g., Figure 66): The variogram function describes the expected spatial variation of a property (RINGROSE and BENTLEY, 2015), i.e., lateral and vertical continuity.

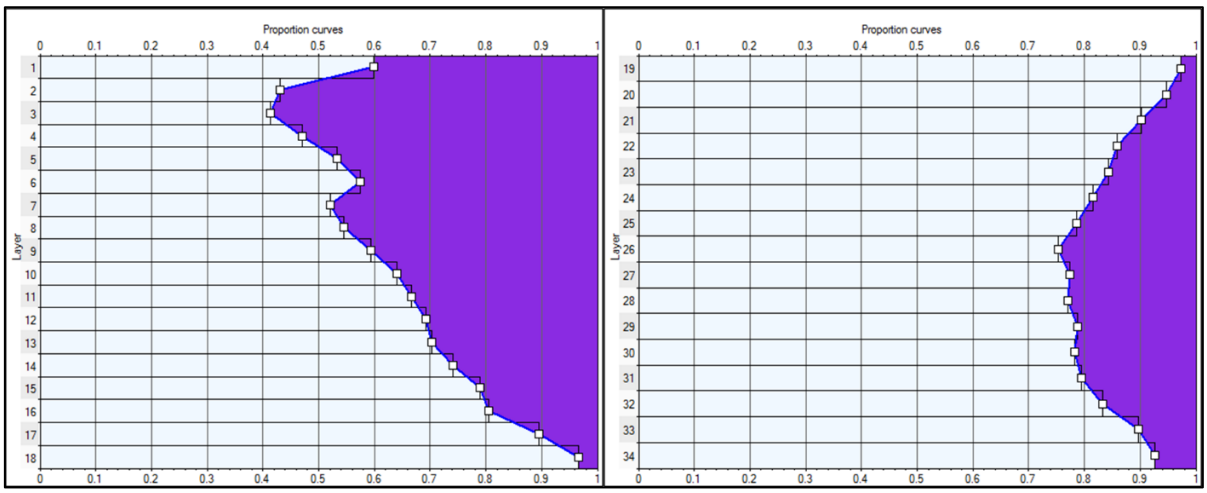

Figure 67: The chart on the left represents the vertical proportion curve for the Upper Bobrikovian zone; the right, the Lower Bobrikovian. The purple colour represents the reservoir 'facies'; the light blue, non-reservoir.

A third step can be necessary in the case of an uneven distribution of wells in the field. Usually, wells are not drilled evenly but are populated in preferential areas. Consequently, some parts of the reservoir are overrepresented in the data set, and the information value of these wells is lower than those wells which are drilled in less populated areas. This difference in information value considering the whole reservoir is accounted for by declustering algorithms (PYRCZ et al., 2006), that calculate weights to balance the misrepresentation, if necessary (after EMERSON, 2019). In the case of Field A, this results in marginal differences (<1% in terms of reservoir ratio), as the field is evenly drilled.

Step 135 is the *Facies modelling* (Processes/Property modelling) job, which contains both the Upper and Lower Bobrikovian. The applied method was SIS (Sequential Indicator Simulation), which is a pixel-based method that assigns, in this case, the facies attribute to each cell on a cell-by-cell basis. Variograms and vertical proportion curves were loaded from the corresponding Data Analysis tab. In the case of Bobrikovian, an additional lateral trend was added (as it was for the Upper and Lower subzones), which represented the probability of reservoir occurrence (Figure 68). *"The sequential simulation works by visiting each point on the grid to be simulated, calculating the conditional distribution at that point and sampling from that distribution. The conditional distribution is the probability distribution for the facies at the point, given knowledge of the facies at nearby well locations and of previously simulated points nearby"* (EMERSON, 2019). The kriging type was ordinary kriging, as it is recommended for a high number wells (RINGROSE and BENTLEY, 2015).

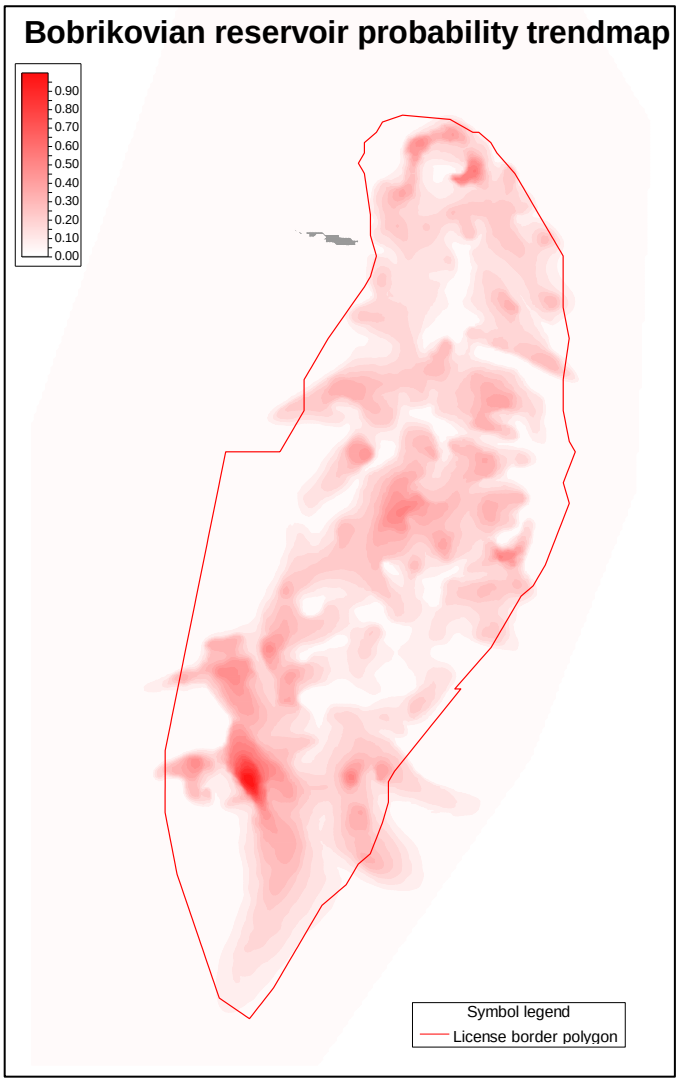

Figure 68: A simplified reservoir probability map based on the integrated interpretation of well log and inflow test data. The higher the value, the higher the probability of the occurrence of reservoir (i.e., sand) layers (based on SZILÁGYI et al., 2021).

Steps 136–138 specify a simple operation, transforming the discrete facies parameter to a continuous net-to-gross type parameter, which is further used in volume calculations.

Steps 139–143 establish a safety feature, removing (i.e., assigning undefined values (U)) any earlier run's result prior to the modelling of the porosity (Figure 64).

Step 144 contains the *Petrophysical modelling* job for the interconnected porosity, where the input is consistently the upscaled porosity. It is biased to the formerly modelled facies (biasing is described in Figure 16) so that flexibility can be saved; both the reservoir and non-reservoir facies' porosity is modelled. (Although the porosity of the Malinov Shale is assigned a value of zero.) Sequential Gaussian Simulation (SGS) is applied, and the variography is mirrored from the Data analysis tab; co-simulation was not possible, as there was no 2D or 3D trend available correlating with the porosity.

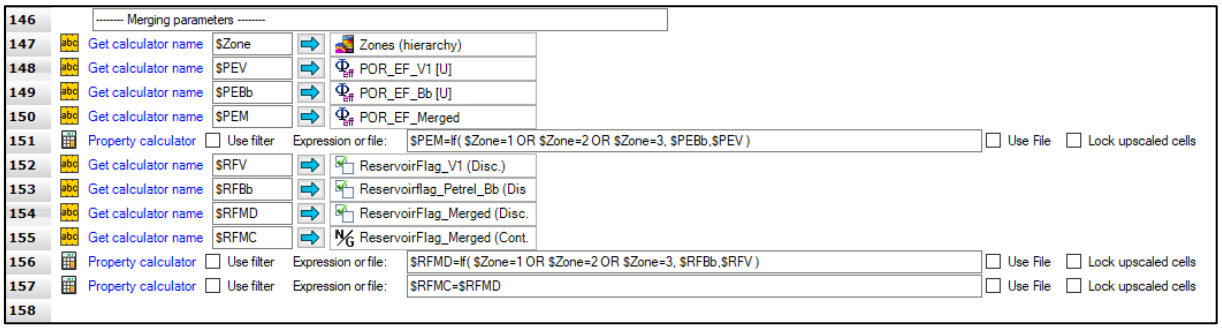

Figure 69: Steps 146-158 in the Stage 4A – Property modelling subworkflow describe an operational set of steps, as they merge the modelled reservoirflag and porosity properties existing in separate parameters until this point.

Steps 147–151 (Figure 69) merge the individual porosity 3D parameters into one merged property (including both Tournaisian, Malinov and Bobrikovian Formations), while steps 152–157 execute the same process for the reservoirflag (i.e., facies/rocktype/net-to-gross) property. Consequently, in the further steps the merged properties were used.

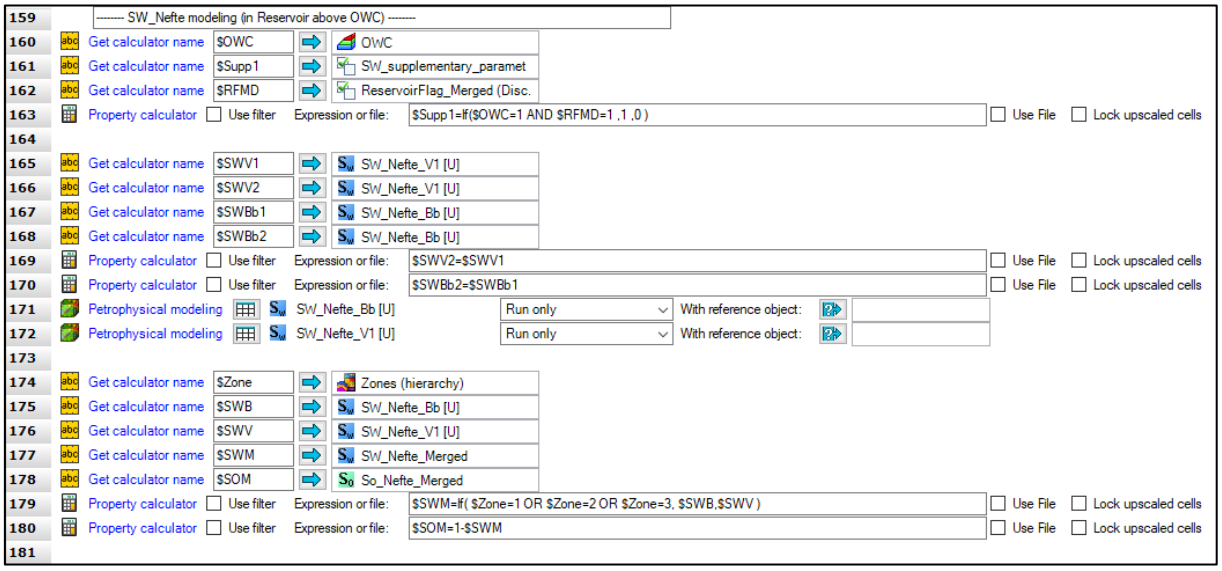

Figure 70: Steps 159–180 in the Stage 4A – Property modelling subworkflow describe the modelling of water saturation, as it is based on the well-log interpreted saturation logs. More specifically, the water saturation logs were upscaled and modelled, but look-up and/or J-functions or any other saturation height functions were not applied during the modelling.

In the case of modelling the initial saturation of an HC reservoir, there are multiple choices at hand depending on data availability and quality (VAVRA et al., 1990; LEVERETT, 1941), from modelling the log-derived initial water saturation to applying look-up functions, fitting Thomeer curves (NEMES, 2016) or calculating J-functions or other unique approaches. In the case of Field A, the initial water saturation for all of the reservoirs was modelled using the log-derived saturation curves and and were propagated in 3D as a continuous parameter. Initial water saturation modelling only happened above the OWC_i and in reservoir cells (based on reservoirflag parameter). In all other cases initial water saturation was assigned at 100%.

To separate the cells where initial water saturation shall be modelled a ‘supplementary’ parameter was created solely for filtering purposes. Steps 160–163 describe the creation of this parameter, which equals one where the cell is ‘reservoir’ and is above the OWC_i of the actual

reservoir. The inherited uncertainty is still present, namely, that the newest wells are most probably already showing a disturbed (non-initial) saturation profile due to the sixty years of fluid production (and water injection) history prior to their being drilled from the 2010s; it was noted and handled as a non-quantified discount factor.

Steps 165–170 (as shown in Figure 70) are the familiar steps of setting the formerly modelled values to undefined so that any inheritance from the 'past' can be avoided.

The Data Analysis was set up focusing on the cells of interest as defined by the supplementary parameter described two paragraphs earlier. In the case of non-reservoir rocktypes, in the Malinov Shale and below the OWC_i (regardless of reservoirflag value), the initial water saturation was assigned 100%.

Steps 171-172 show the *Petrophysical modelling* jobs that are set up for the two modelled formations. Sequential Gaussian Simulation approach was used as well as co-kriging with porosity 3D parameter, where correlation coefficients vary from -0.3 to -0.7. The secondary parameter (i.e., the porosity) was transformed using normal score transformation, and the seed number of the main and the secondary parameters are different.

Steps 174–180 merge the individual properties and, as a last step, calculate the initial oil saturation from initial water saturation.

During the modelling workflow, each step was validated through a comparison of the results' probability distribution to the input data using histograms (as shown in Figure 62), although it is not always a prerequisite that they match due to lateral trends not being captured by the well pattern; hence, the comparison focused on the license area, where the well coverage is basically even.

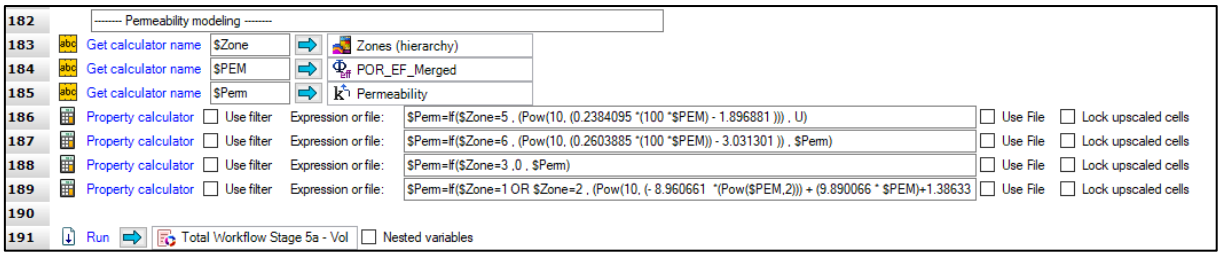

Figure 71: Steps 182–191 in the Stage 4A – Property modelling subworkflow contain the permeability modelling/calculating workflow.

The last property modelled during the geomodelling of Field A was absolute permeability. It is not stochastic modelling, but a deterministic calculation based on core measurements. Steps 183–189 (Figure 71) use the Property calculator to calculate or assign absolute permeability values per zone, based on porosity. Permeability was calculated only in reservoir cells; non-reservoir cells and zones were assigned a value of zero permeability.

The porosity-permeability regressions were identified on core laboratory measurements per reservoir, or in the case of the Tournaisian Formation, per subzone. The regressions are shown in Figure 72 on semi-log plots for the Bobrikovian and Tournaisian Formations.

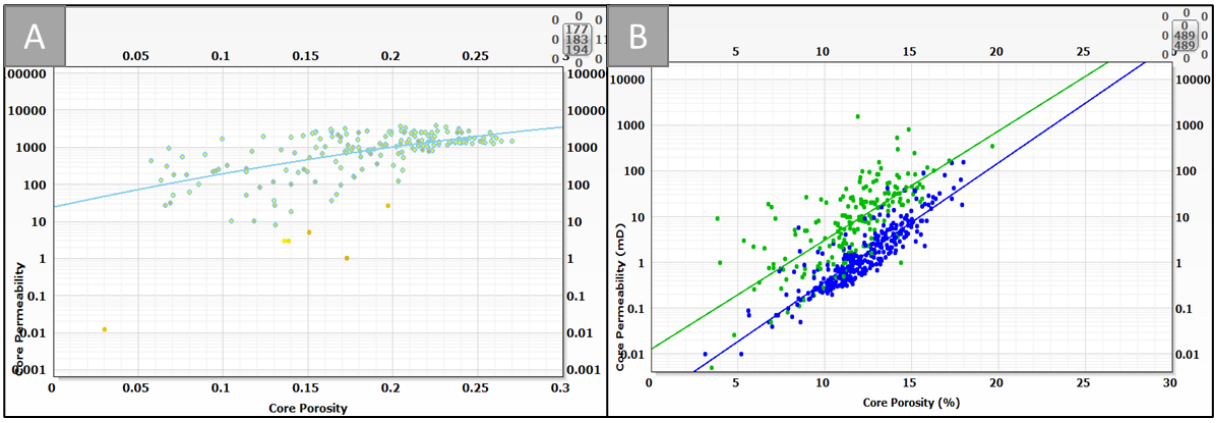

Figure 72: Panel A shows the identified porosity-permeability regression on a semi-log plot in the Bobrikovian Formation, while Panel B shows the same for the Lower- (blue), and Upper-Tournaisian (green). (Courtesy of the project petrophysicists.)

Step 191 is a turning point, where the running of the next subworkflow starts if activated, following the logic of Figure 21.

The Stage 4B – Property modelling subworkflow is highly similar to 4A, and it contains the corresponding steps for the Bashkirian and Serpukhovian reservoirs. In the upper zone the Lower-Serpukhovian has a simplified modelling workflow (as in the water-leg). Also, both A4 and C1s were modelled with the application of the TPM technique.

Due to the high degree of similarity, the 4B subworkflow is not described in detail here.

6.5.1.1 Results

A short list of the outputs and outcomes generated during the Stage 4A and 4B – Property modelling subworkflows is given below:

- geometrical properties (OWC_i, fault segments, cell geometric parameters, administrative properties etc.);
- fluid parameters as properties (Bo_i, fluid density, Boi-Density quotient);
- upscaled well logs (porosity, reservoirflag, water saturation);
- data analysis parametrisation (data transformation sequences, variography, vertical and lateral trends where available);
- QC steps (histograms and descriptive statistics);
- 3D properties modelled stochastically (porosity, initial water saturation (Appendix VIII), and reservoirflag) using different approaches to maximise data value;
- absolute permeability calculated using regression equations based on core analysis;

- auxiliary parameters created to aid filtering, statistical analysis and cross-validating exercises;
- an exhaustive Petrel workflow covering the bullet points above.

6.6 VOLUMETRICS

With the completion of the property modelling, all the input parameters are available in the 3D grid necessary to calculate hydrocarbon initially in-place, which is one of the goals of the modelling. The volume calculation equation is the same as shown in Equation 1 in Chapter Petrophysical modelling and volume calculation (Phase 1).

However, a more correct formulisation of Equation 1 is as follows (after BANKS, 1982 and PÁPAY, 2003):

$$STOIIP = C \sum_{i=1}^{n} \frac{(GRV_i)*(NtG_i)*(\Phi_i)*(1-Swi_i)}{Boi_i} \quad \text{Eq. 2}$$

where C is an optional constant depending on units applied, GRV_i is the bulk volume, NtG_i is the net-to-gross, Φ_i is the interconnected porosity, Swi_i is the initial water saturation and Boi_i is the initial formation volume factor of the i^{th} cell.

Equation 2 states that each incremental volume of the reservoir is discrete. Total volume is the summation (numerical integration) of these discrete values, that is, the integral of the products of discrete values. The integral of the products is not equal to the product of averages (BANKS, 1982). Recently, MA (2018) revisited the deterministic and Monte Carlo methods used for volumetric calculations.

Hydrocarbons in-place are a key indicator of the size of a field, and other important field attributes including future field development options and economic viability. 3D geomodels not only deliver a volume quantification, but also help to identify in-place volume distribution spatially and therefore, in the driving of the drilling of producer and injector wells during primary, secondary and tertiary development methods.

The volumetrics task delivers calculated gross rock, net, pore, hydrocarbon-pore and in-place volumes, along with distribution maps (volume height maps) and the 3D properties that are direct inputs to dynamic modelling. Different filters can be applied to detail the breakdown of final results, for example: share among different administrative areas, different facies and different wells (within a given radius). In addition, if necessary, a preliminary recoverable volume estimation is also possible.

6.6.1 WORKFLOW STAGE 5A AND 5B – VOLUMETRICS

Following the logic of the earlier chapters, only one of the subworkflows is detailed due to the similarity of the two. Subworkflows 5a and 5b consist of six and five steps, respectively, being the shortest of the subworkflows within Field A's Petrel Project. Subworkflow 5a belongs to the lower reservoirs, and this will be described.

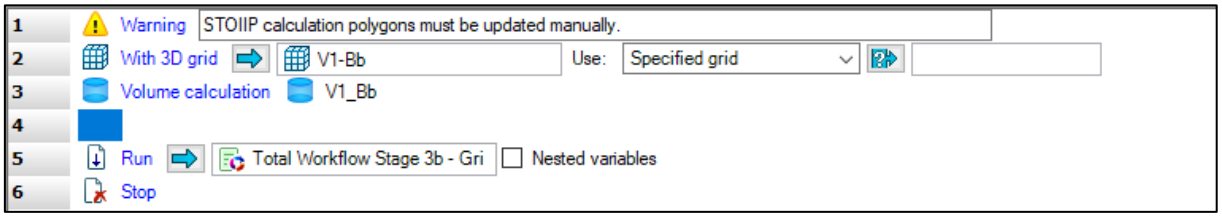

Figure 73: Steps 1–6 in the Stage 5A – Volumetrics subworkflow consists of one main item, the Volume calculation process.

Step 1, *Warning*, shows the user that the actual polygons which limit the area of volume calculation are defined manually and are updated if necessary (Figure 73). These polygons ensure that small artifacts ('tiny structures') which are a great distance from the well coverage are not included as part of the volume estimations.

Step 2 defines the 3D grid to be used through the workflow.

Step 3 is the *Volume calculation* task (Processes/Utilities), which incorporates all the parameters and assigned properties necessary to perform the volume calculation. The corresponding 3D properties, fluid contacts, license or other boundaries are linked in this task, and additional settings are made to deliver the volumetric results.

Step 5 is a decision point; if the 3D model for A4 and C1s also is updated, then it should be active. If the update of the upper reservoirs is not necessary, then it is deactivated, and the workflow stops at Step 6: *Stop* (Utilities/Statements).

In the case of Field A there were several goals and expected volume calculation deliverables:

1. volume reconciliation compared to former studies;
2. the identification of volume share among relevant administrative regions;
3. the calculation of initial in-place volumes within the actual license boundary and surroundings (if any);
4. volumes among formations and subzones being split;
5. the estimation of volumes in the vicinity of dedicated wells.

Once the volume calculation (and the preceding workflow) is set up correctly, all the above goals can be met and updated regularly and automatically as new information or new requests emerge.

The absolute volumes cannot be disclosed due to confidentiality; hence, only relative changes are shown. Compared to former studies, a field-level in-place volume increase was identified of approximately 20-50%. It can also be concluded that the initial in-place volume increased in all four formations. The main drivers of these changes are the change in GRV due to new seismic data and the integrated reinterpretation of petrophysical data. In all cases the full-cycle volumetrics were exported, namely, each parameter from GRV to STOIIP, which made possible a step-by-step comparison, the identification of the contribution of individual parameters to the volume changes, and its visualisation on water-fall diagrams.

The share of the four main formations in the total STOIIP is shown in Figure 74. (Volume maps cannot be disclosed due to their business-critical information content.) The share of in-place volume within the subzonated reservoirs is as follows: Lower Tournaisian to Upper Tournaisian (35% to 65%); Lower Bobrikovian to Upper Bobrikovian (20% to 80%); Lower Serpukhovian to Upper Serpukhovian (0% to 100%). The latter is explained by the modelling approach, as the formation was split into two subzones due to upscaling reasons below the OWC_i and not due to sedimentological considerations.

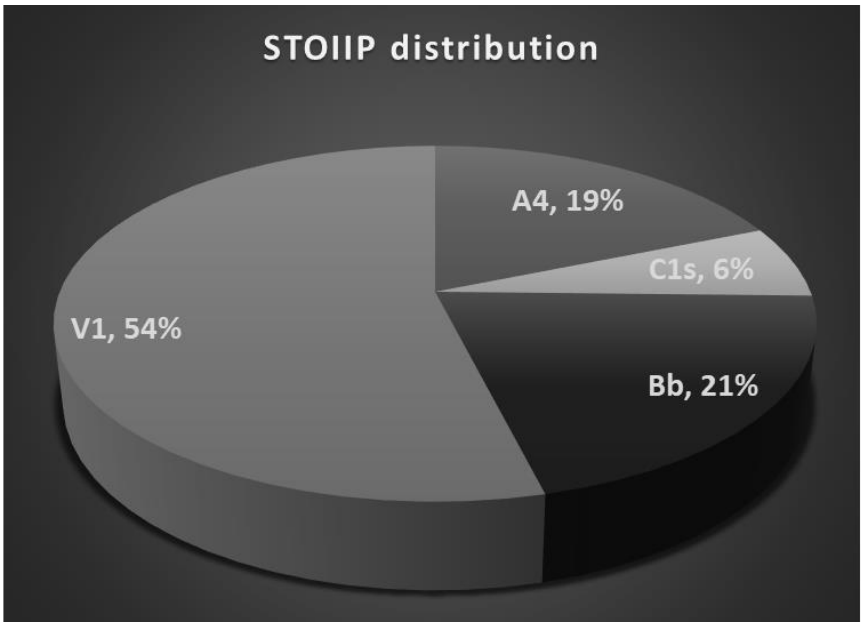

Figure 74: A pie chart showing the ratio of different formations of the total STOIIP. The Tournaisian Formation contains more than 50% of the total STOIIP – it should be noted that the deep reservoirs make up ~75% of the field volume. However, it should also be noted that the Bobrikovian's high lateral heterogeneity makes it challenging as a primary development target, hence, it is usually drilled as an upside potential of Tournaisian wells.

A sensitivity run was performed for the Tournaisian reservoir so that the uncertainty range of the in-place volumes could be pre-screened. An additional cut-off value was introduced as a rule of thumb for oil reservoirs (SABOORIAN-JOOYBARI, 2016): permeability must be a

minimum 1 mD to count as a reservoir. This secondary cut-off had a significant effect (~30%) on the in-place volumes, hence requiring more future focus on net-to-gross identification in the reservoir. Also, it is indicative that due to the additional cut-off, the decrease of in-place volumes mainly occurred in the Lower Tournaisian reservoir, leading to a 50% drop, while in the Upper Tournaisian the drop was around 20-25%.

Auxiliary calculations were made for reporting purposes; the volumes were split according to the administrative boundaries as previously shown in Figure 57.

6.6.1.1 Results

A short list of the outputs and outcomes generated during the Stage 5A and 5B – Volumetrics subworkflows is given below:

- gross rock, net rock, pore, hydrocarbon pore and in-place volume as a 3D property;
- volume height maps;
- volume tables with various breakdowns;
- volume estimations both inside and outside the license area (where applicable);
- Petrel workflow for volume calculations (also, the last subworkflow, closing the geomodelling stream).

7 CONCLUSIONS

This thesis describes in detail the process of building a simple and, subsequently, more complex geological model of Field A with four productive formations (Appendix I). A key focus was put on the workflow building methodology and its advantages and the importance of the preceding data integration.

The last chapter focuses on the outcomes and the pervasive impacts the geomodel (and, necessarily, the dynamic model in most cases) had on the understanding and operation of Field A. Since the geomodel on its own is a tool but not the final goal of the work, it is critical to describe its actual added value. In general, a geomodel supports business decisions, improves understanding and serves as a data sharing and visualisation platform.

It is, on its own, a huge effort to map the size of the task for a project that aims to establish a general understanding of a field which was, despite being discovered in 1947, still not in its mature phase in terms of actual primary recovery factor, and therefore has a huge remaining potential. In other words, by revitalising this field the extracted value can be increased beyond original expectations (PARSHALL, 2012). The opportunity for further investigations and increased exploitation efforts was emphasised by a positive change in *oil initially in-place*, which had already occurred during the Phase 1 modelling (NEMES et al., 2021).

The modelling work has shown its impact in multiple areas, such as subsurface understanding, a revisitation and adjustment of well placement strategy and workover planning processes, an update to field development strategy, a reviving of the investigation into possible upside potential, the optimisation of CAPEX spending, improved data and knowledge sharing with partners, and the building of a team focused on Field A.

7.1 DELIVERABLES AND IDENTIFIED OPPORTUNITIES

The remodelling of Field A used a novel approach of splitting the modelling job into two phases so that room could be made for inevitable updates revealed during the task execution as well as accommodating the business needs requiring the delivery of preliminary results within a short timeframe (accepting the high uncertainty of the results).

7.1.1 PHASE 1 MODELLING

The main result of the Phase 1 modelling exercise was that a huge amount of historical knowledge, experience, seventy years of data and generated information started to become a *structured set of understanding*, where the focus points and gaps were revealed. The preparatory

works, the multidisciplinary interpretation and the modelling all revealed new information or outdated, old, erroneous ‘beliefs’, which are equally important and crucial in terms of the road to transparency (NEMES et al., 2021). It was an immensely useful process, like a rehearsal prior to the big premier. (Although it is rather people-management related, the multidisciplinary work and dedicated focus of the team also had an invaluable impact on forming an effective *project team*, which is a key factor in terms of the quality and time required to deliver a complex task.)

Quantitatively, the main results were the first-pass updated *volumetrics* (and related volume reconciliation) and the reference case 3D geological model with spatially distributed *reservoir parameters*, which could be used to start the dynamic modelling.

Phase 1’s geomodel had already been having a significant impact on ongoing operations in areas such as *new wells planning*, both in number and placing of wells, *field development strategy* and a data acquisition programme (NEMES et al., 2021). The planned wells were fine-tuned, and more than fifty percent of them were moved so that more prospective subsurface targets could be drilled. The drilling of *dedicated Bobrikovian wells* was temporarily suspended, and the *sidetracking* of existing wells was cancelled due to subsurface and economic considerations. The *drilling sequence* of the new wells was optimised to accommodate the post-drill evaluation of individual wells prior to the drilling additional one(s) in the same part of the field, an approach which is called staged drilling.

New (advanced) *well log acquisitions* were proposed in some of the new wells, with the intention of mitigating part of the revealed information gaps (HARRISON, 1995; ASQUITH et al., 2004; DARLING, 2005). *Acoustic density logs* were used in the shallow sections of the wells to update the seismic velocity model lacking information from 0-500 metres of the depth range. *Imaging tool* (image log) was used in order to have an alternative to short well-tests so that the possible role of natural fractures on flow behaviour could be investigated. In a couple of wells the image log acquisition was coupled with coring so that the log interpretation with core structural analysis would be supported. *Nuclear magnetic resonance* tool (NMR) was used so that the in-situ moveable and residual fluid saturation and permeability could be investigated. *LithoScanner* was used to increase the understanding of mineral composition, with an emphasis on anhydrite content, which plays a key role in porosity uncertainty. *Spectralog* was used to differentiate uranium from clay and to validate the relationship of high GR values solely to increased clay content.

Simultaneously, the number of tools run as a conventional *logging set* was *rationalised*, and excess measurements were removed, for example, the induction log (NEMES et al., 2021); in addition, cased hole logging practices were revisited and optimised.

Although from an added value point of view the *revealed gaps* and bottlenecks were lower priority, it was possible they could have a higher impact in the long-term for field development planning, hence, they triggered action plans and the creation of a detailed to-do list for the Phase 2 modelling and the data acquisition prior to the Phase 2 revisit of the field model (NEMES et al., 2021).

Additional *core* (>100 plugs) and *fluid measurements* were requested to fill-in revealed data gaps, mainly for permeability measurements and oil properties.

Geomodel-related data gaps and data discrepancies which were not explicit were revealed, especially in *pressure monitoring*, as a recurring anomaly of 'frozen' pressures was identified. The phenomenon manifested in precisely the same well-head pressure for years in several production wells, which is definitely a data recording anomaly and does not reflect reservoir behaviour. Hence, a pressure measurement campaign was initiated to gather new data and have a better understanding of the actual conditions in the field. In parallel, a programme was initiated to improve the reliability of *production allocation* (as most of the well-groups produce on common pipelines, and production measurement usually takes place at the gathering points and not at the wellhead, making the back allocation challenging).

Detailed geological investigations were initiated based on the recently acquired understanding of (NEMES et al., 2021):

- Bobrikovian facies analysis;
- Bobrikovian old wells petrophysical investigation;
- Serpukhovian paleokarst mapping;
- correlation of intra-formation subzones (Tournaisian and Bobrikovian);
- identification of Tournaisian bottom horizon;
- hardcopy data digitisation (trajectory, production);
- and numerous minor adjustments (e.g., well name contradictions, wellhead coordinates and elevation, logset anomalies).

An unusual subtask was also part of the endgame related to Phase 1. The *software* used for geomodelling needed to be changed, hence, the Phase 1 model built in Roxar Irap RMS 2013.1 was later rebuilt in Schlumberger's Petrel 2015.5 due to business requirements. Consequently, a direct comparison of the two software packages occurred. There were only slight differences in the results of the two packages originating from stochastic deviations, and all the differences were within a standard deviation of the given parameter defined in any of the software packages, meaning that there was no decisive argument on either side. The Phase 2 geological model was initially constructed using Schlumberger's Petrel 2015.5 (later updated to 2016.2) software package for the same business reason (NEMES et al., 2021).

Importantly, based on the results of Phase 1, a *scope of work* and a *timeline* were outlined, with associated subsurface expertise assigned for Phase 2. This was crucial in further decreasing the uncertainty related to the understanding of the field's behaviour and remaining potential (NEMES et al., 2021).

7.1.2 PHASE 2 MODELLING

A schematic overview of the differences between the Phase 1 and Phase 2 models is given in Appendix X with further comments, explanations and quantification.

An overall lesson is that despite the fact that making the subsurface work in a front-loaded way is a slow process, it is critical to dedicate time and focus on *data wrangling* as it is the foundation for each further step, including the final conclusions.

The *dataset* available during the Phase 1 modelling was not final since trajectories, measured and interpreted logsets, core data, finalised completion and production logs, and historical reports were not all integrated, and a fine-tuned seismic interpretation was also missing. The placement of all the data integration, standardising and quality-checking activities into a common *single-source-of-truth database* was in-progress throughout the Phase 1 modelling. These tasks were finished in Phase 2 and incorporated into the subsurface models and subsurface database. Having a comprehensive, clean and structured database has a paramount effect on the time demand involved with data gathering tasks and significantly decreases the chances of misalignments due to the work involved with different vintages and the readiness of input data among experts or disciplines. In order to simplify and standardise the dataflow, the data sharing processes were updated, and *data governance* was implemented. The latter practice had an immediate effect on the smoothness of the data flow and decreased the time necessary to access new data as well as the time spent on redundant work and searching for the correct/latest dataset.

The optimal solution was to use a Petrel and OFM *reference project*, where all the input and interpreted data was loaded (except for special data types that were stored separately, but with strict data governance rules also), at which point the data were labelled as final versions and could be modified by data managers exclusively. These data could be seamlessly loaded into working projects at different locations different experts using the Reference Project Tool so that major datatype conversions, possible information loss or data corruption could be avoided. The same tool(s) provided the opportunity and was/were used to strictly fix the coordinate system, the templates, the nomenclature (*naming conventions* of logs, formations, structural elements, etc.) and unit system applied in order to decrease the chance of inconsistencies among the same data record in different projects (NEMES et al., 2021). (Similar

database challenge phenomena are outlined by CIMIC (2006) related to mature Russian assets planned to be redeveloped and optimised.) As a *quality assurance protocol*, several cross-checks and validation points were implemented during data loading into the Reference projects, such as anomaly detection (e.g., negative values in porosity logs), log-end effect check and wellhead and trajectory reality check.

A *new seismic interpretation* was carried out, incorporating the adjusted and synchronised well-pick set, the newly digitised data and the newly drilled wells. Uncertainty quantification was performed, mainly reflecting the velocity model's uncertainty. The new interpretation mitigated most of the anomalies of Phase 1, such as positive and negative peaks due to erroneous or missing trajectory/elevation data, log shifts or misinterpreted well tops. Hence, the resulting horizons were more realistic and lacked bullseyes.

In *structural modelling* several outlier datapoints had to be removed from horizon adjustment due to anomalous depth values compared to offset wells during Phase 1. The root cause of these anomalies was investigated one-by-one during Phase 2 since they can also have an effect on the spatial distribution of properties as well as completion data and production allocation (NEMES et al., 2021). The structural model was significantly simplified as during the Phase 1 history-matching process, the *in-field faults* showed a marginal impact on the flow pattern; hence, these were not modelled so that the unnecessary complexity involved in increasing the runtime (54 faults with subseismic throw if any were removed) could be avoided.

A particular set of wells (~100 wells) had a high impact on the *Bobrikovian Formation*'s modelling and history matching since these wells provided approximately 50% of the historical production from the formation. In addition, these wells were all drilled in the 1950s and 1960s, and, therefore, possessed limited trajectory data and a very limited petrophysical log suite (SP, GR and/or RES) (CIMIC, 2006). This led to a revisiting of the applied interpretation and modelling techniques, resulting in the maximising of the information value gained from the limited dataset, which influenced the rocktype distribution, especially in the southwest part of the field. This upgrade had a direct impact on the quality of the history matching and, consequently, increased the predictive capabilities of both the geomodel and dynamic model.

In rocktype (and petrophysical) modelling for the Bobrikovian Formation (Bb), the need for *trend maps* became evident so that the high degree of horizontal heterogeneity could be spatially distributed and controlled. The trend maps were created based on core and log data and were used during rocktype modelling in Phase 2. The application of these trend maps on one hand improved the chances of penetrating the Bobrikovian Formation in a favourable reservoir section, and one the other helped to identify areas where the Bobrikovian has a high

probability of being of poor quality, thus, having a direct impact on well placement and production forecasting for new well proposals.

The *subzonation* of the Tournaisian Formation (V1) also had a significant effect on property models, namely, that the lower part of the formation shows lower permeability compared to the upper zone, having a critical effect on saturation profile, productivity, and production-related water encroachment as well as water injection schemes.

The property modelling approach was altered – in three reservoirs (except Bobrikovian) total property modelling (TPM) was implemented so the modelling workflow could be made more flexible and the end results made more realistic geologically. The fine-tuned and *adjusted petrophysical interpretation* was the basis for property modelling including a revisited cut-off set. The new interpretation enabled the incorporation of a higher amount of core data, as the *core dataset* also grew by collecting and structuring existing data and filling in data gaps with new measurements.

The *permeability model* was updated with porosity-permeability regression curves through the incorporation of new core measurement results and subzonation.

The hydrocarbon initially *in-place volume update* is based on the newly updated geomodel, which is the main input for dynamic modelling; it can also be used to identify by-passed oil, which can also drive further field development activities. Although it is not detailed in the thesis, a preliminary 2D volumetrics (map-based) assessment was done for the *Verejskij Formation (A3)* (capping the Bashkirian Fm.) as well, as in some wells it showed inflows and in other fields of the region it was produced in better structural and quality reservoir spots.

A *fully integrated workflow* was outlined (>800 steps) so that the model could be updated on a regular (bi-weekly) basis in a standardised, automatable manner as new data (new wells, adjusted interpretations) arrived. With the workflow in place, the regular model updates are a minimum five times faster (up to ten times) through a significant reduction in the number of clicks and mouse movements compared to fully manual updates; in addition, human mistakes due to the monotonic updating process are overcome with a well-structured workflow (NEMES, 2022). This also means that geoscientists can dedicate more time and energy to creative tasks which really require the cognitive capacity of the expert instead of monotonous clicking. Transparency is key as the operator's partners also use and validate the subsurface models. A total workflow makes the understanding of the process faster and easier for alternative users, helps misunderstandings be avoided and saves time (NEMES, 2022).

Along with the geomodel construction, a quality check *guideline (*a.k.a., *checklist)* for geomodelling was outlined and implemented so that a high-level guidance in terms of quality assurance (two subsections of it are shown in Figure 75) could be provided.

ID	Job family	Job	Description
A	General		
A.1		Regional geology	A general understanding of regional geology. Including source rock, reservoir rocks, seals (sealing capacity), trap type, migration pathways, age, tectonics, stratigraphy, paleogeography and geological evolution.
A.2		Reservoir geological concept	A geological concept or concepts of the AOI, aspects of geological evolution having an effect on reservoir behavior, parameter distribution, Nelson-type.
A.3		Fluid type	Reservoir fluids, oil, gas, water
A.4		Software	Which software used and reasoning.
B	Data loading		
B.1		Data sources	A clear understanding of data sources (seismic, log, core, analogy…) used during geological modeling. Data gaps (also existing but not digitized / loaded, and not existing at all)
B.2		Consistent coordinate system	All input data shall have the same coordinate system.
B.3		Consistent reference level for TVD	True vertical depth's reference level must be unique across the project.
B.4		Consistent reference level for MD	Measured depth reference level must be unique across the project.
B.5		Reference level of seismic elements	Confirmation from seismic interpreter on reference level.
B.6		Domain of seismic elements	Confirmation from seismic interpreter on domain.
B.7		Outlier wellheads and/or trajectories	Visual cross-check of out of range well data.
B.8		Consistent trajectory input	Directional or position logs.
B.9		Consitency of logs and trajectory	No longer log than trajectory shall exist.
B.10		Extreme log values	Cross-check of logs statistics (esp. Key parameters (porosity, shale-content, water saturation) for extreme values.
B.11		Mistyped undefined log values	Fixed and consistent value for undefined data.
B.12		Consistent unit system	SPE Preferred metric / Oilfield
B.13		Consistent naming convention for input data	Log naming, reservoir naming, well naming etc.
B.14		Consistent use of coloring	Standardized use of color schemes for mapping, different cases, presentations etc.
B.15		All relevant data loaded from AOI	With special regard to well data
B.16		Cultural data	License boundaries, seismic acquisition polygons, mining plots, natural conservation areas, surface topography etc.
B.17		Completion data consistency	It shall be consistent with RE's database and discrepancies / out of formation perforations cross-checked.
B.18		Vintage of data	The freeze date of data set used.
B.19		Listing of issues / discrepancies revealed and assumptions	E.g. old wells without logs, trajectories, well picks etc. to be able to follow-up on used dataset at each step
B.20		Handling of old data	E.g. are they aerially concentrated homogenously distributed, how the data gap was bridged and what assumptions were made
B.21		Handling of uncertain data	E.g. in paleokarstic intervals, poor measurement, incomplete log set, old wells etc., uncertain trajectories

Figure 75: A screenshot showing the first two sections of the quality checklist as outlined based on the lessons learnt from Field A's subsurface evaluation process.

7.1.3 THE GEOMODEL'S AFTERLIFE

Although the most evident outcome of the building of the 3D model is the volume calculations, its main power resides in the spatial distribution of the geological properties propagated in the geocellular model, which can be the main input to dynamic simulation, which is the next crucial step in the subsurface modelling workflow. Without dynamic modelling (including history matching), the geomodel is non-valid and should be treated as a first run that needs several loops of iterative work (Figure 18) to reach its final form(s), as an infinite number of realisations is capable of describing the same input data. Only a model that went through this process can be treated as a source of prognosis for future production and as pressure trends, which are direct inputs to operational and financial planning.

During the *history-matching* process, several adjustments were made; in order to keep track of these adjustments (and other changes), an Excel-based *version tracker* was introduced that included all the changes done to the original geomodel with date, goal of the change, affected grids, type of change, the user, and the subworkflow affected due to the change. In order to further detail critical updates or revealed gaps/inconsistencies, a secondary 'buglist' was created in a slidepack.

To avoid information loss during handover, a *short guideline* (a.k.a., Workflow know-how) was drafted about the handling of the workflow and opportunities for upgrades. A summary of these is given in the 7.2 Recommendations subchapter.

The history-matched geomodels and dynamic models are used routinely in both the operation of Field A and for the planning of field development activities, such as:

- production and injector well placement (including targeting by-passed oil), or conversion and post-drill analysis (well success rate increased by minimum 15%);
- workover planning (squeezing, adding perforations, commingling production or, of equal importance, preventing it, and dual completion applicability);
- filtering opportunities of cost optimisation by extending existing wells instead of drilling new ones from the surface (no practical application yet);
- planning well stimulations (e.g., radial jet drilling, hydraulic fracturing) or other production optimisation activities;
- proving the suboptimal manner of actual water injection patterns and the replanning of the strategy sector-by-sector to reenergise the reservoir(s), which is the key challenge in improving the recovery factor in the main reservoirs;
- drilling horizontal wells (in the Lower Tournaisian Formation due to lower reservoir quality, but significant in-place volumes);
- highlighting upside potential in undrilled areas within and outside the actual license area, aiding the decision-making on license extension (if any);
- reinstating drilling of dedicated Bobrikovian wells;
- submission of updated field development plan to related authorities;
- reporting expected production profiles (and recoverable volumes) to related authorities as well as internally to key company stakeholders;
- reconciliation of volumetric data;
- an aid which supports daily operative decisions in the field;
- a tool which supports surface facility and ALS (artificial lift system)-related decisions (e.g., extension of capacity, optimising capacity, change of ALS).

The work delivered an improved level of understanding and triggered a *full reassessment* of the half-century-old development concept, including pressure maintenance system, workover strategy, sidetracking strategy and well stimulation practices applied in the field.

Secondarily – beyond field development planning/optimising – the Petrel project also serves as:

- a source of up-to-date basic data about the field and its wells (as a data repository) and historical information due to having the full-cycle workflow to promptly update the model with new data;

- a source of visual aids (maps, cross- and well-sections, animations), statistical parameters (geological, fluid and dynamic), in-place volumes and production and pressure forecasts for decision-making materials;
- a source of tabular information like well stock reports, well attributes, well tops, and volumetric data;
- an optimisation tool for wellpad utilisation, whereby unnecessary costs and environmental damage can be avoided by building new ones;
- a data and information sharing tool for business partners, as each piece of new information regarding subsurface is loaded and can be easily shared and combined with the version tracker Excel-sheet directly, which shows where changes can be expected;
- an aid during data gathering planning and optimisation (e.g., the earlier-described logging dataset adjustment);
- (with a post-study update) a tool to quantify the untapped oil resources of the Verejskij Formation (above Bashkirian Fm.) and identify further steps (if any).

A work the size of a Field A reevaluation not only has a direct technical impact, but also builds a highly effective *project team* and establishes data and information flow channels (front and back channels as well). This leads to smooth, more effective, collaborative work, which can be an incubator for fresh ideas and innovation.

The goals of the dissertation were set in Chapter 1.3.1, and the inventory of accomplishments is as follows:

I. *Establish a single, quality-checked, standardised database, for both static and dynamic subsurface data*. – Goal met.
II. *Drive a better understanding of the current and past events of the field that can serve as an aid for future planning of data acquisition*. – Goal met.
III. *Build an up-to-date 3D geological model to serve multiple purposes.* – All goals met.
    a. *Serve as a daily tool for reservoir management.*
    b. *Serve as a tool for data visualisation in 1, 2, and 3 dimensions.*
    c. *Serve as a tool for planning mid- and long-term field development, including water injection pattern optimisation, in-fill well drilling placement and upside oil potential identification.*
    d. *To be a direct input to flow simulation modelling.*
    e. *Serve as the basis, from a geological aspect, for updated field development plan documentation.*

   f. *Reestimate initial in-place volumes and its spatial distribution based on newly available data gathered since last modelling exercise.*

IV. *Build a full cycle geomodelling workflow in Petrel to make regular updates faster and smoother.* – Goal met.

V. *Prove that a complete geomodelling workflow can be built that is capable of automatising routine updates in the geomodel.* – Hypothesis proven.

VI. *Make the ever-current model shareable with business partners and third parties if necessary.* – Goal met.

VII. *Introduce the practical implications the work done can have on field development.* – Goal met.

VIII. *Highlight opportunities and risks associated with the area of interest and recommend a way forward.* – Goal met (next subchapter).

The dissertation formulated eight goals and has specified and met all of them (although the documentation described in Point III.e has not yet been compiled and submitted to the relevant authorities). New modelling techniques were introduced in the form of a fully integrated all-round workflow. In addition, most importantly, the link between a computer-based model and a producing oil field has been improved, resulting in short-, mid- and long-term in-field applications.

A main lesson learnt is that a first-pass, non-sophisticated, coarse model (i.e., Phase 1) is already capable of delivering a series of insights that can be directly applied in the daily operations of a field and can deliver significant support in understanding the approximate remaining potential and development opportunities for a mature oil field. However, a more sophisticated and up-to-date tool is needed to fully plan and realise these opportunities and to estimate the associated risks and uncertainties (NEMES et al., 2021).

The Phase 2 modelling was crucial and inevitable for several reasons, such as: newly gathered data; reinterpreted data; digitised old data becoming available; the mitigation of non-suitable modelling steps; the incorporation of experiences gathered during the first-pass history-matching process; the establishment of a fully integrated workflow; and, mainly, to acquire a better tool for the 3D representation of the subsurface characteristics of Field A (NEMES et al., 2021).

7.2 RECOMMENDATIONS

"*There is always room for improvement*": the cliché had already become evident during the creation of the Phase 2 model, as there was a *list of recommendations* of possible improvements created to support the way forward during the process. However, prior to

initiating the implementation of a wide range of adjustments, it was critical to accept that usually the most complicated models are not the best in terms of total errors; hence, a balance between complexity and total errors needed to be struck, which also has a tremendous impact on the time required for modelling jobs. It must always be emphasised that a model is not built for its own purpose; it is built to support and improve business decisions in an industry which deals with high uncertainties.

Further improvement on *dataflow and data loading* to the central database is necessary, both in terms of datatypes and removing the remaining redundancy from the system. (For example, well test and inflow information access from a structured database would deliver added value.) Further adjustments are still necessary, but the data management framework is already in place and optimisation is necessary to fix some discrepant elements/steps and implement lessons learnt.

A new or newly processed *3D seismic* may add value and support the spatial distribution of reservoir properties as the existing dataset was not able to deliver 3D trends applicable for direct use during property modelling.

The building of a *conceptual facies model* for each formation and the incorporation of the possible impacts of diagenesis to better describe the vertical and lateral heterogeneity is recommended.

The role of *faults* should be investigated further, and an attempt could be made to generate fault likelihood attributes to support the interpretation. There is a chance that the structural elements have a slight impact on flow directions. Targeted well tests or interference tests could deliver additional information.

A revisiting of the possible role of *natural fractures* in the carbonate reservoirs and their impact on fluid flow is recommended, as is the creation of a comparative study using the newly acquired image logs and available log information, well test data and production experience, and an adjustment of the geomodel based on the outcome of the study.

The applied initial OWC_i values should be revisited and adjusted, if necessary, employing a multidisciplinary approach including petrophysicists, core experts, well-test engineers and reservoir engineers working on the dynamic simulation. Also, there was a minor indication, that the OWC_i can be different in different segments, but at the very least can vary based on the rocktype of the given sector.

A *rocktyping* investigation should be performed to drive the spatial distribution of properties and better represent reservoir quality (SVIRSKY et al., 2004; PERALTA, 2009) as well as to trigger the applicability of *saturation height functions* for initial saturation modelling. Comprehensive case studies and rocktyping applications were published by MUHAMMAD in

2021 and MUHAMMAD et al. in 2022 regarding a mature Hungarian oil field having a similarly limited amount of log data and carbonate lithology, but with the use of machine learning techniques to boost the information content of the dataset.

In the case of the Serpukhovian Formation (C1s), the effect of paleokarstic features was lacking from the Phase 1 model, both in terms of volumes and flow behaviour. Geological interpretation of paleokarsts was performed by several experts based on well log data and mud loss information during drilling and core information, although the establishing of realistic representations remains a big challenge (CHUNG et al., 2011; LURPROMMAS et al., 2016; SHEN et al., 2019). *Paleokarst modelling* was not part of Phase 2 modelling either (NEMES et al., 2021). The recommendation is a revisiting of the modelling techniques applicable for paleokarsts and the application of trial-and-error tests against the production-history.

Also, in the case of the Serpukhovian reservoir, a *secondary cut-off* should be introduced in order to adjust the log-derived and core-derived ratio of the reservoir/non-reservoir ratio. On core (>150 m recovered) the net-to-gross ratio is evidently lower compared to the log-derived parameter, thus causing an inherent overestimation of in-place volumes. (As the C1s represent the smallest in-place volume, the adjustments were not a high priority during the post-evaluation; see Figure 74.)

The *net-to-gross modelling* was set up with the use of discrete parameters that should be improved by modelling the NtG as a continuous parameter, hence, aiding the history-matching process with improved connectivity. During this process there were partial updates made, and they had a positive impact on the quality of the geomodel in terms of matchability.

During the history-matching process, a scenario involving the application of *permeability cut-offs* should also be tested and included in the sensitivity analysis.

The *horizontal wells* should also be interpreted and the trajectories quality-checked and incorporated during the structural and property modelling. These were bypassed during both stages of modelling as they represent a tiny fraction of total well count (11 wells, ~2% of total wellcount) and complicate the modelling tasks.

In the geomodel a full-cycle *uncertainty quantification* should be performed, incorporating structural, petrophysical and stochastic uncertainty; the application of experimental design methods is advised to control the number of realisations describing the uncertainty space (BILLITER et al., 2008; JAMSHIDNEZHAD, 2015; SULAKSANA et al., 2017; GALIMZHANOV et al., 2017). Multiple stochastic *realisations* should be run and tested for dynamic simulation so that the range of sensitivity depending on the spatial (stochastic) uncertainty of petrophysical properties can be grasped.

With the use of updated in-place volume calculations, a comprehensive, detailed *volume reconciliation* should be initiated to visualise the parameters causing the changes.

The workflow should be amended with any required steps so that the full cycle remains intact. A '*control panel*' could be added to the existing workflow, which is meant to contain all the variables that occur in multiple subworkflows (e.g., range of porosity, cut-off values). In addition, with simple logical switches the run of the total workflow could be setup without the need to open multiple subworkflows and activate/deactivate commands. The overall idea is to have a master workflow where the most frequently altered parameters and steps could be adjusted and referenced in the actual workflows. It would also help in terms of discrepancies being avoided, as it could be the single-source-of-truth for each key parameter. Also, it could help in terms of the need to open the subworkflows one-by-one being avoided.

Finally, the geomodel is not finished without dynamic simulation; *several loops of iterations* are usually necessary to reach an acceptable level of history matching and to arrive at a model applicable for forecasting production and pressure and, hence, for the testing of a wide range of field development scenarios and setups.

In Field A, with the ongoing activities, it is critical to establish a schedule for *regular updates* of the geomodel so that an up-to-date representation of the ever-current knowledge can be maintained.

A set of *dashboards* is advised to be created for different purposes (e.g., drilling activities, workover activities, field overview, production overview) so that the daily monitoring of field life can be supported. A widely accessible platform for these visualisations is Microsoft's PowerBI, connected to the proper data tables (DINIZ et al., 2019). Widely accessible, regularly updated dashboards can create a sense of increased transparency amongst team members and also among management members and business partners.

After all these efforts and cross-validations, the author offers a closing quote as a reminder that believing that a model is an exact, correct representation of reality should be avoided:

"It ain't what you don't know that gets you into trouble. It's what you know for sure that just ain't so."

— Unknown

ACKNOWLEDGEMENTS

First, I would like to thank my family for all the patience and effort they have made to provide me the time to write this thesis. Thanks to Artúr for being a good sleeper. It was a long time ago that I stepped onto this road, so thanks to my wife for not letting me stop moving down it. I'm especially grateful to my father, who planted the seeds of curiosity and interest towards natural sciences in me during my childhood and supported my eversince.

I cannot be grateful enough to my co-authors in the cited papers, Szilvia and István, who not only co-authored, but supported me well beyond that in this work with encouraging words and ideas.

I would like to express my appreciation and greatest gratitude to every former and current colleague who has worked or is still working on the project, be you in Russia, Hungary, Spain, Turkey, Serbia or anywhere else in the world. It was an honour to work with you, to learn from you and to unite our efforts on this exciting, adventurous, challenging, but also professionally and personally highly rewarding road.

REFERENCES AND RESOURCES

1. ABBASZADEH, M., N. KOIDE, Y. MURAHASHI (2000): Integrated characterization and flow modeling of a heterogeneous carbonate reservoir in Daleel Field, Oman. – https://doi.org/10.2118/62514-PA

2. ADELU, A.O., A.A. ADEREMI, A. O. AKANJI, O. A. SANUADE, S. I. KAKA, O. AFOLABI, S. OLUGBEMIGA, R. OKE (2019): Application of 3D static modeling for optimal reservoir characterization. Journal of African Earth Sciences, 152, pp. 184–196.

3. AGBON I.S., G.J. ALDANA, J.C. ARAQUE, A.A. MENDOZA, M.E. RAMIREZ (2003): Resolving historical-data uncertainties for redevelopment of mature fields. – https://doi.org/10.2118/81101-MS

4. AKOUM, M., H. B. HAZZAA (2019): A data governance framework - the foundation for data management excellence. – https://doi.org/10.2118/198593-MS

5. ALBERTINI, C., F. BIGONI, A. COMINELLI, E. DELLA ROSSA, A. FRANCESCONI, V. TARANTINI (2014): Karachaganak, integrated reservoir studies on a giant field. – https://doi.org/10.2118/172274-MS

6. ASQUITH, G., D. KRYGOWSKI (2004): Basic well log analysis. AAPG, 249 pp.

7. AUNG, T.T., S. NOGUCHI, N. OIKAWA, T. KANNO, M. TAMAKI, K. AKIHISA (2011): Integrated facies modeling workflow for methane hydrate reservoir along the eastern Nankai Trough, Japan. – https://doi.org/10.2523/IPTC-15303-MS

8. BAILLIE, J., T. COOMBES, S. RAE (1996): Dunbar reservoir model, a multidisciplinary approach to update brent reservoir description and modelling. – https://doi.org/10.2118/35528-MS

9. BALAJI, K., M. RABIEI, H. CANBAZ, Z. AGHARZEYVA, S. TEK, U. BULUT, C. TEMIZEL (2018): Status of data-driven methods and their applications in oil and gas industry. – https://doi.org/10.2118/190812-MS

10. BANKS, R.B. (1982): New thoughts on an old topic: Reservoir integration (Volumetrics). – https://doi.org/10.2118/11339-MS

11. BAZHENOVA, T.K. (2009): Evolution of oil and gas generation in the Earth's history and petroleum prediction in sedimentary basins. Russian Geology and Geophysics, 50, pp. 308–319.

12. BELLMANN, L.H. (2018): Integrated geological modeling for higher confidence development decisions, Sultanate of Oman. – https://doi.org/10.2118/193043-MS

13. BIGONI F., A. FRANCESCONI, C. ALBERTINI, D. CAMOCINO, E. DISTASO, O. BORROMEO, F.LUONI (2010): Karachaganak - dynamic data to drive geological model. – https://doi.org/10.2118/139881-MS

14. BILLITER, T.C., G. R. KING, K. DAGISTANOVA (2008): Application of brown-field experimental design techniques to a super giant carbonate reservoir. – https://doi.org/10.2118/115422-MS

15. BLOTSKAYA, A.I., G.S. SARDAROV (2020): West Siberia Jurassic Sediments Rock Typing and Digital Models Creating for Geological Model Refining. – https://doi.org/10.2118/201965-MS

16. BOWLER, T. (2015): Falling oil prices: Who are the winners and losers? – BBC News, 19.01.2015.

17. BREIT, V.S., J.A. DOZZO (2004): "State-of-the-art" integrated studies methodologies – An historical review. – https://doi.org/10.2118/87032-MS

18. BRITISH PETROLEUM (2020): Statistical Review of World Energy. 69th Edition. London, UK. 66 pp.

19. CAERS, J. (2005): Petroleum Geostatistics. Society of Petroleum Engineers, pp. 104.

20. CAMPBELL, E. (2017): Standardizing Business Processes within Oil and Gas Markets to Reduce Costs. – https://doi.org/10.4043/27665-MS

21. CAMPOBASSO S., A. GAVANA, G. BELLENTANI, I. PENTOLI, M. PONTIGGIA, L. VILLANI, T.H. ABDELSAMAD (2005): Multidisciplinary workflow for oil fields reservoir studies - case history: Meleiha Field in Western Desert, Egypt. – https://doi.org/10.2118/94066-MS

22. CHUNG E., T. K. KING, O. ALJAAIDI (2011): Karst modeling of a Miocene carbonate build-up in Central Luconia, SE Asia: Challenges in seismic characterisation and geological model building. – https://doi.org/10.2523/IPTC-14539-MS

23. CIMIC, M. (2006): Russian mature fields redevelopment. – https://doi.org/10.2118/102123-MS

24. CORLETT, H., D. HODGETTS, J. HIRANI, A. ROTEVATN, R. TAYLOR, C. HOLLIS (2021): A geocellular modelling workflow for partially dolomitized remobilized carbonates: An example from the Hammam Faraun Fault block, Gulf of Suez, Egypt. Marine and Petroleum Geology, 126, 19 pp.

25. DARLING, T. (2005): Well logging and formation evaluation. Elsevier, 335 pp.

26. DAVID, R. M., L. SAPUTELLI, H. HAFEZ, R. NARAYANAN, P. COLOMBAN, T. AL NAQBI (2017): Upstream data architecture and data governance framework for efficient integrated upstream workflows and operations. – https://doi.org/10.2118/188962-MS

27. DAVIES, A., M. D. SIMMONS (2021): Demand for 'advantaged' hydrocarbons during the 21st century energy transition. Energy Reports, 7, pp. 4483–4497.

28. DEHGHANI, K., S. JENKINS, D. J. FISCHER, M. SKALINSKI (2008): Application of integrated reservoir studies and techniques to estimate oil volumes and recovery—Tengiz Field, Republic of Kazakhstan. – https://doi.org/10.2118/102197-MS

29. DEPERSIO, G. (2019): Why did oil prices drop so much in 2014?. – Investopedia, 06.05.2019.

30. DINIZ, F. C. D. C. B., B. D. N. ESPINDOLA, I. D. AFFONSO, J. L. QUEIROZ, L. Q. OLIVEIRA, G. BARBOZA, C. A. PEREIRA (2019): Data-centrism: A path to digital transformation in engineering design environment. – https://doi.org/10.4043/29860-MS

31. DOLIGEZ, B., Y. HAMON, M. BARBIER, F. NADER, O. LERAT, H.. BEUCHER (2011): Advanced workflows for joint modelling of sedimentary facies and diagenetic overprint, impact on reservoir quality. – https://doi.org/10.2118/146621-MS

32. EBONG, D. E., A.E. AKPAN, J.G. URANG (2019): 3D structural modelling and fluid identification in parts of Niger Delta Basin, Southern Nigeria. Journal of African Earth Sciences, 158, pp. 1–10.

33. EL-BAGOURY, M. A., M. FAHMY, M. KAMAL, A. SAAD, V. VANHEESWIJK, R. KHARBOUTLY (2017): Key learnings from re-development activity and waterflood EOR of mature brown

field: heterogeneous compartmentalized reservoir case study, Western Desert, Egypt. – https://doi.org/10.2118/188574-MS

34. EL-KOUJOK, M., R. GOURIVEAU, N. ZERHOUNI (2011): Reducing arbitrary choices in model building for prognostics: An approach by applying parsimony principle on an evolving neuro-fuzzy system. Microelectronics Reliability, 51, pp. 310–320.

35. ELLIOTT S., H.H. HSU, T. O'HEARN, I. F. SYLVESTER, R. VERCES (1998): The giant Karachaganak Field - Unlocking its potential. Oilfield Review, 10/3, pp. 16–25.

36. EMERSON (2019): Roxar RMS Software Help. Online.

37. FADEEVA N. P., E. V. KOZLOVA, E. N. POLUDETKINA, T. A. SHARDANOVA, N. V. PRONINA, A. V. STUPAKOVA, G. A. KALMYKOV, A. N. KHOMYAK (2015): The hydrocarbon-generation potential of the Domanik rocks in the Volga–Ural Petroliferous Basin. Moscow University Geology Bulletin, 71/1, pp. 41–49.

38. FONTANA, S., N.A. ATMAJASETIADI, F. BREGA, J. VILLACRES, K. ALIYEV, C. CATALANI (2015): Reservoir modelling of a structurally complex deepwater field: A Gulf of Mexico case history. – https://doi.org/10.2118/175045-MS

39. GABNASYROV, A. V., N. A. LYADOVA, I. S. PUTILOV, S. I. SOLOVYEV (2016): Domanik Shale oil: Unlocking potential. – https://doi.org/10.2118/182075-MS

40. GAFFNEYCLINE (2020): Mature fields optimization. GaffneyCline Ltd. 4 pp.

41. GALIMZHANOV, S., E. ISKAKOV, P. LEVCHENKO, A. TURMANBEKOVA, K. ZHUMAGULOV (2017): Application of experimental design for probabilistic IOR evaluation at Korolev Field. – https://doi.org/10.2118/188996-MS

42. GALINDO, R. O., A. GALINDO-NAVA, E. PEREZ-ALVIS, E. ORTUNO (2012): Static/dynamic model for Chac Field based on a novel multidisciplinary workflow. – https://doi.org/10.2118/153708-MS

43. GOLOV, A.A., I.K. KOROLYUK, Y.L. MELAMUD, A.D. SIDOROV, S.A. PUNANOVA (2000): Structural-formational characteristics of Devonian clastic complex of Volga-Ural Province. – Petroleum Geology, 34, pp. 213–222.

44. GOLOVATSKIY, Y., O. PETRASHOV, V. SYRTLANOV, I. VAFIN, N. MEZHNOVA (2015): Huge mature fields rejuvenation. – https://doi.org/10.2118/177334-MS

45. GONG, X., K. GUAN, L. CHEN, T. LIU, C. FU (2021): What drives oil prices? — A Markov switching VAR approach. Resources Policy, 74, 13 pp.

46. GÜLEN, G. (2015): Commodity price cycles: Explained by an expert. The Way Ahead, 11/2, pp. 13–15.

47. GUSEVA, D. M., V. K. BUTENKO, L. I. BORISOVA, R. N. PODOSJAN, N. N. POPOVA (1975): Geologija i razrabotka neftjanyh i gazovyh mestorozdenij Orenburgskoj Oblasti. Juzno-uralskoe ot delenie Vsesojuznogo naucno-iscnedovatelskogo geologorazvedocnogo neftjanogo instituta, Ministerstvo Geologi SSSR, Privolzskoe Kniznoe Izdatelstvo, pp.256. (Original title: Гусева, д. М., В. К. Бутенко, Л. И. Борисова, Р. Н. Подосян, Н. Н. Попова 1975: Геология и разработка нефтяных и газовых месторождений Оренбургской Области. Южно-уральское от деление Всесоюзного научно-исспедовательского геологоразведочного нефтяного института, Министерство Геологии СССР, Приволжское Книжное Издательство, pp. 256.)

48. HANDAYANI N., J. H. SIMAMORA (2012): Challenge in mature field's waterflood project: facing limited GGRP data & budget issue. – https://doi.org/10.2118/149853-MS

49. HAQ, B.U., S.R. SCHUTTER (2008): A chronology of Paleozoic sea-level changes. – Science, 322, pp. 64-68.

50. HARRISON, B. (1995): Russian-style formation evaluation. The London Petrophysical Society and The Geological Society London. 244 pp.

51. HOFFMAN, D.R. (2013): Petrel workflow for adjusting geomodel properties for simulation. – https://doi.org/10.2118/164420-MS

52. HOLLUND, K.U.; R. HAUGE, A. R. SYVERSVEEN, A. JORSTAD, T. LIE, H. C. RONNEVIK (2005): From geological knowledge to good decisions using simple stochastic models: A North Sea case study. – https://doi.org/10.2118/97177-MS

53. HORN, A., D. OSTWALD, M. REISERT, F. BLANKENBURG (2014): The structural-functional connectome and the default mode network of the human brain. NeuroImage. 102/1, pp. 142–151.

54. HUVAZ, O., H. SARIKAYA, T. ISIK (2007): Petroleum systems and hydrocarbon potential analysis of the northwestern Uralsk basin, NW Kazakhstan, by utilizing 3D basin modeling methods. Marine and Petroleum Geology, 24, pp. 247–275.

55. INTERNATIONAL ENERGY AGENCY (2020): World Energy Outlook 2020. 464 pp.

56. JAMSHIDNEZHAD M. (2015): Experimental design in reservoir engineering in Experimental Design in Petroleum Reservoir Studies. Gulf Professional Publishing, pp. 57-98.

57. JOURNEL, A.G. (1995): Geostatistics and Reservoir Geology in YARUS J. M., R.L. CHAMBERS (eds) (1995): Stochastic modeling and geostatistics: principles, methods, and case studies. AAPG Computer Applications in Geology Series, No. 3., 379 pp.

58. KALETA, M., G. VAN ESSEN, J. VAN DOREN, R. BENNETT, B. VAN BEEST, P. VAN DEN HOEK, J. BRINT, T. WOODHEAD (2012): Coupled static/dynamic modeling for improved uncertainty handling. – https://doi.org/10.2118/154400-MS

59. KAMANLI, S.T. (2019): An integrated 3D geological modeling study of a heavy oil field in Southeast Turkey. – https://doi.org/10.2118/198369-MS

60. KETINENI, S.P., Y. TAN, K. L. HOFFMAN, M. JONES, M. GHORAISHY (2019): Unlocking additional barrels from a mature conventional oil field through unconventional technologies: A case study on Rangely oil field, Colorado. – https://doi.org/10.2118/196033-MS

61. KISELEVA, Y. A., T. P. ZHEGLOVA, M. V. DAKHNOVA, S. V. MOZHEGOVA, E. S. NAZAROVA, G. S. NECHITAILO (2017): The role of Domanik deposits in the formation of oil pools in the central areas of the Volga–Ural petroleum province (Buzuluk depression). Russian Geology and Geophysics, 58, pp. 310–321.

62. KOLCHUGIN, A. N., V. P. MOROZOV, E. A. KOROLEV, A. A. ESKIN (2014): Carbonate formation of the Lower Carboniferous in central part of Volga–Ural basin – Research Communication. Current Science, Vol. 107, No. 12., pp. 2029–2035.

63. KOLCHUGIN, A. N., V. P. MOROZOV, E. A. KOROLEV, A. A. ESKIN (2014): Features of the structure of zones of water-oil contacts in carbonate rocks of the Bashkirian Stage (using Akanskoye oilfield in the Volga-Ural Petroleum and Gas Province as an example). Bioscienes Biotechnology Research Asia, 11, pp. 143–149.

64. KONTOROVIC, A.E., L.V. EDER, I.V. FILIMONOVA, M.V. MISENIN, V. J. NEMOV (2016): Neftjanaja promyslennost istoriceski glavnyh centrov Volgo-Uralskoj neftegazonosnoj provincii, elementy i istori, blizajsie i otdalennye perspektivy. Geologija i geofizika, 2016, 57, 12, pp. 2097–2114. (Original title: КОНТОРОВИЧ, А.Э., Л.В. ЭДЕР, И.В. ФИЛИМОНОВА,

М.В. МИШЕНИН, В.Ю. НЕМОВ (2016): Нефтяная промышленность исторически главных центров Волго-Уральской нефтегазоносной провинции, элементы их истории, ближайшие и отдаленные перспективы. Геология и геофизика, 2016, 57, 12, pp. 2097–2114.)

65. KONTOROVIC, A.E., V.R. LIVSHITS (2017): New methods of assessment, structure, and development of oil and gas resources of mature petroleum provinces (Volga–Ural province). Russian Geology and Geophysics, 58, pp. 1453–1467.

66. KRAUSS, C. (2017): Oil prices: What to make of the volatility. – The New York Times, 14.06.2017.

67. KUMAR, S., X.-H. WEN, J. HE, W. LIN, H. YARDUMIAN, I. FAHRURI, Y. ZHANG, J. M. ORRIBO, Y. GHOMIAN, I. P. MARCHIANO, A. BABAFEMI (2017): Integrated static and dynamic uncertainties modeling big-loop workflow enhances performance prediction and optimization. – https://doi.org/10.2118/182711-MS

68. LANG, K., B. R. AUER (in-press): The economic and financial properties of crude oil: A review. North American Journal of Economics and Finance, in-press, 45 pp.

69. LEVERETT, C. M. (1941): Capillary behavior in porous solids. Transactions of the AIME, 142, pp. 152–169.

70. LUKMANOV, R., E. IBRAHIM (2018): Unlocking tight gas volume with integrated multidisciplinary diagnostic approach. – https://doi.org/10.2118/191412-18IHFT-MS

71. LUPU, D. (2019): Current trends in the exploitation of mature gas fields in the context of rehabilitation concept. MATEC Web of Conferences, 290, 10005.

72. LURPROMMAS, T., Y. HAMON, O. LERAT, J. NANTAWUTTISAK (2016): Reservoir characterisation and modelling of the Nang Nuan Oil Field Thailand. – https://doi.org/10.2523/IPTC-18870-MS

73. MA, Y.Z. (2018): An accurate parametric method for assessing hydrocarbon volumetrics: Revisiting the volumetric equation. – https://doi.org/10.2118/189986-PA

74. MANTOPOULOS, A., D. A. MARQUES, S. P. HUNT, S. NG, Y. FEI, M. HAGHIGHI (2015): Best practice and lessons learned for the development and calibration of integrated production models for the Cooper Basin, Australia. – https://doi.org/10.2118/176131-MS

75. MARTINO, L., A. IULIANO, U. SEZAI, C. HERN (2012): Reviewing mature fields - A case history. – https://doi.org/10.2118/152715-MS

76. MCCOMB, T., B. F. TOWLER (2013): How to tackle the challenge of mature field development. The Way Ahead, 9/3, pp. 18–20.

77. MEDDAUGH, W. S. (2015): Improving reservoir forecasts by understanding the relative impacts of sparse data, reservoir modeling workflow and parameter selection, and human bias. – https://doi.org/10.2118/175009-MS

78. MENNING, M., A.S. ALEKSEEV, B.I. CHUVASHOV, V.I. DAVYDOV, F.-X. DEVUYST, H.C. FORKE, T.A. GRUNT, L. HANCE, P.H. HECKEL, N.G. IZOKH, Y.-G. JIN, P.J. JONES, G.V. KOTLYAR, H.W. KOZUR, T.I. NEMYROVSKA, J.W. SCHNEIDER, X.-D. WANG, K. WEDDIGE, D. WEYER, D.M. WORK (2006): Global time scale and regional stratigraphic reference scales of Central and West Europe, East Europe, Tethys, South China, and North America as used in the Devonian–Carboniferous–Permian Correlation Chart 2003 (DCP 2003). Palaeo, 240, 1-2, pp. 318–372.

79. MEYERHOFF, A.A. (1984): Carboniferous oil and gas production in the eastern hemisphere. Journal of Petroleum Geology, 7/2, pp. 125–146.

80. MUHAMMAD, N. A. A. (2021): Naturally fractured basement reservoir characterization in a mature field. – https://doi.org/10.2118/206027-MS

81. MUHAMMAD, N. A. A., I. NEMES, ZS. BIHARI, H. SOLTÉSZ, Á. BÁRÁNY, L. TÓTH, SZ. BORKA, GY. FERINCZ (2022): Naturally fractured carbonate reservoir characterization: A case study of a mature high-pour point oil field in Hungary. – https://doi.org/10.30632/SPWLA-2022-0109

82. MUKHAMETDINOVA, A. Z., A. V. KAZAK, T. I. KARAMOV, N. N. BOGDANOVICH, M. F. SERKIN, I. V. PUTILOV, A. N. CHEREMISIN (2020): Experimental workflow for characterization of storage and transport properties of tight Domanic reservoirs (Russian). – OIJ-2020-11-082-087-RU.

83. NANDURIKAR, N., L. WALLACE (2011): Failure to produce: An investigation of deficiencies in production attainment. – https://doi.org/10.2118/145437-MS

84. NANDURIKAR, N. S., P. M. KIRKHAM (2012): The economic folly of chasing schedules in oil developments and the unintended consequences of such strategies. – https://doi.org/10.2118/162878-MS

85. NEMES, I. (2016): Revisiting the applications of drainage capillary pressure curves in water-wet hydrocarbon systems. Open Geosciences, 8/1, pp. 22–38.

86. NEMES, I. (2022): Applications of automated Petrel workflows in 3D reservoir geologic modelling – A case study. Central European Geology, Akadémiai Kiadó. https://doi.org/10.1556/24.2022.00129.

87. NEMES, I., SZ. SZILÁGYI SEBŐK, I. CSATÓ (2021): Challenges of a mature Russian field's re-development – advantages and disadvantages of quick-look geological modelling. Central European Geology, 64/2, pp.74–90.

88. NG, K. F., T. AFANDI, D. SA'ADON, J. JA'AFAR, M. A. OMAR, N. A. LATIFF, G. I. SANTOSO, K. ALANG, I. D. ROBERTS, N. MURAD, D. PERMANASARI, F. KUTTY (2016): Success Story: A new development concept utilising new advanced technology in a very old complex mature field. – https://doi.org/10.2118/176120-MS

89. O'BRIEN, J., L. SAYAVEDRA, J. L. MOGOLLON, T. LOKHANDWALA, R. LAKANI (2016): Maximizing mature field production - A novel approach to screening mature fields revitalization options. – https://doi.org/10.2118/180090-MS

90. ODEZULU, C., S. OLAWOLE, K. SAIKIA, D. MENTO (2014): Effect of sequence stratigraphy-based facies modeling for better reservoir characterization: A case study from Powder River Basin. – https://doi.org/10.2118/171746-MS

91. OKUYIGA, M., A. BERRIM, R.SHEHAB, S. HADDAD, C. XIAN, M. A. LAWI (2007): Multidisciplinary approach and new technology improve carbonate reservoir evaluation. – https://doi.org/10.2523/IPTC-11528-MS

92. OLEA, R.A. (1994): Fundamentals of semivariogram estimation, modeling, and usage. In J.M. YARUS and R. L. CHAMBERS (eds.) (1994): Stochastic Modeling and Geostatistics Principles, Methods, and Case Studies as part of AAPG Computer Applications in Geology, No. 3. American Association of Petroleum Geologists, pp.342.

93. ONAKO (Orenburgskaja neftjanaja akcionernaja kompanija) (1997): Geologiceskoe stroenie i neftegazonosnost Orenburgskoj Oblasti. Orenburgskoe Kniznoe Izdatelstvo, pp.

43–56. (Original title: Оренбургская нефтяная акционерная компания (ОНАКО) 1997: Геологическое строение и нефтегазоносность Оренбургской Области. Оренбургское Книжное Издательство, pp. 43–56.)

94. PÁPAY, J. (2003): Development of petroleum reservoirs. Akadémiai Kiadó, 940 pp.

95. PARFENOV, A.N., S.S. SITDIKOV, O.V. EVSEEV, V.A. SHASHEL, K.K. BUTULA (2008): Particularities of hydraulic fracturing in dome type reservoirs of Samara Area in the Volga-Urals Basin. – https://doi.org/10.2118/115556-MS

96. PARSHALL, J. (2012): Mature fields hold big expansion opportunity. Journal of Petroleum Technology, 10, pp. 52–58.

97. PEDERSON, J.M., M.S. MOON, H.Y. AL-AJEEL (1998): Data Validation: Key to development of an integrated reservoir model for the Wara Formation, Greater Burgan Field. – https://doi.org/10.2118/50989-PA

98. PERALTA, O. O. (2009): Rock types and flow units in static and dynamic reservoir modeling: Application to mature fields. – https://doi.org/10.2118/122227-MS

99. PETERSON, J.A., J.W. CLARKE (1983a): Geology of the Volga-Ural petroleum province and detailed description of the Romashkino and Arlan oil fields. – USGS Open-File Report pp. 83-711.

100. PETERSON, J.A., J.W. CLARKE (1983b): Petroleum geology and resources of the Volga-Ural Province, U.S.S.R. Geological Survey Circular, 885, 33 pp.

101. PYRCZ, M. (2020): Data analytics and geostatistics – Lecture 1: Statistics. Online course. The University of Texas at Austin.

102. PYRCZ, M. J., E. GRINGARTEN, P. FRYKMAN, C. V. DEUTSCH (2006): Representative input parameters for geostatistical simulation. In COBURN, T. C., J. M. YARUS, R. L. CHAMBERS (eds.): Stochastic modeling and geostatistics: Principles, methods, and case studies, volume II: AAPG Computer Applications in Geology, 5, pp. 123– 137.

103. PYRCZ, M.J., C.V. DEUTSCH (2014): Geostatistical reservoir modeling. Oxford University Press, 449 pp.

104. RAJPUT, S., M. XINJUN, A. BAL, K. RAHMAN, W. JUNWEN (2015): Reducing uncertainty in horizontal well placement for improved field development. – https://doi.org/10.2118/175083-MS

105. REDDEN, J.E., C. T. STRICKLAND (2017): Innovating in the oil and gas industry: A Framework for aligning innovation strategy and tactics. – In: SPE Oklahoma City Oil and Gas Symposium, SPE.

106. RINGROSE, P. (2008): Total-property modeling: dispelling the net-to-gross myth. – https://doi.org/10.2118/106620-PA

107. RINGROSE, P., M. BENTLEY (2015): Reservoir model design - A practitioner's guide. Springer, 250 pp.

108. SABOORIAN-JOOYBARI, H. (2016): A structured mobility-based methodology for quantification of net-pay cutoff in petroleum reservoirs. – https://doi.org/10.2118/183643-PA

109. SAIKIA, K., W. KHAN, S. RAMAKRISHNAN (2015): Challenges in deepwater reservoir characterization: From well log interpretation and well testing to 3D geocellular modeling. – https://doi.org/10.2118/175071-MS

110. SANASI C., L. DAL FORNO, G. R. MACCARINI, L. MUTIDIERI. P. TEMPONE, D. MEZZAPESA, M. DALLA ROSA, A. BUCCI, F. RINALDI, C. ANDREOLETTI (2021): Company data governance transformation to support the business evolution. – https://doi.org/10.2118/207525-MS

111. SARKAR, S., S. KUMAR, K. REDDY, V. SHANKAR, U. S. MISHRA, V. SABHARWAL (2015): Arresting decline in the Ravva field: Success story of Phase-5 drilling campaign. – https://doi.org/10.2118/178753-MS

112. SCHLUMBERGER (2021): Petrel Guru. Build: 20161025.1.

113. SEASHOLTZ, M. B., B. KOWALSKI (1993): The parsimony principle applied to multivariate calibration. Analytica Chimica Acta, 277, pp. 165–177.

114. SELEZNEVA, N. N. (2016): Lower–Middle Devonian rocks at junction of the Volga–Ural Anteclise, Ural Foredeep, and North Caspian Basin: Lithology and perspectives of petroleum potential. Lithology and Mineral Resources, 2016, 51/3, pp. 228–241.

115. SHAKIROV, V.A., D.E. DERYUSHEV, M.A. IVANOV (2015): Current results of overlooked targets identification in the fields of the Orenburg region. – https://doi.org/10.2118/176606-MS

116. SHEN F., K. ZHAO, Y. ZHANG, Y. YU, J. LI (2019): Hierarchical approach to modeling karst and fractures in carbonate karst reservoirs in the Tarim Basin. – https://doi.org/10.2118/197264-MS

117. SHIRAZI, A.F., S.V. SOLONITSYN, I.A. KUVAEV (2010): Integrated geological and engineering uncertainty analysis workflow, Lower Permian Carbonate Reservoir, Timan-Pechora Basin, Russia. – https://doi.org/10.2118/136322-MS

118. SHUDOVA, S. D. (1975): Detalnoe stratigraficheskoe raschenenie Kzanskih otlozheniy mezhdurechya Buzuluka- Ika. In: Geologia I razrabotka neftyanih I gazovih mestorozhdeniy Orenburgskoy oblasti, Ed: M. Guseva,Ministerstvo Geologii SSSR, Pribolzhskoe Knizhnoe Izdatelstvo Saratov, pp.11–19.

119. SMIRNOV, L. P. (1958): Oil-bearing basins on the eastern edge of the Russian Platform – In: Habitat of Oil: American Association of Petroleum Geologists Bulletin, pp. 1168-1181.

120. SPAGNUOLO, M., F. SCALISE, G. LEONI, F. BIGONI, F. M. CONTENTO, P. DIATTO, A. FRANCESCONI, A. COMINELLI, L. OSCULATI (2018): Driving reservoir modelling beyond the limits for a giant fractured carbonate field - Solving the puzzle. – https://doi.org/10.2118/192708-MS

121. SUHAREVICH, P. M., V. I. KAYDALOV, M. N. CHIKIN (1975): Razmeshenie resursov nefti I gaza I osnovnie napravlenia poiskovo-razvedochnih rabot na territorii Orenburgskoy oblasti. In: Geologia I razrabotka neftyanih I gazovih mestorozhdeniy Orenburgskoy Oblasti Ed: M. Guseva,Ministerstvo Geologii SSSR, Pribolzhskoe Knizhnoe Izdatelstvo Saratov, pp. 3–10.

122. SULAKSANA, A., M. CHEERS, H. DOLS, V. YAP (2017): Novel reservoir modeling and experimental design approach to tackle the challenge of modeling highly compartmentalized reservoirs under large uncertainties in a mature offshore field, Malaysia. – https://doi.org/10.2118/188443-MS

123. SVIRSKY, D., A. RYAZANOV, M. PANKOV, P. W. M. CORBETT, A. POSYSOEV (2004): Hydraulic flow units resolve reservoir description challenges in a Siberian oil field. – https://doi.org/10.2118/87056-MS

124. SZILÁGYI SEBŐK, SZ.., I. CSATÓ, I. NEMES (2021): Sedimentology and depositional system of a transitional shallow marine- coastal complex, Lower Visean deposits in the Central Volga-Ural Petroleum Province, Orenburg. Central European Geology, 64/2, pp. 113–132.

125. TARVER, E. (2015): 4 Reasons why the price of crude oil dropped. – Investopedia, 22.10.2015.

126. TIWARI A., N. M. SHANNA, C. MANICKAVASAGAM, P. FARTIYAL (2015): Production optimisation in mature fields. – https://doi.org/10.2118/178090-MS

127. TÖRÖK, J., L. FÜRCHT, T. BÓDI (2012): PVT properties of reservoir fluids. University of Miskolc, 186 pp.

128. TRAVINA, L. M. (1975): Tipi razrezov kamennougolnih otlezhenii v svyazi s tektonicheskim razvitiem territorii Orenburgskoy oblast. In Geologia i razrabotka neftyanih i gazovih mestorozhdeniy Orenburgskoy Oblasti Ed: M. Guseva,Ministerstvo Geologii SSSR, Pribolzhskoe Knizhnoe Izdatelstvo Saratov, pp. 20–26.

129. ULMISHEK, G. F. (1988): Upper Devonian-Tournaisian facies and oil resources of the Russian Craton's eastern margin. Canadian Society of Petroleum Geologists, Memoir 14, pp. 534–535.

130. VAVRA, L. C., G. J. KALDI, M. R. SNEIDER (1992): Geological application of capillary pressure: a review. AAPG Bulletin, 76, pp. 840–850.

131. VERMA, M. K., G. F. ULMISHEK, A. P. GILBERSHTEIN (2000): Oil and gas reserve growth - A model for the Volga-Ural Province, Russia. – https://doi.org/10.2118/62616-MS

132. VO THANH, H., Y. SUGAI, R. NGUELE, K. SASAKI (2019): Integrated workflow in 3D geological model construction for evaluation of CO_2 storage capacity of a fractured basement reservoir in Cuu Long Basin, Vietnam. International Journal of Greenhouse Gas Control, 90, 14 pp.

133. VOLZ, R. F., K. BURN, M. L. LITVAK, S. C. THAKUR, S. SKVORTSOV (2008): Field development optimization of Eastern Siberian giant oil field development under uncertainty. – https://doi.org/10.2118/116831-MS

134. WASKITO, L.B., R. WIDIATMO, H. GUNAWAN, S. PENGXIAO (2015): Integrated offshore mature field revitalization in Asri Basin, North Business Unit Area, Southeast Sumatra, Indonesia. – https://doi.org/10.2118/176250-MS

135. WORDEN, R. H., E. C. HEASLEY, S. A. BARCLAY (1999) The effects of petroleum emplacement on diagenesis : a comparison between sandstone and carbonate reservoirs. Sciences Géologiques, 99, pp. 149–153.

136. ZAKREVSKY, K.E. (2011): Geological 3D modelling. EAGE, 262 pp.

137. ZONENSHAIN, L.P., V.G. KORINEVSKY, V.G. KAZMIN, D.M. PECHERSKY, V.V. KHAIN, V.V. MATVEENKOV (1984): Plate tectonic model of the south Urals development. Tectonophysics, 109, pp. 95–135.

138. ZOZULYA, A., Y. PETRAKOV, Y. KARPEKIN, V. BLINOV, P. WEINHEBER, I. KARIPOV (2016): New life for old fields: Identification of bypassed productive zones, formation evaluation and formation testing through casing with modern wireline tools. – https://doi.org/10.2118/182102-MS

LINKS

[1] https://www.eia.gov/

[2] https://ourworldindata.org/grapher/energy-consumption-by-source-and-region

[3] https://www.youtube.com/watch?v=cnoOZRytULE&t=362s

SUMMARY IN ENGLISH

The main topic of the study is the added value generated through reservoir modelling in a mature oil field, with a special focus on the workflow creation to fully describe the geomodelling process. Multiple authors and studies have been published on the area, but only a few touch base on the details of the workflow. This thesis describes the whole process, from data gathering to the afterlife of the reservoir geological model, through a case study of a mature oil field in the Russian Federation, named Field A.

The author aims to link the current study to the scientific publications related to the wider topic, both to show similar cases and to offer further readings on specific topics. In order to show the broader context, namely, the history of the energy market, and prognosed future subchapters are dedicated to setting the scene.

Due to the global oil price drop in 2014 (*Introduction* chapter), the preventive/reactive measures taken by one oil company included increasing ownership of its assets by reviewing them individually and crosschecking historical volumes and potential and related costs so as to identify marginal or unprofitable elements within their existing portfolio.

In line with the strategy, Field A of the Volga-Ural Basin was also part of an internal reinvestigation. Several unexpected challenges, problems and pitfalls were faced while performing the work, building the database, quality checking and interpreting the data dating back to 1947. To overcome these challenges related to this mature field, new approaches and fit-for-purpose methods were needed while the overall goal to arrive at a reliable estimation of remaining field potential was maintained.

Field A is a mature onshore oil field in the Russian Federation, discovered in 1947 (*Field history* chapter) and put on production in 1949. Geologically, the field is located in the central part of the Volga-Ural Basin, south of the South Tatar Arch. For decades field development was limited; an accelerated drilling campaign started before 2010 as a new operator took over the field. The field is still on production with an active water injection system and more than 500 wells in total.

As detailed in the *Geological background* chapter, the field has four productive formations, of which three are carbonate (Tournaisian, Serpukhovian, Bashkirian Formations) and one is clastic (Bobrikovian Formation), with one underexplored possible upside potential in the Verejskij Formation overlaying the Bashkirian Formation.

The deepest amongst them is the Tournaisian Formation, overlaid by the Bobrikovian, making up the deep reservoirs (~800-1000 m TVDSS depth); the former storing approximately 50% of the total oil initially in-place of the field. The Serpukhovian and the Bashkirian Formations comprise the shallow reservoirs (~500-600 m TVDSS). The same chapter also

positions the field in the extended region by giving a short overview of the regional geology and tectonic settings referencing several authors dedicated to the studies of the Volga-Ural Basin.

The total cumulative oil produced as of 2020-03-01 was almost 13 million m^3 (~82 million barrels). However the actual recovery factor is only approximately 10–14% (depending on STOIIP case), providing room for a detailed investigation so that the development strategy can be optimised. Based on analogous fields and calculations, the expected final recovery in similar reservoirs could be between 25-35%, or even higher with modern secondary and tertiary methods (PÁPAY, 2003).

All of the reservoirs are undersaturated oil reservoirs (hence, no primary gas cap exists), with medium-type black oil having an API gravity of 25-27°. The prevailing driving mechanism is weak to moderate aquifer drive and depletion. The dissolved gas content is low (5–40 m^3/m^3), and therefore plays an ancillary role as a driving mechanism.

Due to non-technical reasons, a double modelling workstream was outlined and followed; two geomodels were built: a first-pass simplified one (Phase 1); and consequently a second, more detailed and established one of higher quality and greater quantity of input data (Phase 2).

The Phase 1 model (*Discussion of the first pass geological model (Phase 1)* chapter), a first-pass 3D geological model, was constructed along with wrangling, filtering and interpreting seventy years of subsurface data.

The chapter describes the challenges and mitigative actions concerning the Phase 1 model, describes the geomodelling workflow followed during Phase 1, and shows the immediate and long-term added value of a simplified model. It was evident since the beginning that the first-pass model requires revisiting from multiple aspects regarding input dataset, applied methods and depth of analysis. It also aims to highlight how and why several decades of data and information can and should be structured, following a consistent workflow, to maximise the information value from existing data and to identify critical gaps that were worth investing time and capital in.

The next step was the creation of the Phase 2 geomodel (*Discussion of the main geological model (Phase 2)* chapter). The Phase 2 model aimed at overcoming the shortcomings of Phase 1 in several aspects: data quality and quantity; applied methods; applied software; and workflow.

The differences between the two models are shown and described in detail. A special focus is put on the discussion of how an integrated full-cycle Petrel workflow was created to optimise future model updates and usage. Each geomodelling task is described in theory and

practice and shows how the workflow handles the given step. Prior to describing the subworkflows, an introduction is given about the concept.

Each subworkflow is covered in a separate subchapter, from initialisation to volumetric calculations. The subchapters start with a general overview, then detail the script, and conclude with a list of outcomes.

The Phase 2 geocellular model was built for all four formations and was separated into two 3D grid models (Number 1 – the Tournaisian and Bobrikovian Formations; Number 2 – the Serpukhovian and Bashkirian Formations). The complete workflow, which is capable of updating the whole reservoir geological model, consists of more than 800 steps, grouped into ten subworkflows.

The *Conclusions* chapter is subdivided into two main parts, describing the deliverables of both the Phase 1 and Phase 2 models individually and outlining a way forward in the form of recommendations for future model updates.

The *Deliverables and identified opportunities* subchapter describes the results and insights gained from the modelling exercises and, most importantly, how these insights can be used to generate additional recoverable volumes, that is, additional income for the company. The palette ranges from optimised data gathering programmes to the reinitiated drilling of horizontal wells and a reshuffled water injection well pattern.

The Petrel workflow was successfully built and in subsequent model updates and allowed the model to be shared with business partners and the methodology on reviews and audits to be explained. The created workflow significantly decreased the time necessary to incorporate new data into the geomodel and run general updates. Beyond that it created transparency, as each step can be recreated and cross-checked if necessary by any interested parties.

The *Recommendations* subchapter focuses on possible updates/upgrades that are recommended to be made both to the model or the workflow in the future to improve its speed, transparency and applicability.

The thesis is framed in such a way that in the first chapter a group of eight goals are set, and in the last chapter each of these are revisited and reflected upon. Each of the goals were fulfilled over the course of the work. The following paragraph details these goals and the summarised corresponding resolution (in *italics*).

1) Establish a single, quality-checked, standardised database for both static and dynamic subsurface data. – *Petrel Reference Project (static data) and OFM*

Reference Project (dynamic data) were built, and data loading guidelines and processes were put into operation.

2) Drive a better understanding of the current and past events in the field that can aid in the future planning of data acquisition. – *The integrated reevaluation of Field A had an impact on almost all aspects of the ongoing field development (data acquisition, drilling, well workovers, further potential).*
3) Build an up-to-date 3D geological model to serve multiple purposes. – *The model was built with a full-cycle Petrel workflow, proving all of its benefits. The model is used for visualisation, source of data and statistics, input to full-field dynamic modelling, and reconciliation of initial in-place volume.*
4) Build a full-cycle geomodelling workflow in Petrel to make regular updates faster and smoother. – *The workflow was outlined from data loading to volumetric calculation; it is modular, and can be automatically run as new data arrive or other updates are necessary.*
5) Prove that a complete geomodelling workflow can be built that is capable of automatising routine updates in the geomodel. – *This was proven as the whole workflow was used in practice multiple times following the completion of the geomodel.*
6) Make the ever-current model shareable with business partners and third parties, if necessary. – *The reference projects, the working geomodel (Phase 2) and the workflow itself are shareable and were continuously shared after the finish of the geomodel as well. All the updates and adjustments can be followed in a version tracker sheet so that transparency can be maintained.*
7) Introduce the practical implications the work done can have on field development. – *The outcomes are described in detail for both Phase 1 and Phase 2 modelling and beyond.*
8) Highlight opportunities and risks associated with the area of interest and recommending a way forward. – *The last subchapter lists the identified recommendations (which at the same time highlight the weak points of the model) for a way forward, which have already been partially implemented since the since the study was completed.*

SUMMARY IN HUNGARIAN

A tanulmány fő témája a rezervoármodellezés hozzáadott értéke érett szénhidrogén-mezők esetén, külön figyelmet fordítva a modellezés teljes menetét leíró lépéssorra (*„workflow”*). Számos szerző és publikáció foglalkozik érett mezőkkel, de csak néhány tér ki a modellezés menetét leíró lépéssor részletes tárgyalására. Jelen tanulmány a teljes folyamatot leírja az adatgyűjtéstől a geomodel utóéletéig, mindezt egy az Orosz Föderáció területén található érett mező (*Mező A*) esettanulmányán keresztül.

A szerző egyik célja, hogy elhelyezze a jelen tanulmányt a rendelkezésre álló, releváns nemzetközi szakirodalomban és bizonyos specifikus témákban további forrásokra mutasson rá. Ahhoz, hogy a témát szélesebb kontextusban is el lehessen helyezni az első fejezet rövid kitekintést tartalmaz az energiaszektorra és annak jövőjére.

A 2014-es olajáresés új folyamatokat indított el az szénhidrogén termeléssel és kutatással foglalkozó vállalatok között (*Introduction fejezet*). Ez a globális olajáresés az olajcégeknél egy portfólió-felülvizsgálati hullámot indított el. Mezőik mélyebb és pontosabb megértése és kivizsgálása kezdődött, hogy a fennmaradó potenciált, még kitermelhető mennyiségeket és a várható költségeket feltérképezzék, a nem, vagy csak marginálisan profitábilis elemeket pedig leírják.

A Volga-Ural-medencében található Mező A is egy ilyen, felülvizsgálat alá eső elem volt. Számos váratlan kihívás és probléma jelentkezett már az adatbázis építés, minőségellenőrzés és adatértelmezés fázisában, mivel az adatok 1947-től fogva folyamatosan keletkeztek. Az ehhez hasonló érett mezőket érintő áthidalandó kihívások újszerű, esetenként egyedi megoldásokat kívántak, hogy az eredeti cél, azaz a mező még fennmaradó potenciálja pontosítható legyen.

Mező A egy érett – 1947-ben felfedezett, 1949-ben termelésbe állított - szárazföldi olajmező az Orosz Föderáció területén (*Field history fejezet*). A mező geológiailag a Volga-Ural-medence központi részén található. A mezőfejlesztés évtizedekig lassú tempóban haladt, fokozott aktivitás 2010-ben kezdődött, amikor a jelenlegi operátor átvette az üzemeltetést. A mező jelenleg is termel, összesen több mint 500 kúttal rendelkezik, és aktív nyomásfenntartás történik, vízbesajtolás révén.

A *Geological background fejezet* részletesen leírja a mező tektono-sztratigráfiai jellemzőit, a mezőben négy produktív formáció található, melyek közül három karbonátos (Tournaisian, Serpukhovian, Bashkirian Formációk), és egy sziliciklasztos (Bobrikovian Formáció), illetve egy még termelésbe nem állított, alulkutatott sekély formáció, a Verejskij, a Bashkirian Formáció fölött.

A legmélyebben a Tournaisian Formáció található, melyre a Bobrikovian települ, együttesen alkotják a mély rezervoárokat (~800-1000 mtsza). Előbbi tárolja a mező teljes kezdeti földtani vagyonának ~50%-át. A Serpukhovian, és a Bashkirian Formációk alkotják a sekély rezervoárokat (~500-600 mtsza). Ugyanez a fejezet a mezőt elhelyezi a regionális geológiai képben felhasználva a rendelkezésre álló nemzetközi szakirodalmat a Volga-Ural-medencéhez kapcsolódóan.

A 2020.03.01-ig összesen kitermelt olaj majdnem elérte a 13 milló m^3-t (~82 millió hordó). Mindazáltal a mezőszintű aktuális kihozatali tényező mindössze ~10-14%, ami további fejlesztéseknek ad teret a mező üzemeltetését és termeltetését illetően. Analóg mezők alapjám hasonló rezervoárokban az elsődleges kihozatali tényező elérheti a 25-35%-ot, másodlagos, harmadlagos eljárások alkalmazásával pedig ennél magasabban is (PÁPAY, 2003).

Minden rezervoár alultelített olajtelep (azaz nincs elődleges gázsapkájuk), fluidumuk medier típusú kőolaj, 25-27 °API sűrűségű. A jellemző hajtási mechanizmus gyenge vagy közepes erősségű aquifer és kimerülés. A kezdeti oldottgáz-tartalom minimális, jellemzően 5-40 m^3/m^3, ezért elhanyagolható a nyomásfenntartó szerepe.

Nem technikai okok miatt, hanem üzletpolitikai megfontolásból két geomodell készült. Egy első, egyszerűbb (Phase 1), és ezt követően egy részletesebb, több bemenő adatra építő és az első hiányosságait áthidaló második (Phase 2).

A Phase 1 három dimenziós geomodel készítésével párhuzamosan zajlott a több, mint 70 évnyi bemeneti adat gyűjtése, rendszerezése, szűrése és értelmezése. (*Discussion of the first pass geological model (Phase 1) fejezet*).

A fent jelzett fejezet bemutatja a Phase 1 geomodellezés kihívásait és azok megoldásait, leírja a modellezés menetét és a rövid-, valamint hosszútávú hozzáadott értéket, amit a modell képvisel. A modellezés kezdetétől bizonyos volt, hogy az első, egyszerűsített modellt felül kell később vizsgálni, mind bemenő adatok, mind a használt eljárásokat tekintve. Szintén a fejezet célja, hogy bemutassa miért és hogyan lehetséges több évtizednyi adattömb módszeres rendszerezése és értelmezése, ezzel maximalizálva annak információ-tartalmát., valamint a kritikus adathiányok feltárását.

Következő lépésben készült el a Phase 2 geomodell (*Discussion of the main geological model (Phase 2) fejezet*). A Phase 2 modell deklarált célja volt a Phase 1 változat hiányosságainak orvoslára adatminőségi és -mennyiségi, metodológiai és “workflow” szempontból is.

A két modellváltozat különbségeit és hasonlóságait részletesen tárgyalja a dolgozat. Kiemelt hangsúlyt fektetve a részletes és teljes “Petrel workflow”-ra, amely hivatott a jövőbeni frissítéseket és mindennapi használatot felgyorsítani, optimalizálni. A geomodellezés minden

lépésének elméleti háttere is röviden bemutatásra kerül, együttesen a gyakorlati alkalmazással és a “workflow”-ban elfoglalt helyével. Minden „subworkflow” bemutatása előtt röviden összefoglalásra kerül az adott részt koncepciója, kiindulópontja és célja.

Minden “subworkflow” - az adatbetöltéstől a volumetrikus számításokig - egy-egy külön alfejezetet képez. Az alfejezetek általános áttekintéssel kezdődnek, majd lépésről-lépésre bemutatják az összeállított „workflow”-t, annak kódsorát és összefoglalást adnak az adott rész kimenő adatairól, eredményeiről.

A Phase 2 geomodell szintén tartalmazza a négy termelt formációt, de két grid modellre bontva, az egyikben a mélyebb formációk a Tournaisian és a Bobrikovian található, míg a másikban a sekélyek, azaz a Serpukhovian és a Bashkirian Formáció.

A teljes „workflow”, amely lehetővé teszi a geomodell átfogó frissítését több mint 800 lépésből áll és 10 „subworkflow”-ra van bontva.

A *Conclusions fejezet* két fő részre osztható, az egyik foglalkozik a Phase 1 illetve a Phase 2 modellek eredményeivel, hozzáadott értékével (*Deliverables and identified opportunities alfejezet*). A második fő rész (*Recommendations alfejezet*) pedig az esetleges további fejlesztési lehetőségekre tesz javaslatot.

The *Deliverables and identified opportunities alfejezet* leírja a modellezésből levezethető eredményeket és lehetőségeket, és hogyan konvertálhatóak ezek az eredmények addicionális készletekké, termeléssé, azaz üzleti értékké a vállalat számára. A paletta széles az optimalizált adatszerzési programoktól az újra elindított horizontális fúrási programig és az felülvizsgálat és optimalizált vízbesajoltó rendszerig terjed.

A Petrel “workflow” elkészült, és az azt követő modellfrissítsek, üzleti partnerekkel történő modellmegosztások, zsűrik és auditok során sikeresen alkalmazásra került. A készített “workflow” jelentősen csökkenti a modell frissítéséhez szükséges időt, ezzel is növelve a hatékonyságot. Mindemelett nagyban növeli az átláthatóságot, mivel minden lépés megismételhető, ellenőrizhető, frissíthető ha szükséges.

A *Recommendations alfejezet* azokra a jövőbeni lehetséges frissítésekre, javításokra fokuszál, amelyek tovább tudják növelni a “workflow” hatékonyságát és áttekinthetőségét, alkalmazhatóságát.

A dolgozat keretét adja az annak elején kitűzött tételszerű nyolc cél, amely célok mindegyikére reflektál a szerző az utolsó fejezetben. Minden cél teljesült, a következő felsorolás ezen célokat és a teljesülésük (*dőlt betűvel*) vázlatos összefoglalóját adja.

1) Standardizált, ellenőrzött statikus és dinamikus adatokat tartalmazó adatbázis létrehozása.. – *Petrel Reference Project (statikus adatok) és OFM Reference Project*

(dinamikus adatok) készületek, melyek kiegészülnek az adatok betöltését, ellenőrzését tartalmazó folyamatleírással.

2) A mező előéletének alaposabb megismerése által felülvizsgálni a jövőbeni terveket és lehetőségeket az adatszerzés területén. – *A mező újrafeldolgozása az adatszerzésen messze túlmenően, a művelés szinte minden aspektusára hatással volt. (adatszerzős, fúrás, átképzések, maradék potenciál …).*
3) Egy multifunkciós, aktualizált 3D geomodell felépítése. – A modell elkészült, a teljes folyamatot leíró Petrel „workflow”-val egyetemben, utóbbinak minden előnyével. *A modell vizualizációs, operációs, számítási, szimulációs célokat szolgál, valamint a volumetrikus felülvizsgálat alapja.*
4) Egy a teljes geomodellezés leíró Petrel „workflow” felépítése, a modell frissítésnek gyorsabbá és átláthatóbbá tétele céljából. – *A “workflow” elkészült, a folyamatot az adatbetöltéstől a volumetrikus számításokig leírja, moduláris és új adatok/információk esetén automatikusan futtatható.*
5) Annak bebizonyítása, hogy egy a teljes geomodellezést leíró „workflow” felépíthető. – *Bizonyítást nyert, mivel az elkészített “workflow” számos alkalommal alkalmazásra került a geomodell frissítése során.*
6) A mindenkori aktuális geomodell megoszthatóságának biztosítása üzleti partnerek és harmadik felek számára. – *A referencia projektek, a geomodell (Phase 2), és a “workflow” is megosztható. Minden frissítés naplózásra kerül egy verziókövető táblában.*
7) Az elvégzett modellezés gyakorlati alkalmazásainak bemutatása. – *Mind a Phase 1, mind a Phase 2 modellezési periódus eredményei és gyakorlati hatásai bemutatásra kerültek.*
8) További lehetőségek és kockázatok felvázolása a vizsgálat területet illetően. – *Az utolsó fejezet bemutatja az azonosított lehetőségeket, javaslatokat, és párhuzamosan rávilágít a geomodell gyengeségeire, határaira. (A felvázolt további lehetőségek egy része a tanulmány lezárása óta már megvalósult.)*

APPENDIX

Appendix II: *Panel A* – Structural map of the pre-Paleozoic basement of the Volga-Ural basin; the black rectangle indicates the vicinity of Field A (depth contours digitised after PETERSON and CLARKE, 1983a; IHS MARKIT). The Volga-Ural basin, with its acreage of cca. 700,000 km^2, is the second most prolific HC region in the Russian Federation – after Western Siberia – spreading from the Urals geosyncline in the east to the Volga River and Russian platform in the west and the Caspian basin at the south (PARFENOV et al., 2008; MEYERHOFF, 1984). *Panel B* – Generalised lithological column and geological stages of the Early Devonian-Permian in the AOI, indicating the main reservoir formations in Field A (modified after HAQ et al., 2008 and PETERSON and CLARKE,1983a, IHS MARKIT, SZILÁGYI et al., 2021).

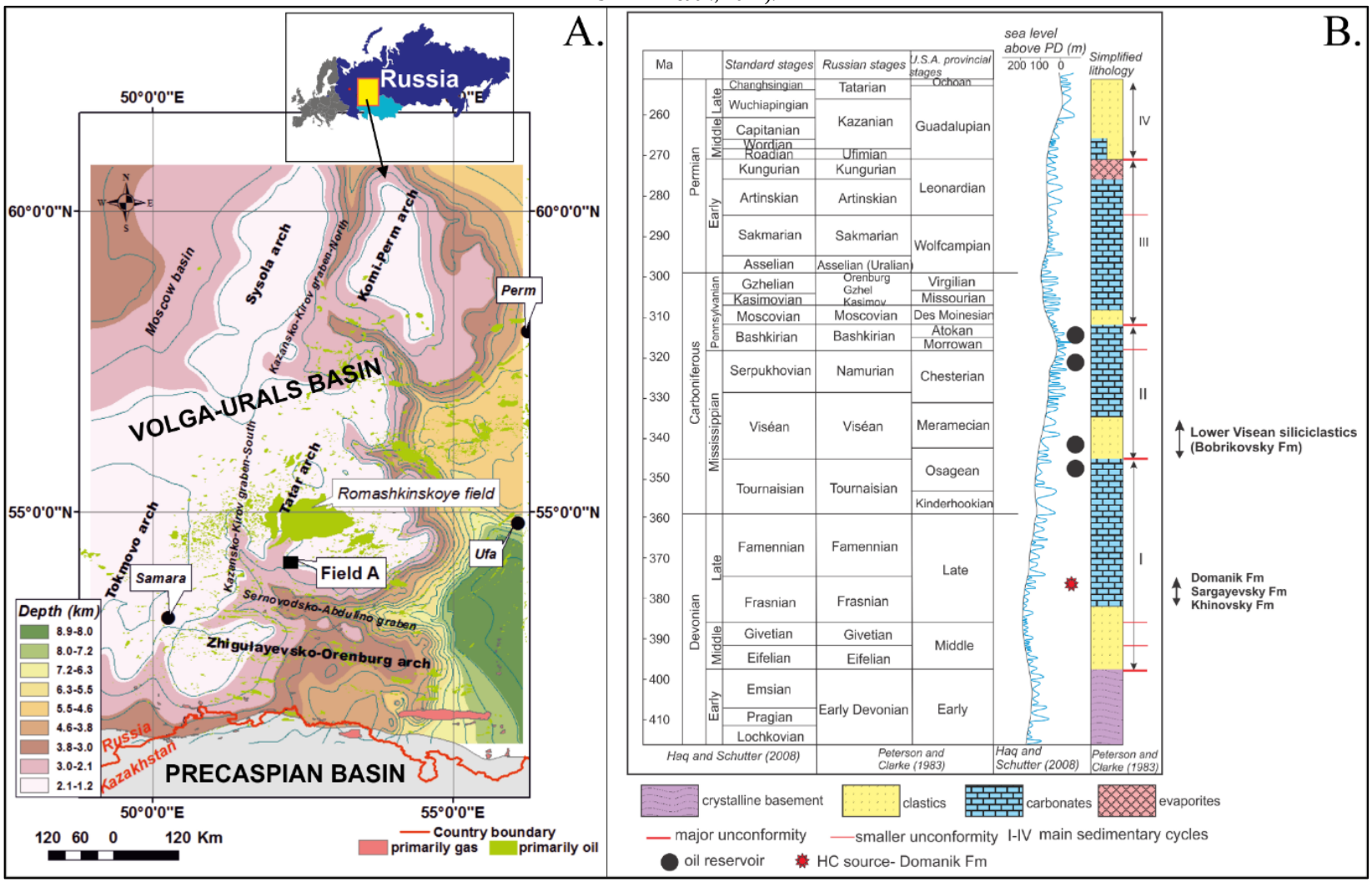

Appendix III: A structural top map of C1s Formation in the AOI (depth domain) with well picks used for anchoring the depth horizon (green discs), indicating 3D seismic coverage (white) and official license boundary polygon (blue). The easternmost N-S strike-slip fault is the eastern bounding fault of the field (along the license boundary); from other directions structural deepening bounds the HC accumulations (dark green line indicates the external OWC polygon) (Source: NEMES et al., 2021).

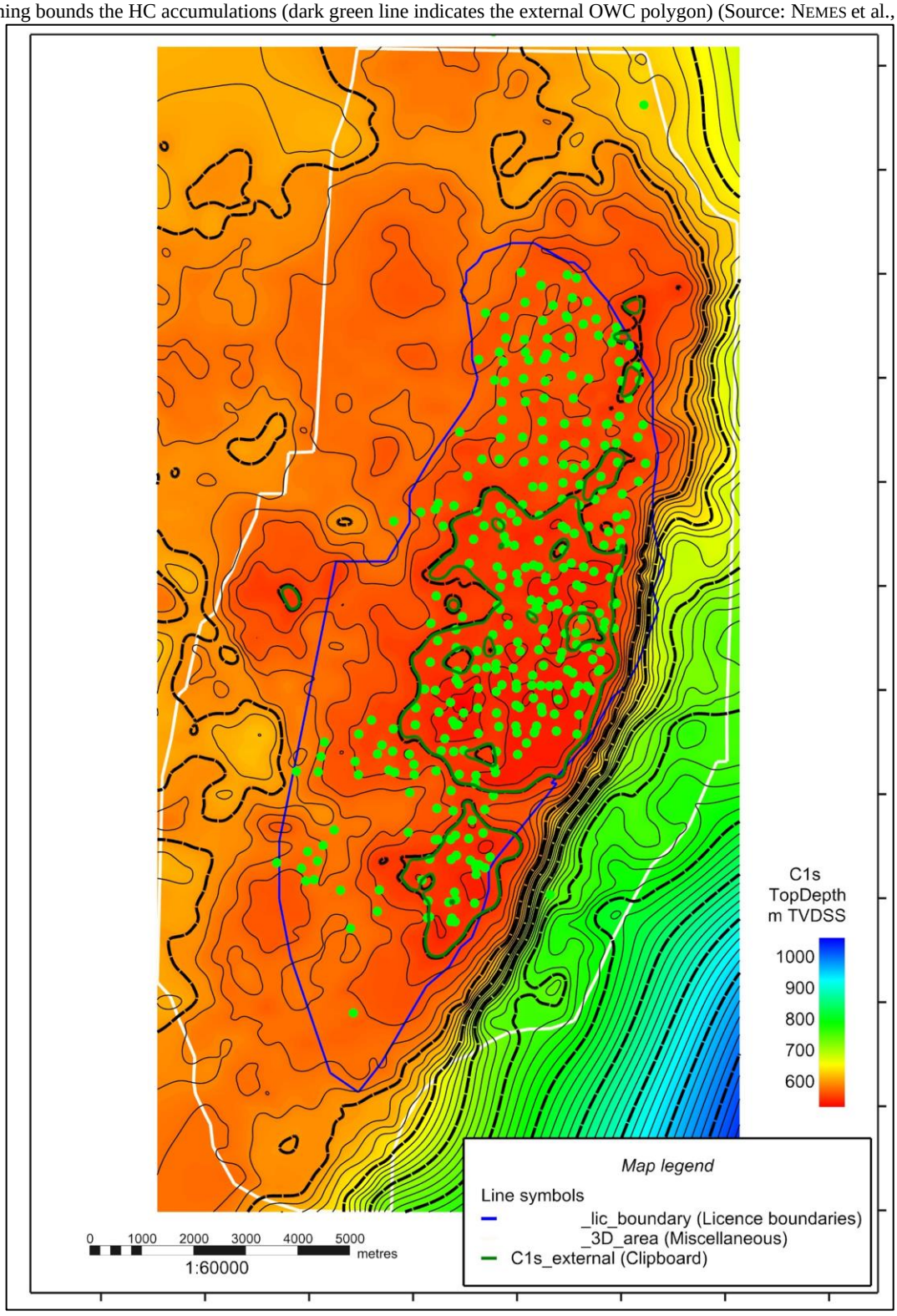

Appendix IV: The production license boundary of Field A is indicated with a yellow solid line, the 3D seismic acquisition coverage by a striped white line. The underlying map is a topographic map of the surrounding area.

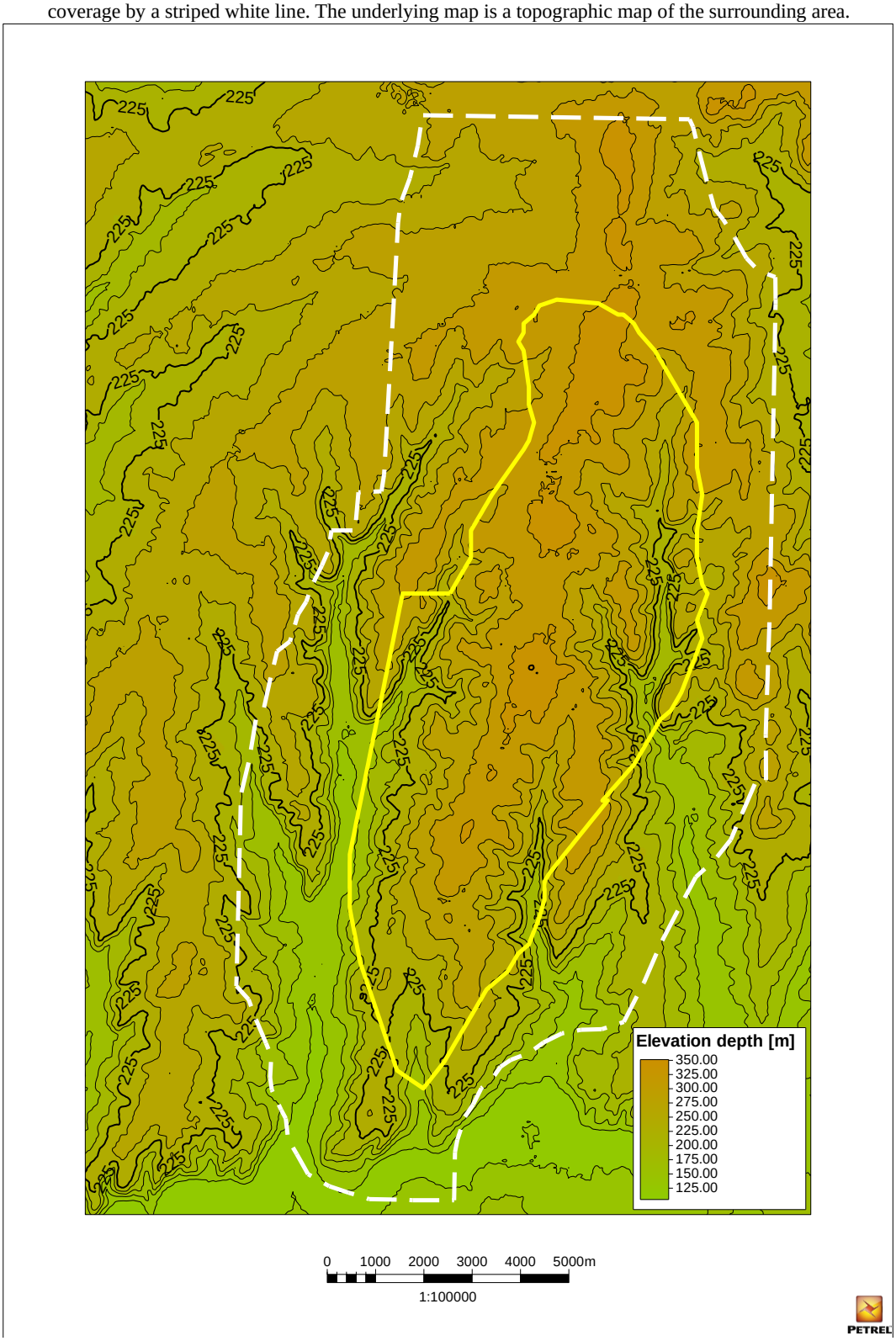

Appendix V: A4 – Bashkirian top surface in depth domain, as prepared for structural modelling. The white squares represent the well tops used for adjustment. The white solid line shows the eastern bounding fault's polyline at the given depth. The red polygon represents the production license boundary. The high well density within the license area should be noted.

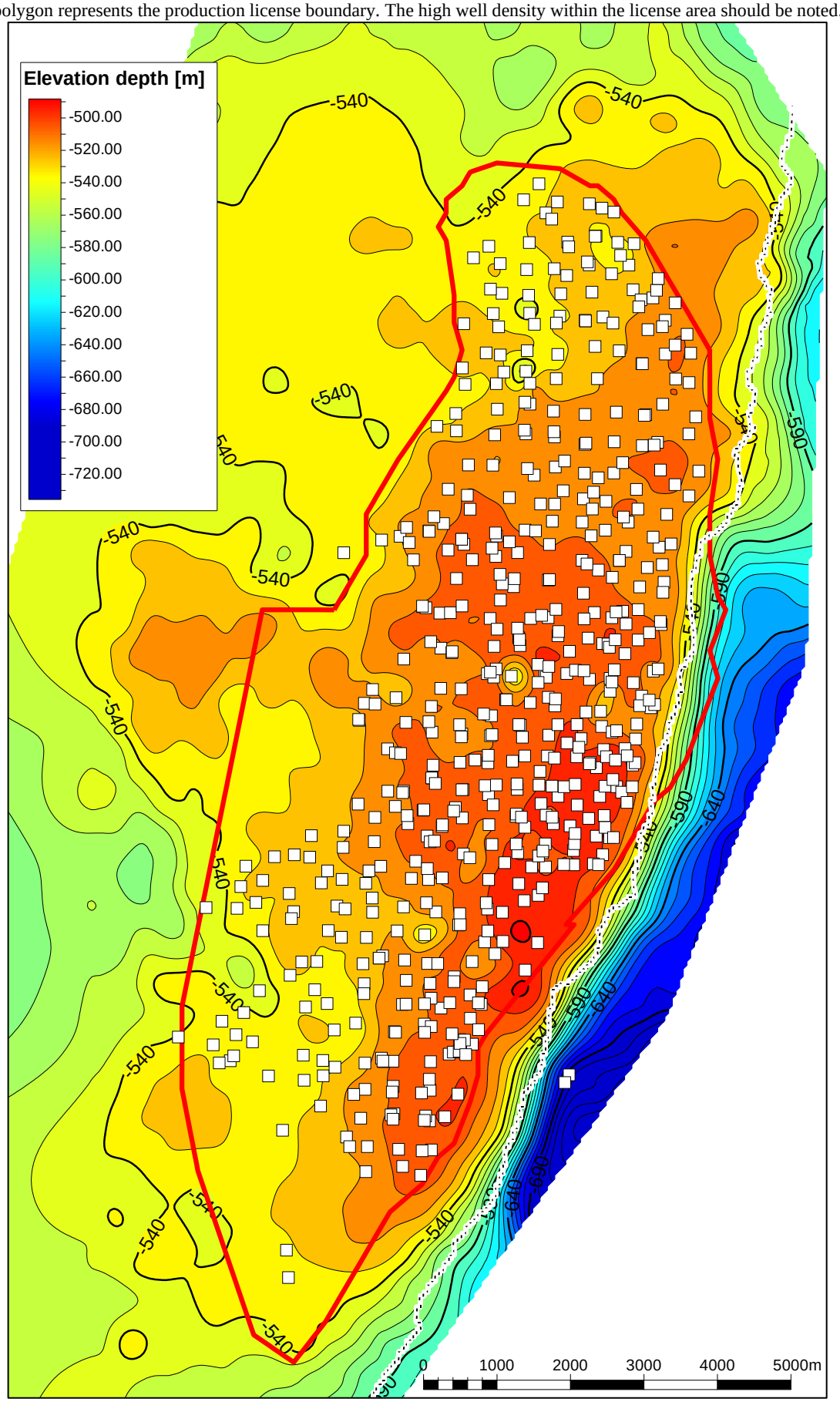

Appendix VI: True vertical thickness (TVT) map of the Tournaisian Formation. The gross thickness in the AOI is greatly uniform; minimal thickness changes can be identified.

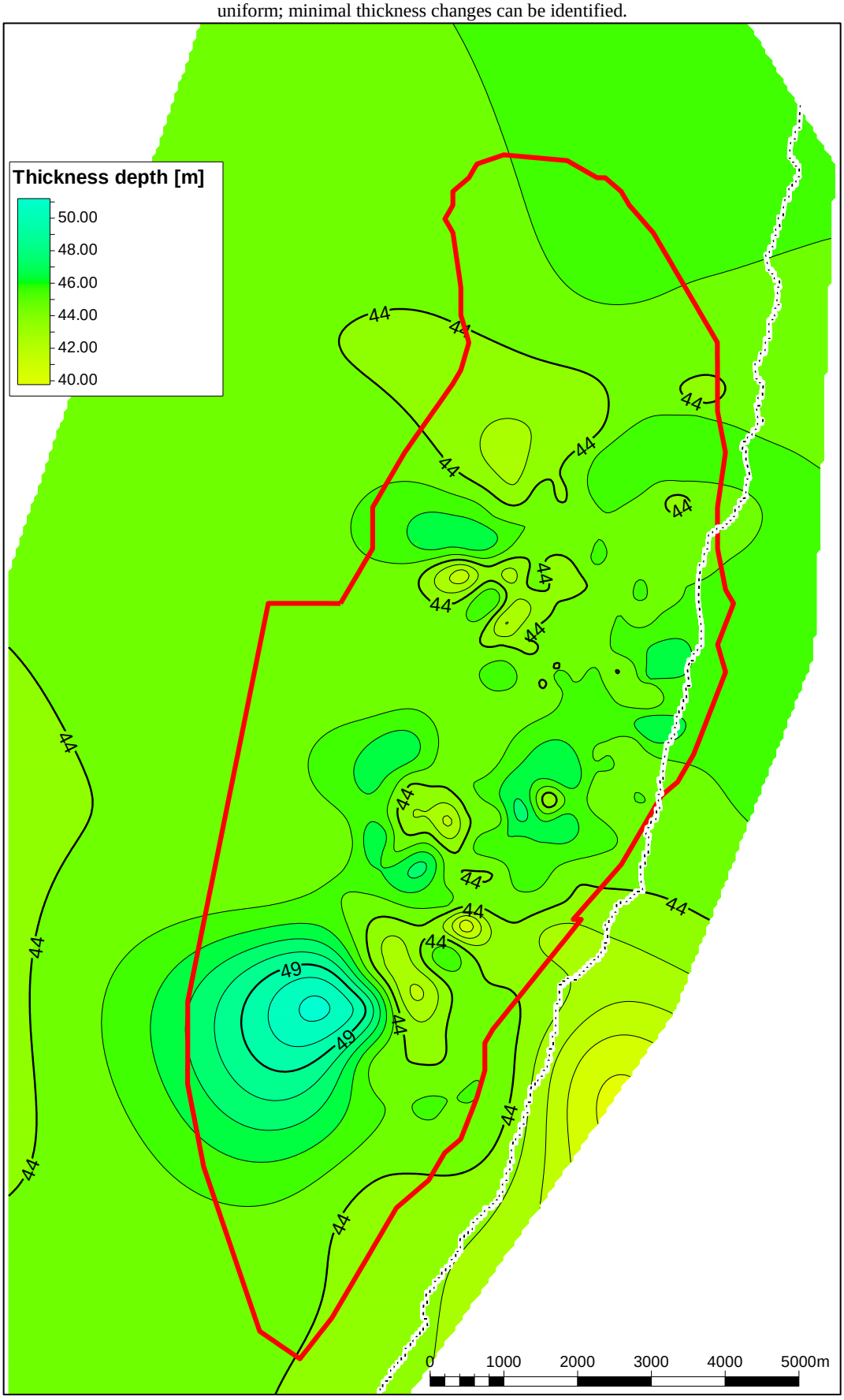

Appendix VII: The contours and the colouring depict the top of C1s reservoir. The green polygon is the geomodel's boundary; the red is the production license boundary. The dashed blue polygon represents the outer oil-water contact at 549 m TVDSS. Outer oil-water contact is the intersection of the top of the reservoir and the depth surface of the OWC. Consequently, the inner OWC is the intersection with the bottom of the reservoir. In the case of C1s, inner OWC is non-existent since the bottom and the OWC do not intersect.

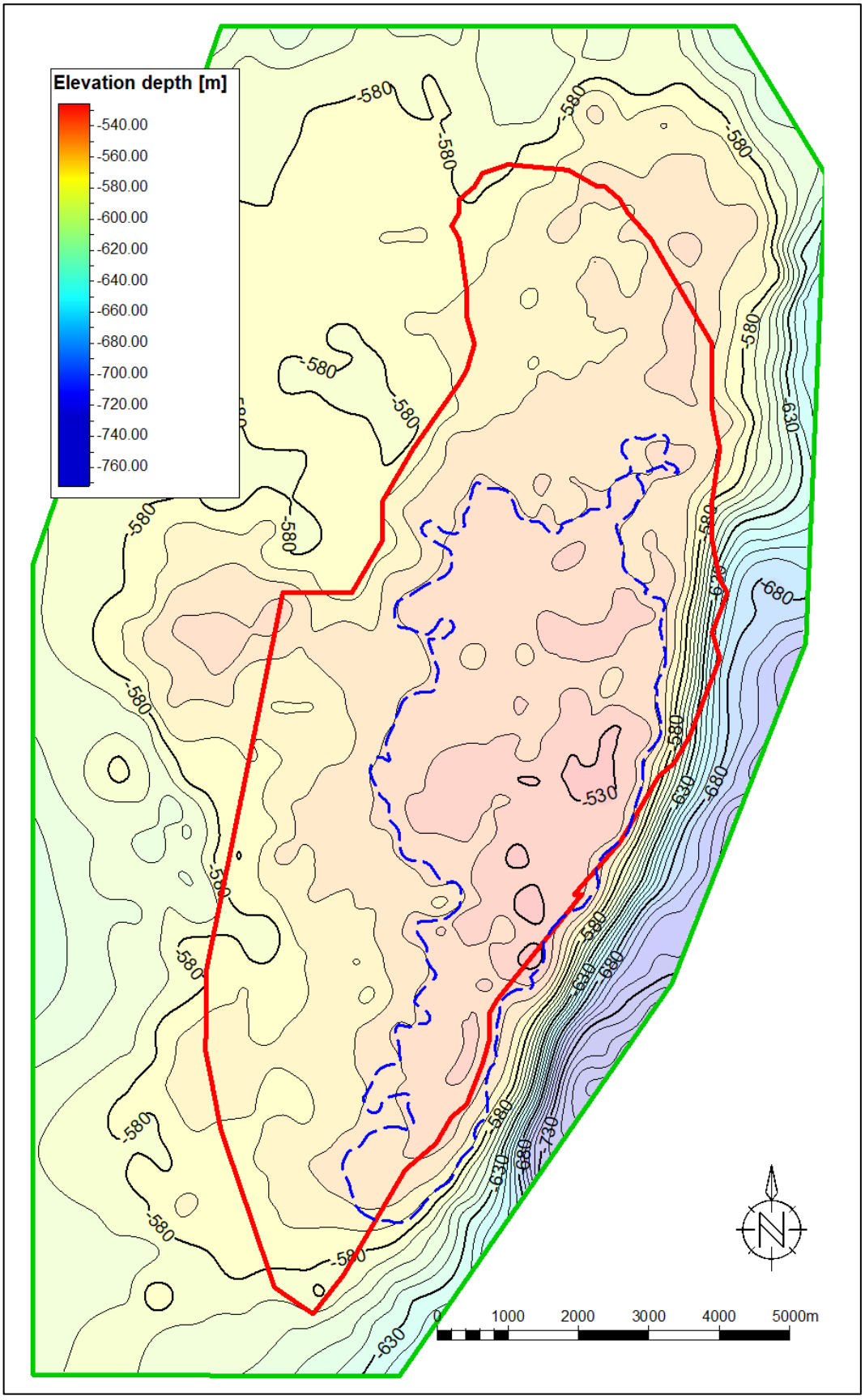

Appendix VIII: A panel showing the main grid properties in fence filtering of the 3D grid representing the Bobrikovian and Tournaisian reservoirs (Z-scale=25). *Panel A* – Reservoirflag parameter, where purple shows the reservoir, while grey represents the non-reservoir zones. Tournaisian's excellent NtG ratio is high, in contrast to Bobrikovian's low ratio (Appendix IX). *Panel B* – The interconnected porosity values show higher homogeneity in the lower part (Tournaisian), although Bobrikovian is represented by a wider range. *Panel C* – A screenshot showing the initial water saturation model of lower formations; the blue parts show the reservoir under OWC_i, consequently, $Sw_i=1$, while the higher above OWC_i (more precisely, free water level – FWL), the lower the Sw_i, as buoyancy and capillary forces drive the initial saturation profile (NEMES, 2016). Panel D – The modelled (calculated) absolute permeability of Bobrikovian and Tournaisian. Bobrkovian has excellent permeabilities in the best part of the reservoir, while Tournaisian's is two orders of magnitude lower (Appendix IX).

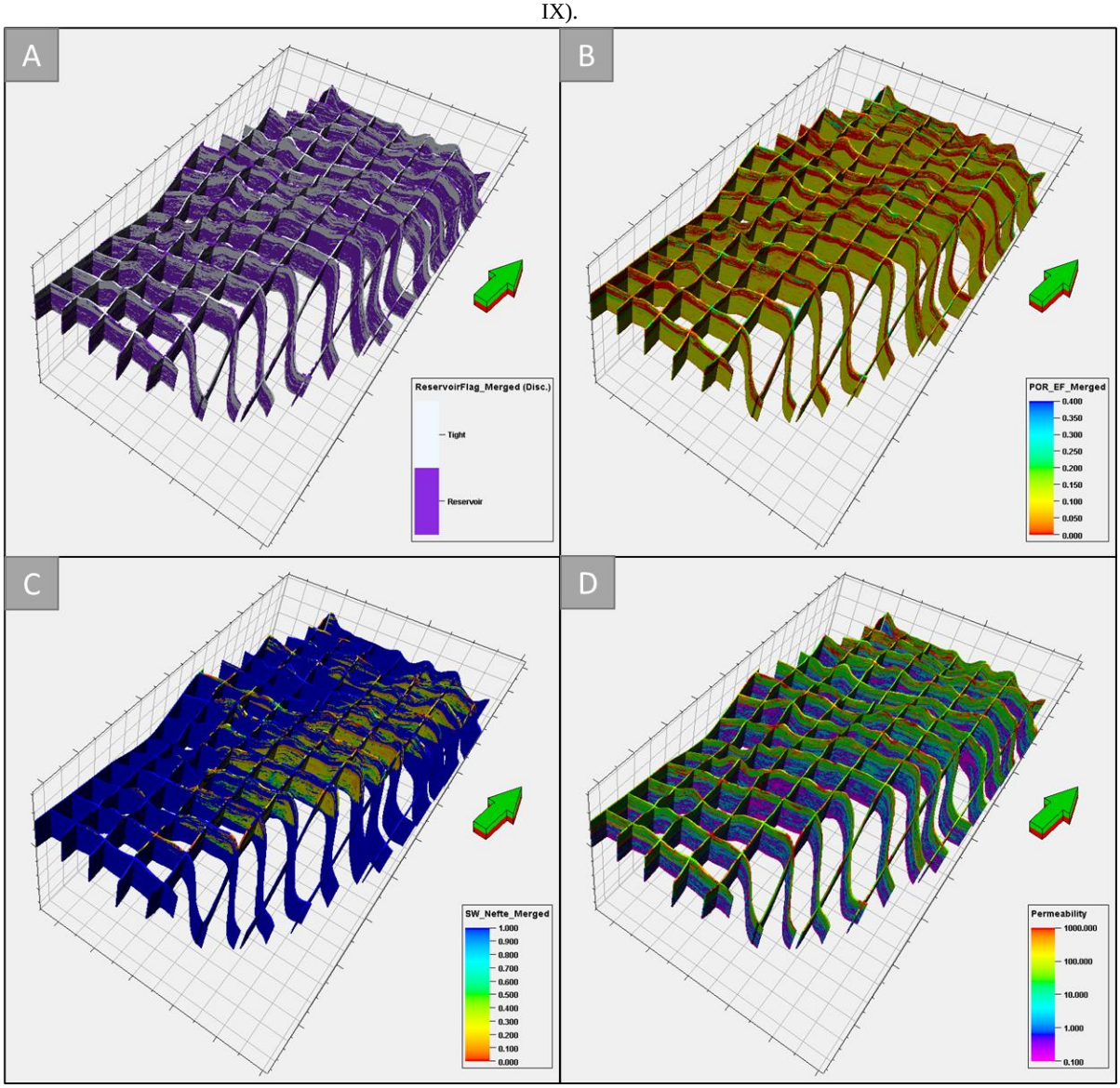

Appendix IX: A overview table summarising the key geological, dynamic and technical data of Field A.

Parameter	Unit	Formation				Comment
		A4	C1s	Bb	V1	
Number of wells	-	551	542	415	413	Number of wells that penetrated, at a minimum, the top of the formation.
Average well distance	m	400	400	550	550	-
Total length of core recovered	m	558	167	243	597	-
Area	km^2	80-100	15-30	80-120	60-90	Total area.
Thickness (TVT)	m	37	57	18	44	-
Trapping mechanism	-	Structural (fault and anticline) and OWC	Structural (fault and anticline) and OWC	Structural (fault and anticline) and OWC	Structural (fault and anticline) and OWC	-
OWCi	m TVDSS	535	549	930	941	-
Net-to-gross ratio (range)	%	25-40%	50-70%	20-40%	60-90%	-
Cut-off porosity	%	8.7%	8.0%	11.0%	8.4%	-
Porosity type	-	matrix and vuggy	vuggy	matrix	matrix	-
Interconnected porosity (arithmetic mean range)	%	10-13%	11-14%	15-17%	10%-12%	In the reservoir zones.
Permeability	mD	1 - >1000	2 - >1000	250 - >1000	1 - 875	In the reservoir zones.
Initial water saturation (arithmetic mean range)	%	10-70%	10-70%	10-60%	10-50%	In the pay zones.
Water salinity	g/l	55	55	230	230	-
Ratio of initial in-place volume	%	19%	6%	21%	54%	-
Main fluid type	-	undersaturated oil	undersaturated oil	undersaturated oil	undersaturated oil	-
Boi	m^3/sm^3	1.000	1.024	1.025	1.035	-
Absolute oil density at ambient conditions	t/m^3	0.901	0.903	0.892	0.893	-
API-gravity	°API	25.5	25.2	27.1	27.0	
Rs_i at p_i	m^3/m^3	5-10	5-10	15-20	25-35	-
CO_2-content in associated gas	%	7-10	7-10	3-7	3-7	-
H_2S-content in associated gas	ppm	0	0	1900-2800	1900-2800	-
Viscosity (@reservoir conditions)	cP	35-45	35-45	20-30	20-30	-
Ratio of total produced volume	%	10%	4%	31%	55%	@2022.01.01
Reservoir temperature	°C	19-21	19-21	25-27	25-27	-
Initial reservoir pressure	bar	66	73	108	109	-
Reference depth	m TVDSS	535	549	930	940	-
Bubble point pressure	bar	26	25	38	40	-
Driving mechanism	-	weak aquifer drive and depletion	moderate aquifer drive and depletion	weak aquifer drive and depletion	weak aquifer drive and depletion	-
Main production method	-	artifical lifting (SRPs)	artifical lifting (SRPs)	artifical lifting (SRPs)	artifical lifting (SRPs)	-

Appendix X: A comparative overview of Phase 1 and Phase 2 models summarising the most important aspects and the upgrade (if any). A short recommendation on the way-forward is also given.

Comparative overview of Phase 1 and Phase 2 geomodels					
Category	**Aspect**	**Phase 1**	**Phase 2**	**Recommendation for a future phase**	**Change**
General	Used software for modelling	Emerson's RMS 2013.1 (64-bit MS Windows 7)	Schlumberger's Petrel 2015.5 (64-bit MS Windows 7)	Schlumberger's Petrel latest stable version. (or piloting Rock Flow Dynamics's tNavigator)	↑
General	Vintage date	2016-01-01	2017-07-15	Update the vintage at a pre-defined frequency (~quick update continuously, detailed update annually).	↑
General	Modelled area	210	170	No further cut on the grid extenstion is recommended in order to cover the possible potential in the AOI.	↑
General	Coordinate system	Specific local projection and datum system.	Specific local projection and datum system.	-	→
General	Total number of wells in the model	459	557	Include the wells drilled since the vintage date. Update any trajectory where newly digitized data became available.	↑
General	Repeatable workflow	Simple workflow was built.	Detailed full-cycle workflow was constructed.	Fine-tune the workflow (correct manual steps, add the "control panel").	↑
Structural modelling	Vintage of seismic interpretation	2015	2017	Update and incorporate new wells and data	↑
Structural modelling	Number of reservoirs modelled	4	4	6 - Incorporate possible shallow and deep exploration targets also	↑
Structural modelling	Number of subzones modelled	0	7	No further sub zonation is recommended.	↑
Structural modelling	Number of welltops	350 welltops for Bashkirian Formation top and 179 for Tournasian Formation bottom. (Total number: 2,389)	551 welltops for Bashkirian Formation top and 165 for Tournasian Formation bottom. Complete re-interpretation with unified approach. (Total number: 2,909)	-	↑
Structural modelling	Number of faults modelled	54	1	Revisit the role of faults on flow pattern.	→
Facies modelling	Methodology of rock-typing	Based on one set of cut-off criteria per zone	Based on one set of cut-off criteria per subzone	A more sophisticated methodology in order to differentiate relevant rocktypes driving the flow pattern. (e.g. MICP-based, or composition-based, or fracture-based).	↑
Facies modelling	Methodology of facies modelling	Sequential Indicator Simulation	Sequential Indicator Simulation	Object-based modelling at least for Bobrikovian Formation.	→
Property modelling	Application of trend maps	No trend maps were applied	Trend maps applied only in the Bobrikovsky Formation	Incorporate trend maps for other formations also, especially for Serpukhovian karsts.	↑
Property modelling	Application of seismic-based trends	Not available	Not available	It is worth a re-visit with new software and cutting-edge methods.	→
Property modelling	Petrophysical interpretation	First pass interpretation with several wells missing.	Complete re-interpretation and calibration to core data, adding ~100 wells with interpretation.	Re-visit intrepretability of more wells, and quantify uncertainty.	↑
Property modelling	Porosity modelling	Interconnected porosity modelled biased to the reservoirflag (a.k.a. rocktypes) per formation.	First interconnected porosity modelled in 3D, and the reservoirflag calculation was performed in the grid per subzone. (Except for Bobrikovsky Formation).	If new rocktype model will be built, this must have an impact on the porosity model also.	↑
Property modelling	Water saturation modelling	Based on log-derived water saturation.	Based on log-derived water saturation of an updated petrophysical interpretation.	J-functions or look-up functions should be calculated and used. Apply Thomeer-method for measured MICP-curves in order to maximize information-value.	↑
Property modelling	Permeability modelling	Poro-perm regressions were used per formation.	Poro-perm regressions were used as per subzone, with increased amount of evaluated data.	White noise should be added to the permeability distribution, as well as permeability anisotropy should be modelled.	↑
Volume calculation	Stochastic uncertainty quantification	Not quantified	Not quantified	Minimum of 50 stochastic realizations should be run.	→
Volume calculation	Uncertainty quantification	Not quantified	Not quantified	Structural and petrophysical uncertainty range should be modelled and quantified for initial in-place volumes-	→